Publication No. R79-31 Order No. 654

MIT

Seismic Behavior and Design of Buildings

Report No. 2

INELASTIC SEISMIC RESPONSE OF A TORSIONALLY UNBALANCED SINGLE-STORY BUILDING MODEL

by

H.M. IRVINE

and

G.E. KOUNTOURIS

DEPARTMENT
OF
CIVIL
ENGINEERING

SCHOOL OF ENGINEERING
MASSACHUSETTS INSTITUTE OF TECHNOLOGY
Cambridge, Massachusetts 02139

July 1979

Sponsored by the National Science Foundation

Applied Science and Research Applications

Grant ENV77-14174

Additional Copies May Be Obtained from:

National Technical Information Service

U.S. Department of Commerce

5285 Port Royal Road

Springfield, Virginia 22161

50272-101

REPORT DOCUMENTATION PAGE	1. REPORT NO. NSF/RA-790389	2.	3. Recipient's Accession No. PB80-164197
4. Title and Subtitle: Inelastic Seismic Response of a Torsionally Unbalanced Single-Story Building Model (Seismic Behavior and Design of Buildings, Report No. 2)			5. Report Date: July 1979 6.
7. Author(s): H. M. Irvine, G. E. Kountouris			8. Performing Organization Rept. No.: Publication No. R79-31
9. Performing Organization Name and Address: Massachusetts Institute of Technology School of Engineering Department of Civil Engineering Cambridge, Massachusetts 02139			10. Project/Task/Work Unit No.: Order No. 654 11. Contract(C) or Grant(G) No. (C) (G) ENV7714174
12. Sponsoring Organization Name and Address: Engineering and Applied Science (EAS) National Science Foundation 1800 G Street, N.W. Washington, D.C. 20550			13. Type of Report & Period Covered 14.

15. Supplementary Notes

16. Abstract (Limit: 200 words)

The dynamic effects of coupling between torsion and translocation using a simple torsionally unbalanced single-story building model are described. The investigation deals with a two-degree-of-freedom model in which two frames support a diaphragm the center of mass of which may be offset from the center of stiffness. Frames are assumed to behave as simple elastic-plastic springs and to have the same stiffness and strength levels. A comprehensive parameter study was undertaken to identify trends in the peak ductility demands of the worst situated frame. Results are plotted and interpreted. A simple frequency domain analysis outlines why the peak ductility demands occur in the frame farthest from the center of mass. The study indicates that the most important parameter is one involving the product of diaphragm mass and spectral acceleration normalized by a yield level in the frame. For wide ranges of other parameters, the peak ductility demand is roughly linear in this parameter, a characteristic of symmetric structures. Eccentricity does not appear to be a significant parameter. A regression analysis of the data yielded simple confidence levels for peak ductility demands.

17. Document Analysis a. Descriptors

Earthquake resistant structures
Dynamic structural analysis
Buildings
Mathematical models
Earthquakes
Ductility

b. Identifiers/Open-Ended Terms

c. COSATI Field/Group

18. Availability Statement: NTIS	19. Security Class (This Report)	21. No. of Pages
	20. Security Class (This Page)	22. Price

(See ANSI-Z39.18) See Instructions on Reverse

OPTIONAL FORM 272 (4-77)
(Formerly NTIS-35)
Department of Commerce

17

Massachusetts Institute of Technology
Department of Civil Engineering
Constructed Facilities Division
Cambridge, Massachusetts 02139

Seismic Behavior and Design of Buildings

Report No. 2

INELASTIC SEISMIC RESPONSE OF A TORSIONALLY UNBALANCED SINGLE-STORY BUILDING MODEL

by

H. M. Irvine

and

G. E. Kountouris

July 1979

Sponsored by the National Science Foundation
Applied Science and Research Applications
Grant ENV77-14174

Publication No. R79-31

Order No. 654

B

ABSTRACT

An investigation of the inelastic seismic response of a simple torsionally unbalanced building is reported. The studies undertaken here concern a two-degree-of-freedom model in which two frames support a diaphragm the center of mass of which may be offset from the center of stiffness. The frames are assumed to behave as simple elastic-plastic springs and to have the same stiffness and strength levels.

A comprehensive parameter study is undertaken in an attempt to identify trends in the peak ductility demands of the worst situated frame, which is frequently, but not always, the one nearest the center of mass. The results are presented in an extensive series of plots and the trends present are discussed. A simple frequency domain analysis is outlined in an attempt to explain why, in some cases, the peak ductility demands occur in the frame farthest from the center of mass.

From this work it is concluded that the most important parameter is one involving the product of diaphragm mass and spectral acceleration normalized by a yield level in the frame. For wide ranges of the other parameters the peak ductility demand is roughly linear in this parameter—a result well known for symmetric structures. Surprisingly, eccentricity does not appear to be a particularly significant parameter. A regression analysis of the data is performed to yield simple confidence levels for the peak ductility demands.

PREFACE

This is the second report prepared under the research project entitled "Seismic Behavior and Design of Buildings," supported by National Science Foundation Grant ENV77-14174.

The purpose of the project is: To perform a more comprehensive evaluation of various definitions of ductility used at present in dynamic analysis programs, assessing their physical meaning and their relation to expected structural damage; to evaluate different design procedures, particularly those recommended by present codes, in terms of the behavior of the resulting frames and the expected level of damage under various earthquake motions; to develop if needed alternate design procedures or recommendations to ensure the adequacy of the behavior; and to evaluate further some of the complex models used at present for special structures (such as nonlinear finite element models for reinforced concrete structures).

The first report produced was:

Biggs, John M., Lau, Wai K., and Persinko, Drew, "Seismic Design Procedures for Reinforced Concrete Frames."

The project is supervised by Professors J. M. Biggs and H. M. Irvine, and Research Assistants who have contributed to the Project are Hooshang Banon, George Kountouris, Wai K. Lau and Drew Persinko.

TABLE OF CONTENTS

LIST OF FIGURES

CHAPTER I - INTRODUCTION

1.1 Scope

In this report the dynamic effects of coupling between torsion and translation are investigated using a simple eccentric single-story building model. Both elastic and inelastic responses to selected strong ground motions are examined, with most attention being paid to endeavoring to assess trends in inelastic response.

Many investigations into elastic response have been carried out in the past, reviews of which may be found in Hoerner (1) and in Dempsey (2). Most investigators have concluded that current torsional provisions in loadings codes may be inadequate, but the means of remedying the situation are unclear. Very little work has been done on inelastic response of torsionally unbalanced buildings, at least in so far as systematic studies are concerned. The object of the present work is, therefore, to attempt to fill in some of the gaps in present knowledge.

In many respects the work is an extension of that reported by Dempsey and Irvine (2), in which analytical solutions were obtained for peak elastic response quantities. It is there too that, for the first time, a general criterion was given for the occurrence of full modal coupling, in a simple two-degree-of-freedom model. The inelastic case is obviously much more complicated, and the use of a digital computer is essential since step-by-step integration methods are required. It occasionally happens that elastic analytical work can be used to predict and explain features of inelastic response and this, it turns out, is true of the present work. For the most part, however, one must rely on numerical methods and be able to sift through the vast quantities of information that the process provides.

Our main concern is with peak ductility demands in parts of an eccentric model and the output has been tailored accordingly.

It is to be expected that inelastic response studies of a torsionally unbalanced building, even in an idealized case such as this, involve several parameters, many of which may be profoundly important. Our efforts are aimed primarily at isolating those that appear to be of prime importance; it is realized, of course, that results obtained in this manner for this model are, at best, difficult to extrapolate to more realistic multistory systems.

1.2 Organization of the Report

In Chapter 2 a review of the elastic analysis of a partially symmetric building model is made. Modal analysis of the equations of motion is performed, the eigenvalues and eigenmodes are extracted, and the total response is decomposed into the response due to the lateral and torsional vibration modes. Various cases of modal coupling are shown and full modal coupling is investigated. The maximum seismic response of the model is expressed in terms of two equivalent static actions—the horizontal shear and the torque. Results are plotted continuing the maxima by addition, subtraction, SRSS and modified SRSS.

Chapter 3 presents the formulation of the equations of motion for an inelastic 2-DOF single-story building model. The modeling is discussed, for this appears to be the simplest inelastic model for eccentricity studies. Frequency domain analysis is performed on the equations in the elastic case in order to show general trends and to predict (what was later confirmed) various aspects of inelastic response to seismic excitation. The important

parameters of the problem are pointed out and a commonly used non-dimensionalization is performed in order to facilitate the parametric study.

In Chapter 4 the program used is briefly presented, and several features of the program closely related to the parametric study are discussed. The different parameters and their range are investigated. Then the results of the parametric studies are presented in 108 plots for the four different earthquake motions. The results represent a total of 3888 actual cases.

In Chapter 5 there is a detailed discussion of the results. The various trends are explained and the influence of the different parameters, and their significance, are evaluated. Since both real and artificial motions are used, the importance of the specific earthquake motion in the ductility requirements is pointed out and the variability to the response to a real earthquake versus an artificial one is discussed. Finally, Chapter 5 contains the conclusions of this study. The results are summarized and their implications on design are discussed.

CHAPTER II

REVIEW OF THE ELASTIC ANALYSIS OF A SIMPLE 2-DOF PARTIALLY SYMMETRIC BUILDING MODEL

The inelastic seismic response of a torsionally unbalanced two-degree-of-freedom system is much more complex than the elastic case. In the elastic case analytical formulae can be used to evaluate the seismic response, whereas this is impossible for the inelastic case. Dempsey and Irvine (2) have derived analytical formulae for the peak response of the simplest form of torsional unbalance, which is an idealized single-story shear building subjected to horizontal ground shaking. The following is a brief review of that work.

The model consists of a rigid floor diaphragm and resisting elements that are limited to deform elastically in horizontal shear. Since the ground shaking is purely translatory, any torsional response is attributable solely to the torsional unbalance inherent in the asymmetric distribution of mass and stiffness.

The model is shown in Figure 2.1. The small circle (o) and star (*) in this figure denote the center of mass and center of stiffness respectively; e is the calculated eccentricity.

For massless resisting elements the undamped equations of motion with respect to the center of mass are

$$\begin{bmatrix} M & 0 \\ 0 & J_o \end{bmatrix} \begin{bmatrix} \ddot{V}_o + \ddot{u}_g \\ \ddot{\theta} \end{bmatrix} + \begin{bmatrix} K^v & K^v e \\ K^v e & K_o^\theta \end{bmatrix} \begin{bmatrix} V_o \\ \theta \end{bmatrix} = \begin{bmatrix} 0 \\ 0 \end{bmatrix} \qquad (2.1)$$

where M = mass of floor diaphragm

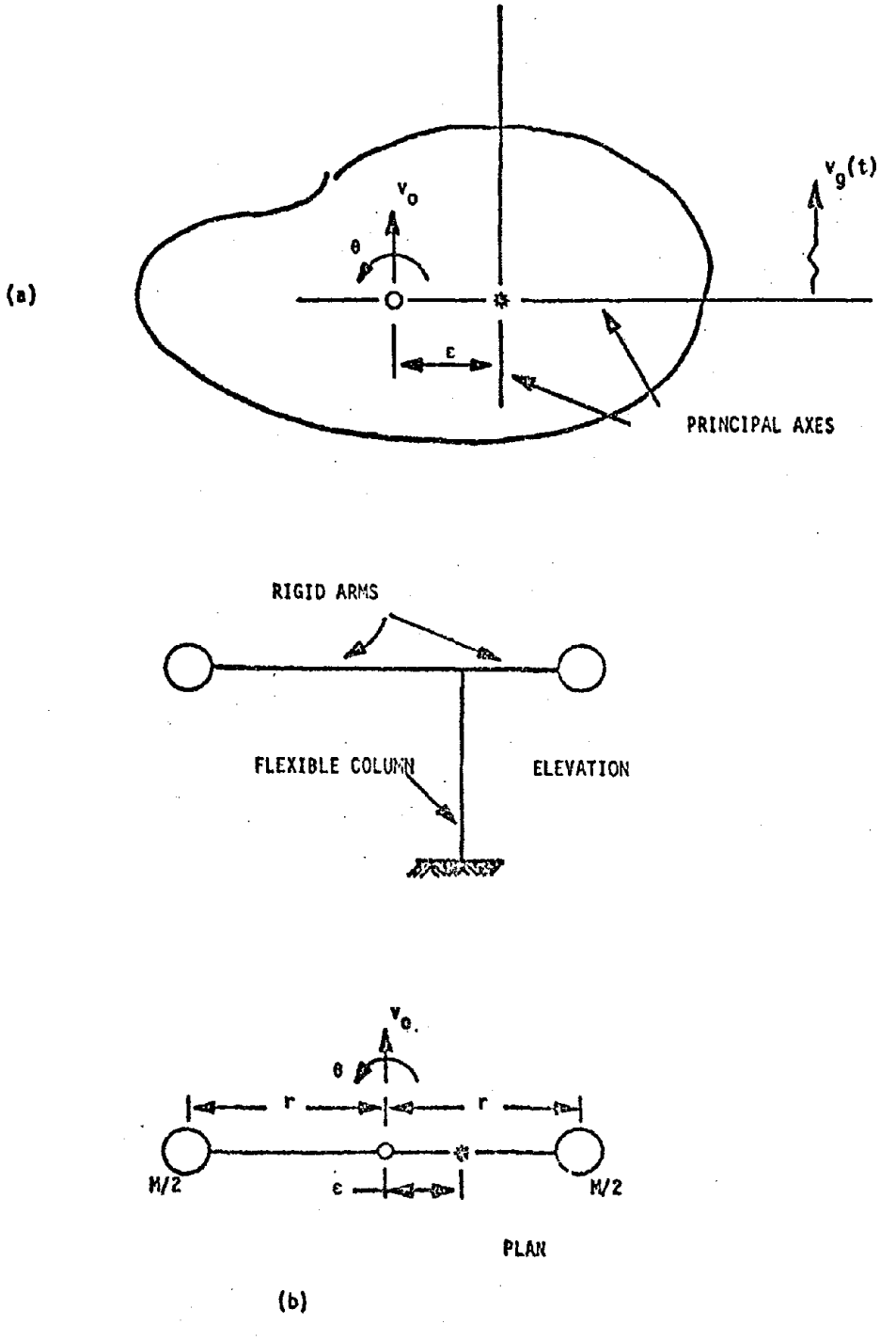

Figure 2.1 - Definition Diagrams for Model (2).

J_o = polar moment of inertia of the diaphragm about the center of the mass

e = eccentricity

$V_o(t)$ = displacement of center of mass relative to ground

$\theta(t)$ = counterclockwise angle of rotation of the diaphragm

K^v = translational stiffness in the direction of the ground shaking

K_o^θ = torsional stiffness for a stationary center of mass.

The eigenvalue problem reduces to the equation

$$\lambda^4 - (1 + \mu_o^2)\lambda^2 + \mu^2 = 0 \quad ,$$

which has the two roots, λ_v, λ_θ, and where λ_v and λ_θ are the ratios of the "coupled natural frequencies" to the balanced translational natural frequency, respectively.

$$\mu_o^2 = K_o^\theta / K^v r^2 \quad ,$$

r = radius of gyration

$$\mu^2 = \mu_o^2 - \delta^2 \qquad \text{and}$$

$$\delta = e/r \quad .$$

The two eigenvalues are

$$\lambda_v^2 = \frac{1 + \mu_o^2}{2} + \text{sgn}\,(1 - \mu_o)\sqrt{\left(\frac{1 - \mu_o^2}{2}\right)^2 + \delta^2}$$

$$\lambda_\theta^2 = \frac{1 + \mu_o^2}{2} - \text{sgn}\,(1 - \mu_o)\sqrt{\left(\frac{1 - \mu_o^2}{2}\right)^2 + \delta^2}$$

and the eigenmode matrix Φ is

$$\Phi = \begin{bmatrix} \cos\psi & -\text{sgn}\,(1-\mu_o)\sin\psi \\ \text{sgn}\,(1-\mu_o)\sin\psi & \cos\psi \end{bmatrix}$$

where

$$\cos\psi = \sqrt{\frac{1}{2} + \text{sgn}\,(1-\mu_o)\frac{(1-\mu_o^2)}{4\sqrt{\left(\frac{1-\mu_o^2}{2}\right)^2+\delta^2}}}$$

$$\sin\psi = \sqrt{\frac{1}{2} - \text{sgn}\,(1-\mu_o)\frac{(1-\mu_o^2)}{4\sqrt{\left(\frac{1-\mu_o^2}{2}\right)^2+\delta^2}}}$$

The angle ψ is bounded by $0 \leq \psi \leq \pi/4$ and provides a measure of the modal coupling. The modes are fully coupled at the center of mass when $\psi = 45°$. Then $\mu_o = 1$, and

$$\mu = \sqrt{1-\delta^2} \qquad \phi = \frac{1}{\sqrt{2}}\begin{bmatrix} 1 & -1 \\ 1 & 1 \end{bmatrix}$$

If viscous damping is included in the model, then the normal coordinate equations of motion can be written

$$\ddot{\xi}_v + 2\zeta_v\omega_v\dot{\xi}_v + \omega_v^2\xi_v = -\alpha_v\ddot{u}_g$$

$$\ddot{\xi}_\theta + 2\zeta_\theta\omega_\theta\dot{\xi}_\theta + \omega_\theta^2\xi_\theta = -\alpha_\theta\ddot{u}_g$$

where $\omega_v = \lambda_v\sqrt{K^v/M}$ and $\omega_\theta = \lambda_\theta\sqrt{K^v/M}$ are the natural frequencies and

where ζ_v, ζ_θ fractions of critical damping and α_v, α_θ are modal participation factors, given by

$$\alpha_v = \cos \psi$$

$$\alpha_\theta = -\operatorname{sgn} (1 - \mu_o) \sin \psi.$$

The solution of them for zero initial conditions is

$$V_o = D_v \cos^2\psi + D_\theta \sin^2 \psi$$

$$r\theta = \operatorname{sgn} (1 - \mu_o)(D_v - D_\theta) \sin \psi \cos \psi$$

where

$$D_v(t) = -D(\zeta_v, \omega_v, t, \ddot{v}_g)$$

$$D_\theta(t) = -D(\zeta_\theta, \omega_\theta, t, \ddot{v}_g)$$

and $$D(\zeta,\omega,t,\ddot{u}_g) = \frac{1}{\omega\sqrt{1-\zeta^2}} \int_o^t \exp[-\zeta\omega(t-\tau)] \sin \omega\sqrt{1-\zeta^2}\,(t-\tau)\ddot{u}_g(\tau)d\tau \ .$$

The maximum seismic response is expressed in terms of the horizontal shear S_* and the torque T_*, which act at the center of stiffness.

$$S_* = K^v V_*(\max)$$

$$T_* = K^\theta \theta \ (\max) \ .$$

The positive directions of shear and torque are shown in Figure 2.2.

If we use the idealized design spectrum of Figure 2.3, where

$$S_a(\zeta,\omega) = \begin{cases} S_a(\zeta,\omega_1) & T \le T_1 \\ \\ S_a(\zeta,\omega_1)(T_1/T) & T \ge T_1 \end{cases} ,$$

then it is found that

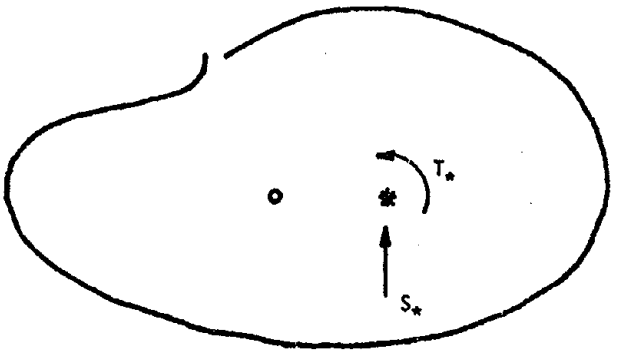

Figure 2.2 - Diagram Showing Positive Directions of Shear and Torque (2)

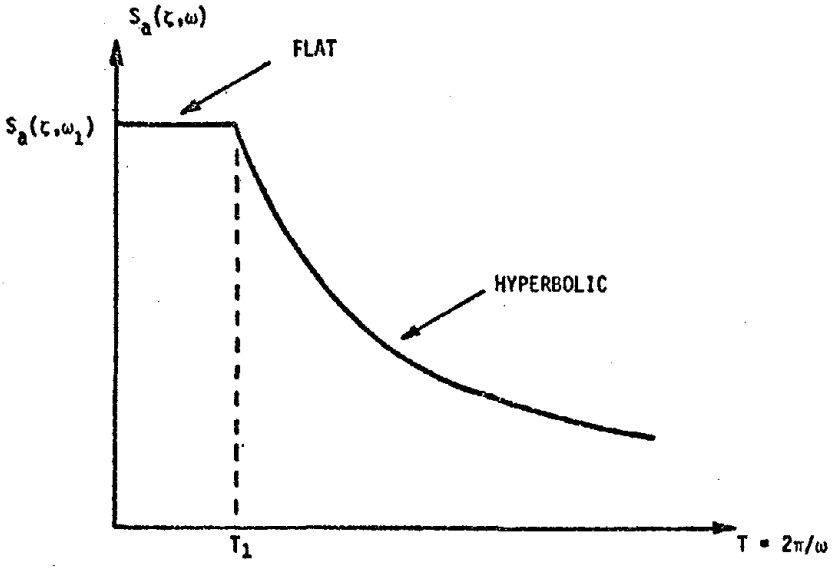

Figure 2.3 - Diagram Illustrating Spectra Used (2)

$$\bar{S}_{*_V} = \frac{1}{\lambda_V^2} \frac{S_a(\zeta,\omega_V)}{S_a(\zeta,P_V)} [\cos^2\psi + \text{sgn}\ (1-\mu_o)\ \delta \sin\psi \cos\psi]$$

$$\bar{S}_{*_\theta} = \frac{1}{\lambda_\theta^2} \frac{S_a(\zeta,\omega\ )}{S_a(\zeta,P_V)} [\sin^2\psi - \text{sgn}\ (1-\mu_o)\ \delta \sin\psi \cos\psi]$$

$$\bar{T}_{*_V} = \text{sgn}\ (1-\mu_o)\ \frac{\mu^2}{\lambda_V^2} \frac{S_a(\zeta,\omega_V)}{S_a(\zeta,P_\theta)} \sin\psi \cos\psi$$

$$\bar{T}_{*_\theta} = \text{sgn}\ (1-\mu_o)\ \frac{\mu^2}{\lambda_\theta^2} \frac{S_a(\zeta,\omega_V)}{S_a(\zeta,P_\theta)} \sin\psi \cos\psi$$

where

$$\bar{S}_* = \frac{S_*}{MS_a(\zeta,P_u)} \qquad \bar{T}_* = \frac{T_*}{MS_a(\zeta,P_\theta)}$$

and

$$P_V = \sqrt{K^V/M} \qquad P_\theta = \sqrt{K^\theta/J_*}$$

Now the question arises as to how to combine the modal maxima. As a preliminary investigation one could algebraically add them or subtract them in order to get a feeling of the response.

If the frequencies are well separated, then we can use the SRSS to estimate the maximum response. The SRSS combination functions are

$$\bar{S}_* = \sqrt{\bar{S}_{*_V}^2 + \bar{S}_{*_\theta}^2} \qquad \bar{T}_* = \sqrt{\bar{T}_{*_V}^2 + \bar{T}_{*_\theta}^2}$$

The computed results are shown in Figure 2.4.

A major disadvantage of the SRSS is that the sign is lost. However, as we will see in the following chapter, the sign of the maximum response has some interesting and particular implications for the response.

If the natural frequencies are close, then a modified SRSS can be used

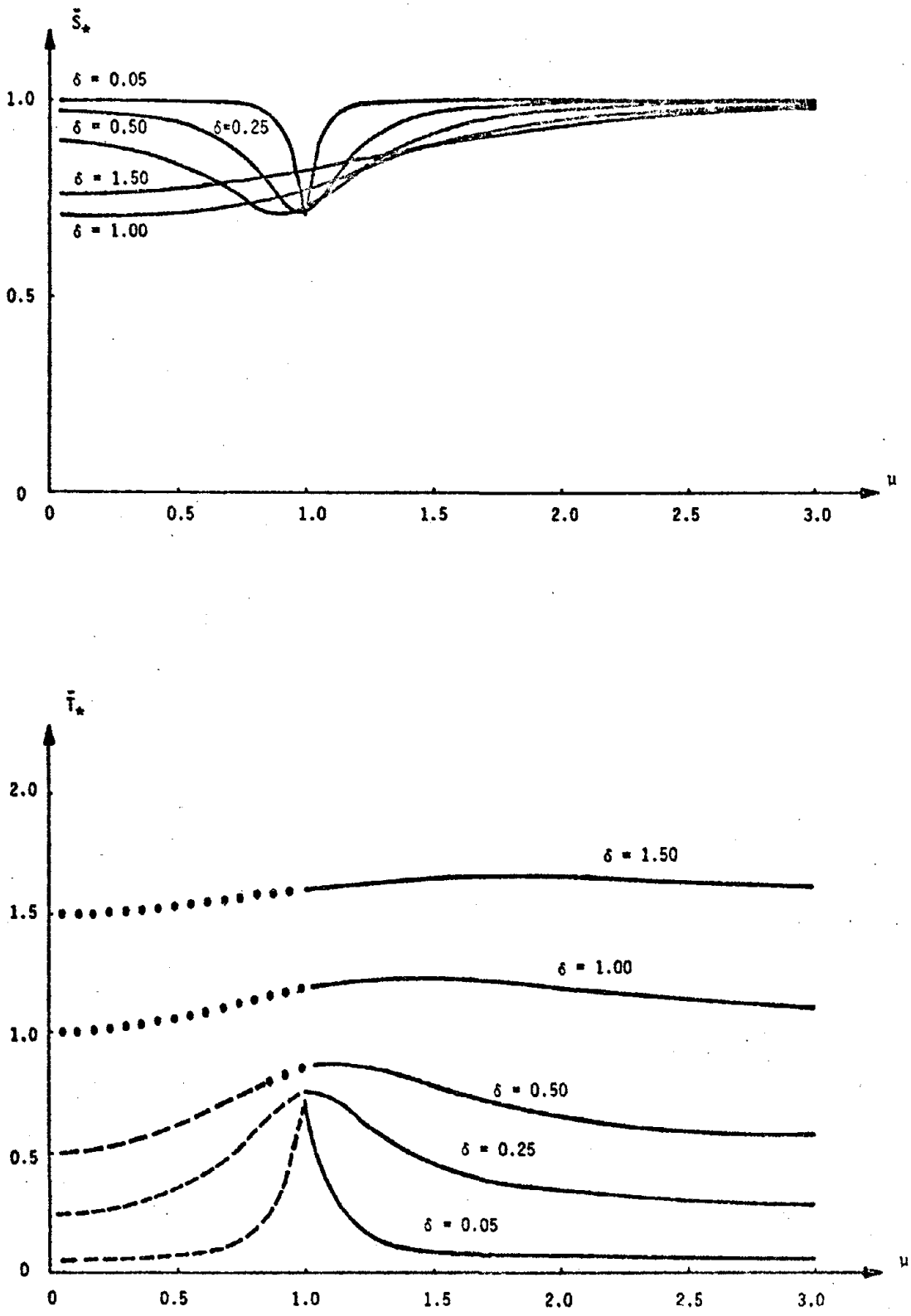

Figure 2.4 - Maximum Values of $\bar{S}_*$ and $\bar{T}_*$ Evaluated Using the SRSS Combination Rule. Inferred torque signs: --- positive, —— negative, ··· both negative and positive (2)

effectively. This approach has been derived by Rosenblueth and Elorduy. According to them, the maximum earthquake response is

$$Q^2 = \sum_{i=1}^{N} Q_i^2 + \sum_{i=1}^{N-1} \sum_{j=i+1}^{N} \frac{2Q_iQ_j}{1 + \varepsilon_{ij}^2}$$

where Q_i and Q_j are the i^{th} and j^{th} modal maxima and $\varepsilon_{ij} = \dfrac{|\omega_i - \omega_j|}{(\zeta_i\omega_i + \zeta_j\omega_j)}$,

In Dempsey and Irvine's work the best estimates were:

$$\overline{S}_* = \sqrt{\overline{S}_{*v}^2 + \overline{S}_{*\theta}^2 - 2 \exp\left\{-40\left(\frac{\omega_v - \omega_\theta}{\omega_v + \omega_\theta}\right)^2\right\}|\overline{S}_{*v}| \cdot |\overline{S}_{*v\theta}|}$$

$$\overline{T}_* = \sqrt{\overline{T}_{*v}^2 + \overline{T}_{*\theta}^2 + 2 \exp\left\{-40\left(\frac{\omega_v - \omega_\theta}{\omega_v + \omega_\theta}\right)^2\right\}|\overline{T}_{*v}| \cdot |\overline{T}_{*\theta}|}$$

The computed results are shown in Figure 2.5 for all frequency spacings.

In Figures 2.4 and 2.5 it may be observed that there are regions where the maximum torque is positive, which at first glance seems improbable. We will see later that this happens at low values of the "rotational" to "translational" periods, and we will attempt to give a mathematical justification and a physical explanation for it.

As a conclusion to the above analysis of the single-story shear building, it should be emphasized that only for an elastic analysis can analytical formulae be derived. Also, the results are plotted for the maximum

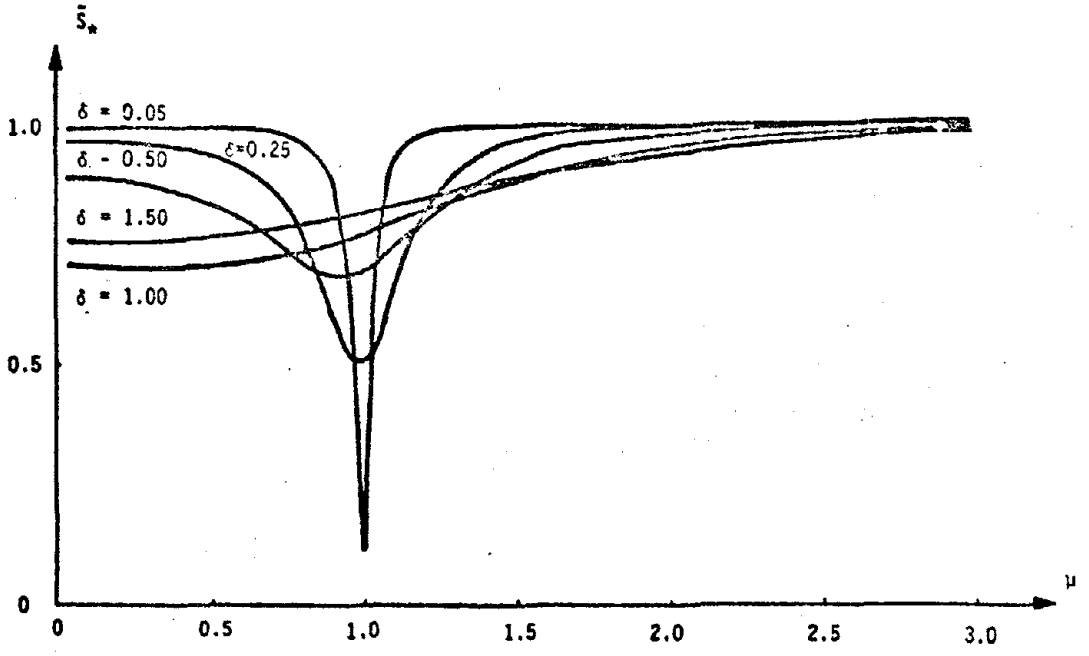

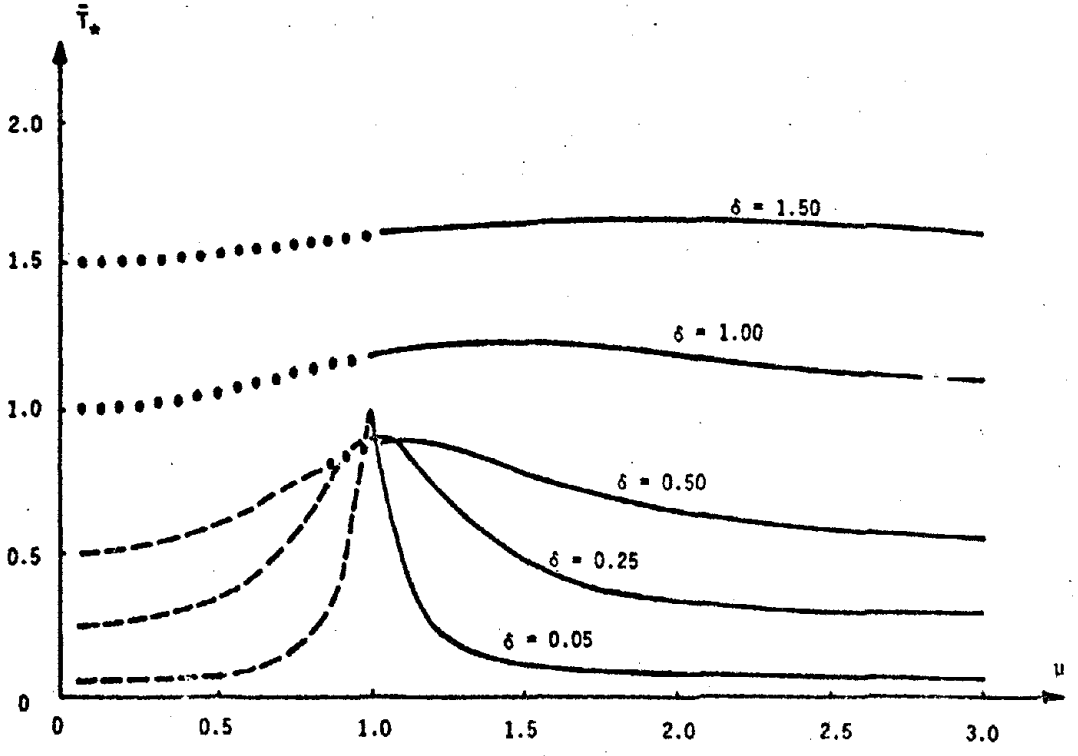

Figure 2.5 - Final Results for the Maximum Normalized Shears and Torques Evaluated Using Modified Forms of the SRSS Combination Rule: ---- positive, ——negative, ··· both positive and negative (2).

response using the simplifying concept of the flat-hyperbolic design spectrum. The results of Figure 2.5 provide an insight into the problem of the torsional imbalance in the elastic case as well as some information for the studies of the inelastic case. Finally, it should be noted that these analytical results are dependent on just two parameters; such simplicity cannot be expected when inelastic demands are to be met.

CHAPTER III - FORMULATION OF THE MODEL

3.1 Equations of Motion

In order to study the inelastic seismic response of a torsionally unbalanced building, a single-story building model has been devised (see Figure 3.1.1).

The model consists of two identical one-bay frames parallel to each other and supporting a diaphragm, which is assumed to be rigid and of mass M. The two frames are assumed to be massless and to exhibit elasto-plastic behavior. The diaphragm's center of mass is offset from the center of stiffness so that there is an eccentricity and the model is torsionally unbalanced. Consequently, for an earthquake motion which coincides with the direction of the two identical frames, both translation in the direction of the earthquake motion and rotation of the diaphragm will occur. Translation and rotation are thus the two degrees of freedom in this single-story building model. If the center of mass coincides with the center of stiffness, then the rotational mode of the building will not be excited and this is the symmetric case, which is a useful reference case. A schematical representation of the model is in Figure 3.1.2.

The mass is offset distance X from the left frame. Each frame is designated a stiffness K. Taking the sum of forces and the sum of moments with respect to the left-hand frame, we obtain the two equations

$$\begin{aligned} \sum F^V = 0 \quad & M(\ddot{V}_o + \ddot{u}_g) + KV_1 + KV_2 = 0 \\ \sum M = 0 \quad & Mx(\ddot{V}_1 + \ddot{u}_g) + (J_o + Mx^2)\ddot{\theta} + KV_2L = 0 \quad , \end{aligned} \tag{3.1.1}$$

where J_o is the moment of inertia, V_o is the relative displacement, and θ is the rotation of the center of the mass. So

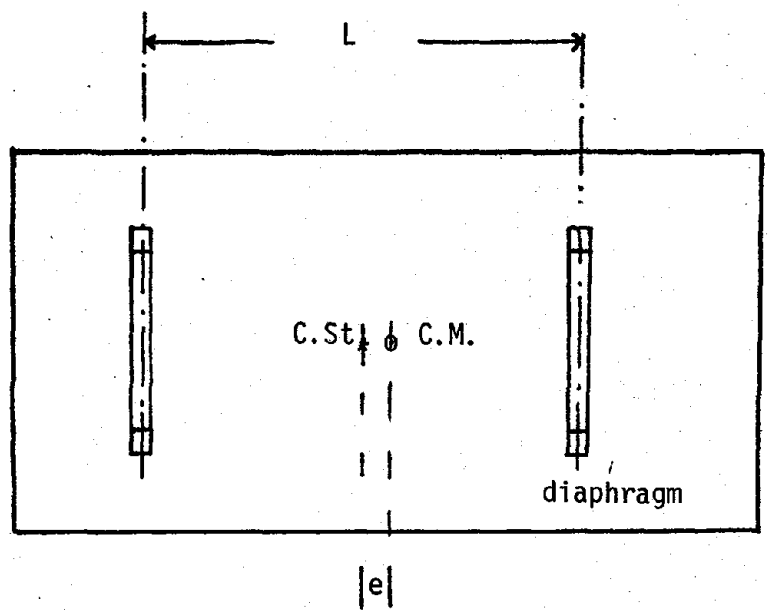

Figure 3.1.1 - Plan View of the Model

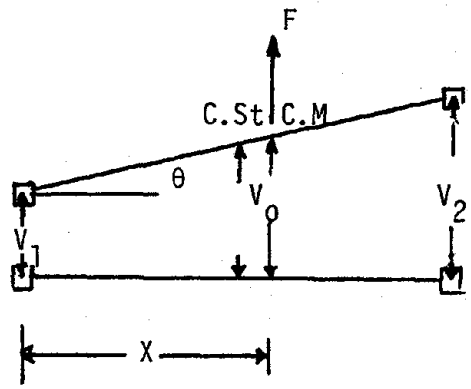

Figure 3.1.2 - Schematic View of the Model

$$V_o = V_1 + \frac{V_2 - V_1}{L} X$$

$$\theta = \frac{V_2 - V_1}{L} \qquad (3.1.2)$$

Substituting eqn. (2) in eqn. (1), we obtain

$$\begin{vmatrix} M(1 - \frac{X}{L}) & M\frac{X}{L} \\ M(1 - \frac{X}{L})X - \frac{J_o}{L} & M\frac{X}{L}X + \frac{J_o}{L} \end{vmatrix} \begin{vmatrix} \ddot{V}_1 \\ \ddot{V}_2 \end{vmatrix} + \begin{vmatrix} K & K \\ 0 & KL \end{vmatrix} \begin{vmatrix} V_1 \\ V_2 \end{vmatrix} = \begin{vmatrix} -M\ddot{u}_g \\ 0 \end{vmatrix}$$

or by multiplying the first by X and subtracting

$$\begin{vmatrix} M(1 - \frac{X}{L}) & M\frac{X}{L} \\ -\frac{J_o}{L} & \frac{J_o}{L} \end{vmatrix} \begin{vmatrix} \ddot{V}_1 \\ \ddot{V}_2 \end{vmatrix} + \begin{vmatrix} K & K \\ -KX & K(L-X) \end{vmatrix} \begin{vmatrix} V_1 \\ V_2 \end{vmatrix} = \begin{vmatrix} -M\ddot{u}_g \\ 0 \end{vmatrix} \qquad (3.1.3)$$

The same result can be obtained by substituting in eqn. (2.1.1)

$$V_o = V_1 - X\theta$$

$$\theta = \frac{V_1 - V_2}{L}$$

Let K^V be the total translational stiffness. Then

$$K^V = 2K$$

$e = X - \frac{L}{2}$. Hence eqn. (3.1.3) becomes

$$\begin{vmatrix} \frac{1}{2} - \frac{e}{L} & \frac{1}{2} + \frac{e}{L} \\ -\frac{r^2}{L} & \frac{r^2}{L} \end{vmatrix} \begin{vmatrix} \ddot{V}_1 \\ \ddot{V}_2 \end{vmatrix} + \frac{K^V}{2M} \begin{vmatrix} 1 & 1 \\ -\frac{L}{2} - e & \frac{L}{2} - e \end{vmatrix} \begin{vmatrix} V_1 \\ V_2 \end{vmatrix} = \begin{vmatrix} -\ddot{u}_g \\ 0 \end{vmatrix} \qquad (3.1.4)$$

where r is the radius of gyration with respect to the center of mass. In the above equation K^V is generally a function of V_1 and V_2 and can be out of the parentheses for the linear problem and some other general cases. In the general nonlinear problem, the equation of motion can be written:

$$\begin{vmatrix} \frac{1}{2} - \frac{e}{L} & \frac{1}{2} + \frac{e}{L} \\ -\frac{r^2}{L} & \frac{r^2}{L} \end{vmatrix} \begin{vmatrix} \ddot{V}_1 \\ \ddot{V}_2 \end{vmatrix} + \frac{1}{M} \begin{vmatrix} 1 & 1 \\ -\frac{L}{2} - e & \frac{L}{2} - e \end{vmatrix} \begin{vmatrix} f(V_1) \\ f(V_2) \end{vmatrix} = \begin{vmatrix} -\ddot{u}_g \\ 0 \end{vmatrix} \qquad (3.1.5)$$

where $f(V_1)$, $f(V_2)$ are the forces due to the nonlinear stiffnesses.

3.2 Frequency Domain Analysis

A frequency domain analysis is performed herein for the case when $K = K^V/2$ = constant. This analysis can show clearly the trends of the response of each one of the two frames and enables an exploration to be made as a function of the independent parameters.

For an earthquake excitation in the direction of the frames, the equations of motion are:

$$\begin{vmatrix} \frac{1}{2} + \varepsilon & \frac{1}{2} - \varepsilon \\ -\xi & \xi \end{vmatrix} \begin{vmatrix} \ddot{V}_1 \\ \ddot{V}_2 \end{vmatrix} + \frac{K^V}{2M} \begin{vmatrix} 1 & 1 \\ -\frac{1}{2} + \varepsilon & \frac{1}{2} + \varepsilon \end{vmatrix} \begin{vmatrix} V_1 \\ V_2 \end{vmatrix} = \begin{vmatrix} -\ddot{u}_g \\ 0 \end{vmatrix} \qquad (3.2.1)$$

where we have now nondimensionalized r and e by writing $\xi = r^2/L^2$ and $\varepsilon = e/L$. Eqn. (3.2.1) is equivalent to eqn. (3.1.4), except for an unimportant change in sign of the eccentricity.

Now, in attempting to find the steady state solution, let us assume that

$$\ddot{u}_g = \ddot{U}_g e^{i\Omega t}$$

$$V_1 = U_1 e^{i\Omega t}$$

$$V_2 = U_2 e^{i\Omega t}$$

Substituting in eqn. (3.2.1) we obtain

$$\left\{ - \begin{vmatrix} \frac{1}{2} + \varepsilon & \frac{1}{2} - \varepsilon \\ -\xi & \xi \end{vmatrix} \Omega^2 + \frac{K^V}{2M} \begin{vmatrix} 1 & 1 \\ -\frac{1}{2} + \varepsilon & \frac{1}{2} + \varepsilon \end{vmatrix} \right\} \begin{vmatrix} U_1 \\ U_2 \end{vmatrix} = \begin{vmatrix} -\ddot{U}_g \\ 0 \end{vmatrix} \qquad (3.2.2)$$

The equations of motion have the form of a system of two simultaneous equations with two unknowns. Setting $V_1 = U_1 e^{i\Omega t}$ etc. is equivalent to performing a Fourier transform on eqn. (3.2.1) with zero initial conditions. Eqn. (3.2.2) can be written

$$\left\{ - \begin{vmatrix} \varepsilon' & -\varepsilon'' \\ -\xi & \xi \end{vmatrix} \Omega^2 + A \begin{vmatrix} 1 & 1 \\ \varepsilon'' & \varepsilon' \end{vmatrix} \right\} \begin{vmatrix} U_1 \\ U_2 \end{vmatrix} = \begin{vmatrix} -\ddot{U}_g \\ 0 \end{vmatrix} \qquad (3.2.3)$$

where $\varepsilon' = \frac{1}{2} + \varepsilon$ $\qquad A = \frac{K^V}{2M}$

$\varepsilon'' = -\frac{1}{2} + \varepsilon$ $\qquad \xi = \frac{r^2}{L^2}$

Solving the system in eqn. (3.2.3), we obtain:

$$U_1 = -\ddot{U}_g \frac{-\xi\Omega^2 + \varepsilon' A}{(\varepsilon\xi\Omega^4 + \varepsilon' A^2 - \xi A\Omega^2 - \varepsilon'^2 A\Omega^2) - (\xi\varepsilon''\Omega^4 + \xi A\Omega^2 + A\varepsilon''^2 + A\varepsilon''^2)}$$

and a similar expression for U_2. Simplifying, we obtain

$$U_1 = -\ddot{U}_g \frac{-\xi\Omega^2 + \frac{A}{2} + \varepsilon A}{\xi\Omega^4 - A\Omega^2\left(\frac{1}{2} + 2\varepsilon^2 + 2\xi\right) + A^2}$$

$$U_2 = -\ddot{U}_g \frac{\xi\Omega^2 - \frac{A}{2} + \varepsilon A}{\xi\Omega^4 - A\Omega^2\left(\frac{1}{2} + 2\varepsilon^2 + 2\xi\right) + A^2} \qquad (3.2.4)$$

The denominator has two positive roots corresponding to the two resonant frequencies. For earthquake excitation with a power spectral density function of $G(\Omega)$ we can determine the standard deviation of the response of the two frames as

$$\sigma_{u_1}^2 = \int_0^\infty \left| \frac{-\xi\Omega^2 + \frac{A}{2} + \varepsilon A}{\xi\Omega^4 - A\Omega^2\left(\frac{1}{2} + 2\varepsilon^2 - 2\xi\right) + A^2} \right|^2 G(\Omega)\, d\Omega$$

and

$$\sigma_{y_2}^2 = \int_0^\infty \left| \frac{\xi\Omega^2 - \frac{A}{2} + \varepsilon A}{\xi\Omega^4 - A\Omega^2\left(\frac{1}{2} + 2\varepsilon^2 + 2\xi\right) + A^2} \right|^2 G(\Omega)\, d\Omega \qquad (3.2.5)$$

In eqns. (3.2.4) observe that if ε is replaced by $-\varepsilon$, then

$$U_1 = -\ddot{U}_g \frac{-\xi\Omega^2 + \frac{A}{2} - \varepsilon A}{\xi\Omega^4 - A\Omega^2\left(\frac{1}{2} + 2\varepsilon^2 + 2\xi\right) + A^2} = +\ddot{U}_g \frac{\xi\Omega^2 - \frac{A}{2} + \varepsilon A}{\xi\Omega^4 - A\Omega^2\left(\frac{1}{2} + 2\varepsilon^2 + 2\xi\right) + A^2} = -U_2$$

Observing eqns. (3.2.4) we realize that, in absolute value, U_1 is larger than U_2 when

$$\left|-\xi\Omega^2 + \frac{A}{2} + \varepsilon A\right| > \left|\xi\Omega^2 - \frac{A}{2} + \varepsilon A\right|$$

or $$\left(-\xi\Omega^2 + \frac{A}{2} + \varepsilon A\right)^2 - \left(\xi\Omega^2 - \frac{A}{2} + \varepsilon A\right)^2 > 0$$

or $$2\varepsilon A(-2\xi\Omega^2 + A) > 0 \qquad (3.2.6)$$

The above relation holds when

$$\xi < \frac{A}{2\Omega^2} \quad \text{or}$$

$$r^2 < \frac{K^V}{M} \frac{1}{\Omega^2} \left(\frac{L}{2}\right)^2 \tag{3.2.7}$$

Obviously in the symmetric case $\varepsilon = 0$ and, from eqn. (3.2.6), we obtain

$$|U_1| = |U_2| \quad .$$

However, if

$$r^2 > \frac{K^V}{M} \frac{1}{\Omega^2} \left(\frac{L}{2}\right)^2 \tag{3.2.8}$$

which implies that if the diaphragm's radius of gyration is large with respect to the torsional stiffness, then the frame farthest from the center of mass exhibits larger displacements. Since $K^V(\frac{L}{2})^2$ is the torsional stiffness with respect to center of stiffness K_*^θ and Mr^2 is the polar moment of inertia with respect to the center of mass, then, when the forcing frequency is such that

$$\Omega > \sqrt{K_*^\theta / J_o} \quad ,$$

a larger response is observed in the frame farthest from the center of mass.

The above result holds for single frequency excitation. In the case of an earthquake motion, the model will exhibit the "larger-offset" behavior depending on the Fourier Amplitude Spectrum of the specific earthquake. Since the ratio K_*^θ/J_o is known, we can examine how much power lies below that characteristic frequency. If there is sufficient power below this characteristic frequency, then this behavior can and does occur. These considerations are taken up again later.

3.3 Non-dimensionalization of the Equations of Motion

It is of particular advantage to non-dimensionalize the equations of motion of the single-story building model. By doing this the parameters of the problem become apparent and the parameter study will be based on these parameters.

In the case of an earthquake excitation of a single-degree-of-freedom system, the equation of motion can be written

$$m\ddot{u} + c\dot{u} + Ku = - m\ddot{u}_g .$$

We can always define a new variable $z = u/u_y$ so that

$$m\ddot{z} + c\dot{z} + Kz = - \frac{m\ddot{u}_g}{u_y}$$

or

$$\ddot{z} + 2\beta\omega\dot{z} + \omega^2 z = -\omega^2 \frac{m\ddot{u}_g}{Ku_y}$$

or

$$\ddot{z} + 2\beta\omega\dot{z} + \omega^2 z = -\omega^2 \left(\frac{m\ddot{u}_g}{F_y}\right) \quad , \qquad (3.3.1)$$

where F_y is the yielding force; u_y is the yielding displacement.

Hence we see that in the earthquake excitation of a one-degree-of-freedom system the important parameters are the natural frequency ω, the percentage of the critical damping β, and the ratio $m\ddot{u}_g/F_y$, which is called parameter α.

The value of $\ddot{u}_g$ to use in a particular parameter study is not obvious. One possibility is to use the maximum ground acceleration $\ddot{u}_g$. Another is to use the spectral acceleration for the particular natural frequency ω. Sometimes the latter tends to more rational results since the value of the spectral acceleration, even if it is taken out of an elastic response spectrum, includes extra information about the earthquake, which the maximum ground acceleration alone cannot.

In the inelastic case the equation can be written

$$\ddot{z} + 2\beta\omega\dot{z} + \omega^2 f(z) = -\omega^2\left(\frac{m\ddot{u}_g}{f_y}\right) \qquad (3.3.2)$$

where now for the elastoplastic case:

$$f(z) = z \qquad \text{for } z \leq 1$$

$$f(z) = 1 \qquad \text{for } z \geq 1 \ .$$

Usually the above equation is solved using numerical methods (4).

For our model the equations of motion are (3, 2, 1).

$$\begin{vmatrix} \frac{1}{2} + \frac{e}{L} & \frac{1}{2} - \frac{e}{L} \\ -\frac{r^2}{L^2} & \frac{r^2}{L^2} \end{vmatrix} \begin{vmatrix} \ddot{V}_1 \\ \ddot{V}_2 \end{vmatrix} + \frac{K^V}{2M} \begin{vmatrix} 1 & 1 \\ -\frac{1}{2} - \frac{e}{L} & \frac{1}{2} + \frac{e}{L} \end{vmatrix} \begin{vmatrix} V_1 \\ V_2 \end{vmatrix} = \begin{vmatrix} -\ddot{u}_g \\ 0 \end{vmatrix}$$

Let $V_1 = u_y z_1$, $V_2 = u_y z_2$; then

$$\begin{vmatrix} \frac{1}{2} - \frac{e}{L} & \frac{1}{2} - \frac{e}{L} \\ -\frac{r^2}{L^2} & \frac{r^2}{L^2} \end{vmatrix} \begin{vmatrix} \ddot{z}_1 \\ \ddot{z}_2 \end{vmatrix} + \frac{K^V}{2M} \begin{vmatrix} 1 & 1 \\ -\frac{1}{2} + \frac{e}{L} & \frac{1}{2} + \frac{e}{L} \end{vmatrix} \begin{vmatrix} f(z_1) \\ f(z_2) \end{vmatrix} = \begin{vmatrix} -\frac{K^V}{M}\left(\frac{M\ddot{u}_g}{F_y}\right) \\ 0 \end{vmatrix} \qquad (3.3.3)$$

where $f(z_1)$, $f(z_2)$ are nonlinear functions of displacements z_1, z_2 .

Hence we see that the parameters for our model are:

(1) the eccentricity e/L

(2) the translational "frequency" $\sqrt{K^V/M}$

(3) the ratio $M\ddot{u}_g/f_y$ or α (alpha)

(4) the radius of gyration r

(5) the distance between the frames L.

Observing that the torsional stiffness for the symmetric case is

$$K^{\theta} = K^{V} \left(\frac{L}{2}\right)^2$$

and

$$J_o = Mr^2 \quad ,$$

then

$$\frac{K^{\theta} / J_o}{K^{V}/M} = \frac{K^{V}(L/2)^2 \frac{1}{Mr^2}}{\frac{K^{V}}{M}} = \left(\frac{L}{2r}\right)^2 \quad ,$$

which indicates that L/2r is a parameter depending on the "frequency" ratio. Since our purpose is to compare the response of the torsionally unbalanced building model to the torsionally balanced one, we consider as a parameter the translational "frequency" of the building model, and we vary the ratio of the rotational to translational "frequency."

Thus the parameters in the study of the inelastic response of the building model include:

(i) the eccentricity ratio

(ii) the translational "frequency,"

(iii) the "frequency" ratio

(iv) the ratio $m\ddot{u}_g/F_y$

Instead of the peak ground acceleration $\ddot{u}_{g_{max}}$ in term (iv), the spectral acceleration for the specific translational frequency has been used.

Damping in eqns. (3.3.3) will be introduced by Kuzak's method. This method guarantees specified modal damping in each mode. A value of 5% critical modal damping has been used, since this is a typical value for buildings.

CHAPTER 4 - STUDIES ON THE BUILDING MODEL

4.1 Program Used for Analysis

Computer program STAVROS was amended in order to be able to perform parametric studies. The program is written in Fortran IV and uses 520K of primary memory on an IBM 370/155 computer. No secondary storage is required. The program is designed for buildings having a maximum of 30 stories, 30 different structural elements (in plan) and 3000 points of ground acceleration in each direction.

Each floor can have a maximum of three degrees of freedom: x-translation, y-translation and rotation. In each floor the total stiffness of the various structural elements is calculated and becomes the equivalent stiffness of the floor. This formulation is not accurate for tall buildings which exhibit large bending deformations, but for up to 30 stories the "shear beam" is considered sufficiently accurate. After the stiffnesses are calculated a standard IBM eigenvalue routine extracts the eigenvalues and eigenmodes of the elastic system. Having already computed the dynamic properties of the building in the elastic range, we proceed with the time-history analysis.

If we are to include viscous damping, which is described by a damping matrix, C, then these equations take the form

$$\ddot{Mu} + \dot{Cu} + Ku = -\begin{bmatrix} M_x \ddot{u}_g \\ M_y \ddot{v}_g \end{bmatrix} = R \quad ,$$

where $\ddot{u}_g$, $\ddot{v}_g$ are ground accelerations in x and y directions respectively.

These are the differential equations of motion in matrix form, for a multi-D.O.F. system, excited by a ground acceleration in the x and y direc-

tions. However, in the inelastic case, K is not constant, and it is more appropriate to write:

$$M\ddot{u} + C\dot{u} + f(u) = R \quad , \tag{4.1.1}$$

where f(u) is a vector of forces and a function of the displacement vector u.

The damping is introduced by Kuzak's method, which produces a C matrix that gives any desired percentage of critical damping in any mode. This matrix is given as the product

$$C = M\Phi B\Phi^T M \quad ,$$

where M = mass matrix

B = diagonal matrix with elements $2\beta_i\omega_i$

β_i = percentage of critical damping in the i^{th} mode

ω_i = circular frequency of the i^{th} mode

Φ = matrix whose columns are the eigenvectors of the system (normalized with respect to M).

Equation (4.1.1) is solved numerically using a step-by-step integration procedure. The procedure is called the "constant velocity method" and assumes that velocities are constant within the time step. Under this assumption the recurrence formulas for velocities and accelerations are:

$$\dot{u}_n = \frac{1}{2\Delta t}(u_{n+1} - u_{n-1})$$

$$\ddot{u}_n = \frac{1}{\Delta t^2}(u_{n+1} - 2u_n + u_{n-1}) \quad .$$

Replacing these two expressions in eqn. (4.1.1) we obtain

$$u_{n+1} = \left[\frac{1}{\Delta t^2} M + \frac{1}{2\Delta t} C\right]^{-1}\left[R_n - F_n + \frac{2}{\Delta t^2} Mu_n - \left(\frac{1}{\Delta t^2} M - \frac{1}{2\Delta t} C\right)u_{n-1}\right]. \tag{4.1.2}$$

The above equation can be used for the calculation of the displacement vector at time step n+1 in terms of the displacement vectors at steps n and n-1 and the force vector F at n.

Step-by-step integration methods are very sensitive to the selected time interval Δt. Instability of the system solution may occur for Δt larger than a certain value. However, a $\Delta t = 0.02$ is adequate for the stability of the system (3), and this number has been used in the parametric study. In equation (4.1.2) the first parenthesis on the right-hand side remains unchanged throughout the step-by-step integration. The R_n depends on the acceleration time history of the particular earthquake and F_n on the inelastic model used. In the parametric study of the building model the bilinear model has been used. The first slope of the bilinear model OA accounts for the primary stiffness and the AB accounts for the secondary stiffness, which is the stiffness in the inelastic range and is 3% of the primary stiffness (Figure A.2.1).

For the bilinear stiffness the subroutine "BILIN" was used. Having the displacements at n and n-1 known, as well as the force vector at n, one can calculate the displacements u at n+1. Then using subroutine BILIN we specify F at n+1. An analysis of subroutine BILIN is given in Appendix II.

After the step-by step integration is completed, the maximum displacement is stored and the maximum ductility of each structural element calculated.

The STAVROS program was amended in order to adjust to the parametric study requirements. The new version of the program is able to handle 216 cases at the same time. IBM software routines have been modified and duplicate the 370 system environment. The program plots in a desired way the results of the parametric study.

4.2 Parameters in the Nonlinear Analysis of the Inelastic Single-story Building Model.

As mentioned in Section 3.1, the single-story building model consists of two identical one-bay frames parallel to each other and supporting a diaphragm of mass M. The frames are spaced at a distance L from each other, are considered massless, and exhibit elastoplastic behavior. The diaphragm has a radius gyration r. As was found before, the ratio L over r is a measure of the rotational to translational "frequency" ratio, equal to the parameter μ in Dempsey and Irvine's paper, namely:

$$\frac{K^{\theta}/J_o}{K^{V}/M} = \left(\frac{L}{2r}\right)^2 ,$$

since K^{θ} is equal to $K^{V}L^2/2$ for the symmetric elastic case.

By changing the position of the center of mass of the diaphragm with respect to the center of stiffness, we alter the eccentricity of the single-story building model..

By increasing the peak acceleration, we change the value of the ratio MS_a/F_y. Even if the mass of the diaphragm M and the yield strength F of the structural elements remains constant, S_a is affected not only by peak acceleration, but also by the shape of the time history of the input earthquake accelerations. Of course, additionally, the translational frequency affects results. As was mentioned earlier, by inspecting equation (3.3.3), we realize that both the translational and rotational periods are essential in the analysis. However, since our purpose is to compare non-symmetric with symmetric response, the translational period is fixed and the ratio of torsional to translational "period" is varied.

It is possible to tabulate the constructions among the parameters, starting with the higher ranking ones and moving downwards to the lower ranking ones.

Parameter 1.	Earthquake
	↓
Parameter 2.	Translational period
	↓
Parameter 3.	Ratio L/2r or parameter M' on the plots
	↓
Parameter 4	Eccentricity e
	↓
Parameter 5	Ratio MS_a/F_y ↔ Ductility or parameter α

The hierarchy of the above scheme can be illustrated as follows. A parameter is called higher ranking if its parameter number is less than some other parameter. A higher ranking parameter will not vary until all the possible combinations of lower ranking parameters are performed. For example, the value of eccentricity will be constant until all the different values of the ratio MS_a/F_y have been used in the calculations. Similarly, for one translational period all the different frequency ratios, eccentricities and ratios MS_a/F_y should have been used already.

Values of Parameters

As far as was possible, realistic values of the different parameters have been chosen for the parametric study.

For Parameter 1, four different earthquake motions have been used:

EL CENTRO	N-S	1940
PACOIMA DAM	S16E	1971
KERN COUNTY TAFT	N21E	1952
ARTIFICIAL MOTION		

The last is a motion generated artificially to meet the requirements of a prescribed response spectrum. An artificial motion portrays less variation than a real earthquake motion.

Considering Parameter 2, we allowed four different values of translational periods:

$$T_1 = 0.5 \text{ sec.}$$
$$T_2 = 1.0 \text{ sec.}$$
$$T_3 = 1.5 \text{ sec.}$$
$$T_4 = 2.0 \text{ sec.}$$

The translational period affects also the value of Parameter 5 (ratio MS_a/F_y) since the value of the response spectrum is taken for the above specified periods.

As far as Parameter 3 is concerned, which is the ratio $K^{\theta}/J_o \div K^{V}/M$, or $L/2r$, we considered six values, with a minimum of 0.5 and a maximum of 1.75, namely:

0.5 0.75 1.0 1.25 1.5 1.75 .

Values outside the above range seem unrealistic for commonly encountered buildings. A common value of this ratio for framed buildings is close to unity.

Parameter 4 is the eccentricity ratio which is the ratio of the distance between the center of mass and center of stiffness to the distance L between the frames of the building model. Values of eccentricity ratio greater than 0.25 are unusual for buildings. By the same token, an eccentricity ratio of zero would mean that the building model is symmetric: an unobtainable situation in practice. Six different values of eccentricity have been used, and these are

$$e_1 = 0.00 \qquad e_3 = 0.10 \qquad e_5 = 0.20$$
$$e_2 = 0.05 \qquad e_4 = 0.15 \qquad e_6 = 0.25$$

Finally, for the last Parameter 6, which is the ratio of mass times the spectral acceleration to the yield strength of the structural elements, six values of the last parameter are used:

$$\frac{MS_a}{F_y} = 2,\ 4,\ 6,\ 8,\ 10,\ 12 \quad .$$

The way the parametric study was undertaken is as follows. First the two frames were proportioned and the diaphragm mass was adjusted in order to yield a period of 0.5 seconds. Then, for subsequent values of translational periods, the mass was increased in order to account for the new periods. Simultaneously the peak acceleration was adjusted—or, equivalently, the earthquake was scaled—in order to retain the values 2, 4, 6, 8, 10, and 12 in the parametric study.

The ratio L/2r was adjusted by varying the radius of gyration r or equivalently the moment of inertia J_o.

The eccentricity e was changed by keeping the coordinates of the center of stiffness constant and varying the coordinates of the center of mass.

The ratio MS_a/F_y was adjusted by varying the mass M, yield strength F_y and spectral acceleration for reference earthquake magnitude and scaling the peak acceleration. Scaling the peak acceleration may not be valid or appropriate (9), but this scheme has been used for convenience and is accurate enough for the purpose of this parameter study.

4.3 Parametric Studies on the Nonlinear Response of the Single-Story Building Model.

In the following pages the results of the parametric studies are displayed. Each graph represents 36 cases, since it is the combination of six values of eccentricity with the six values of the parameter α for a certain value of L/2r. The abscissa represents values of the parameter α and the ordinate values of the ductility μ of the frame closest to the center of mass. Whenever the ductility of the frame farthest from the center of mass is recorded in the ordinate, this will be emphasized.

The motions are

El Centro	1940	N-S
Pacoima Dam	1971	S16E
Kern County - Taft	1952	N21E
Artificial Motion		

and the results will be displayed in this order. For each motion the results will start being displayed for a period of 0.5 sec. and for the closest frame to the center of mass. Then for a period of 0.5 sec. (the same) the ductility of the other frame will be displayed. Subsequently the ductility demands of the closest frame will be displayed for periods of 1.0 sec., 1.5 sec., and 2.0 sec. This scheme is repeated for the other three motions.

The above results are displayed, starting from the next page, and their order can be schematized as follows:

	Period	Frame	Plots
El Centro Earthquake	0.5	Closest	
		Farthest	
	1.0	Closest	1-30
	1.5	Closest	
	2.0	Closest	
Pacoima Dam	0.5	Closest	
	1.0	Closest	31-54
	1.5	Closest	
	2.0	Closest	
Kern County	0.5	Closest	
	1.0	Closest	55-78
	1.5	Closest	
	2.0	Closest	
Artificial Motion	0.5	Closest	
		Farthest	
	1.0	Closest	79-108
	1.5	Closest	
	2.0	Closest	

EL CENTRO N-S 1940

PLOTS 1 - 30

EL-CENTRO N-S 1940

PERIOD= 0.5 SEC M'= 0.50

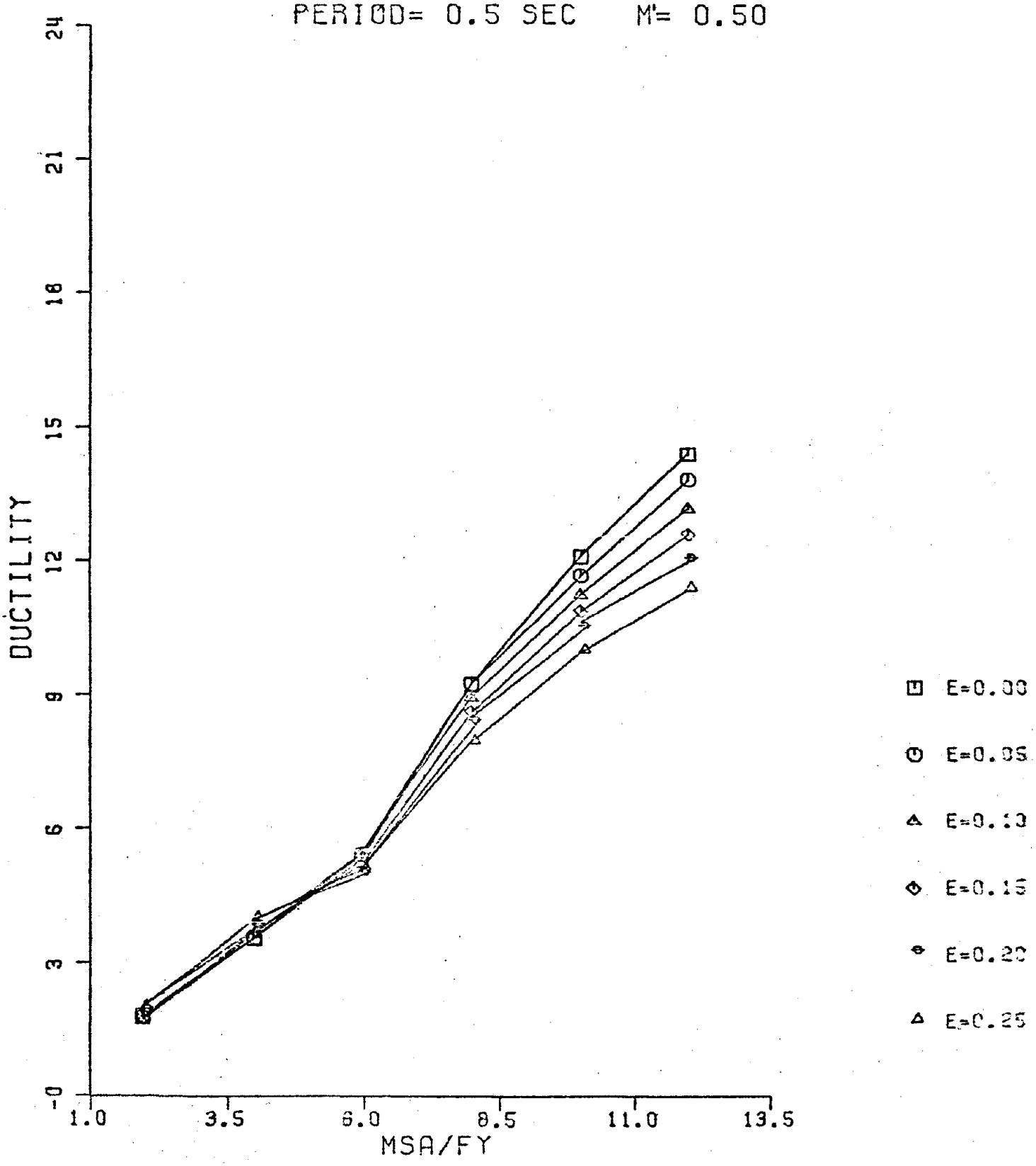

PLOT #1

EL-CENTRO N-S 1940

PERIOD= 0.5 SEC M'= 0.75

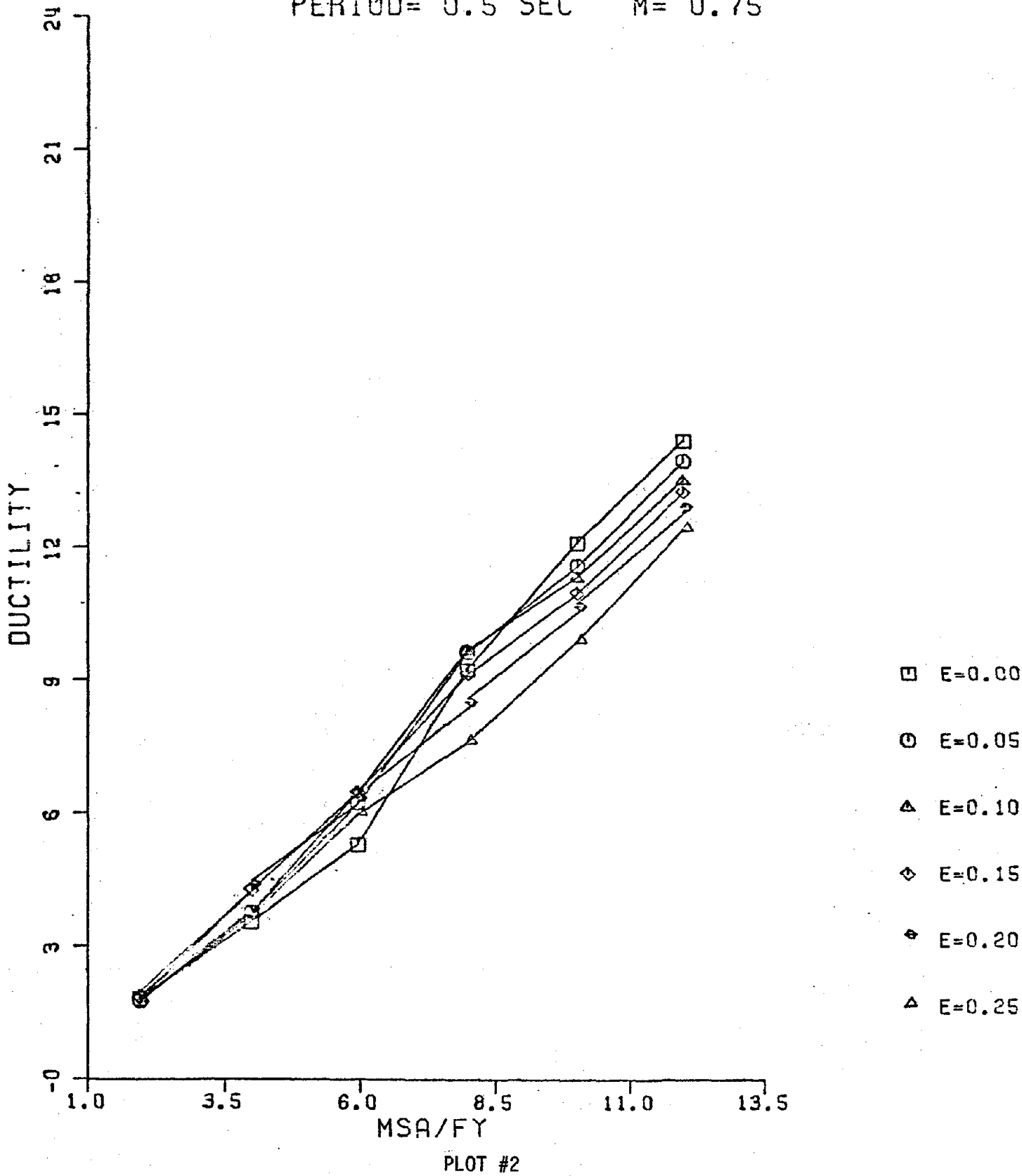

PLOT #2

EL-CENTRO N-S 1940

PERIOD= 0.5 SEC M= 1.00

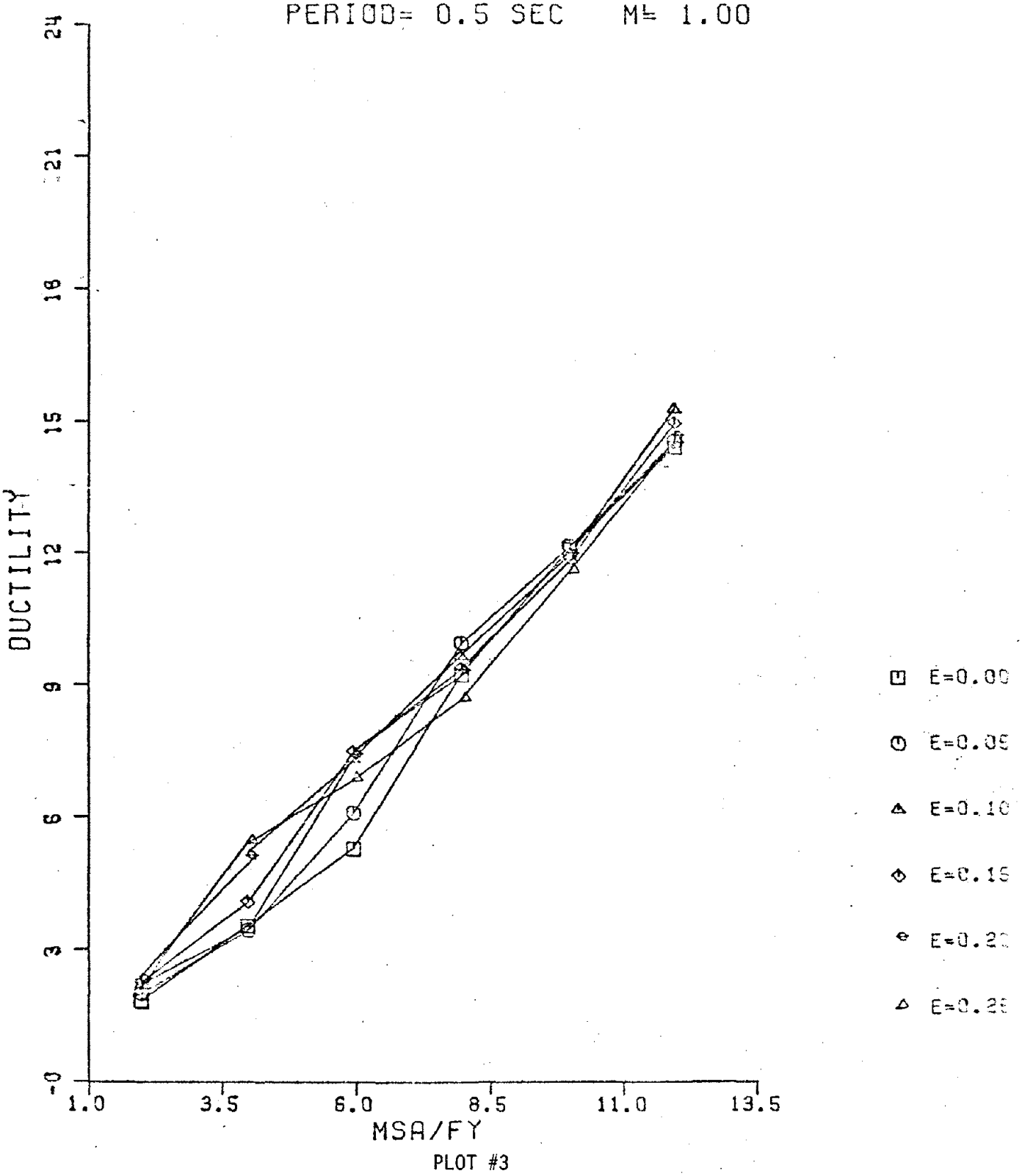

PLOT #3

EL-CENTRO N-S 1940

PERIOD= 0.5 SEC M'= 1.25

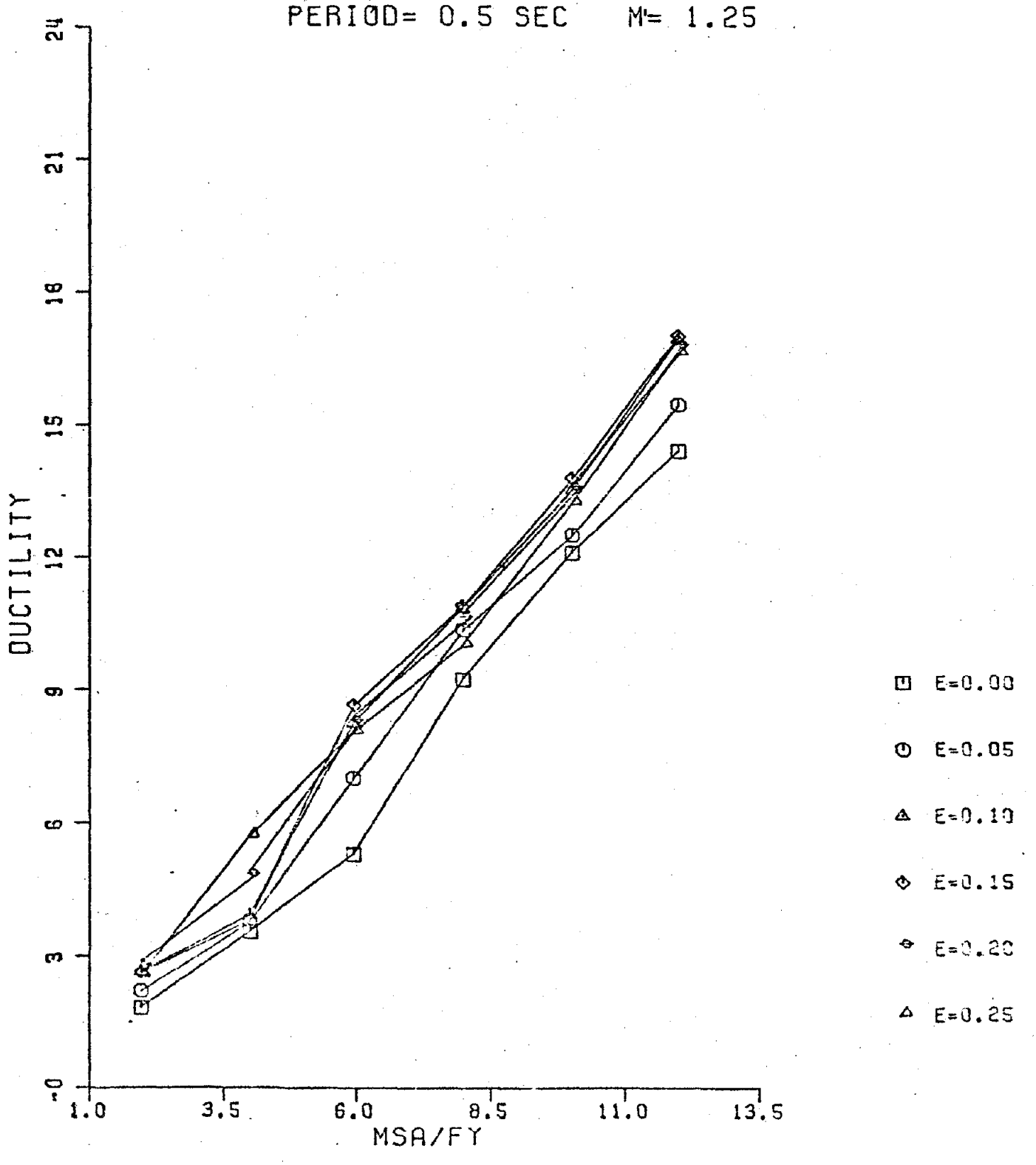

PLOT #4

EL-CENTRO N-S 1940

PERIOD= 0.5 SEC M= 1.50

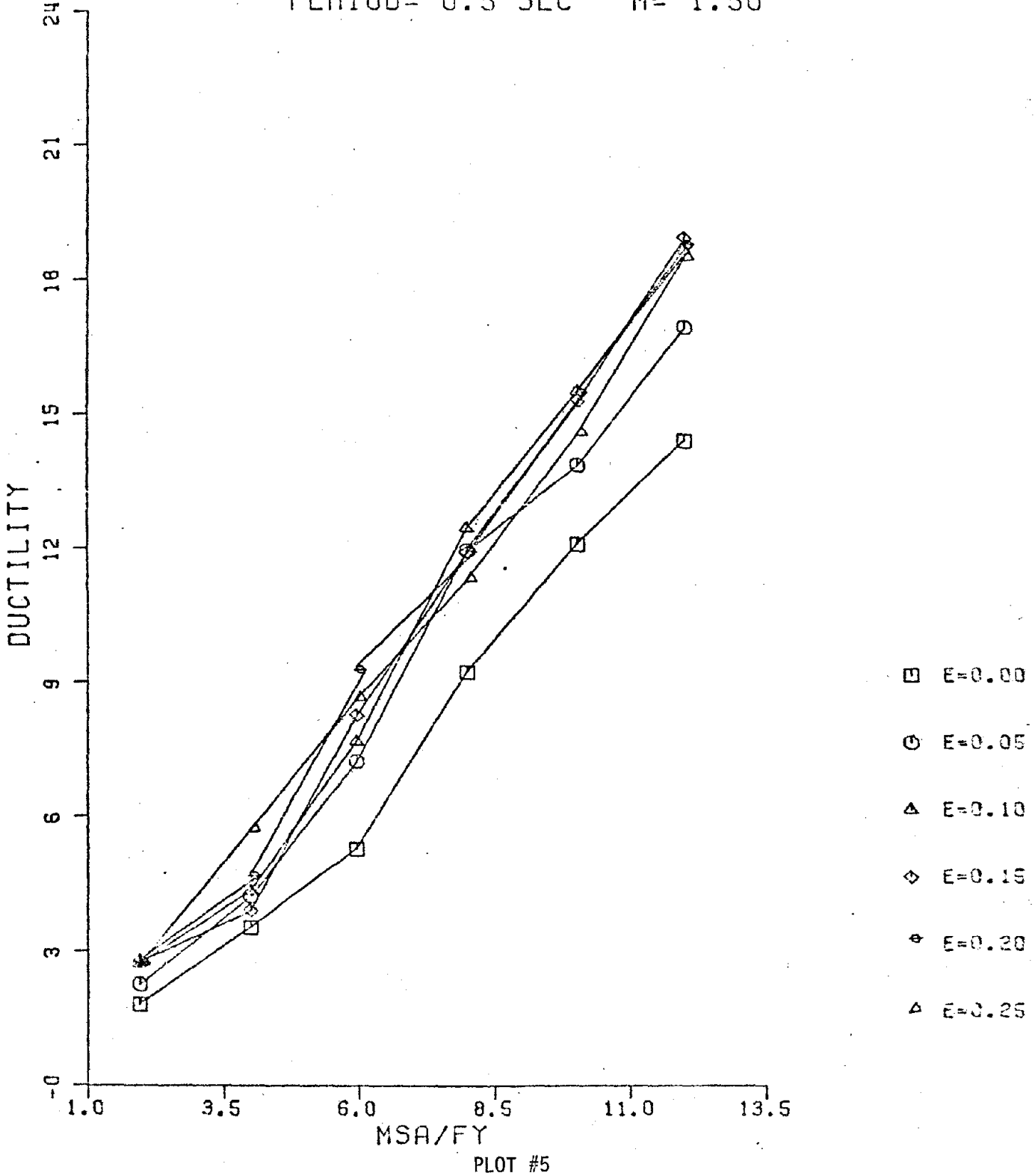

PLOT #5

EL-CENTRO N-S 1940

PERIOD= 0.5 SEC M= 1.75

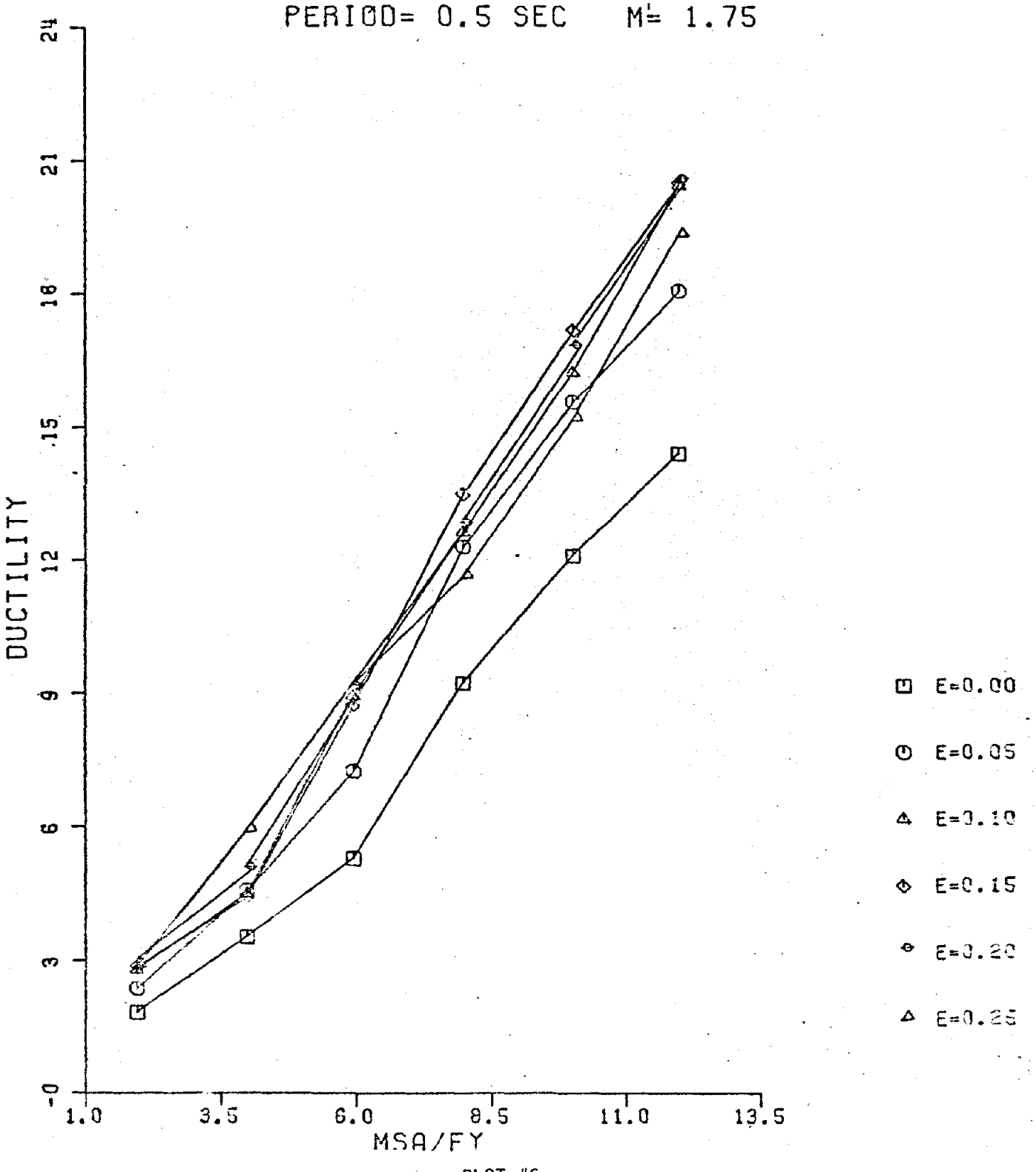

PLOT #6

EL-CENTRØ N-S 1940

PERIØD= 0.5 SEC M'= 0.50

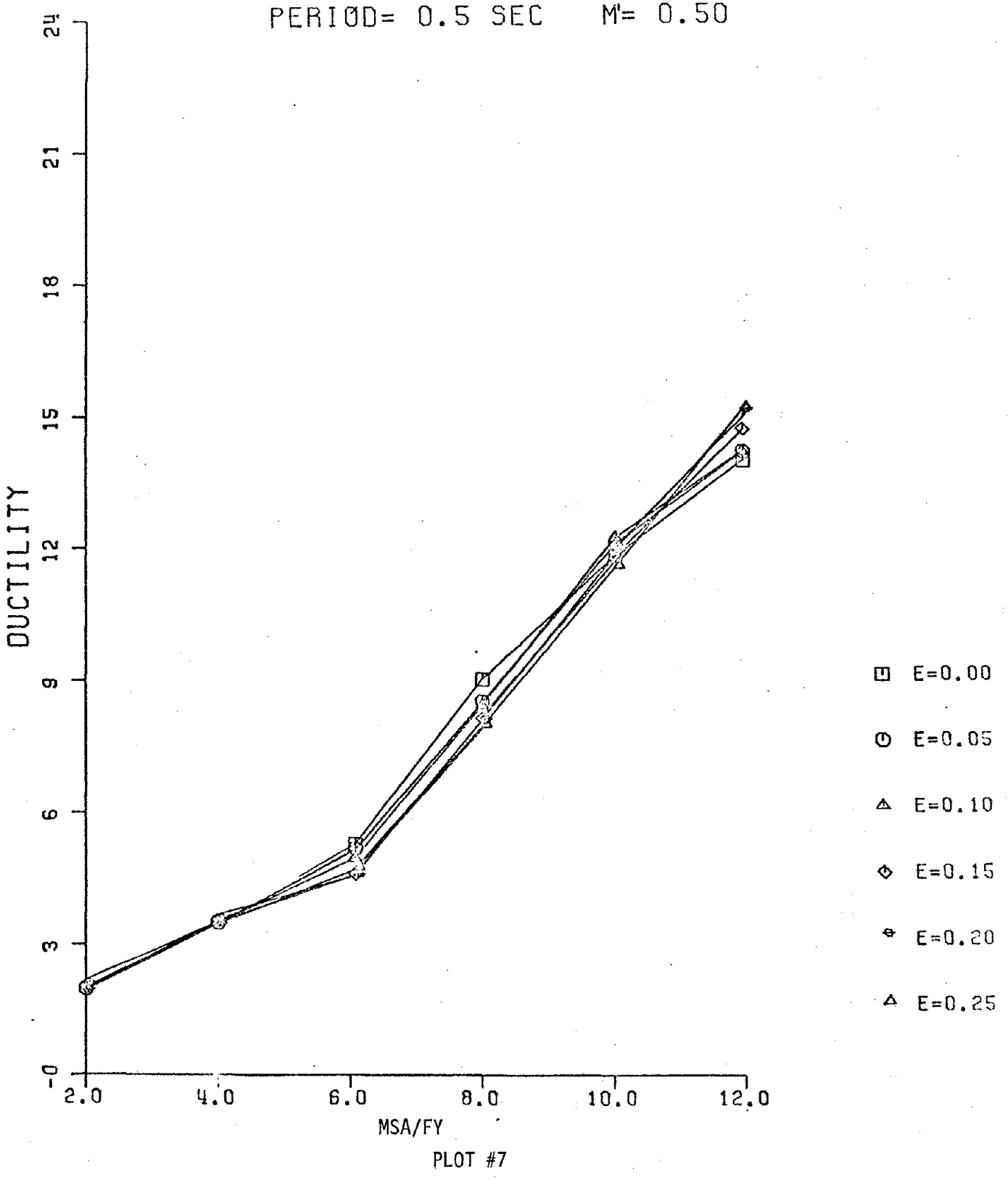

PLOT #7

EL-CENTRO N-S 1940

PERIOD= 0.5 SEC M= 0.75

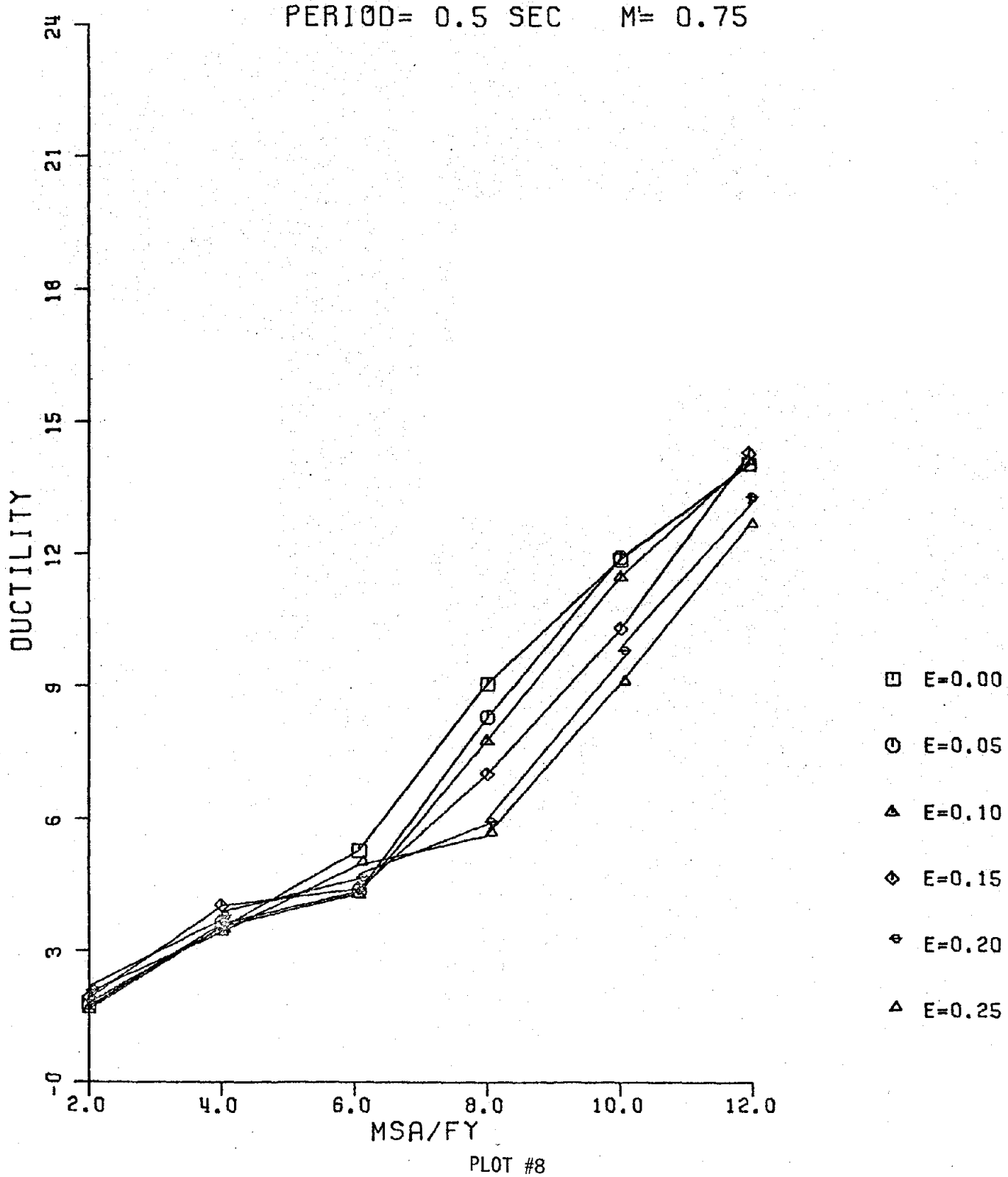

PLOT #8

EL-CENTRØ N-S 1940

PERIØD= 0.5 SEC M'= 1.00

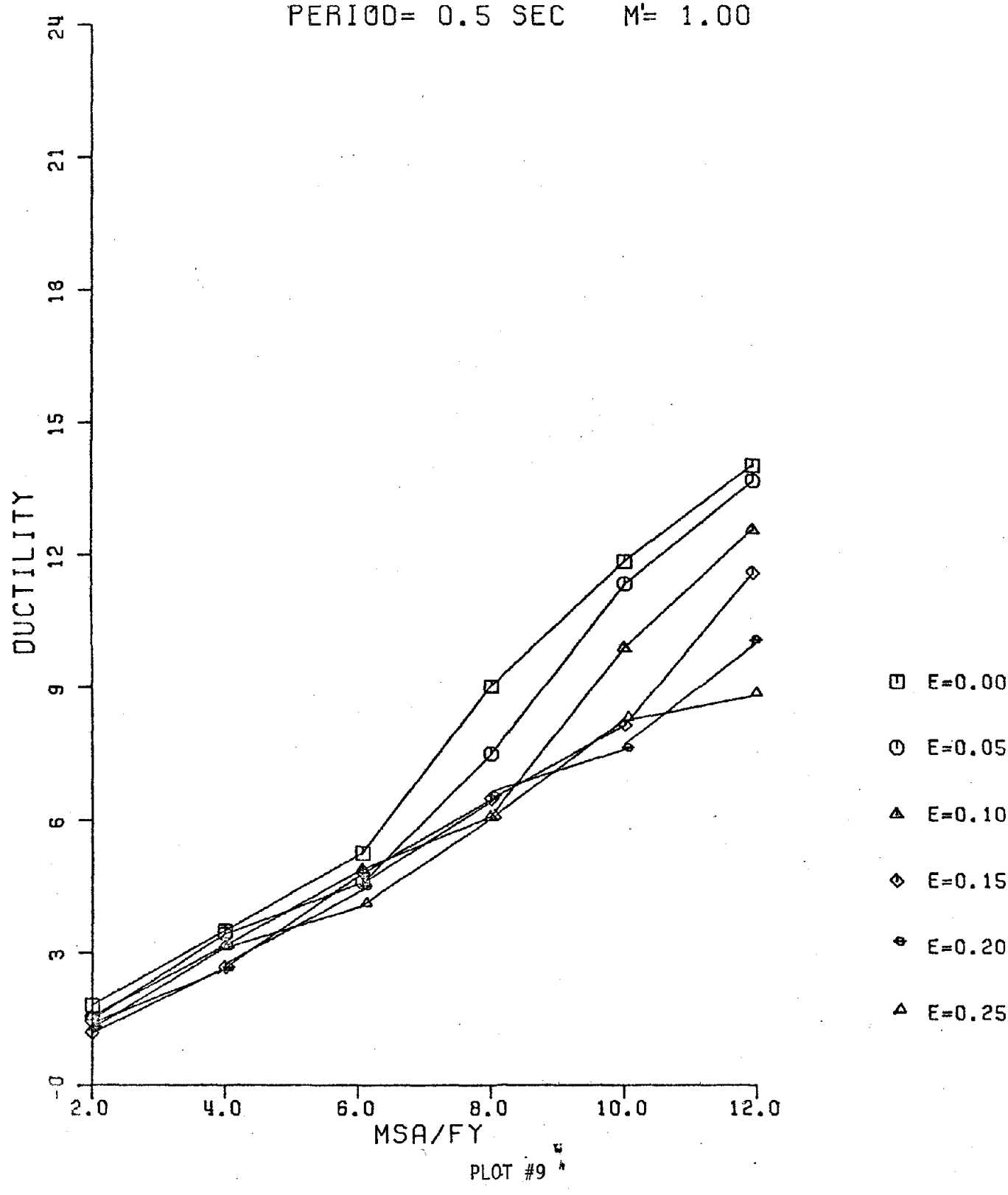

PLOT #9

EL-CENTRO N-S 1940

PERIOD= 0.5 SEC M'= 1.25

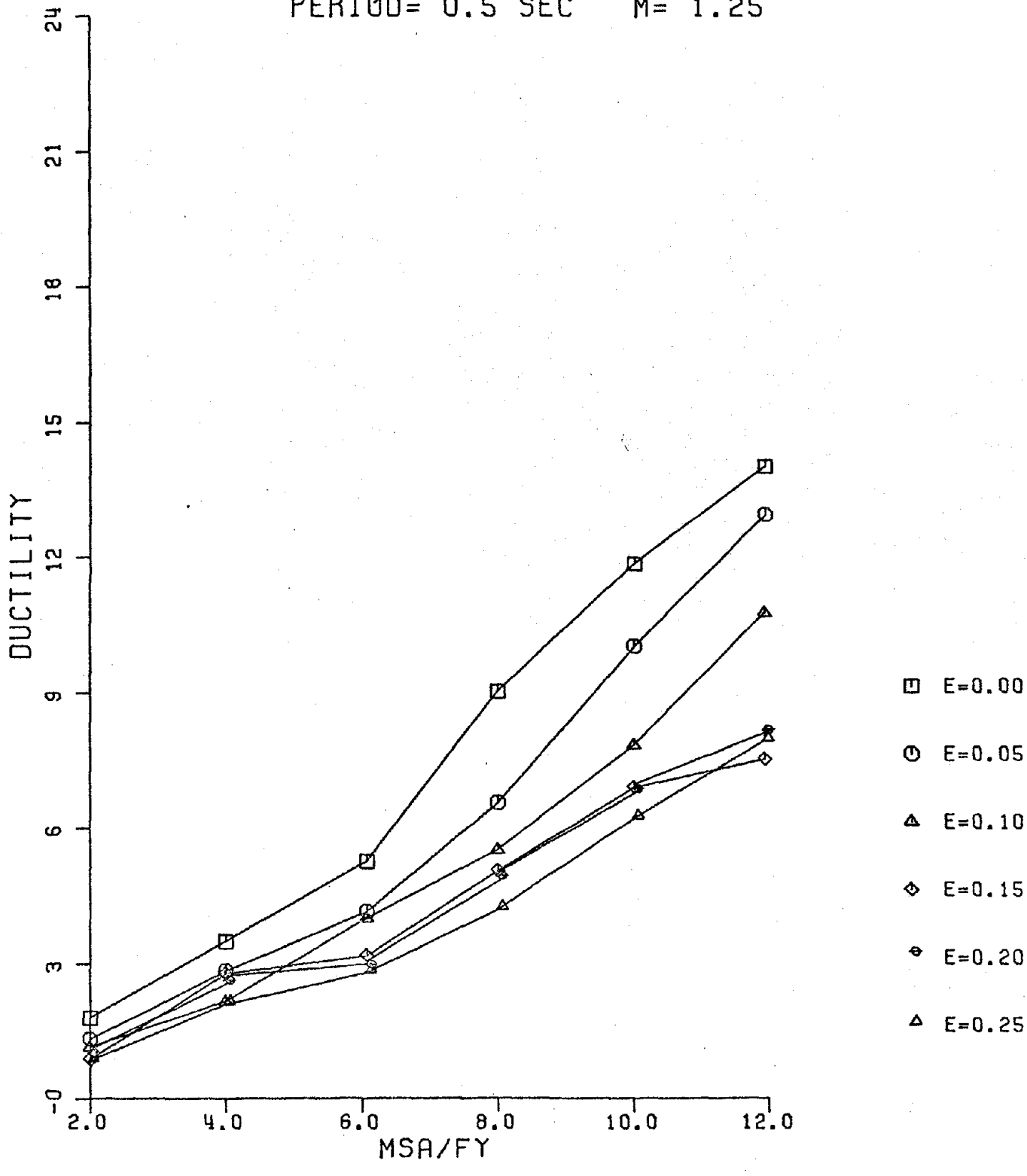

PLOT #10

EL-CENTRØ N-S 1940

PERIØD= 0.5 SEC M'= 1.50

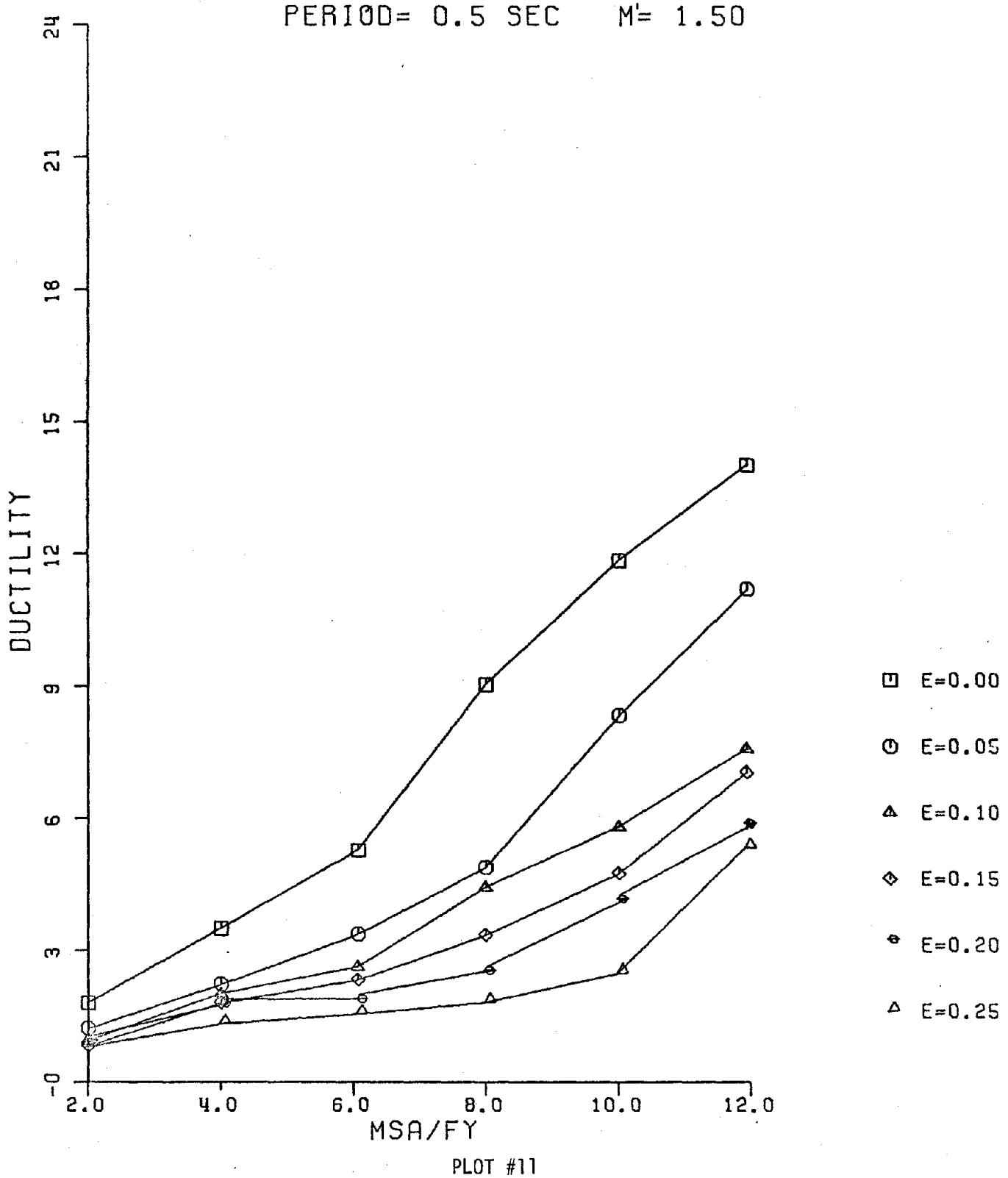

PLOT #11

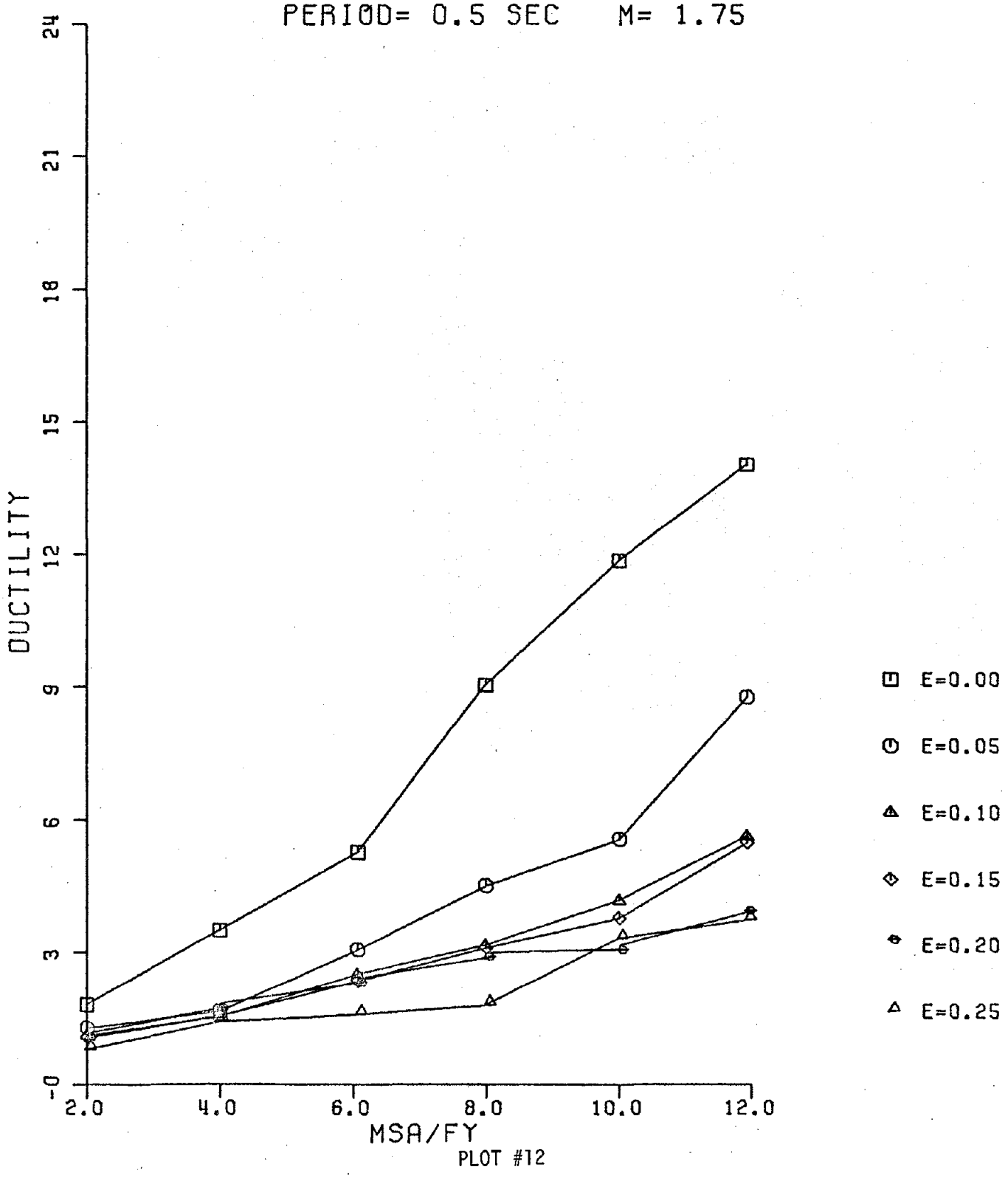
EL-CENTRØ N-S 1940
PERIØD= 0.5 SEC M= 1.75
DUCTILITY
-0
3
6
9
12
15
18
21
24
2.0
4.0
6.0
8.0
10.0
12.0
MSA/FY
PLOT #12
E=0.00
E=0.05
E=0.10
E=0.15
E=0.20
E=0.25

EL-CENTRO N-S 1940

PERIOD= 1.0 SEC M'= 0.50

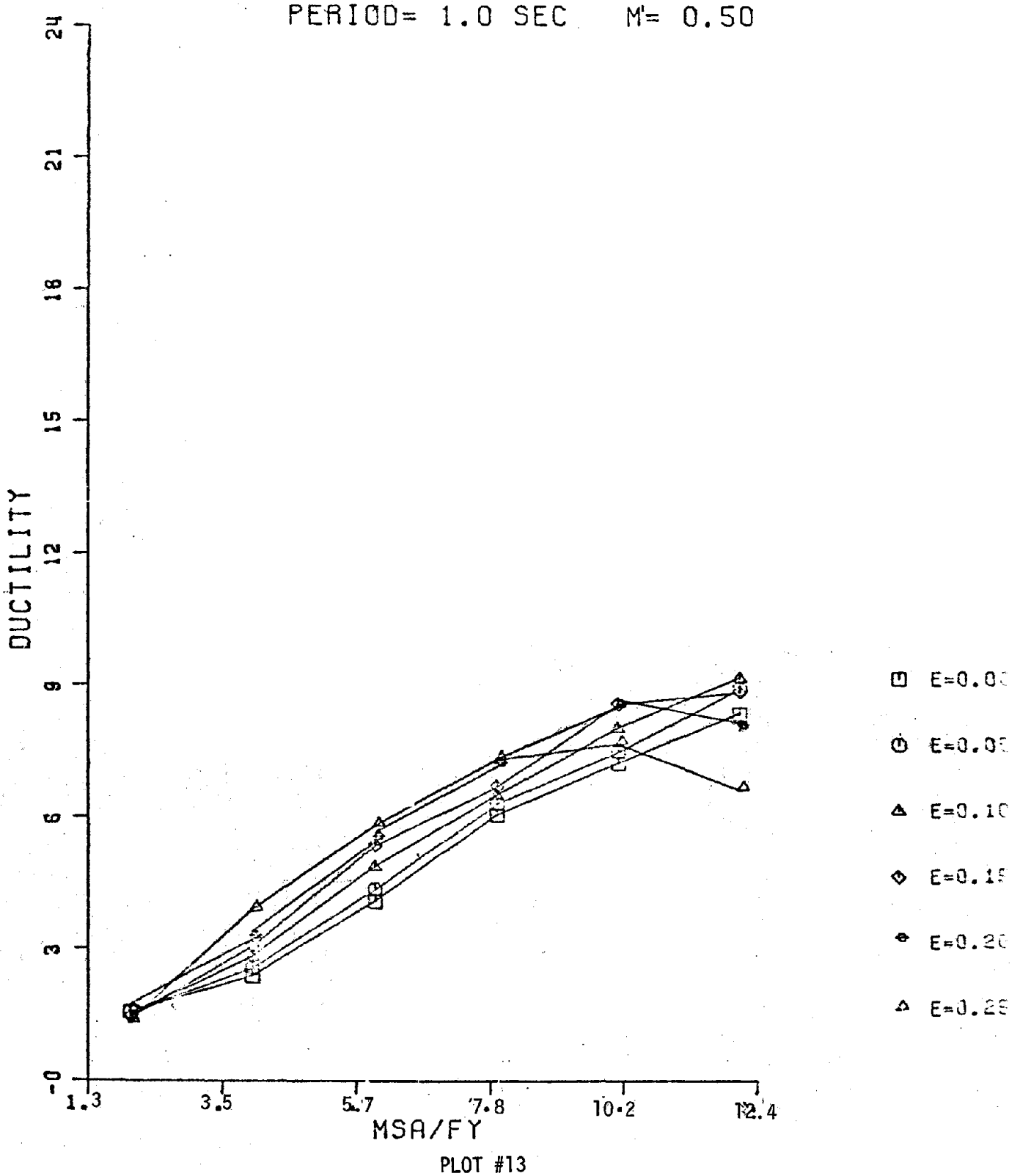

PLOT #13

EL-CENTRO N-S 1940

PERIOD= 1.0 SEC M= 0.75

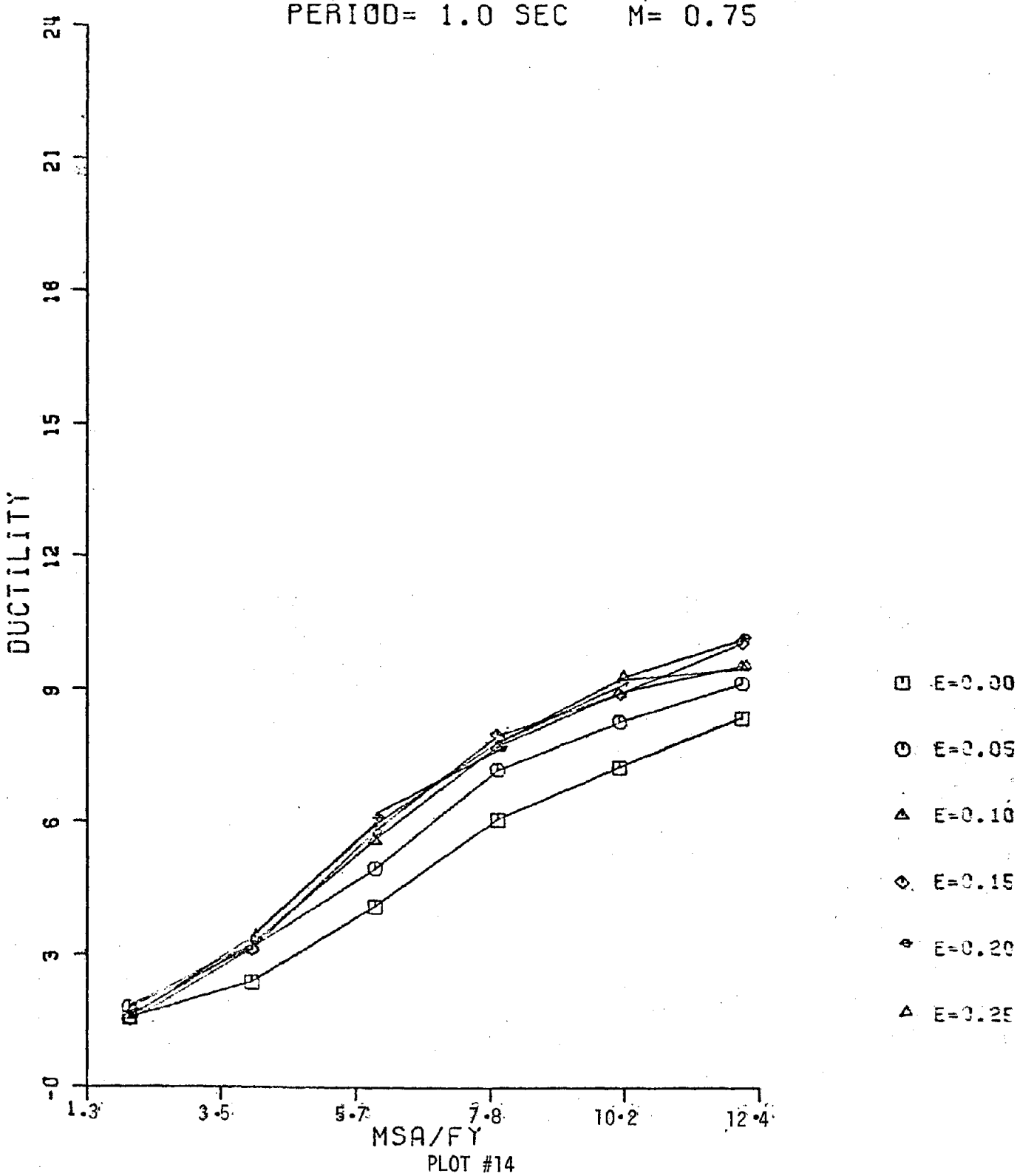

PLOT #14

EL-CENTRO N-S 1940

PERIOD= 1.0 SEC M'= 1.00

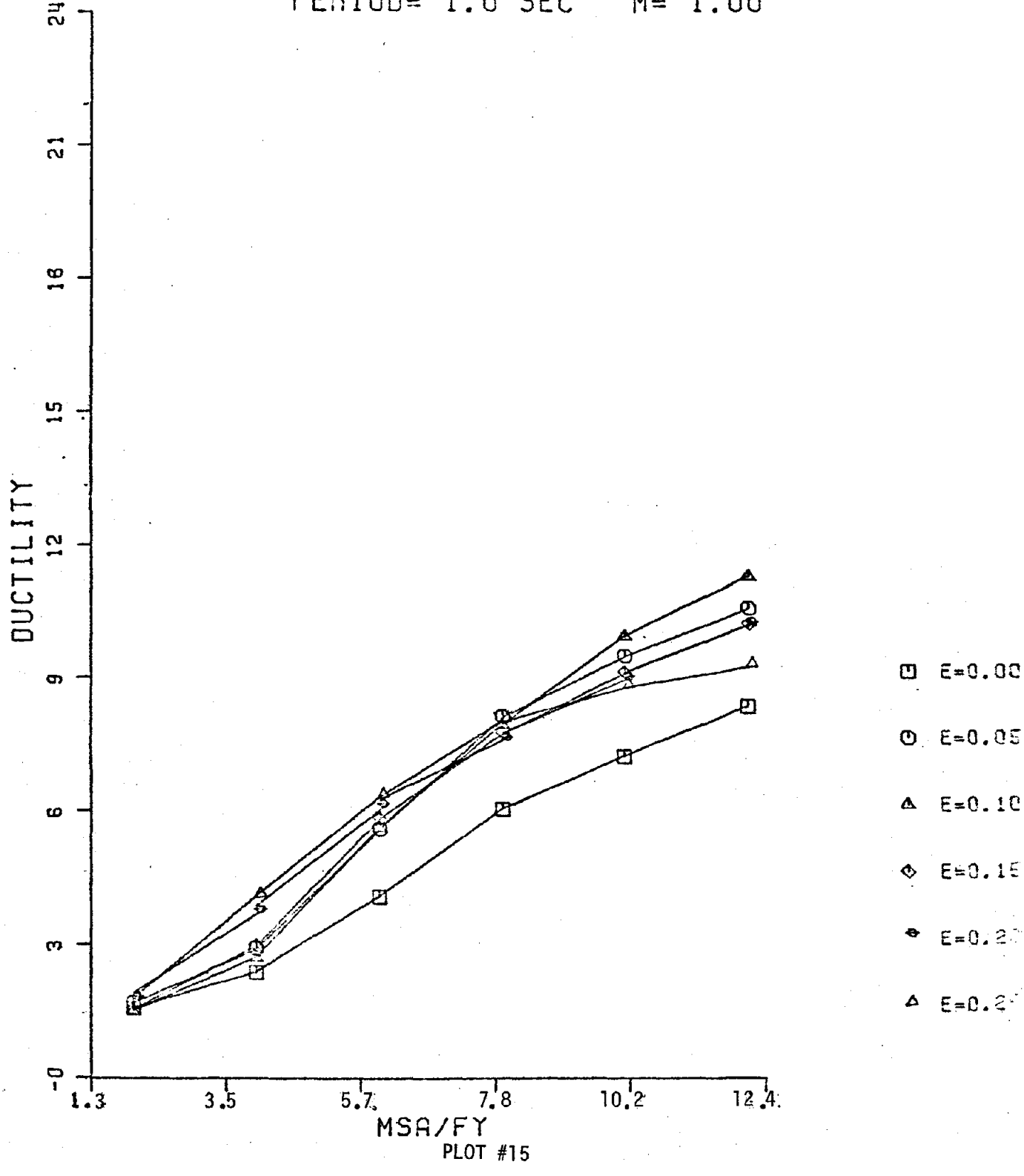

PLOT #15

EL-CENTRO N-S 1940

PERIOD= 1.0 SEC M'= 1.25

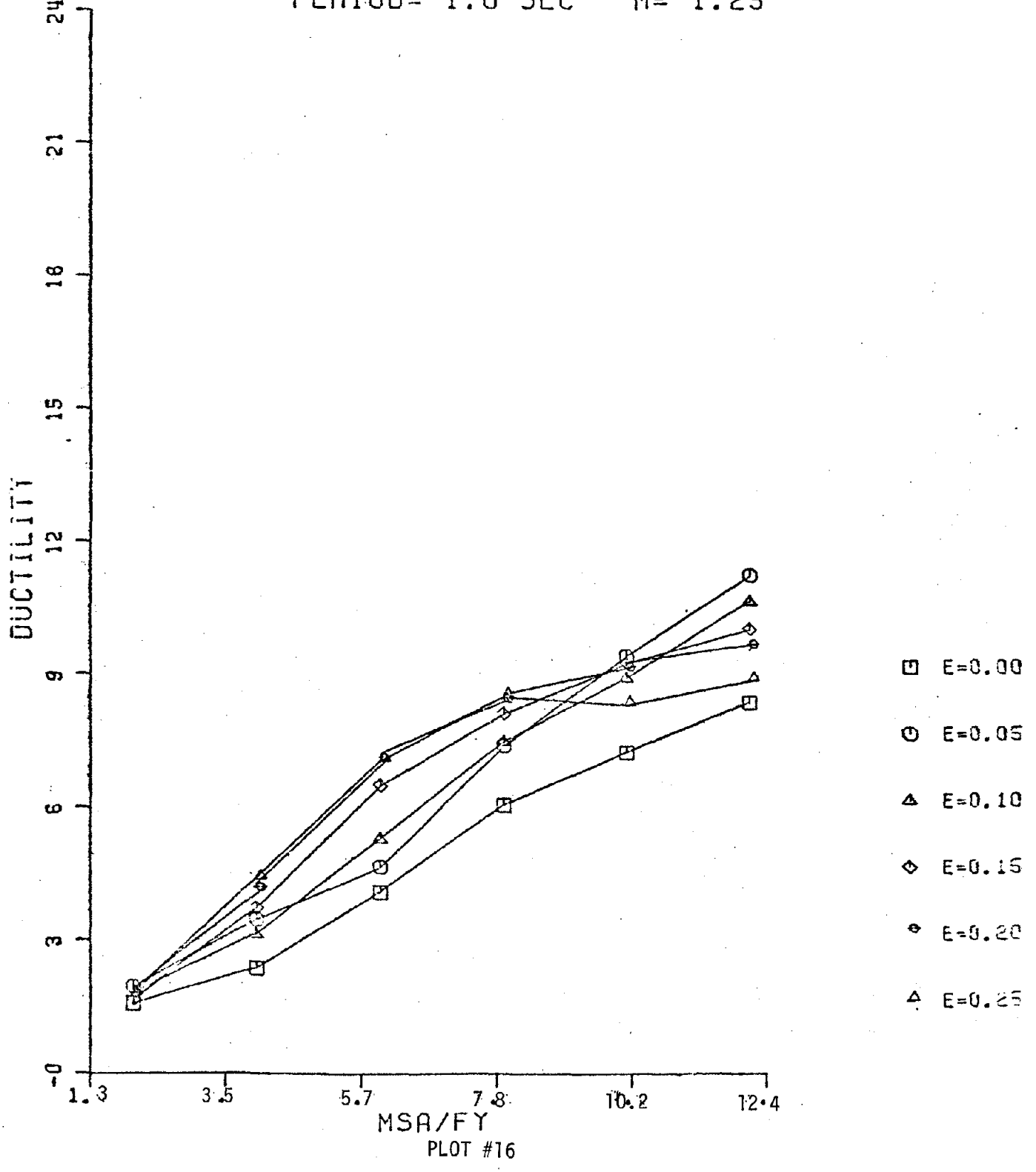

PLOT #16

EL-CENTRO N-S 1940

PERIOD= 1.0 SEC M= 1.50

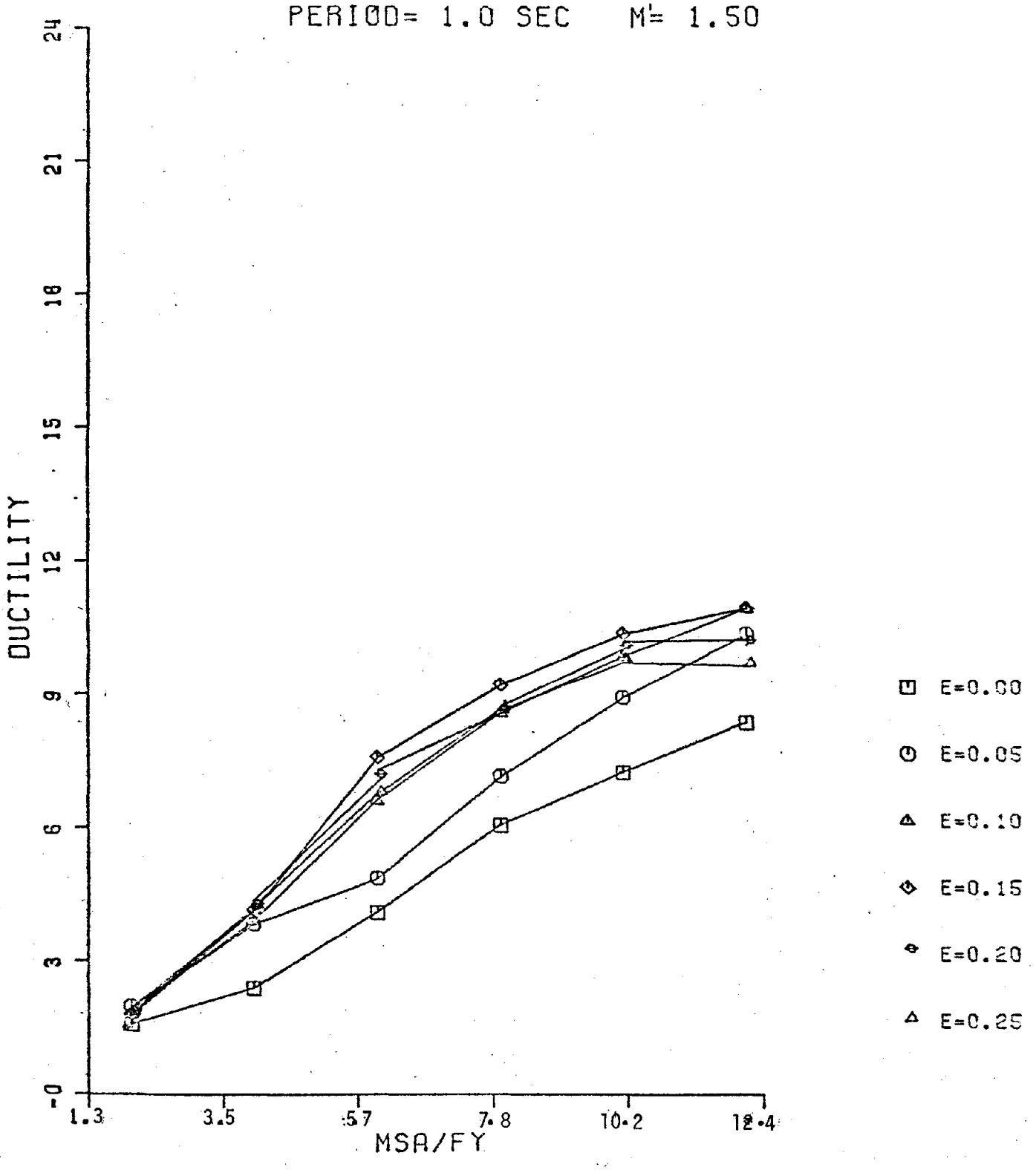

PLOT #17

EL-CENTRO N-S 1940

PERIOD= 1.0 SEC M'= 1.75

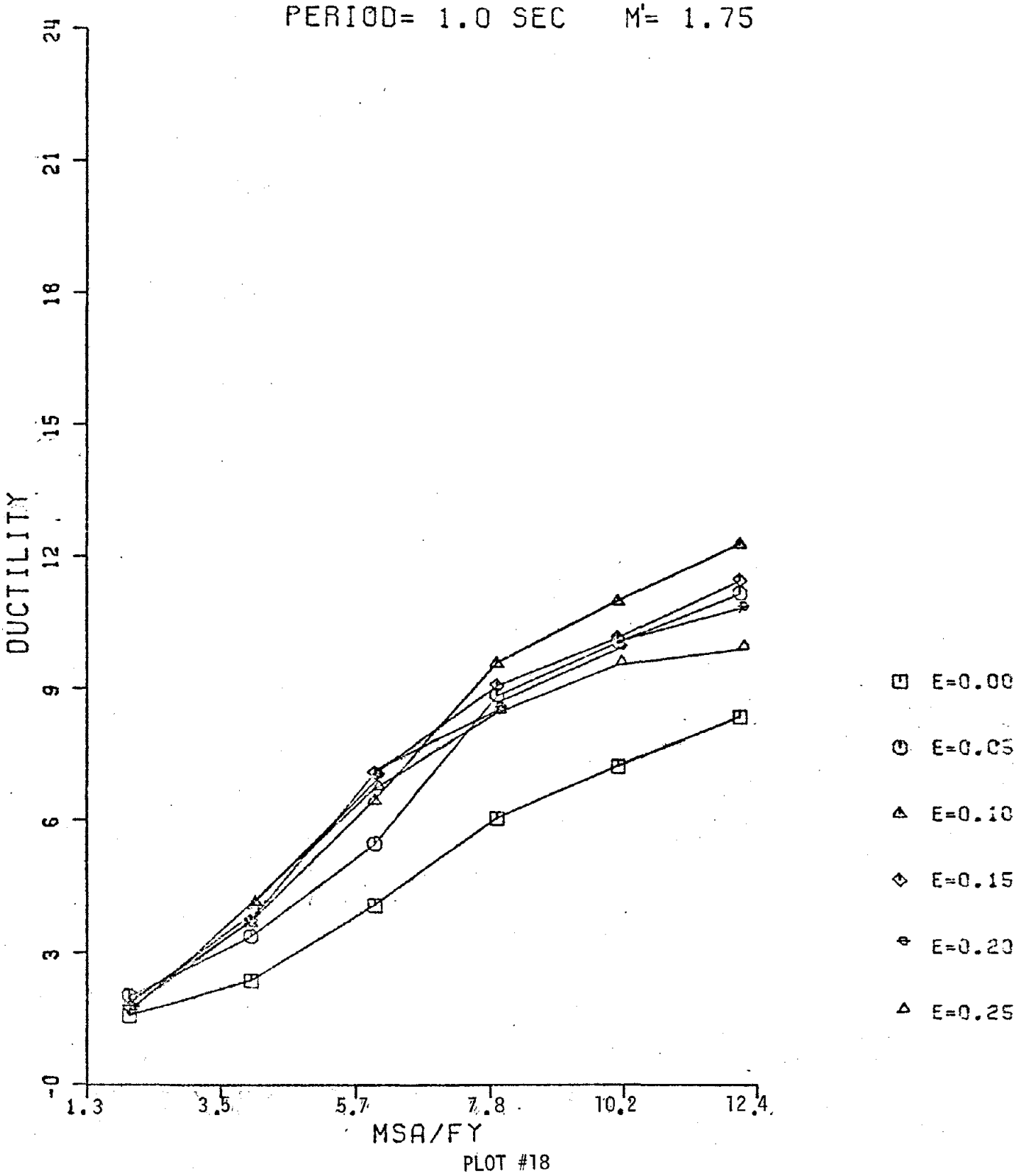

PLOT #18

EL CENTRO N-S 1940

PERIOD= 1.5 SEC M'= 0.50

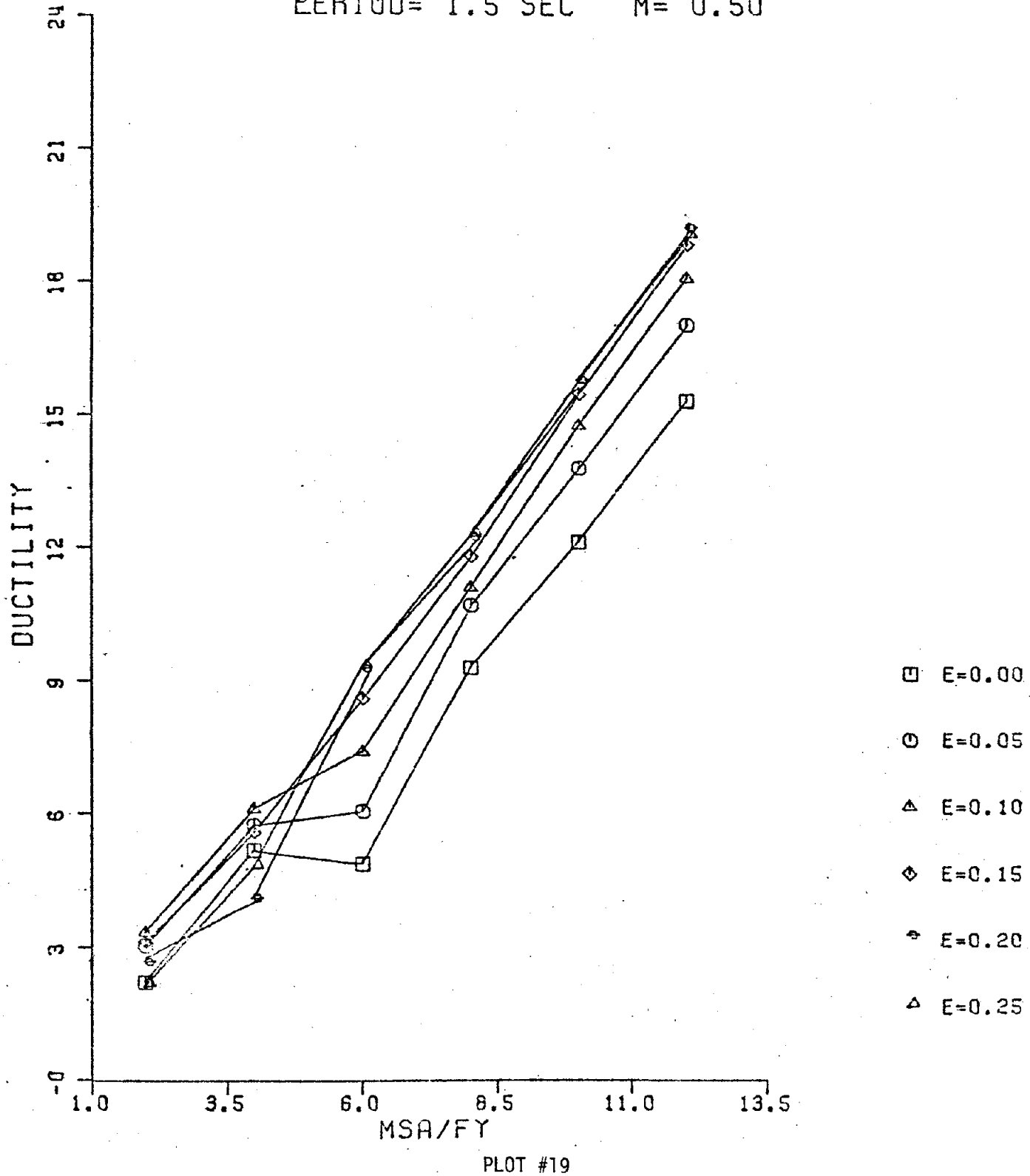

PLOT #19

EL-CENTRO N-S 1940

PERIOD= 1.5 SEC M= 0.75

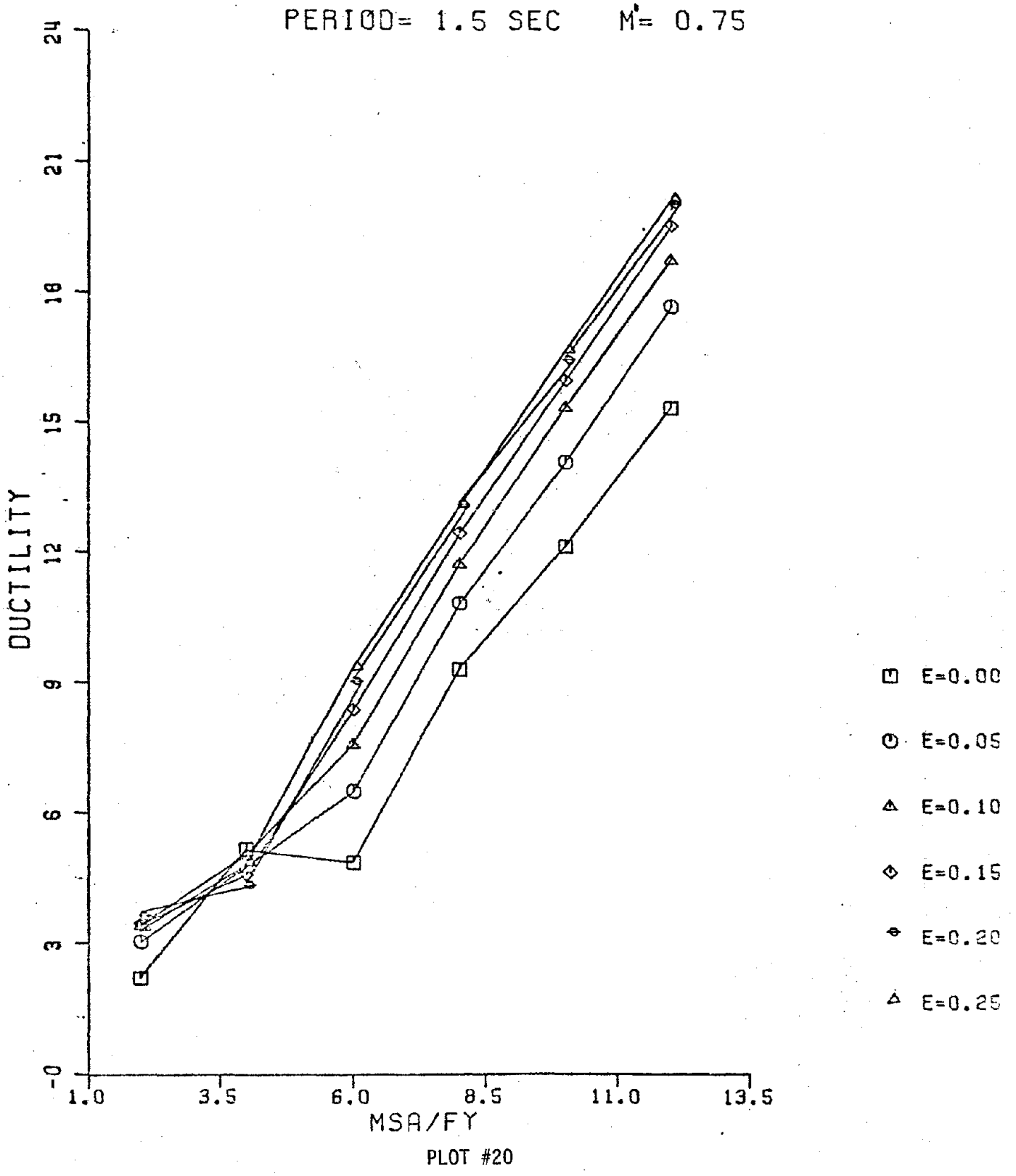

PLOT #20

EL-CENTRO N-S 1940

PERIOD= 1.5 SEC M= 1.00

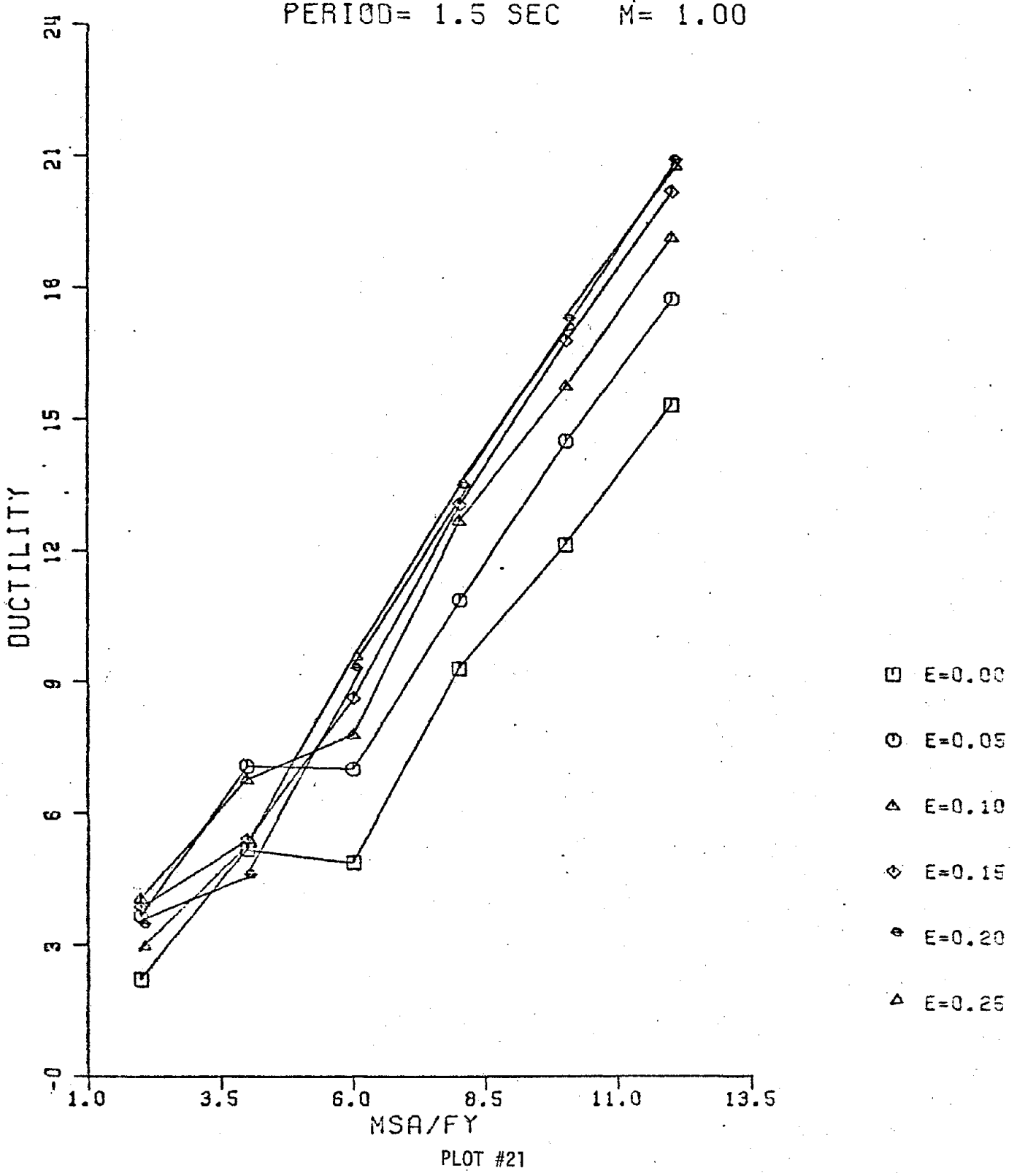

PLOT #21

EL-CENTRO N-S 1940

PERIOD= 1.5 SEC M= 1.25

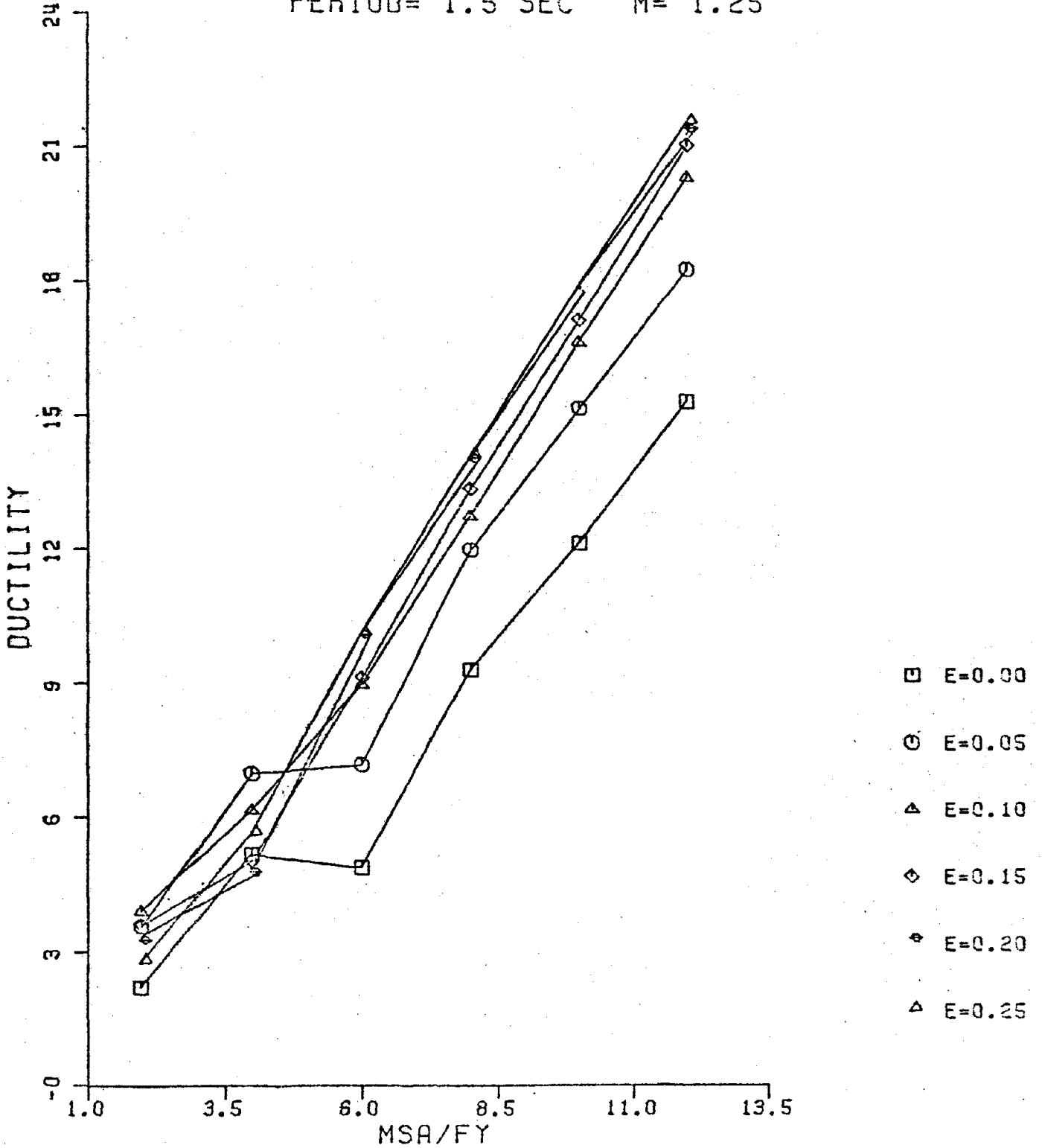

PLOT #22

EL-CENTRO N-S 1940

PERIOD= 1.5 SEC M= 1.50

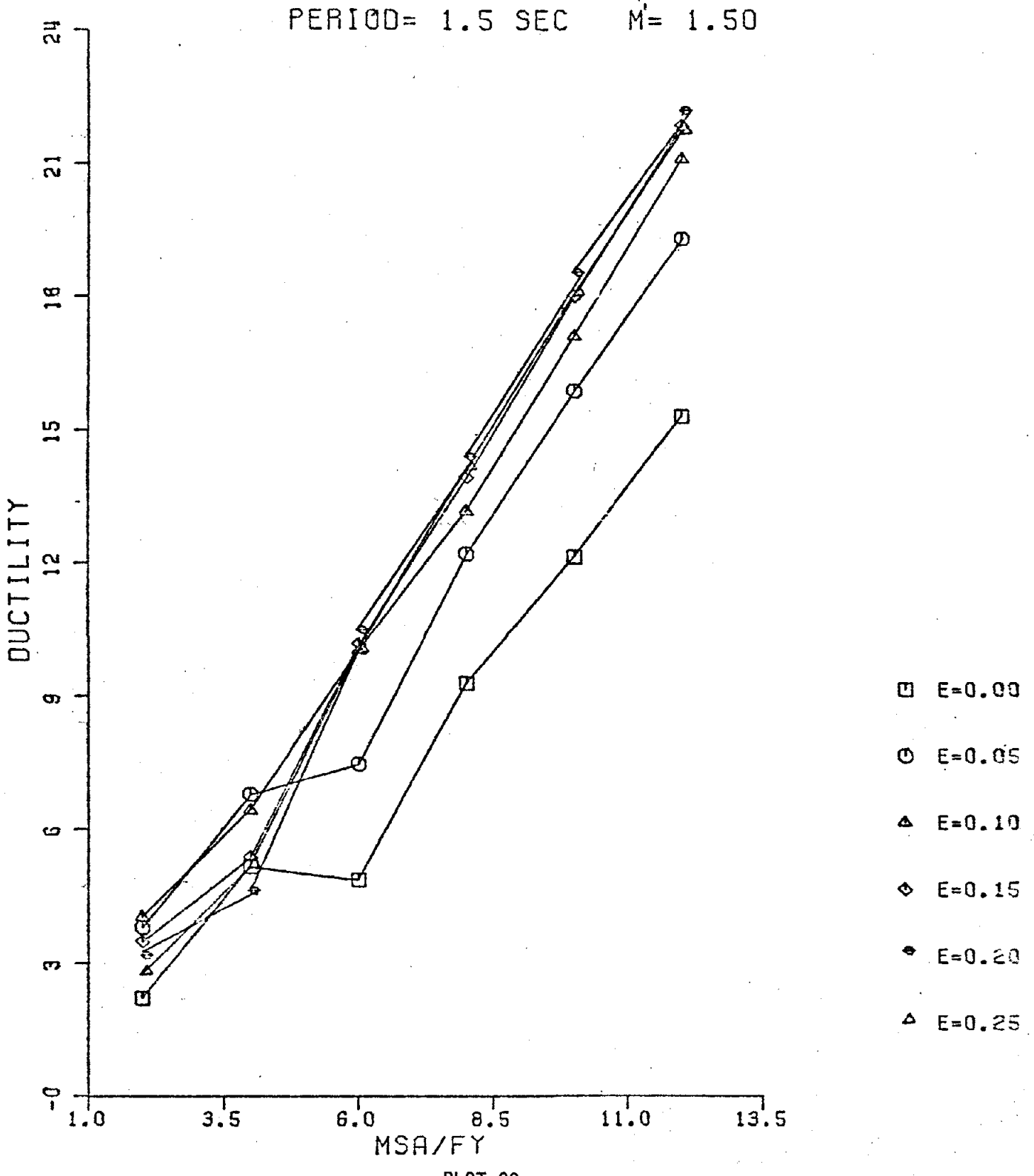

PLOT 23

EL-CENTRO N-S 1940

PERIOD= 1.5 SEC M= 1.75

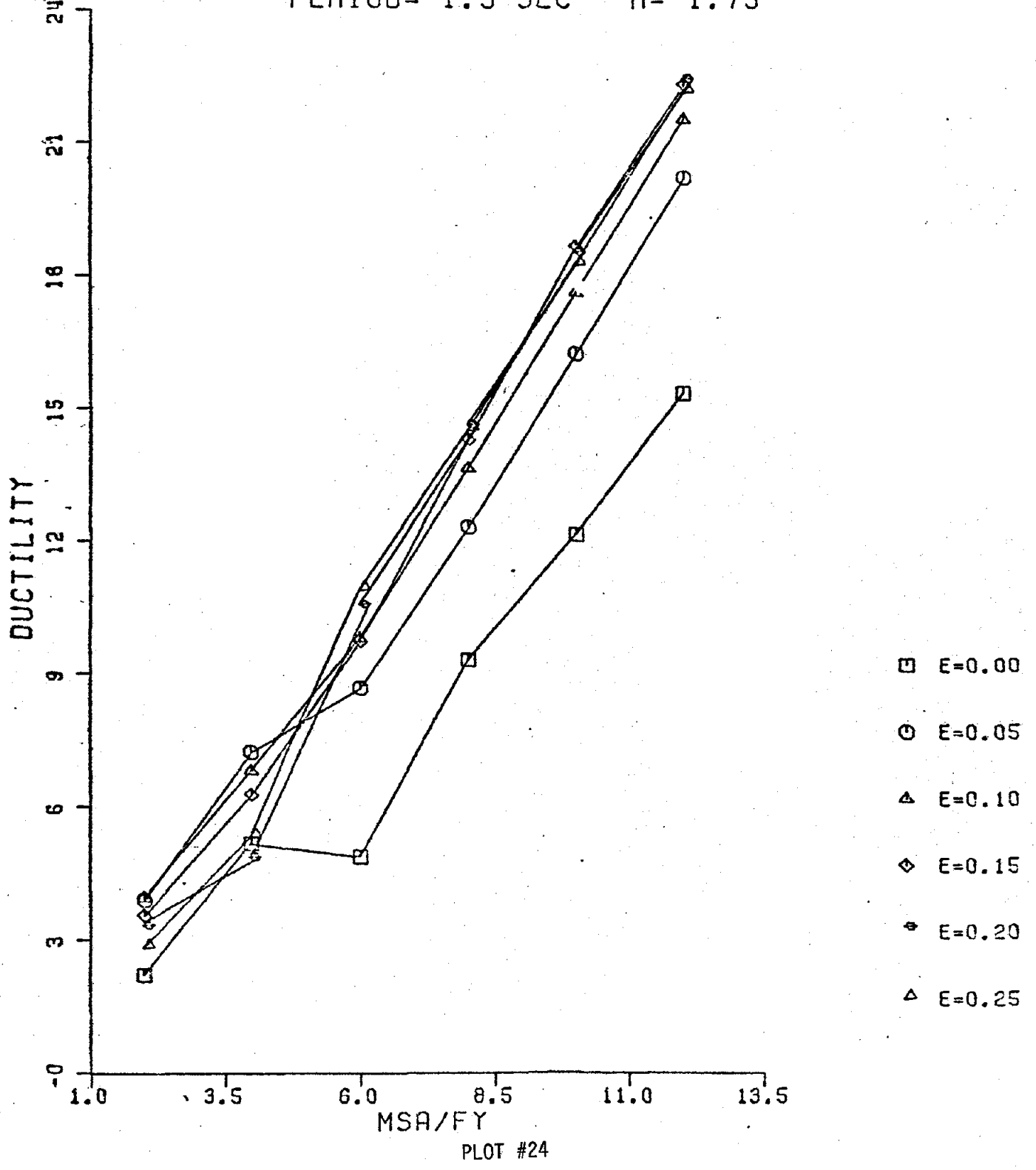

PLOT #24

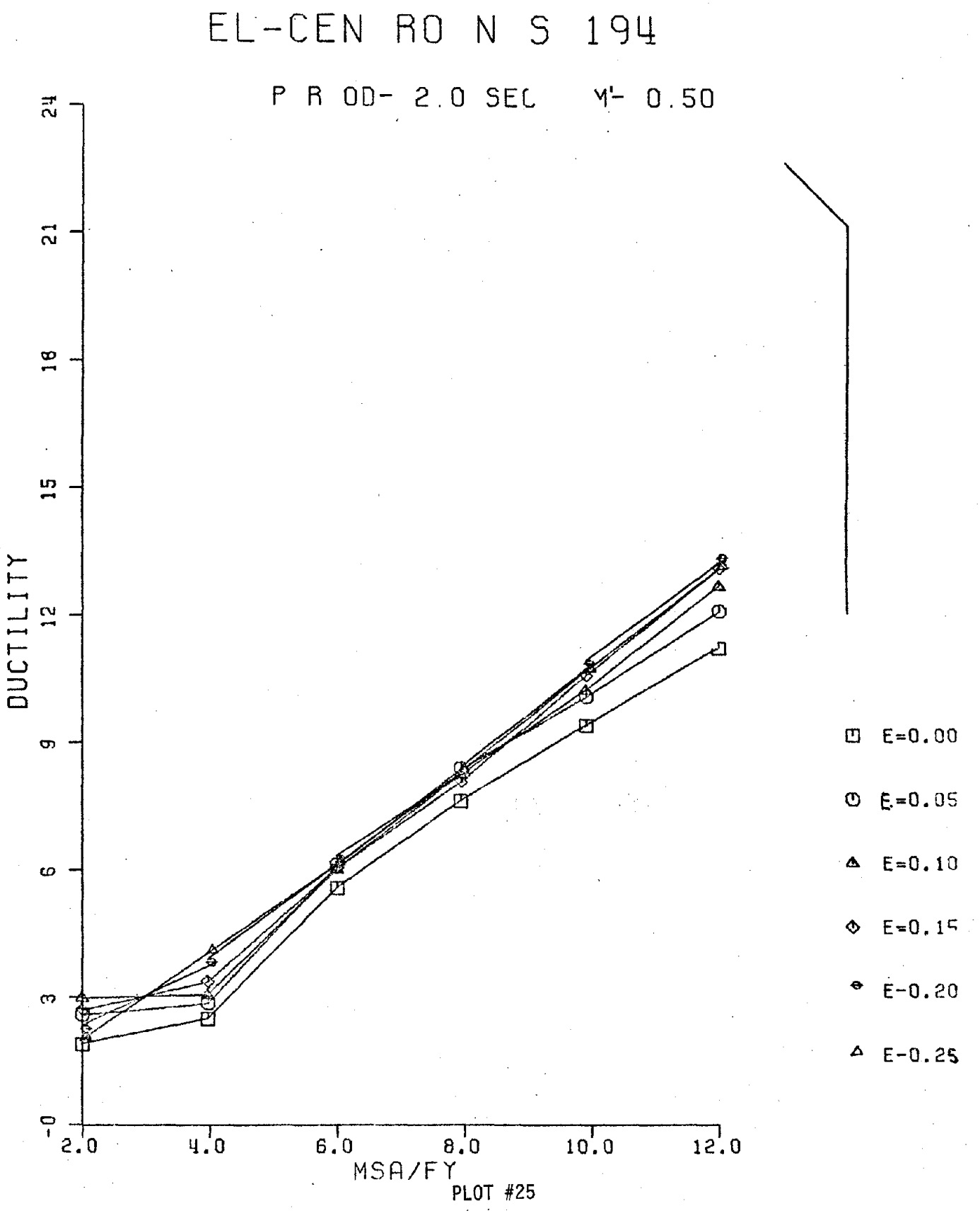
EL-CEN RO N S 194
P R OD- 2.0 SEC Y- 0.50
DUCTILITY
0
3
6
9
12
15
18
21
24
2.0
4.0
6.0
8.0
10.0
12.0
MSA/FY
PLOT #25
E=0.00
E=0.05
E=0.10
E=0.15
E-0.20
E-0.25

EL-CENTRO N-S 1940

PERIOD= 2.0 SEC M= 0.75

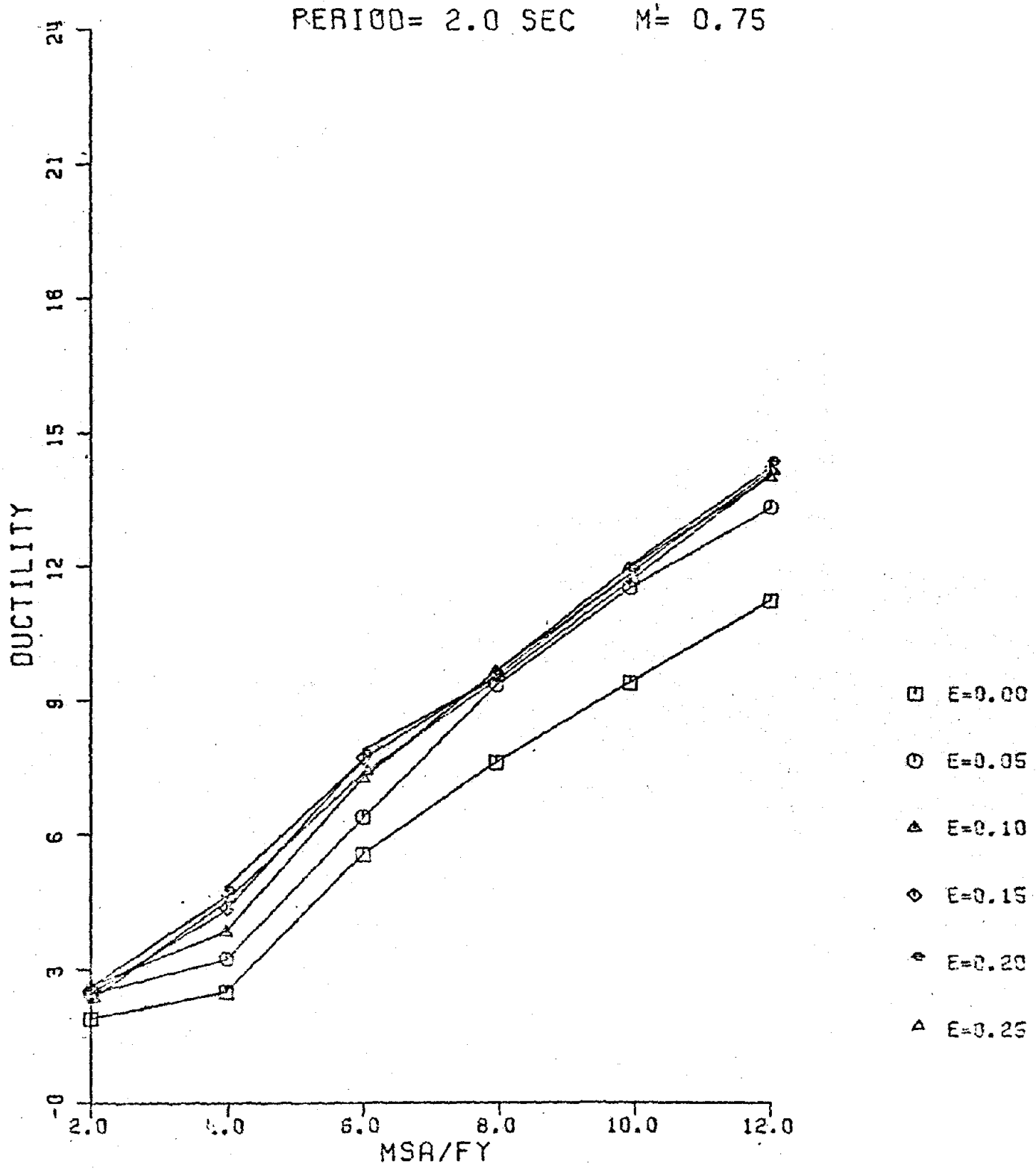

PLOT #26

EL-CENTRO N-S 1940

PERIOD= 2.0 SEC M'= 1.00

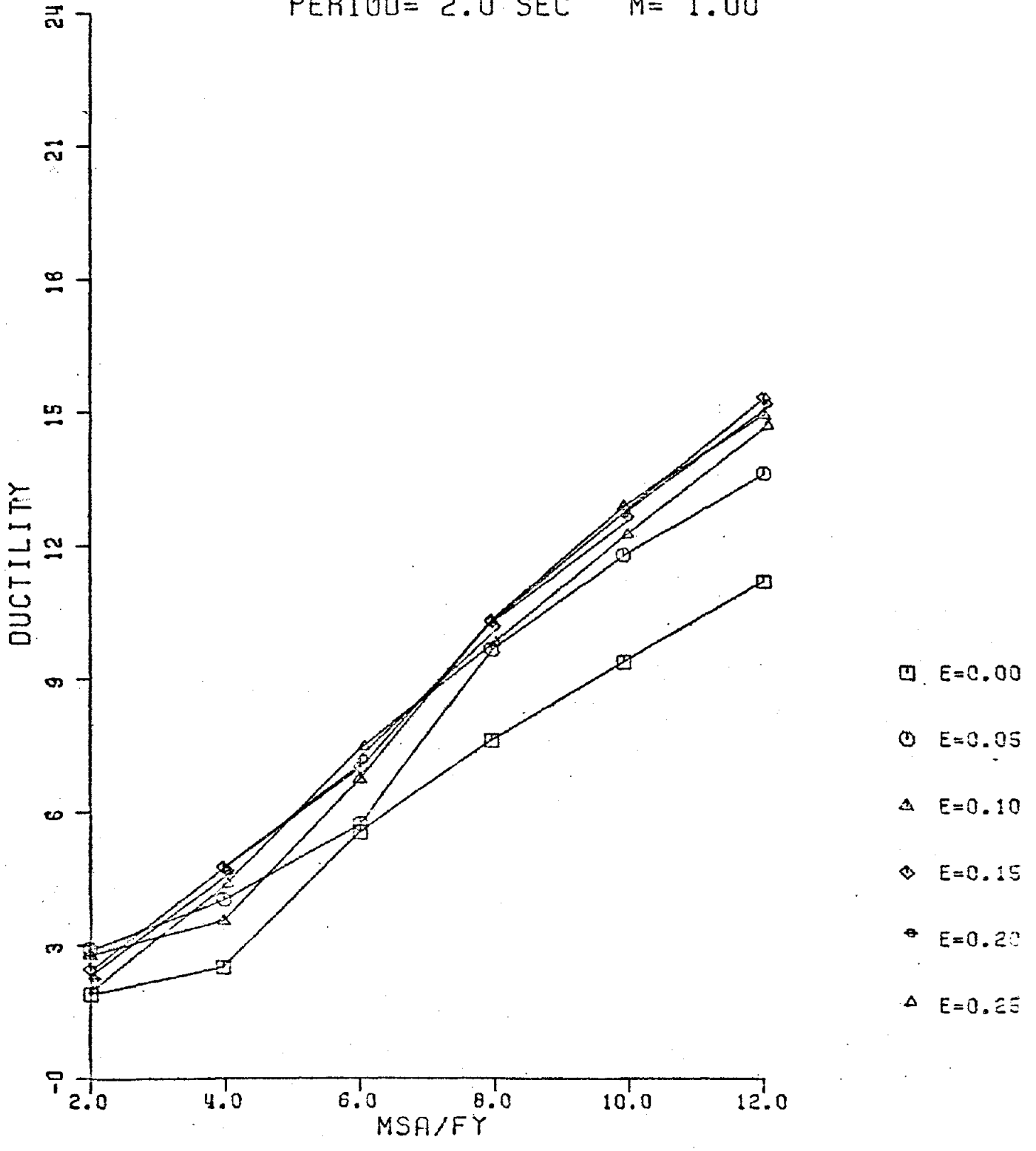

PLOT #27

EL-CENTRO N-S 1940

PERIOD= 2.0 SEC M= 1.25

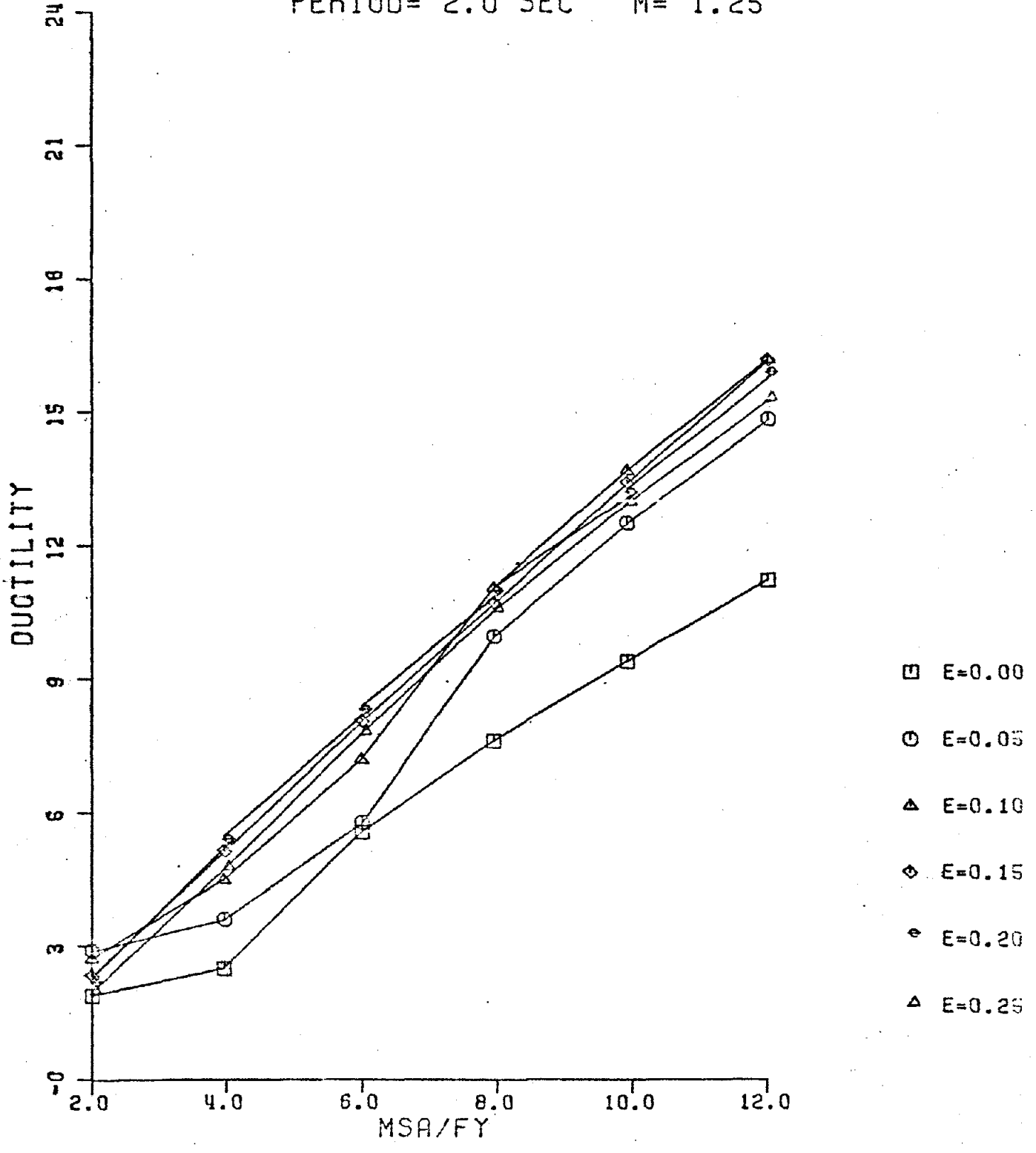

PLOT #28

EL-CENTRO N-S 1940

PERIOD= 2.0 SEC M'= 1.50

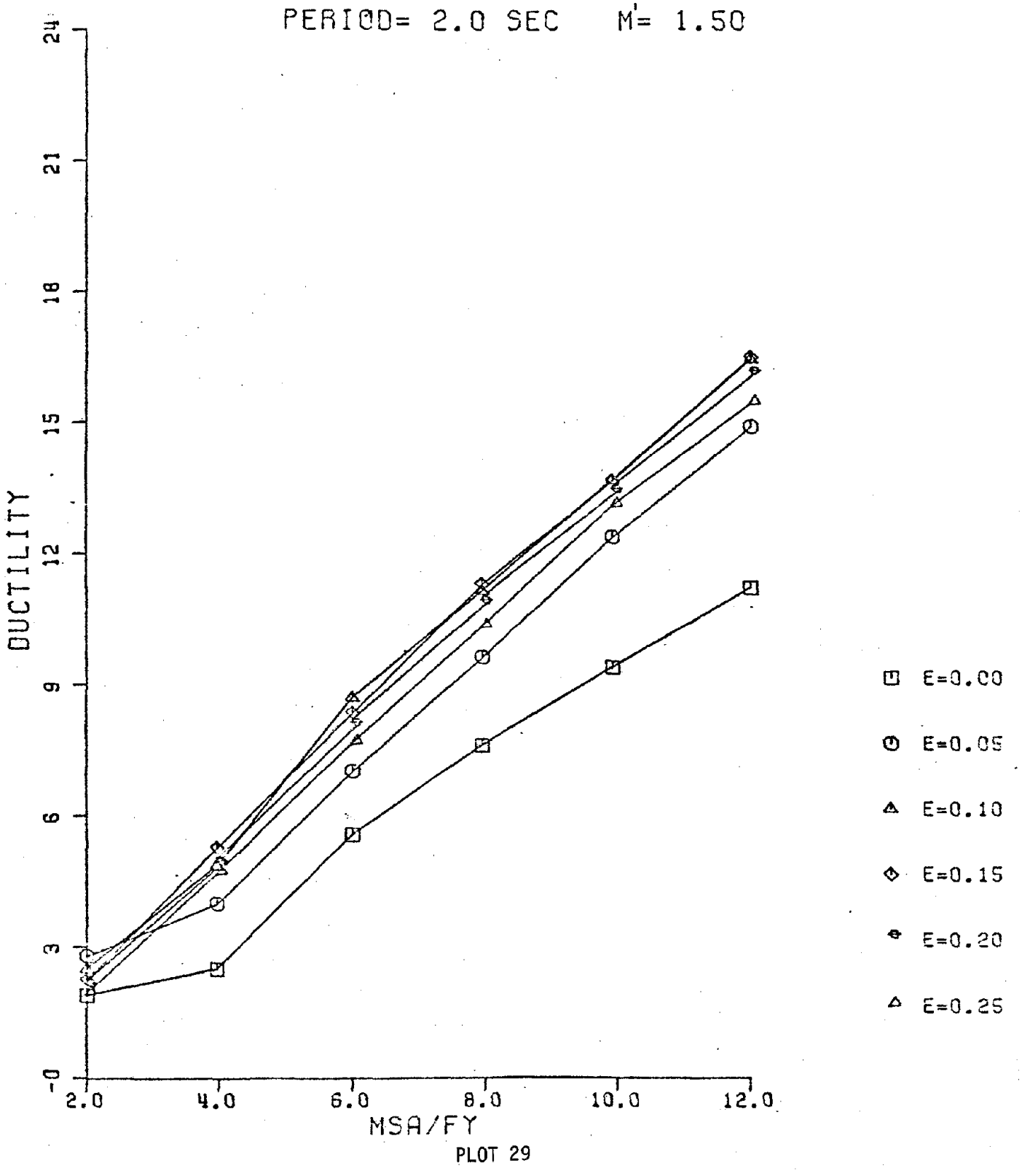

PLOT 29

EL-CENTRO N-S 1940

PERIOD= 2.0 SEC M= 1.75

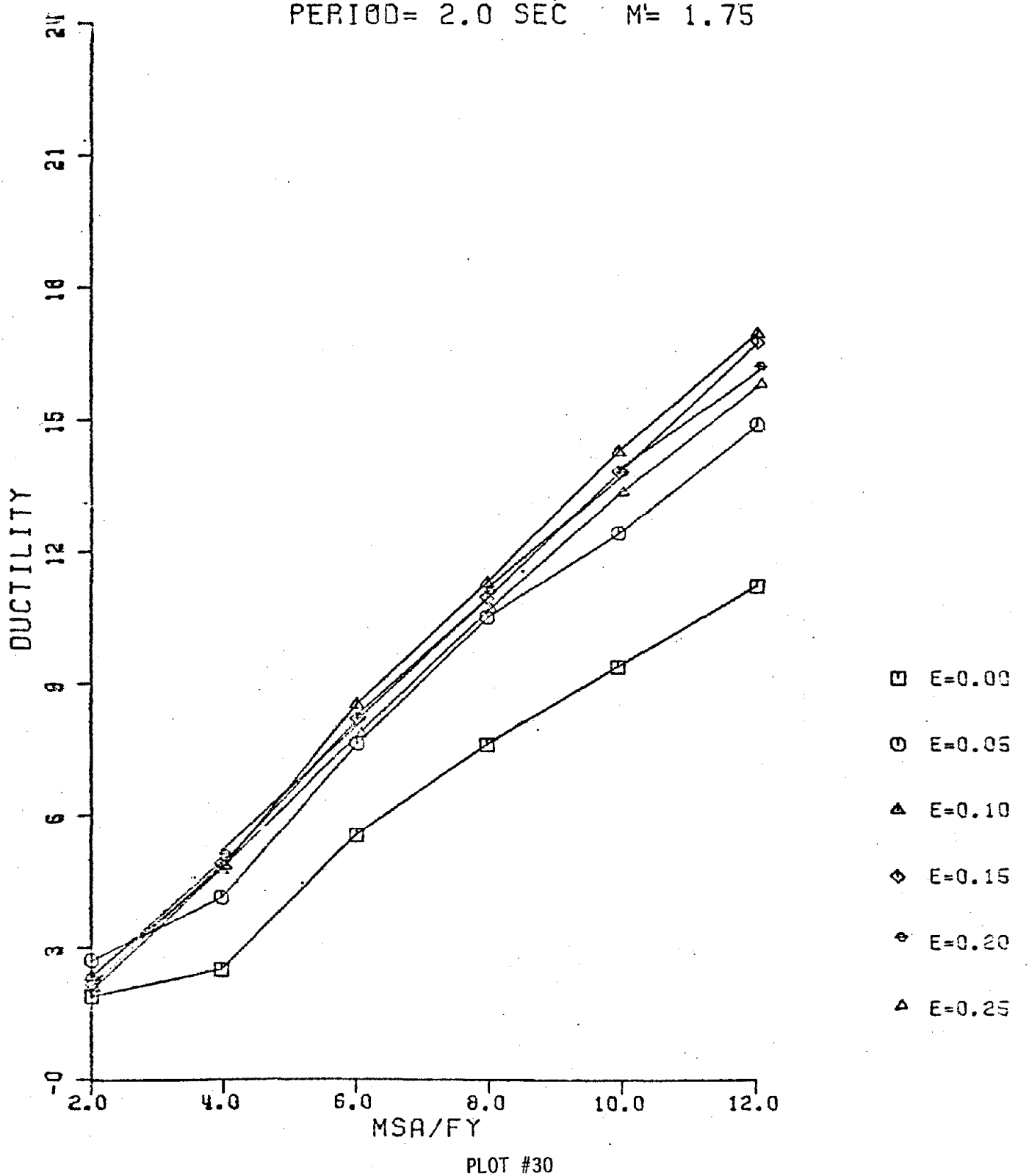

PLOT #30

PACOIMA DAM 1971 S16E

(San Fernando)

PLOTS 31 - 54

PACOIMA DAM S16E

PERIOD= 0.5 SEC M'= 0.50

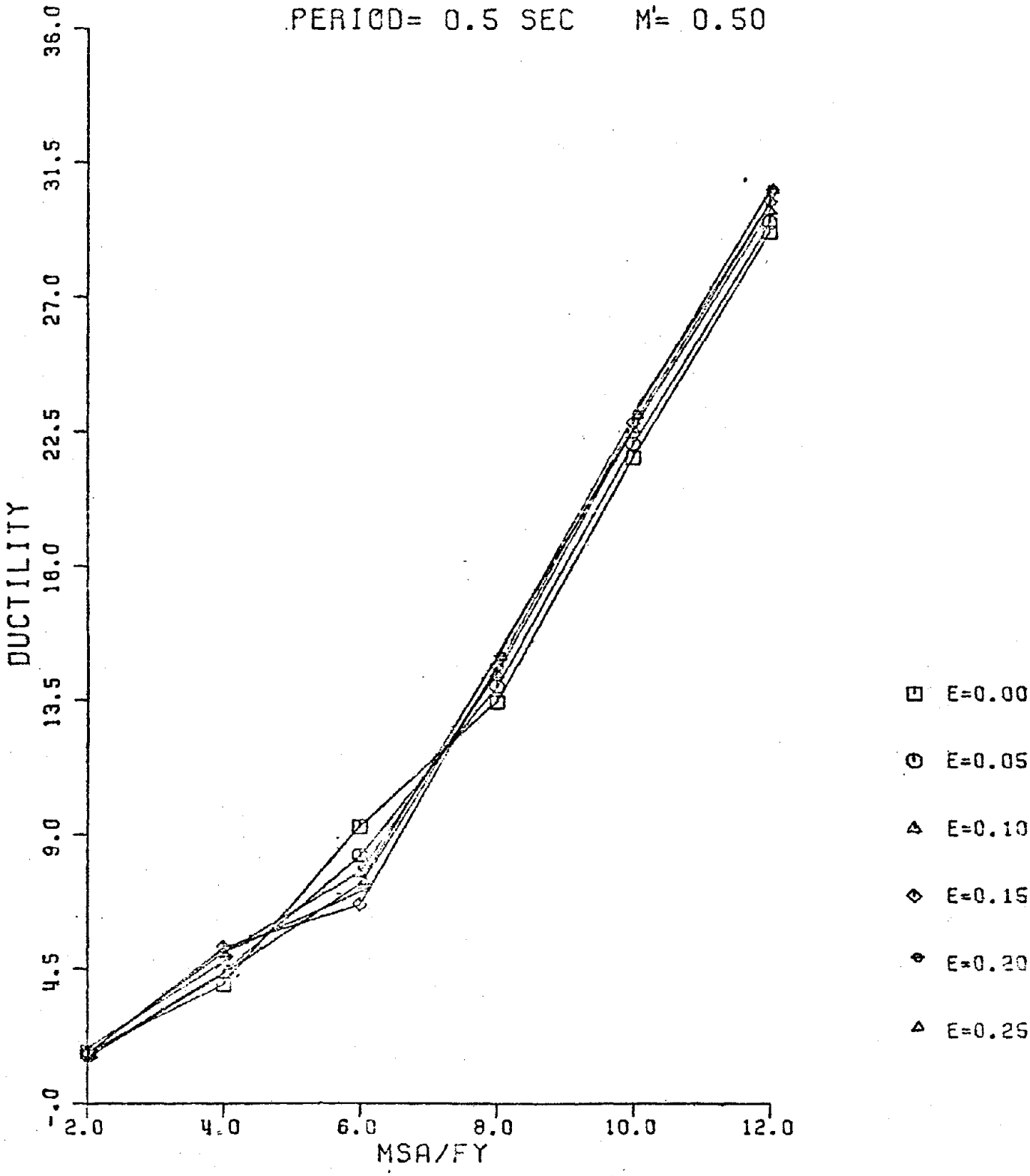

PLOT #31

PACOIMA DAM S16E

PERIOD= 0.5 SEC M'= 0.75

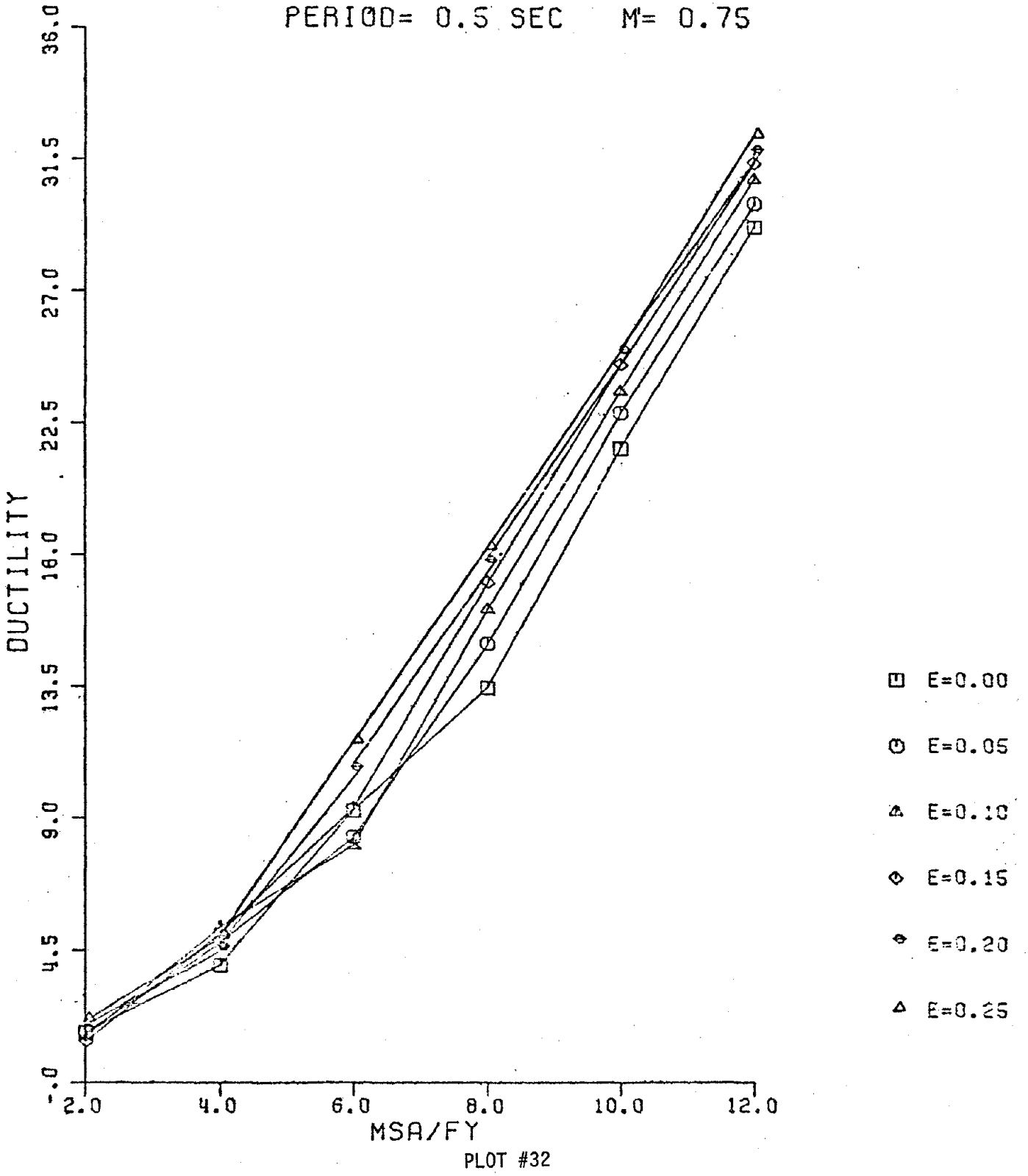

PLOT #32

PACOIMA DAM S16E

PERIOD= 0.5 SEC M= 1.00

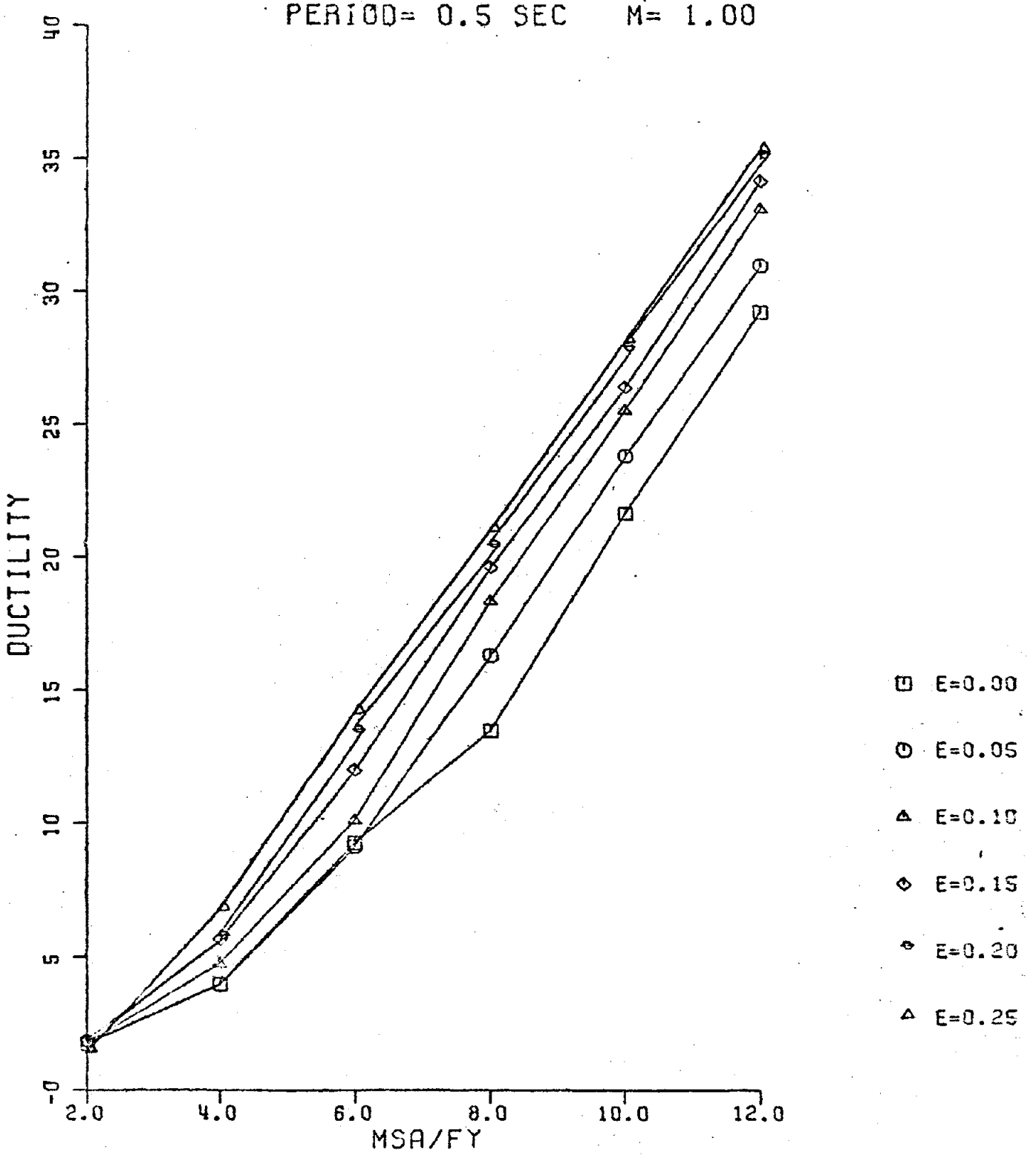

PLOT #33

PACOIMA DAM S16E

PERIOD= 0.5 SEC M= 1.25

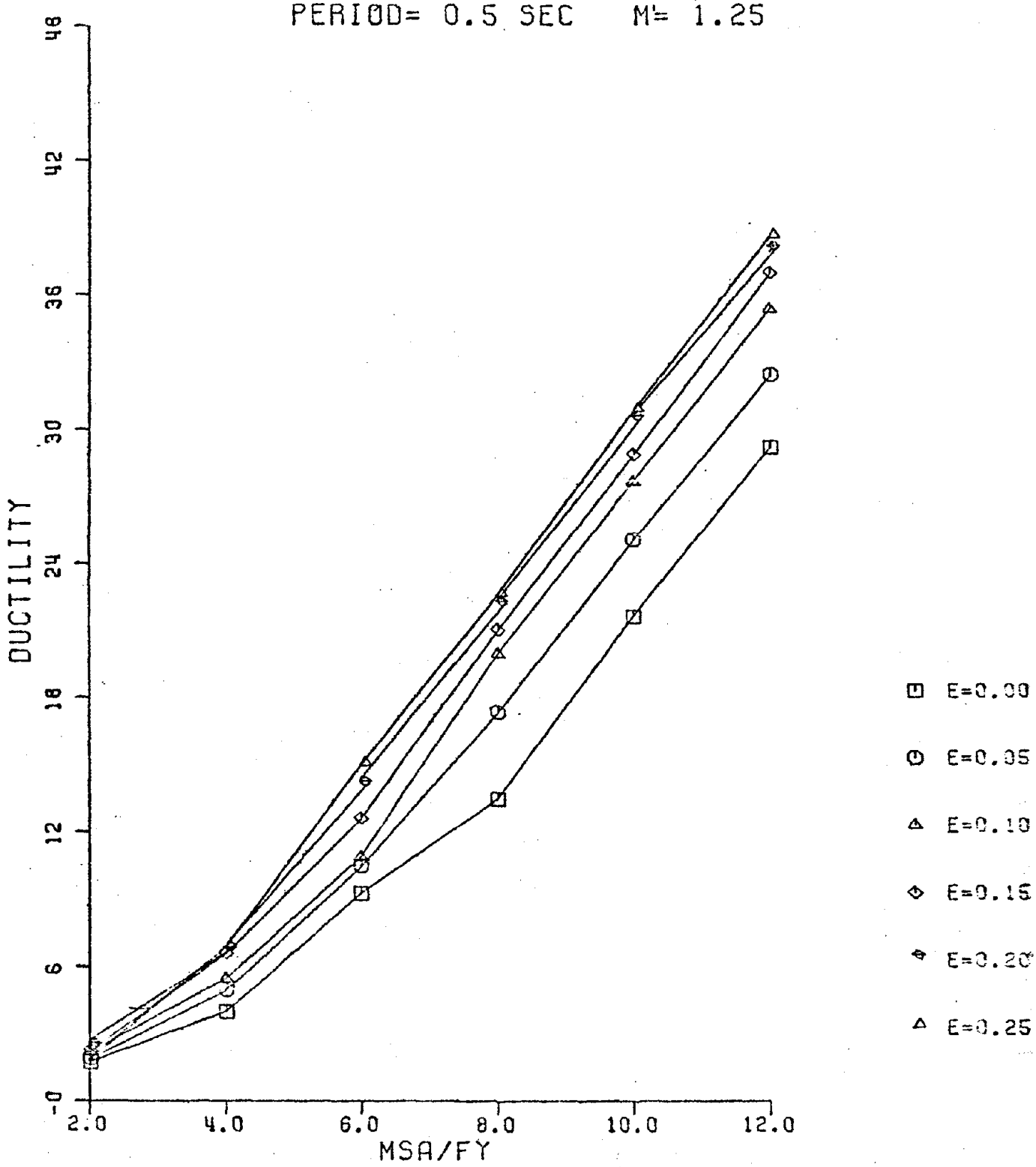

PLOT #34

PACOIMA DAM S16E

PERIOD= 0.5 SEC M= 1.50

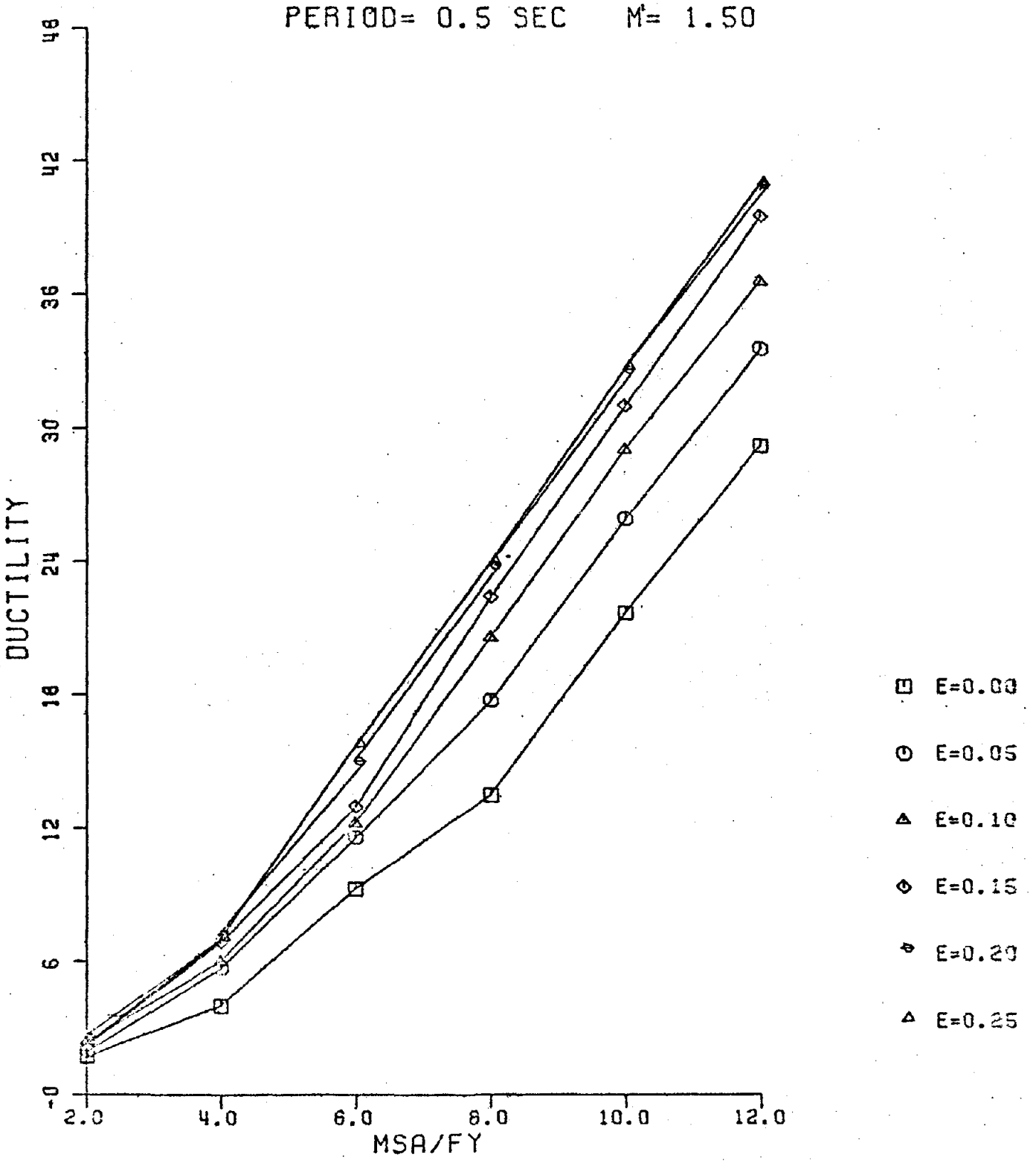

PLOT #35

PACOIMA DAM S16E

PERIOD= 0.5 SEC M= 1.75

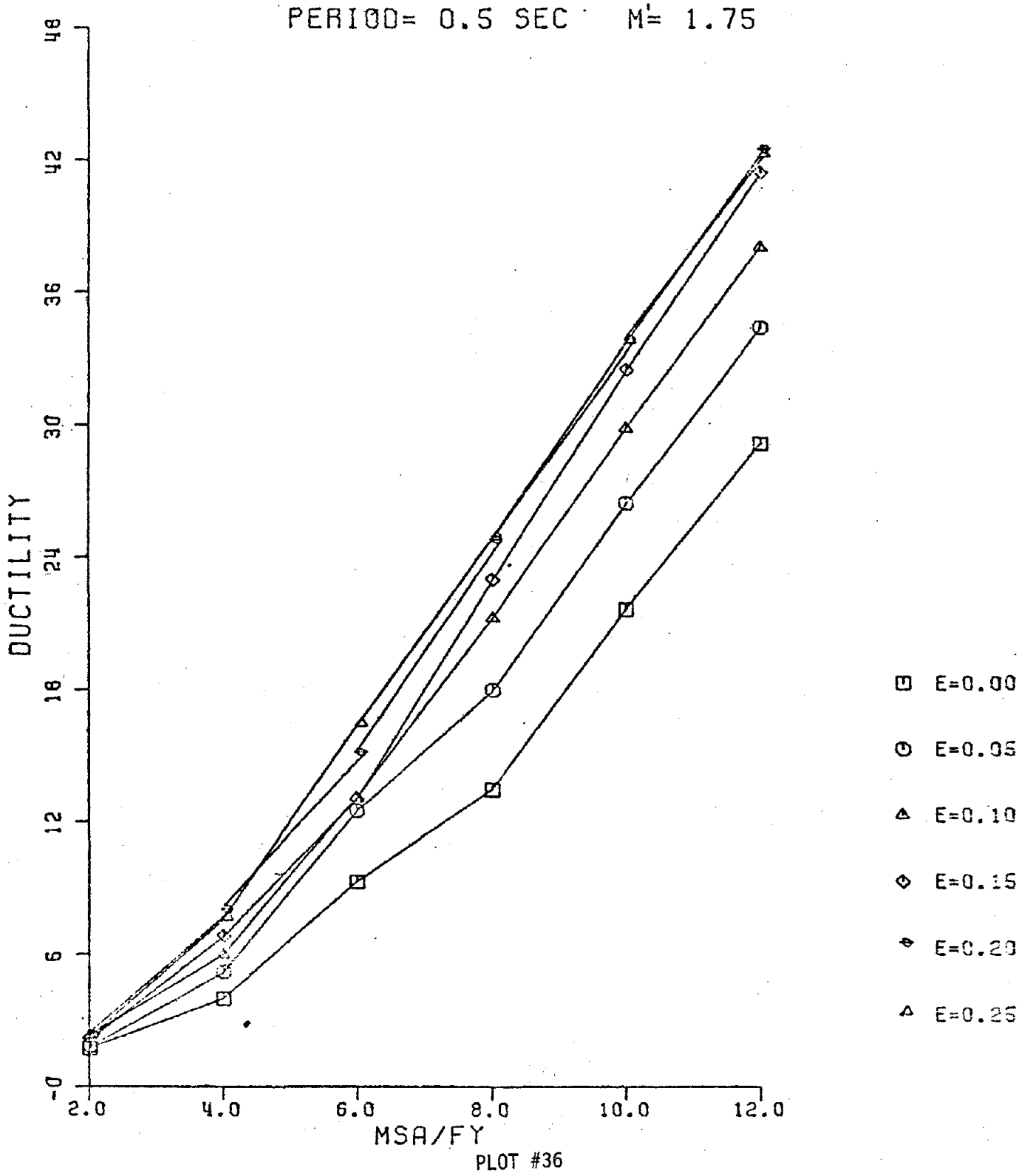

PLOT #36

PACOIMA DAM S16E

PERIOD= 1.0 SEC M'= 0.50

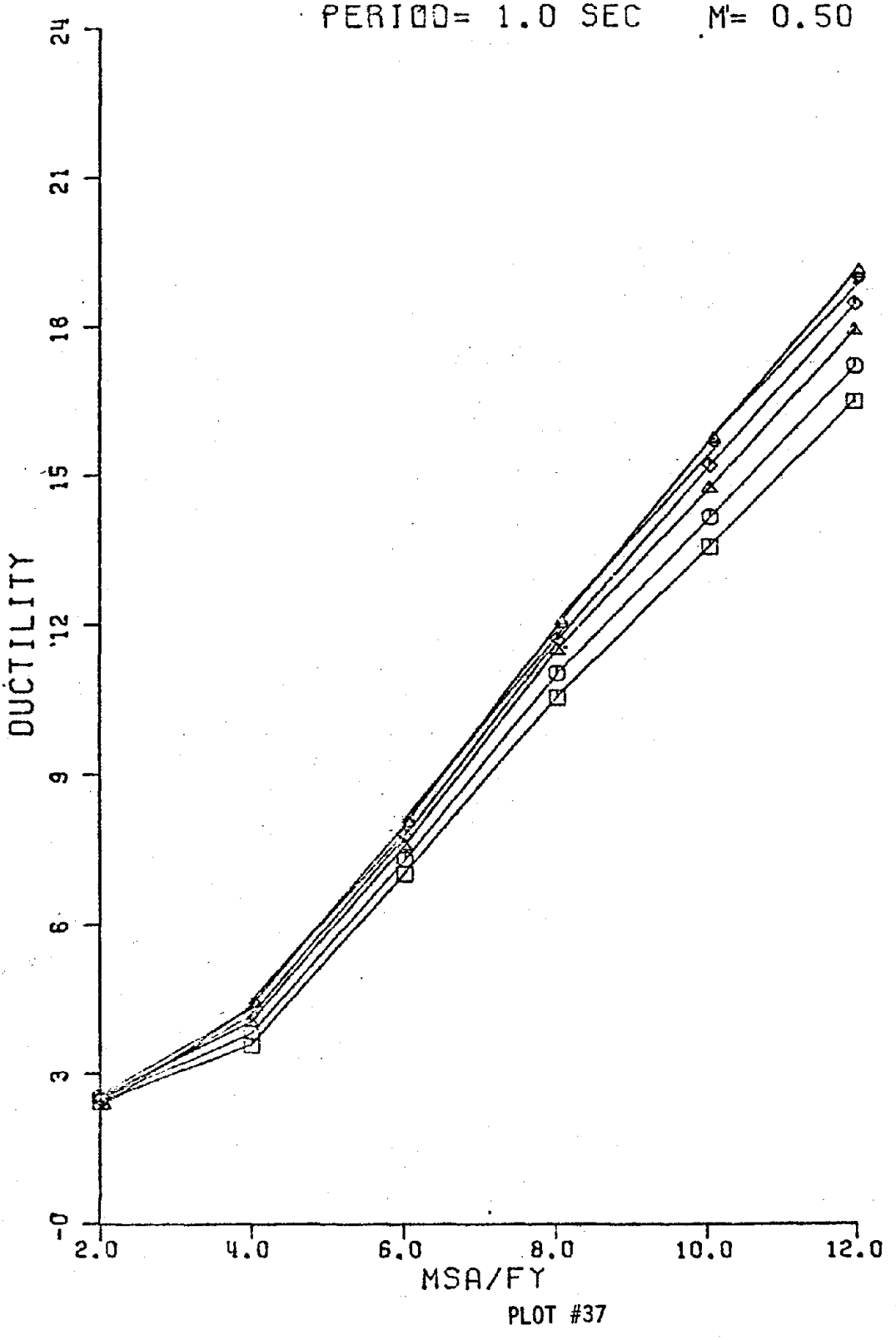

PLOT #37

PACOIMA DAM S16E

PERIOD= 1.0 SEC M'= 0.75

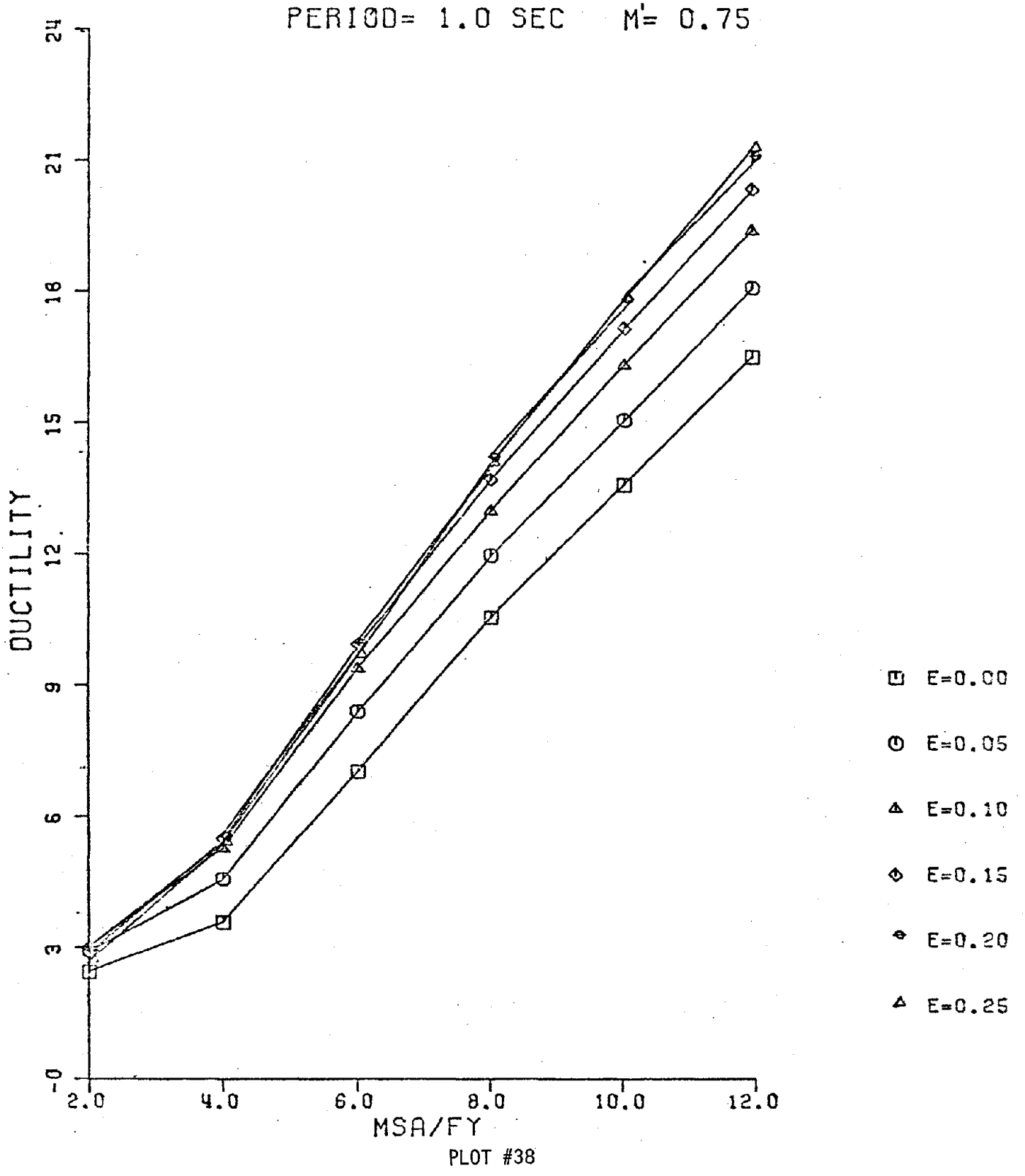

PLOT #38

PACOIMA DAM S16E

PERIOD= 1.0 SEC M= 1.00

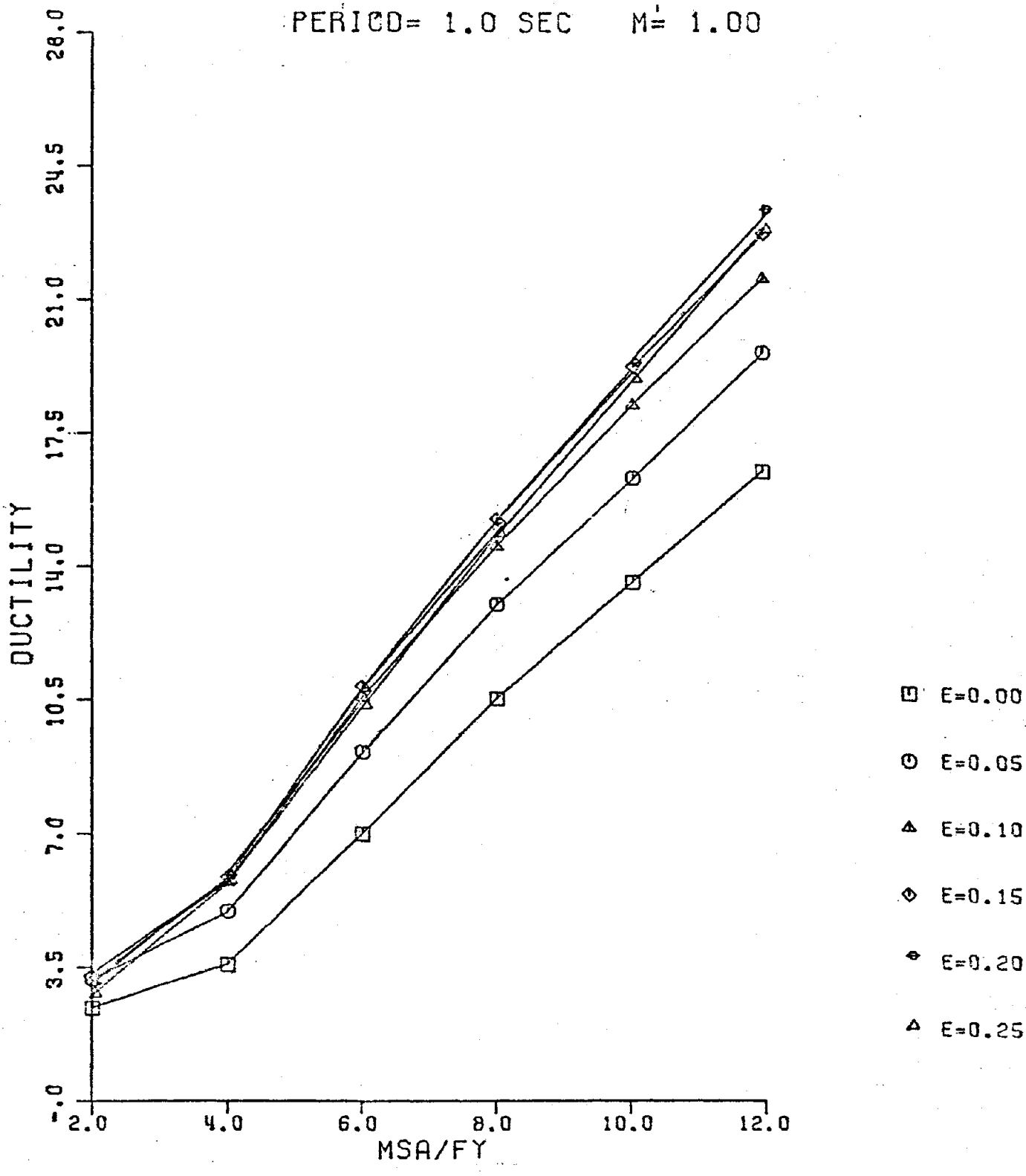

PLOT #39

PACOIMA DAM S16E

PERIOD= 1.0 SEC M'= 1.25

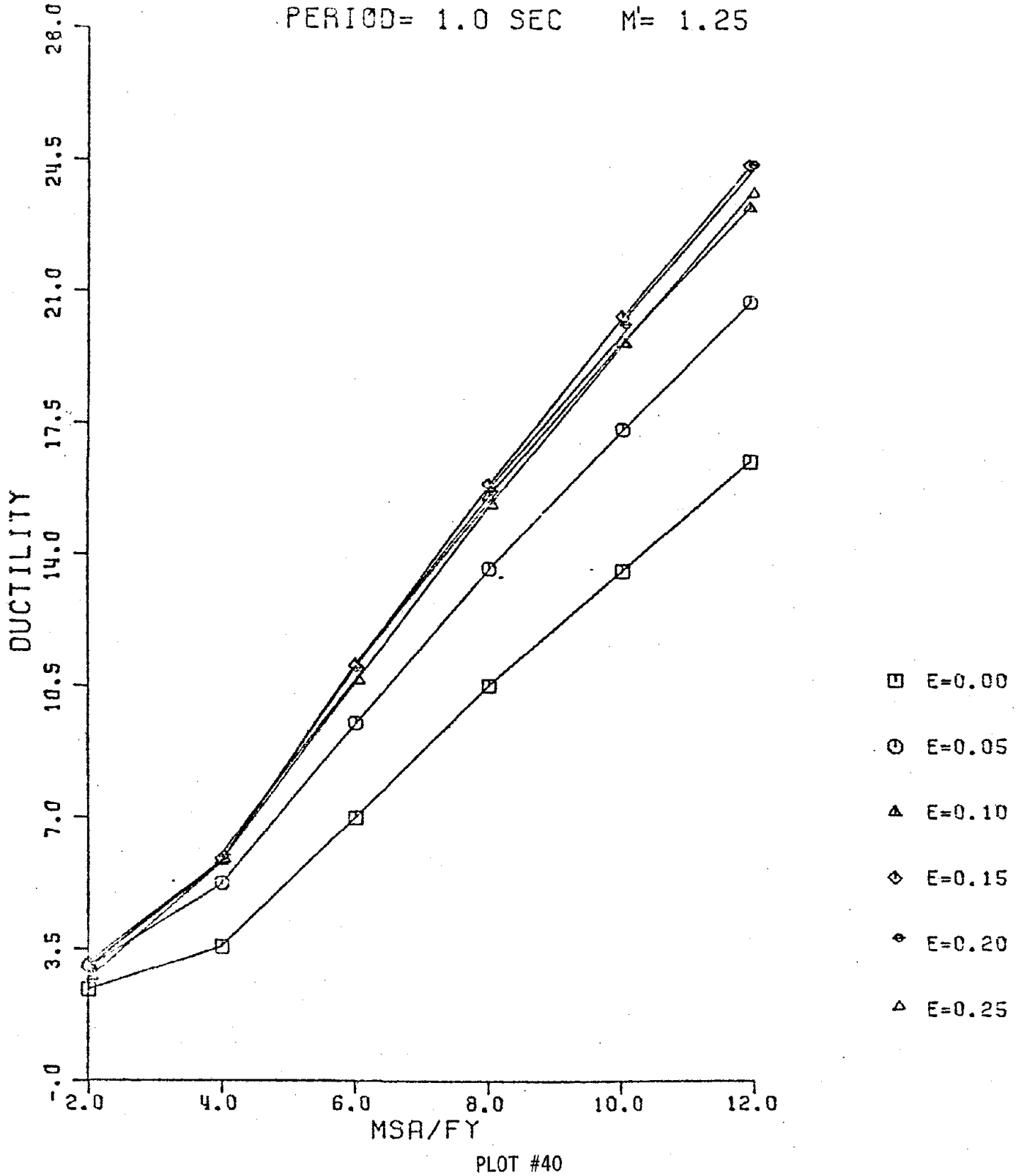

PLOT #40

PACOIMA DAM S16E

PERIOD= 1.0 SEC M= 1.50

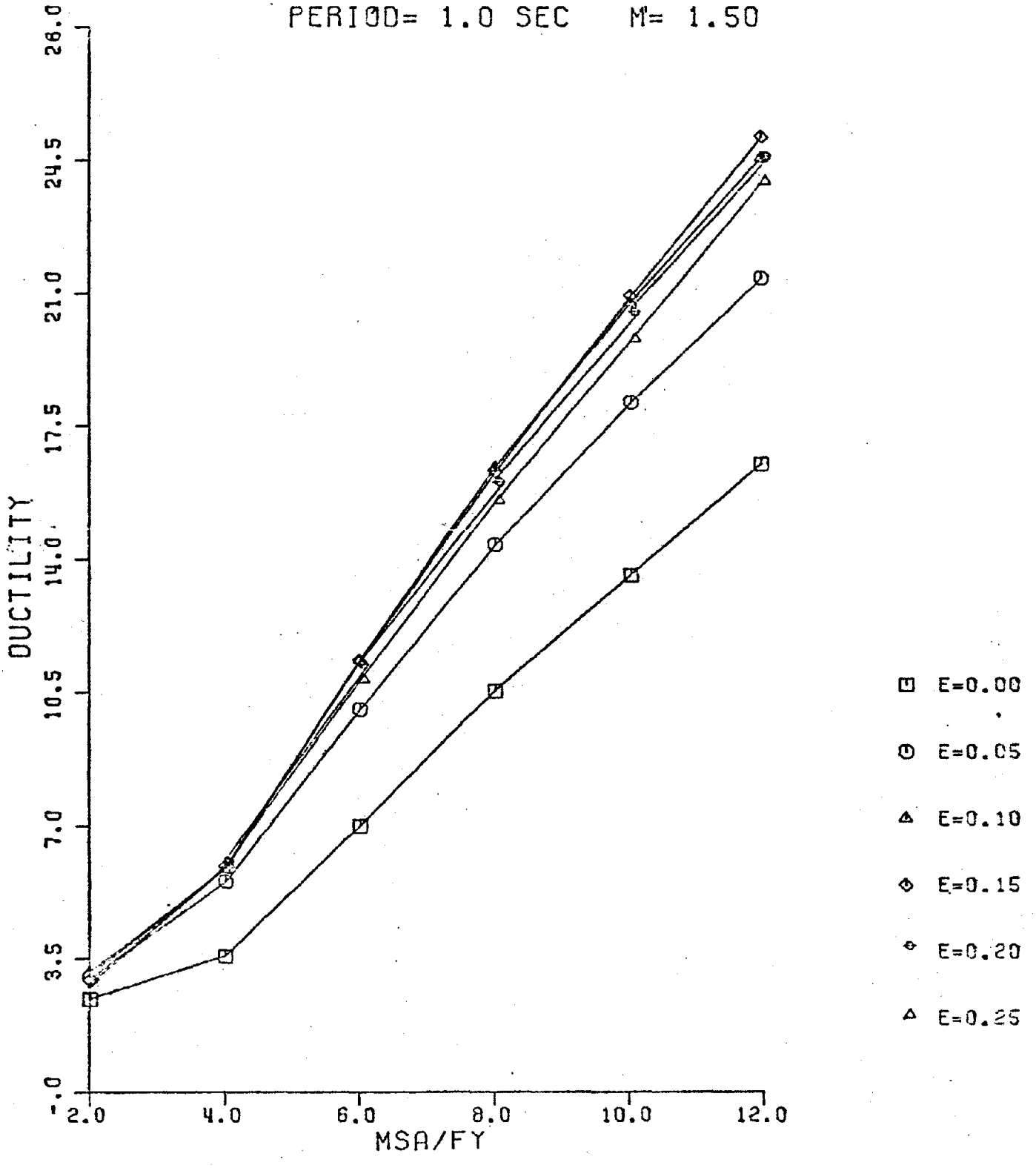

PLOT #41

PACOIMA DAM S16E

PERIOD= 1.0 SEC M= 1.75

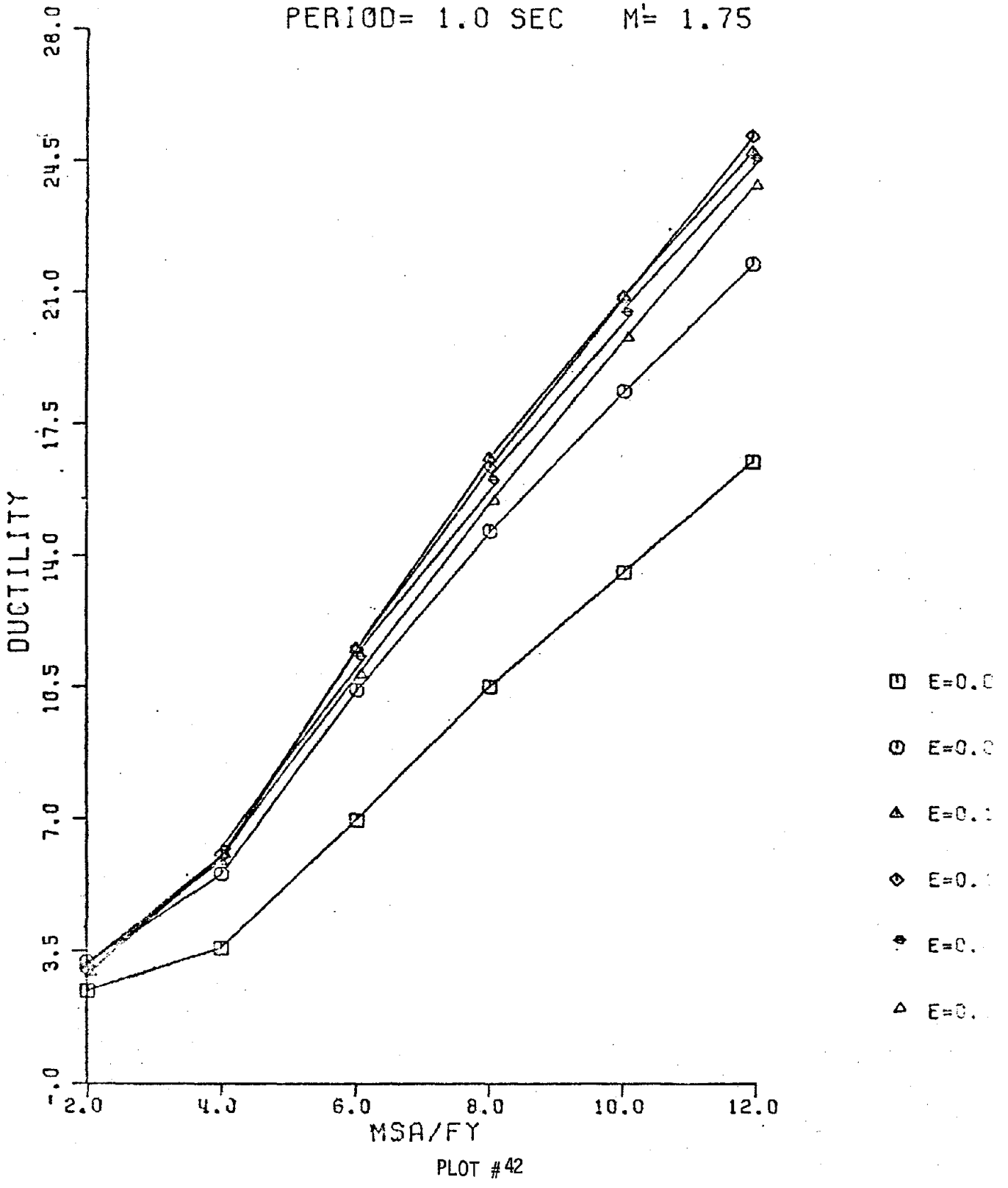

PLOT #42

PACOIMA DAM S16E

PERIOD= 1.5 SEC M= 0.50

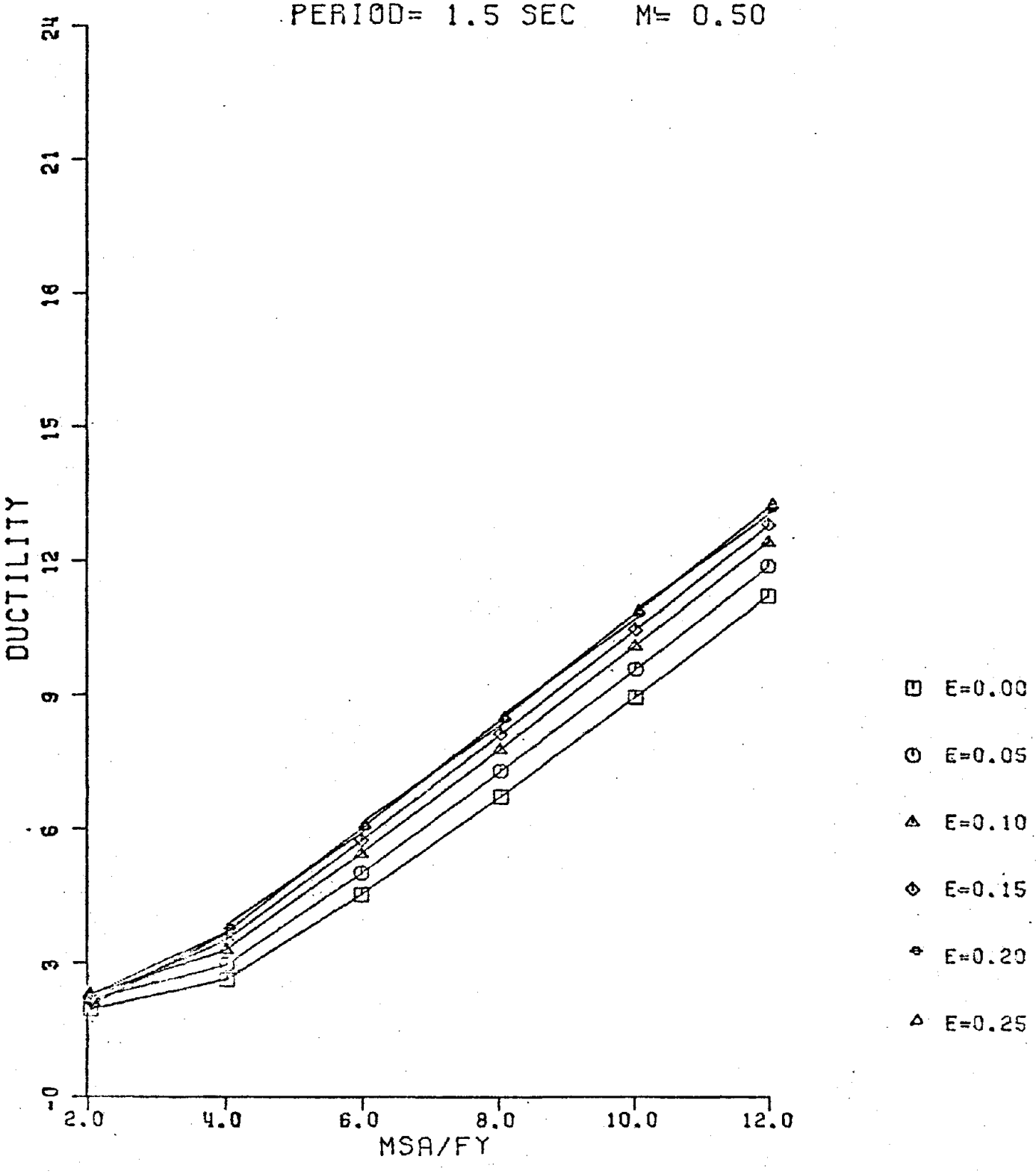

PLOT #43

PACOIMA DAM S16E

PERIOD= 1.5 SEC M= 0.75

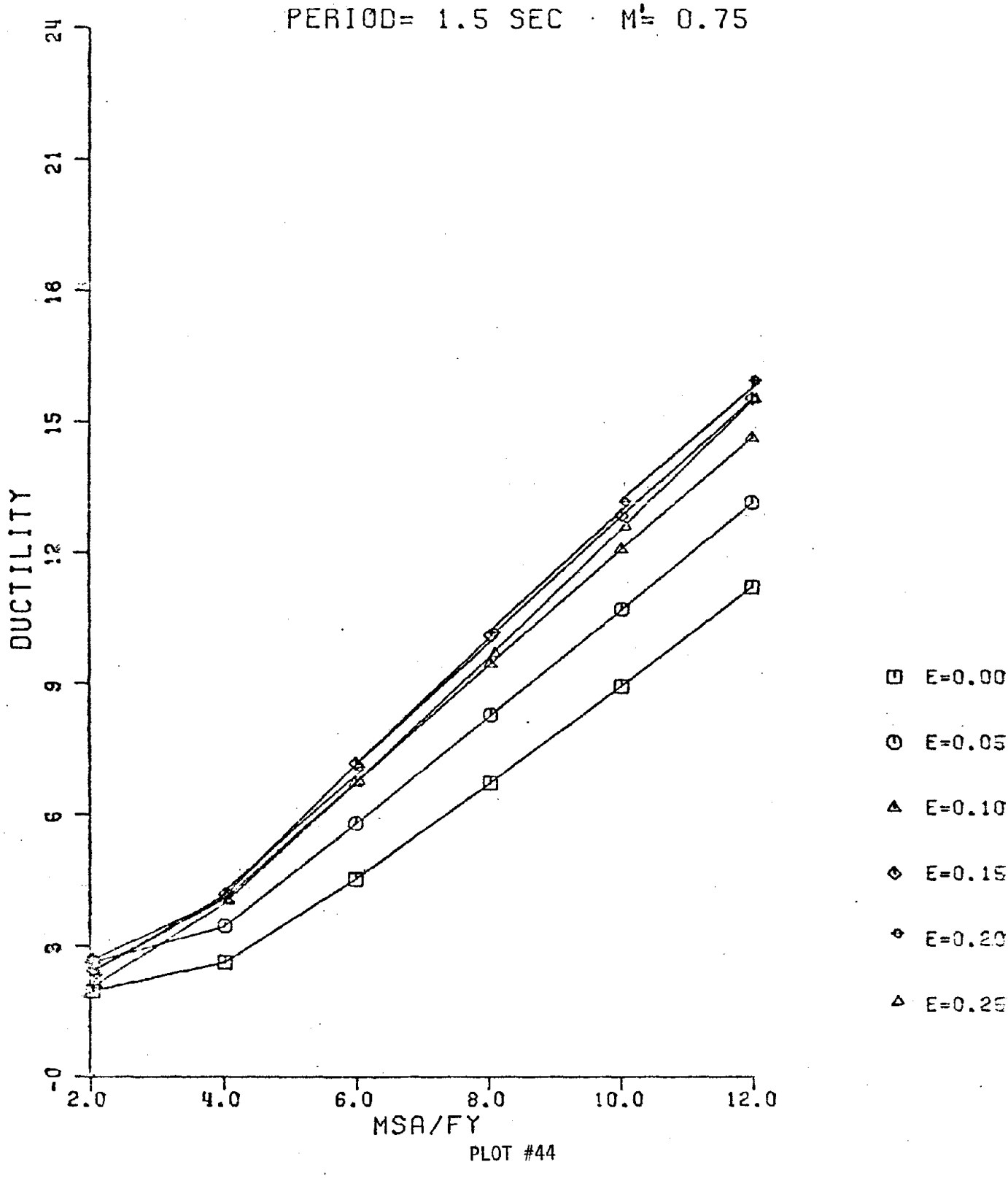

PLOT #44

PACOIMA DAM S16E

PERIOD= 1.5 SEC M= 1.00

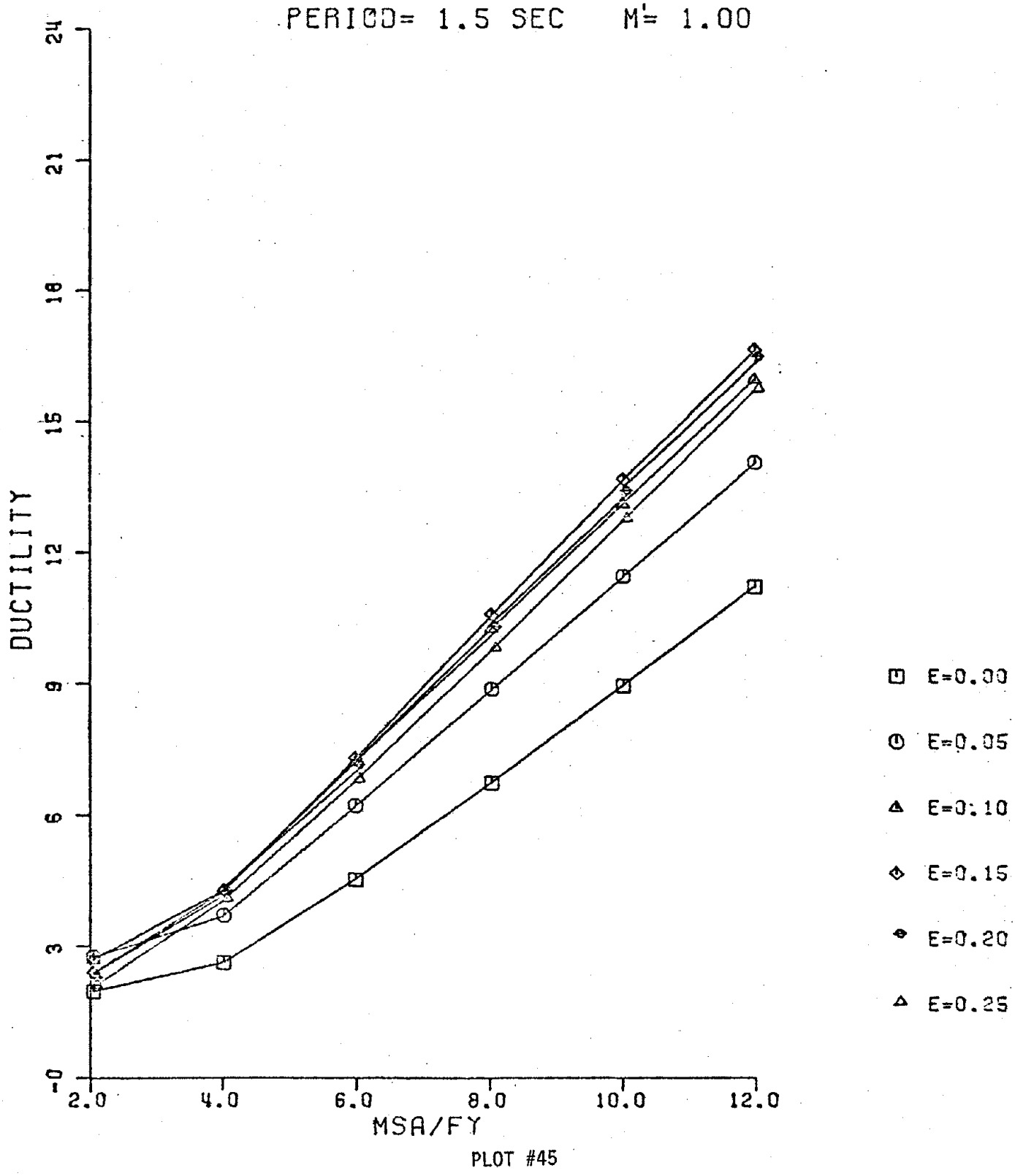

PLOT #45

PACOIMA DAM S16E

PERIOD= 1.5 SEC M'= 1.25

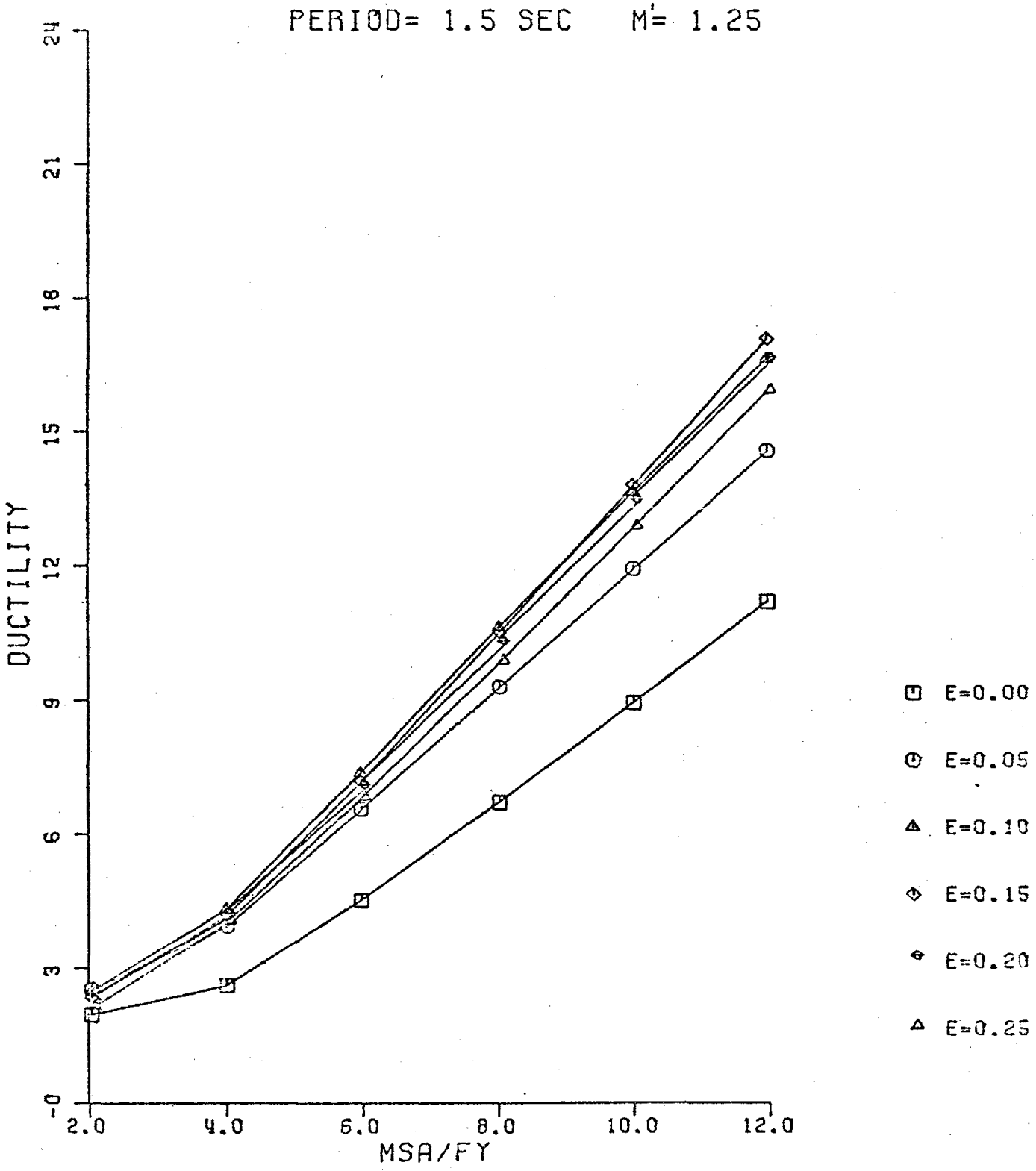

PLOT #46

PACOIMA DAM S16E

PERIOD= 1.5 SEC M= 1.50

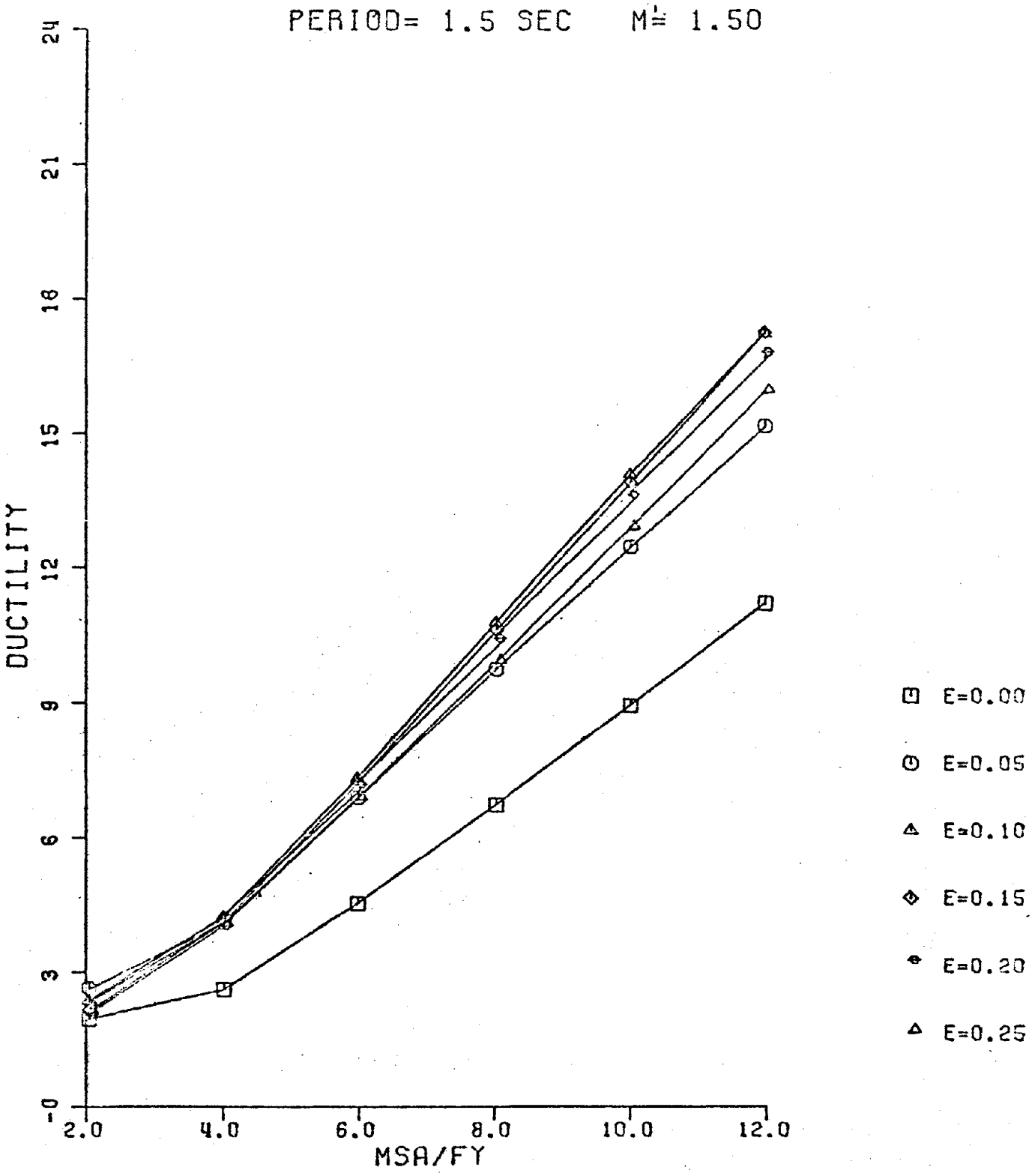

PLOT #47

PACOIMA DAM S16E

PERIOD= 1.5 SEC M= 1.75

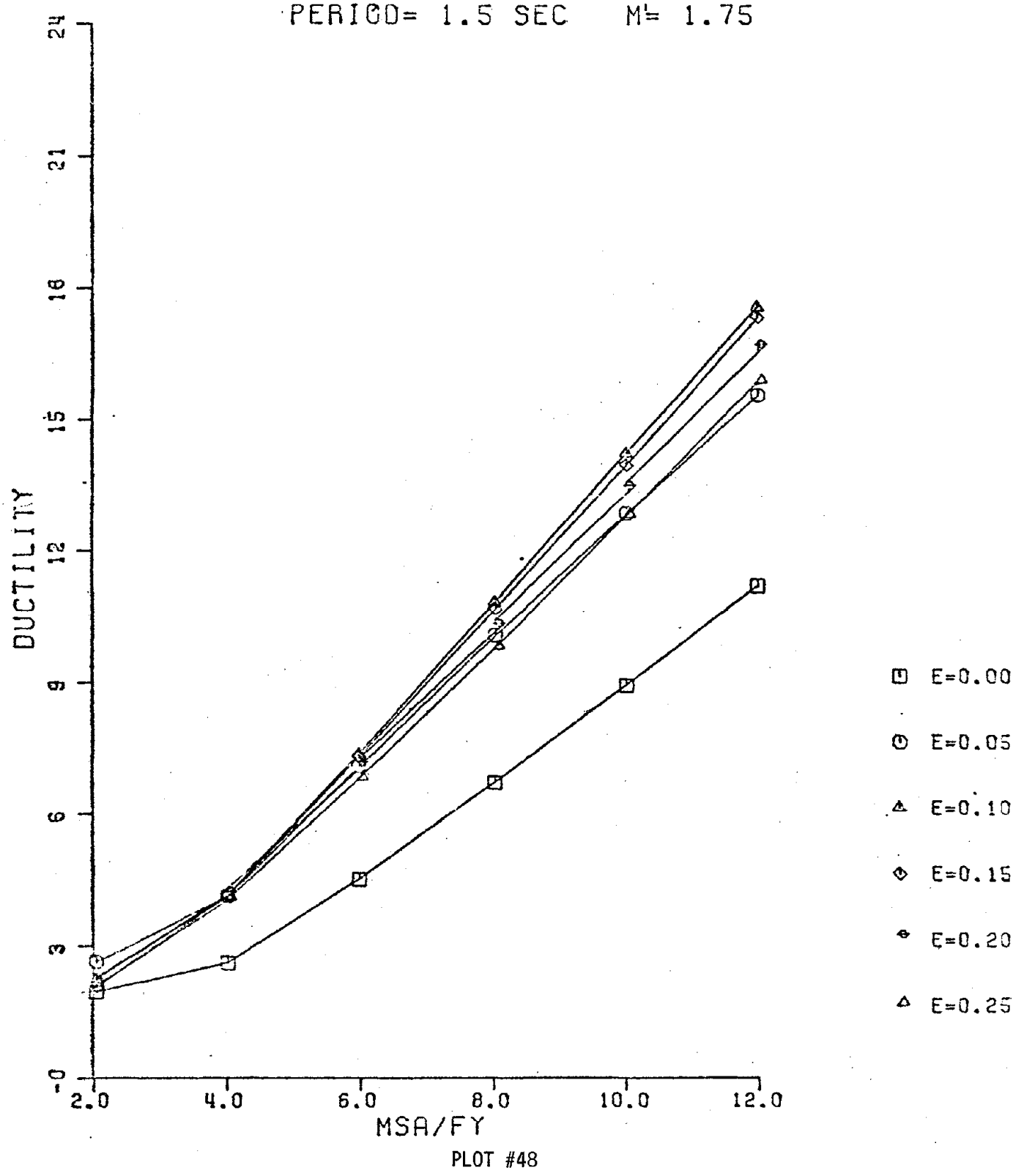

PLOT #48

PACOIMA DAM S16E

PERIOD= 2.0 SEC M= 0.50

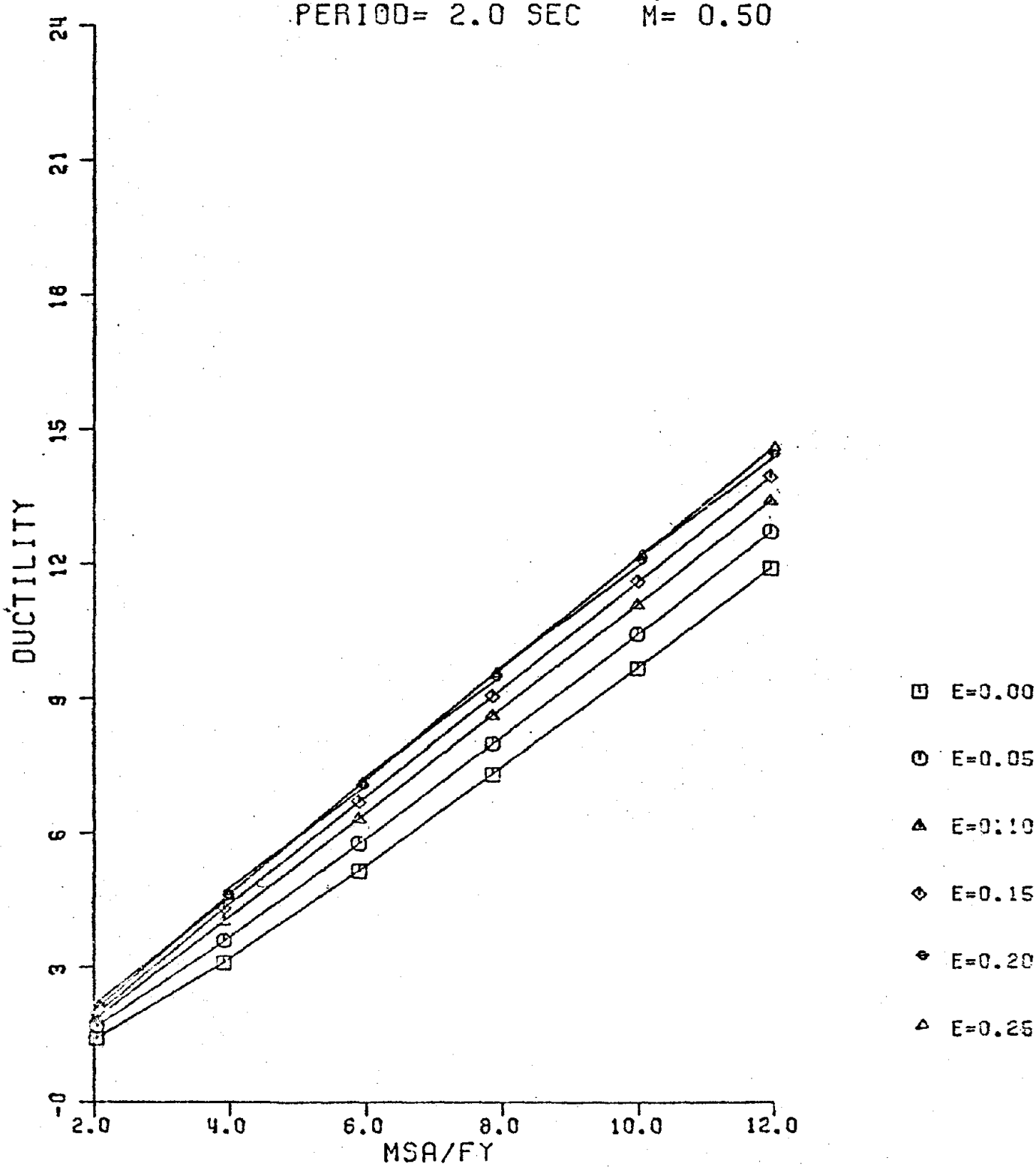

PLOT #49

PACOIMA DAM S16E

PERIOD= 2.0 SEC M'= 0.75

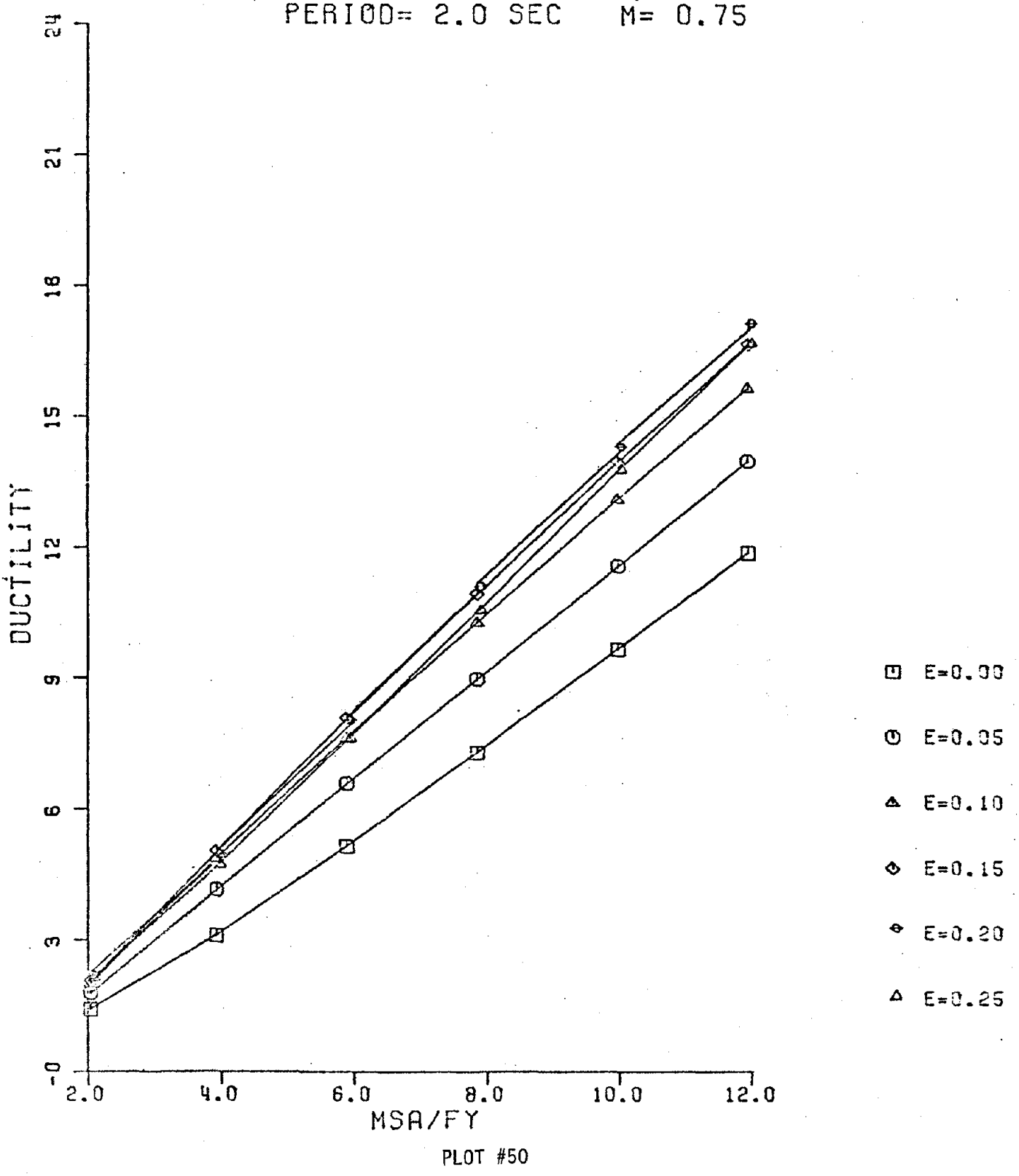

PLOT #50

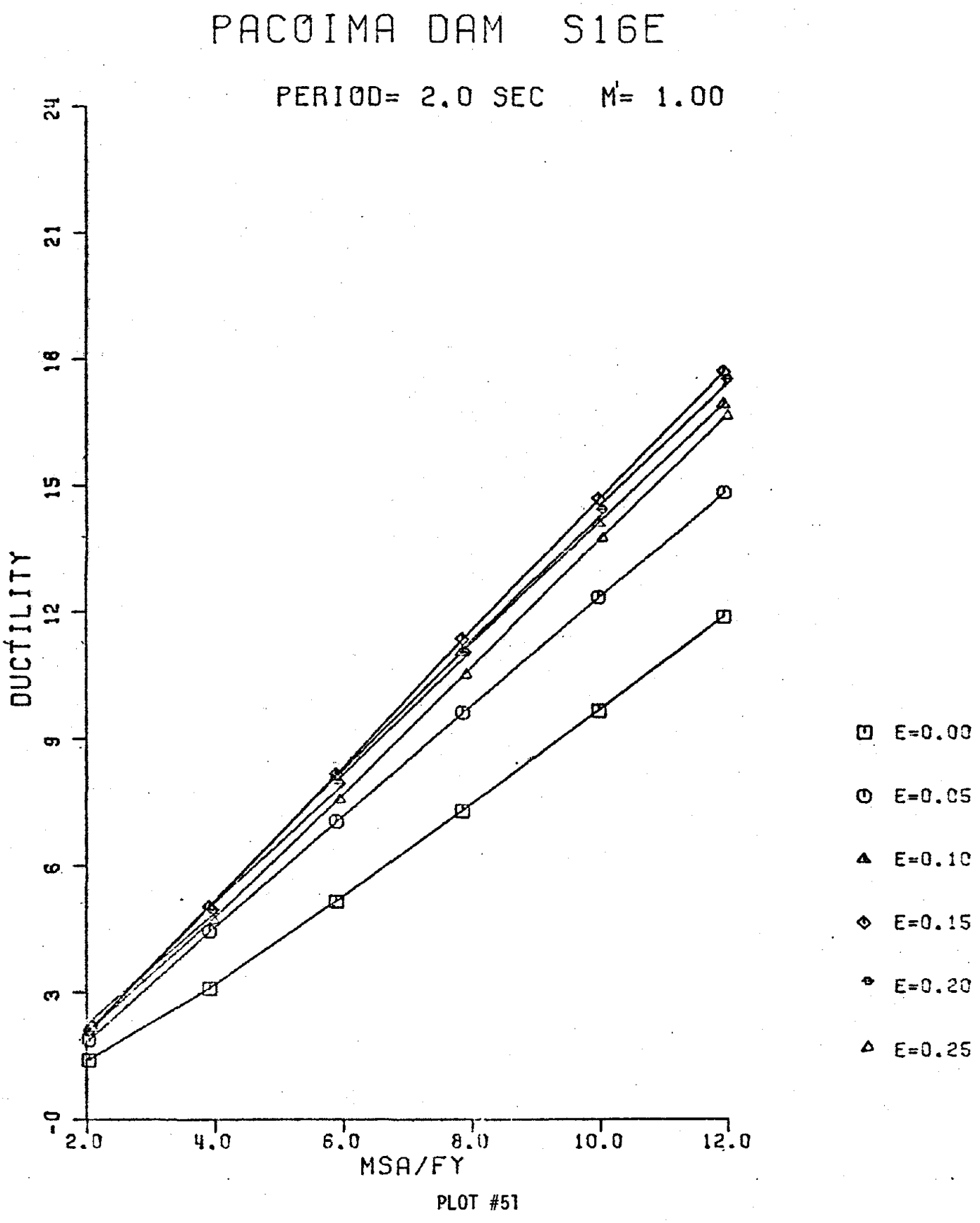
PACOIMA DAM S16E
PERIOD= 2.0 SEC M= 1.00
DUCTILITY
-0
3
6
9
12
15
18
21
24
2.0
4.0
6.0
8.0
10.0
12.0
MSA/FY
E=0.00
E=0.05
E=0.10
E=0.15
E=0.20
E=0.25

PLOT #51

PACOIMA DAM S16E

PERIOD= 2.0 SEC M'= 1.25

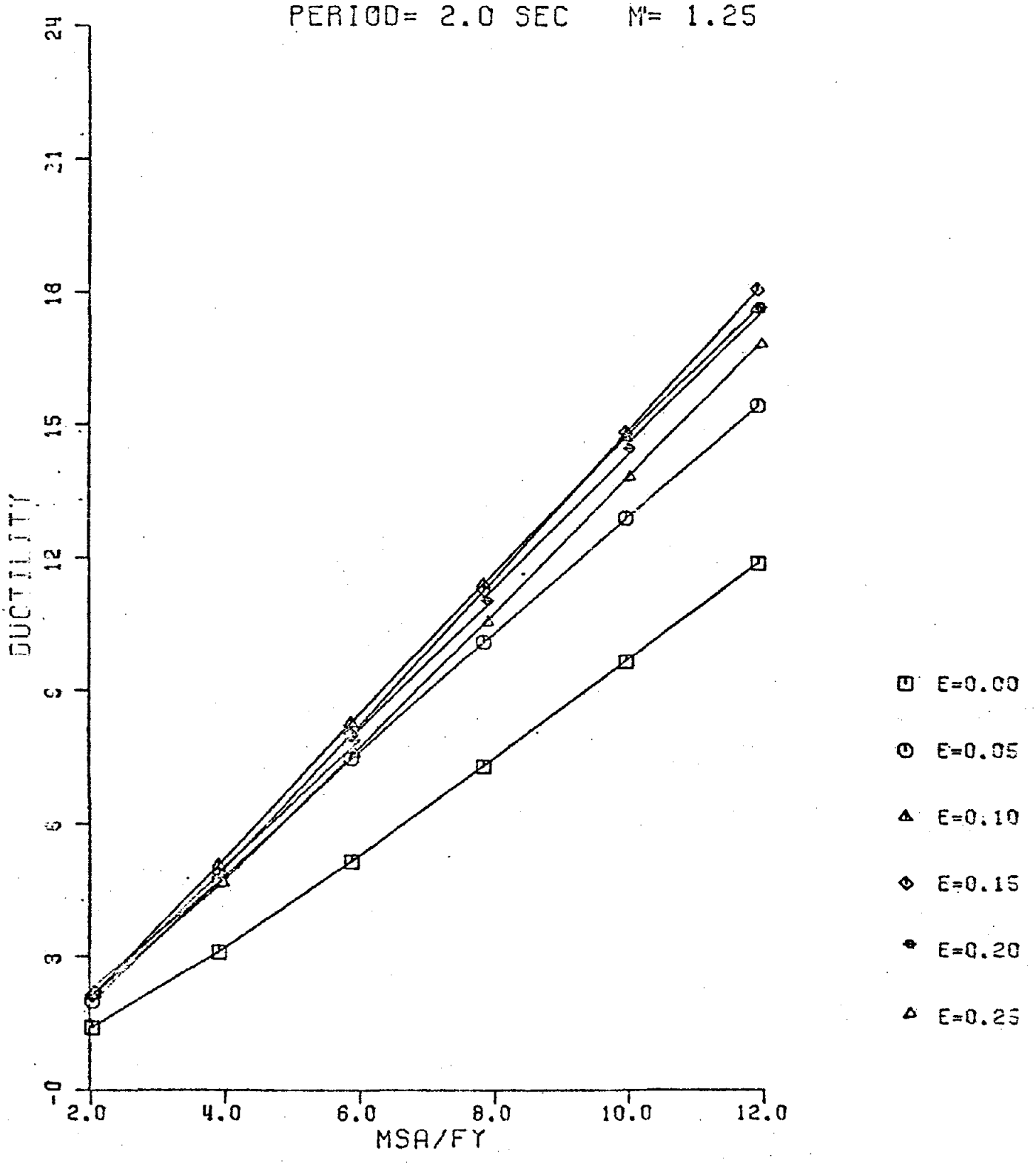

PLOT #52

PACOIMA DAM S16E

PERIOD= 2.0 SEC M= 1.50

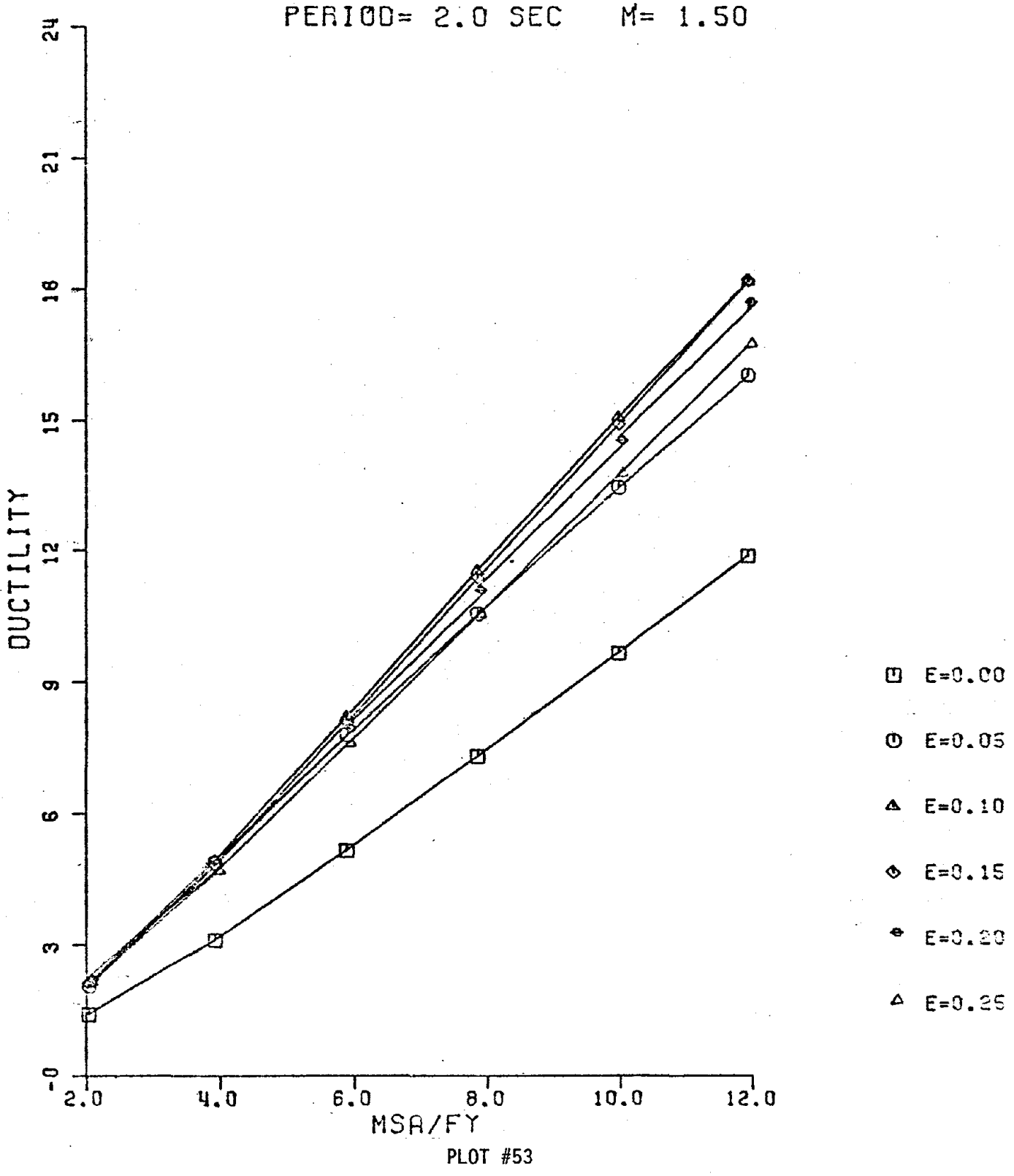

PLOT #53

PACOIMA DAM S16E

PERIOD= 2.0 SEC M= 1.75

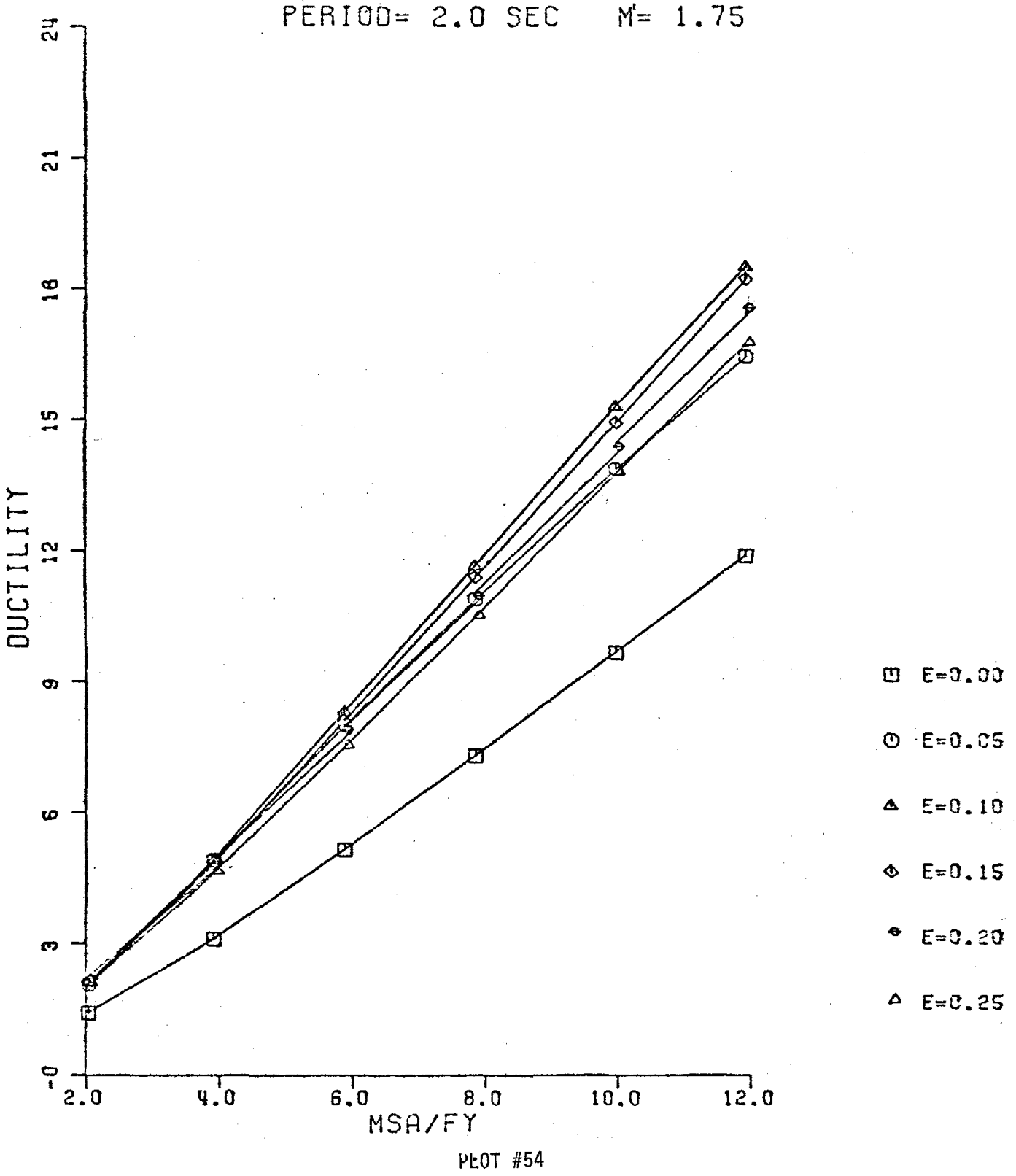

PLOT #54

KERN COUNTY - TAFT 1952 N21E

PLOTS 55 - 78

KERN COUN., TAFT N21E

PERIOD= 0.5 SEC M'= 0.50

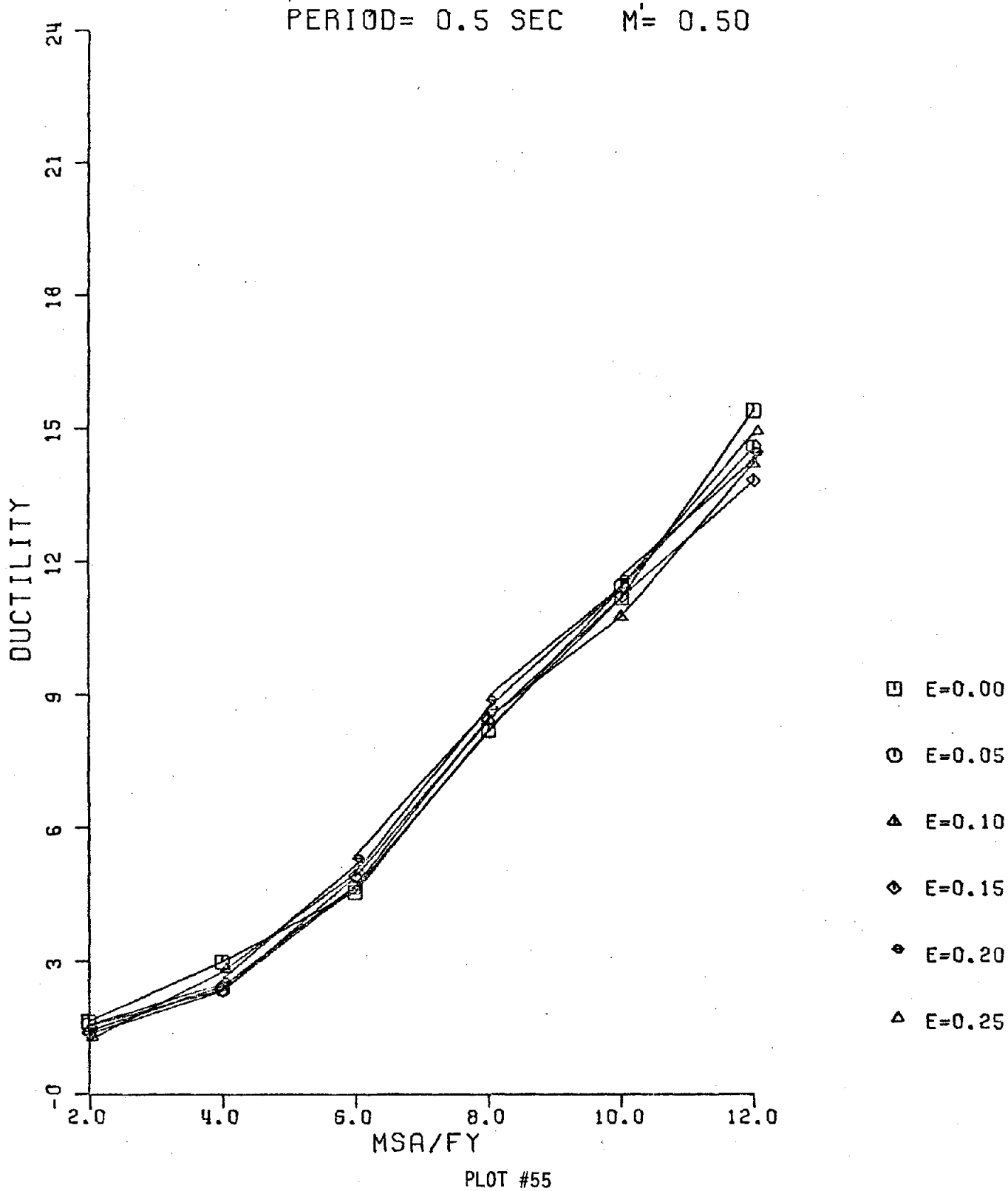

PLOT #55

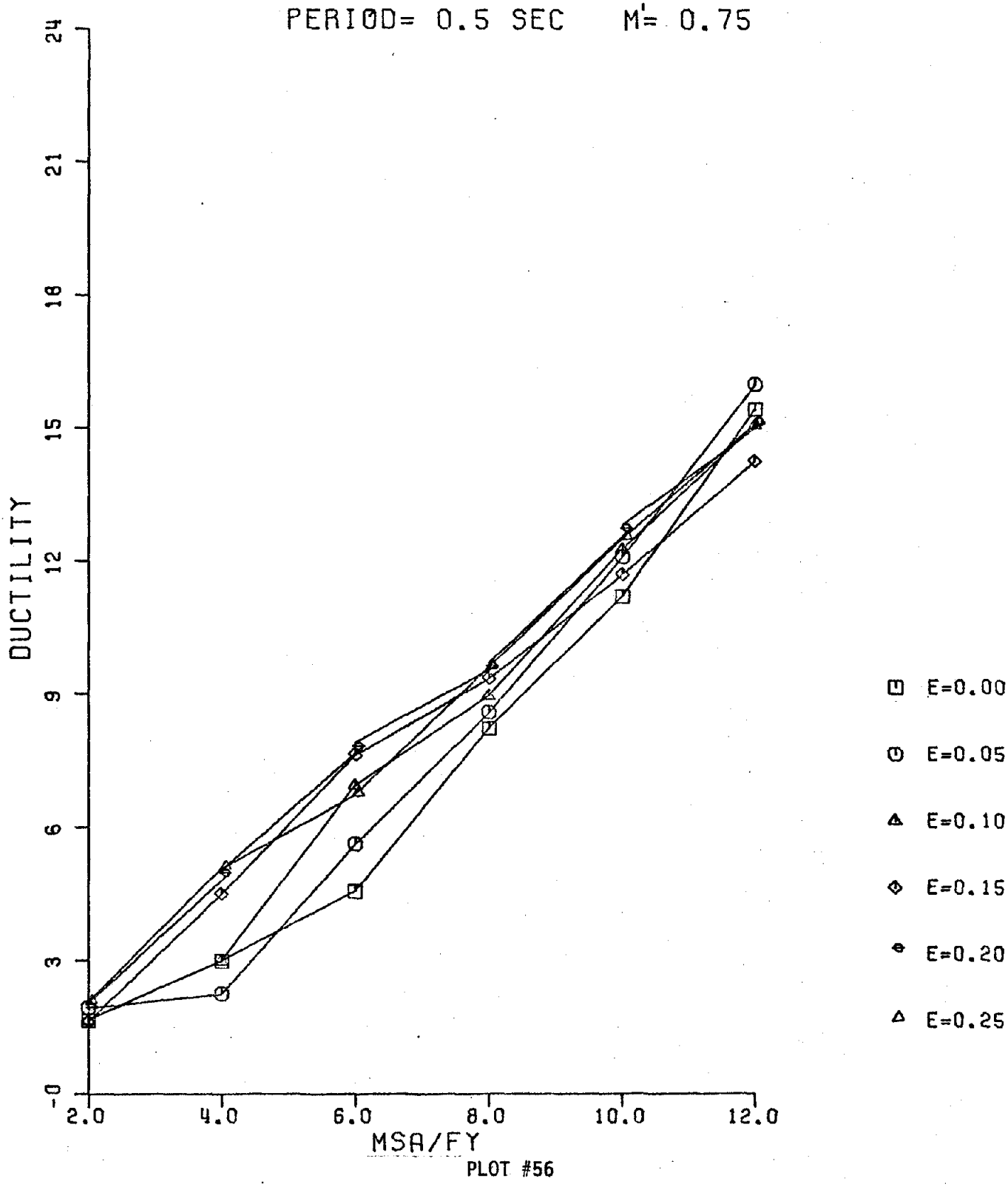
KERN COUN., TAFT N21E
PERIOD= 0.5 SEC M'= 0.75
DUCTILITY
-0
3
6
9
12
15
18
21
24
2.0
4.0
6.0
8.0
10.0
12.0
MSA/FY
PLOT #56
E=0.00
E=0.05
E=0.10
E=0.15
E=0.20
E=0.25

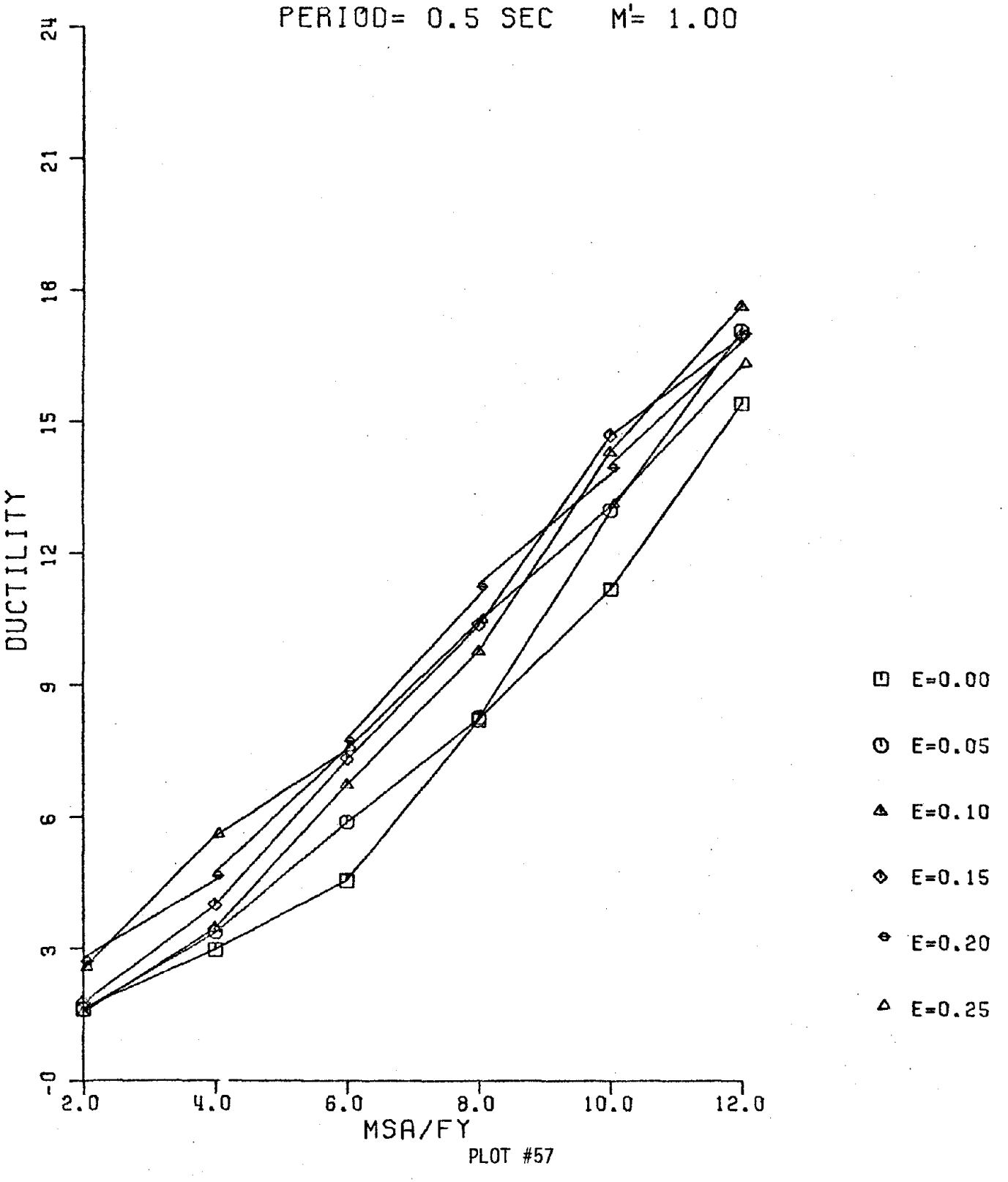
KERN COUN., TAFT N21E
PERIOD= 0.5 SEC M'= 1.00
DUCTILITY
MSA/FY
-0
3
6
9
12
15
18
21
24
2.0
4.0
6.0
8.0
10.0
12.0
E=0.00
E=0.05
E=0.10
E=0.15
E=0.20
E=0.25
PLOT #57

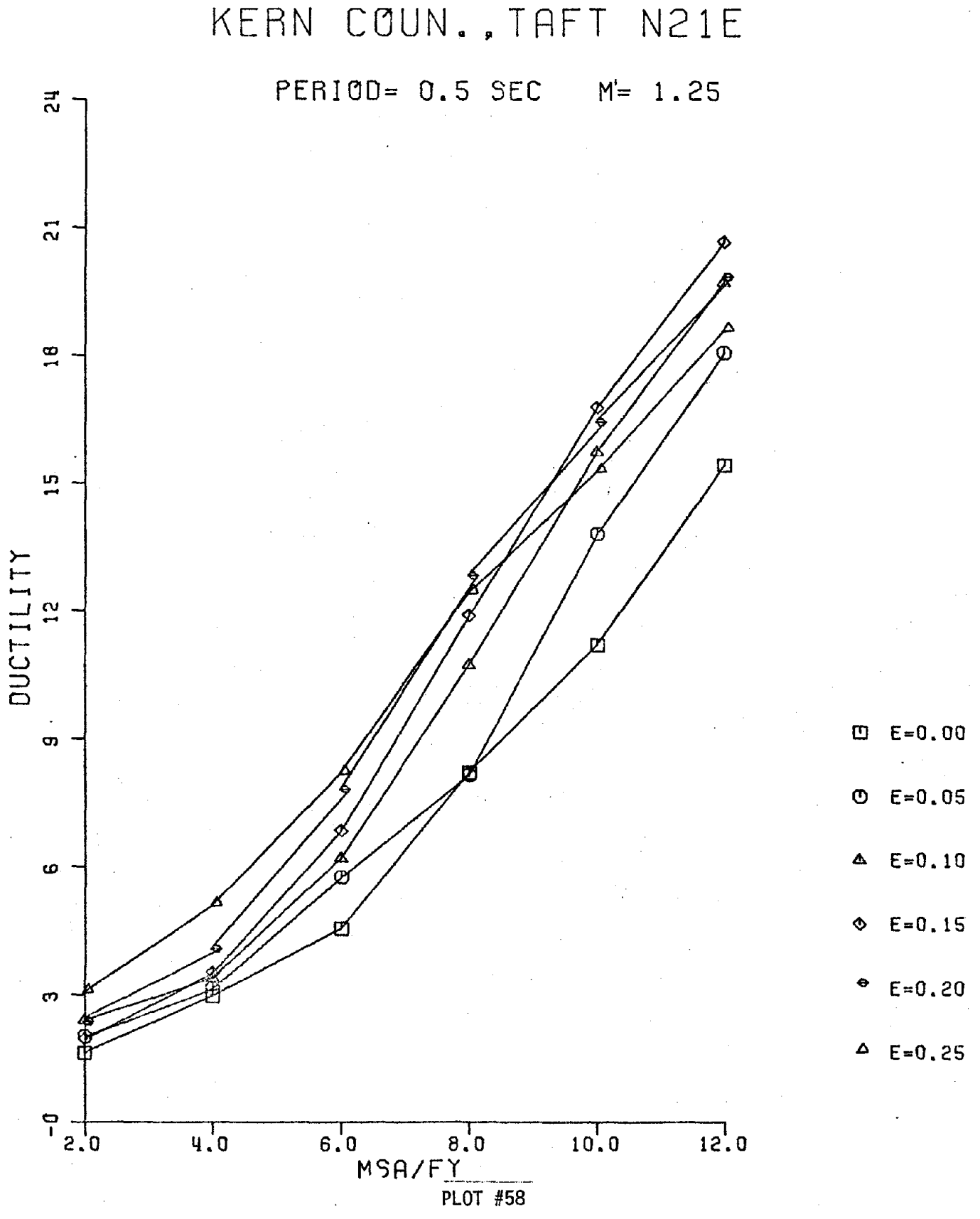
KERN COUN., TAFT N21E
PERIOD= 0.5 SEC M'= 1.25
DUCTILITY
-0
3
6
9
12
15
18
21
24
2.0
4.0
6.0
8.0
10.0
12.0
MSA/FY
PLOT #58
E=0.00
E=0.05
E=0.10
E=0.15
E=0.20
E=0.25

KERN COUN., TAFT N21E

PERIOD= 0.5 SEC M'= 1.50

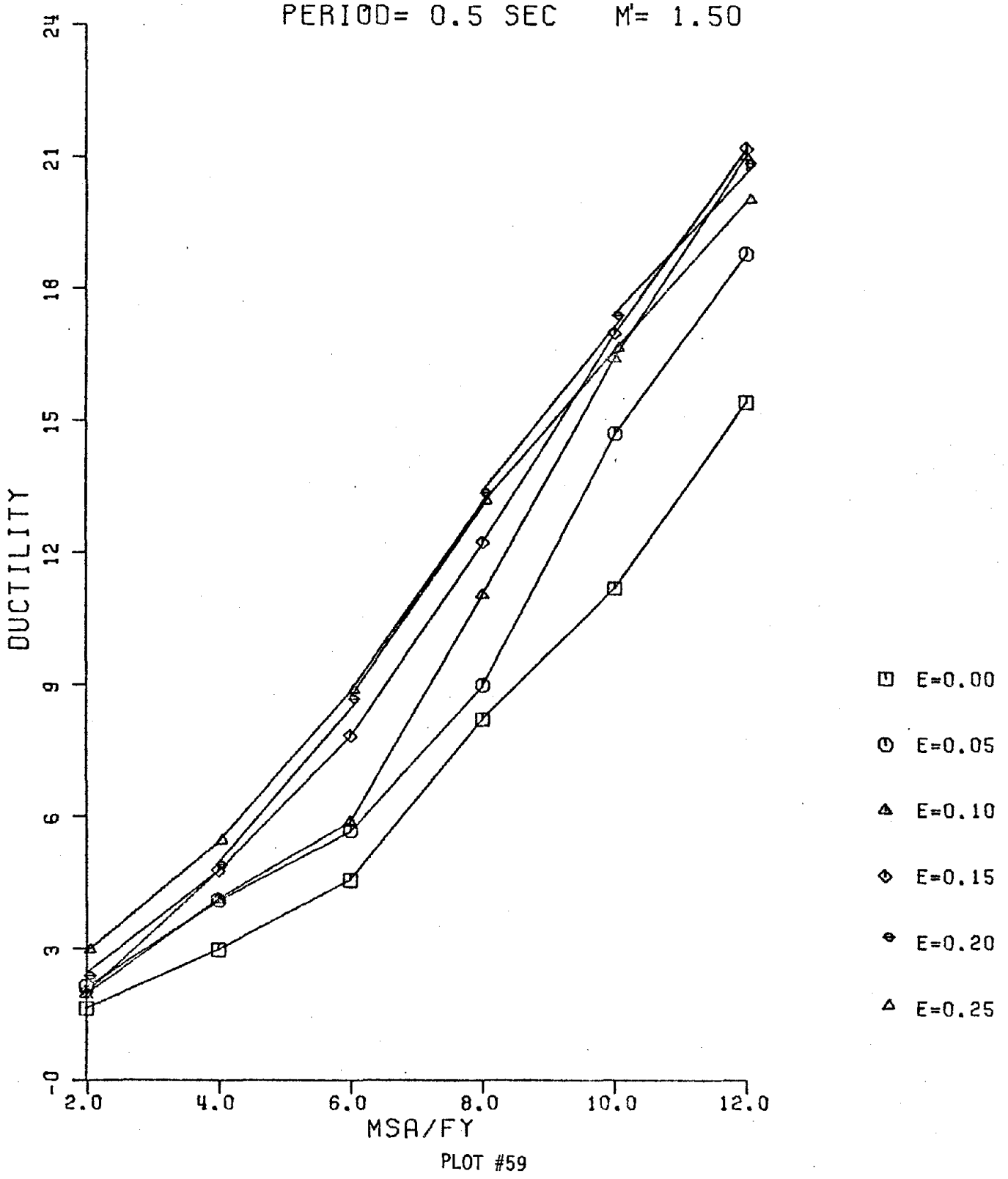

PLOT #59

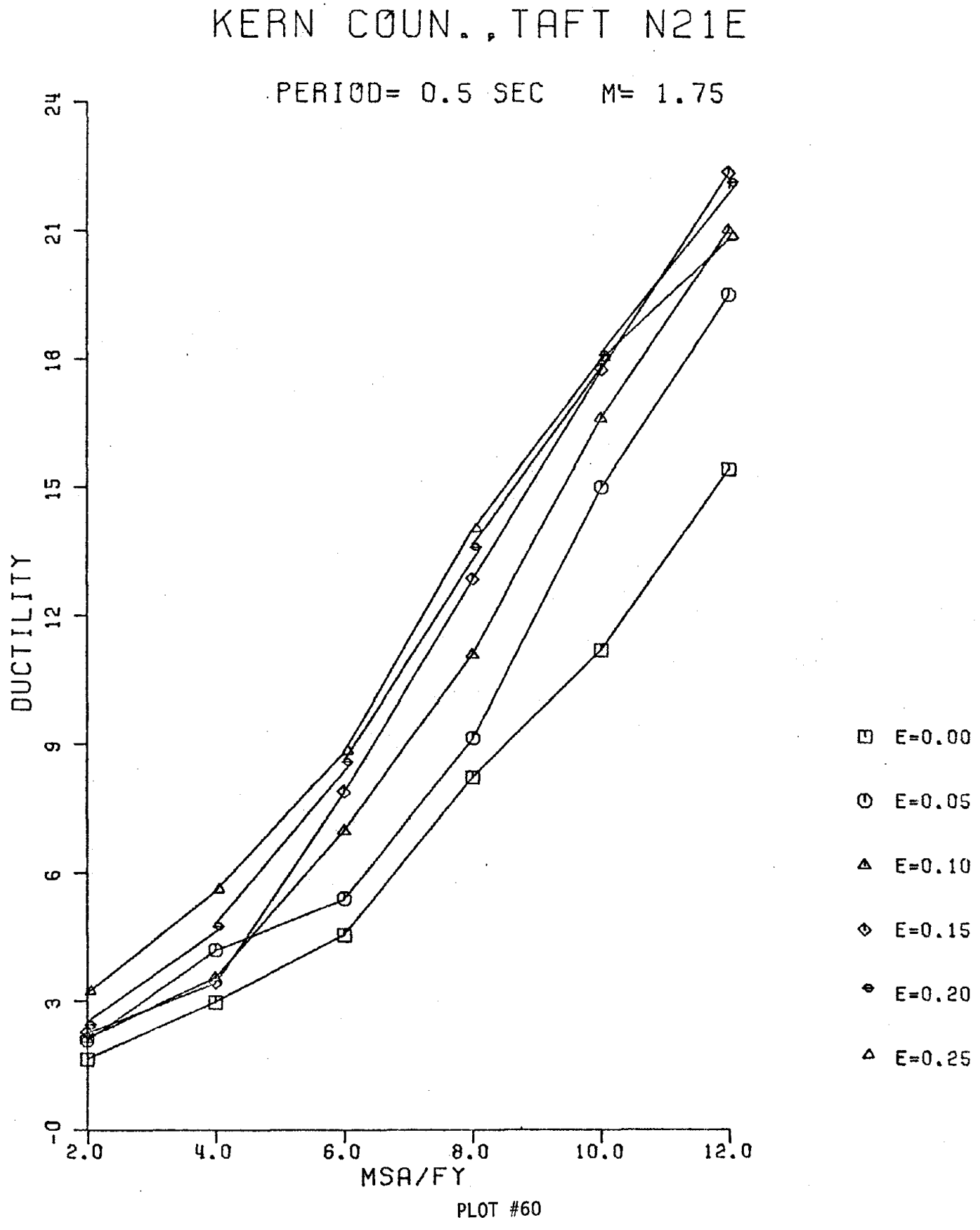
KERN COUN., TAFT N21E
PERIOD= 0.5 SEC M= 1.75
DUCTILITY
MSA/FY
PLOT #60
E=0.00
E=0.05
E=0.10
E=0.15
E=0.20
E=0.25

KERN COUN., TAFT N21E

PERIOD= 1.0 SEC M'= 0.50

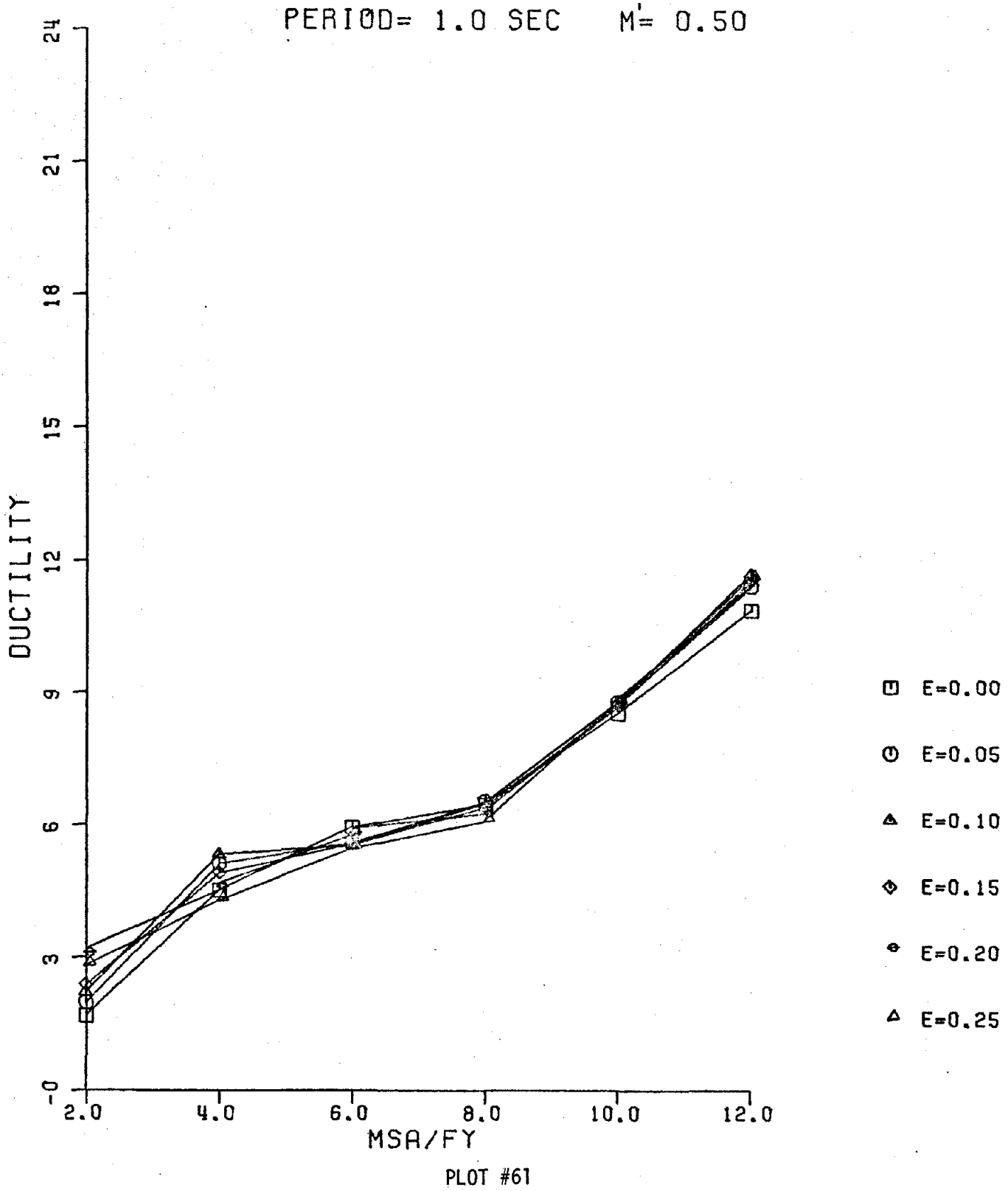

PLOT #61

KERN COUN., TAFT N21E

PERIOD= 1.0 SEC M= 0.75

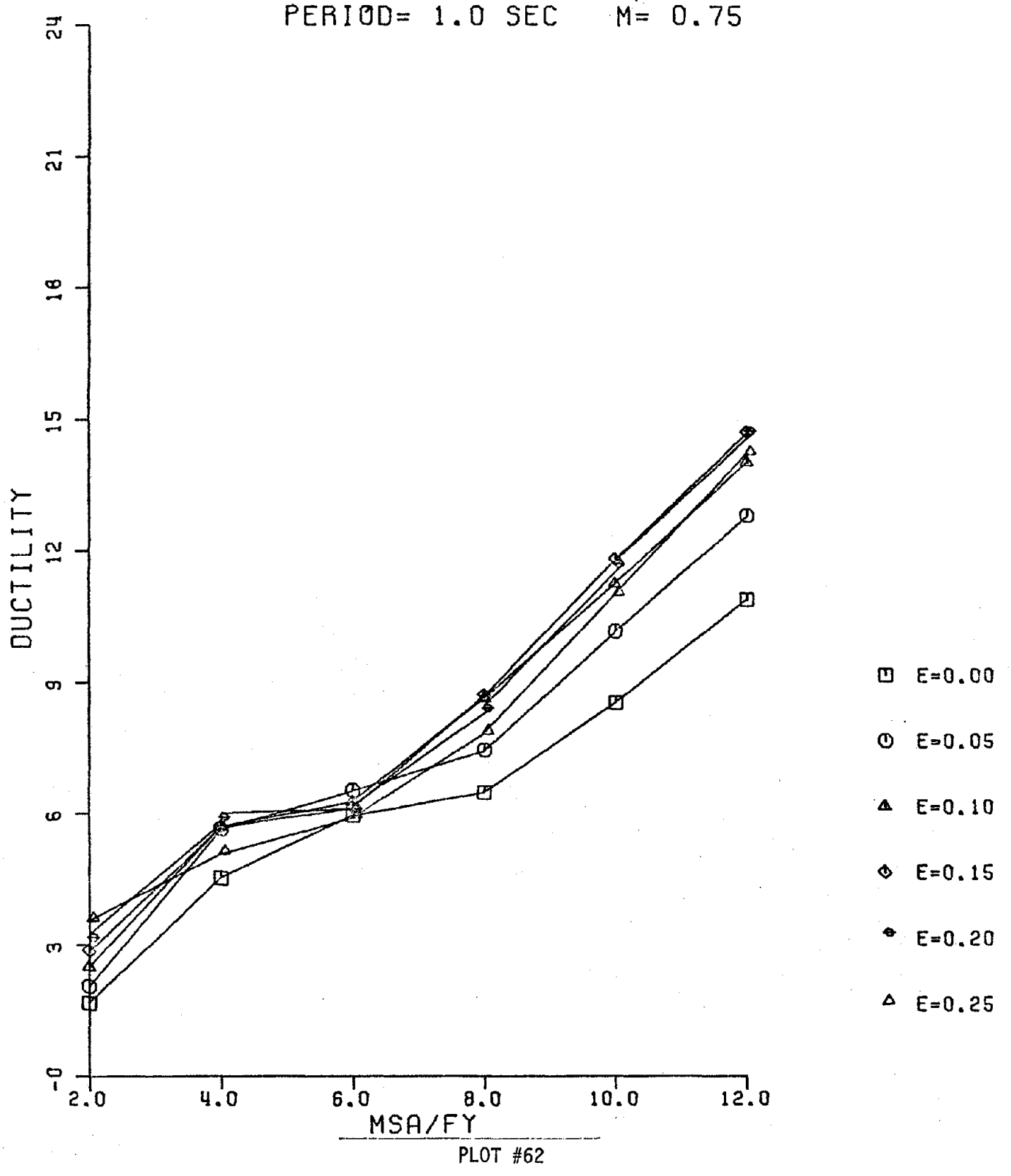

PLOT #62

KERN COUN., TAFT N21E

PERIOD= 1.0 SEC M'= 1.00

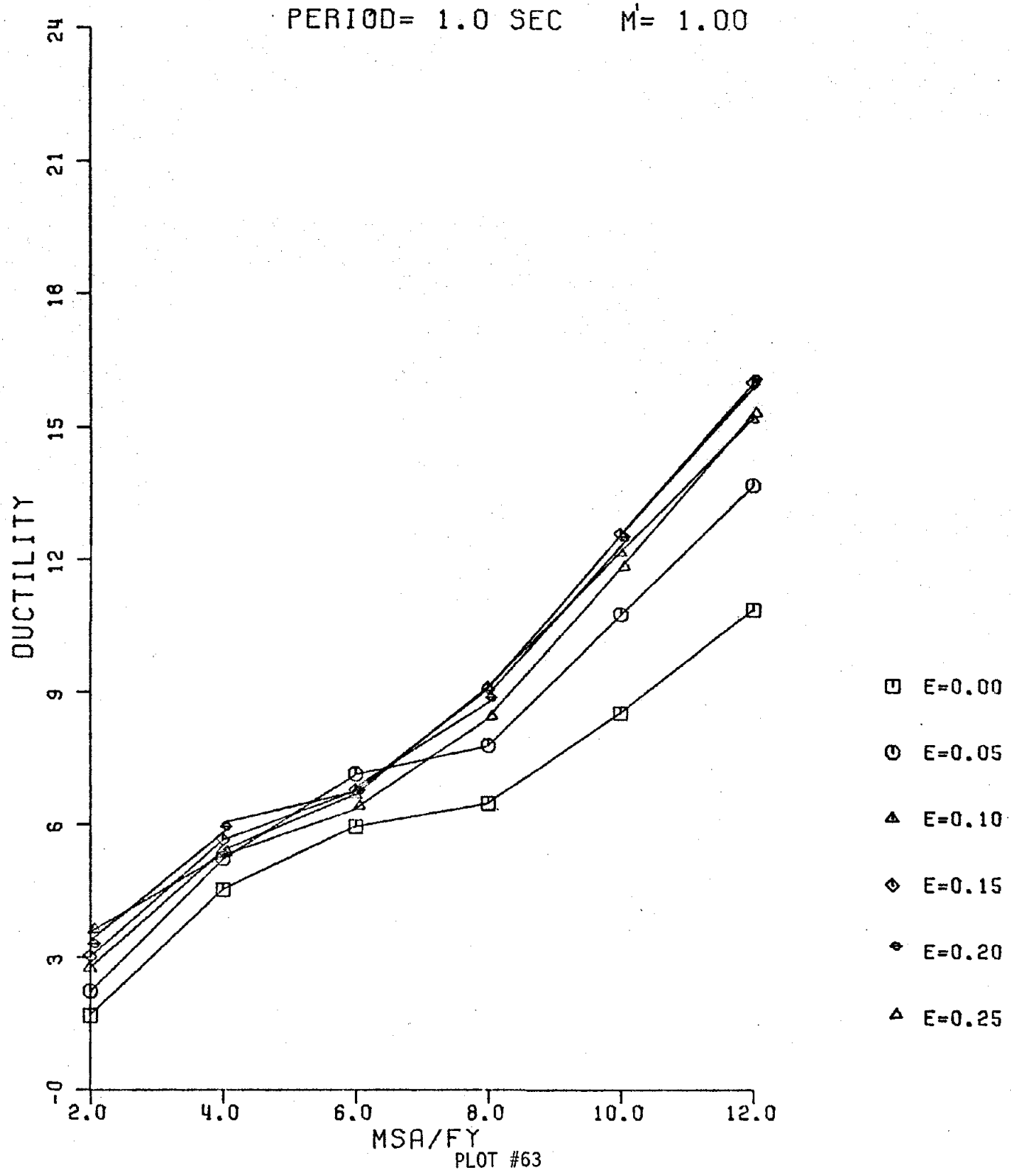

PLOT #63

KERN COUN., TAFT N21E

PERIOD= 1.0 SEC M'= 1.25

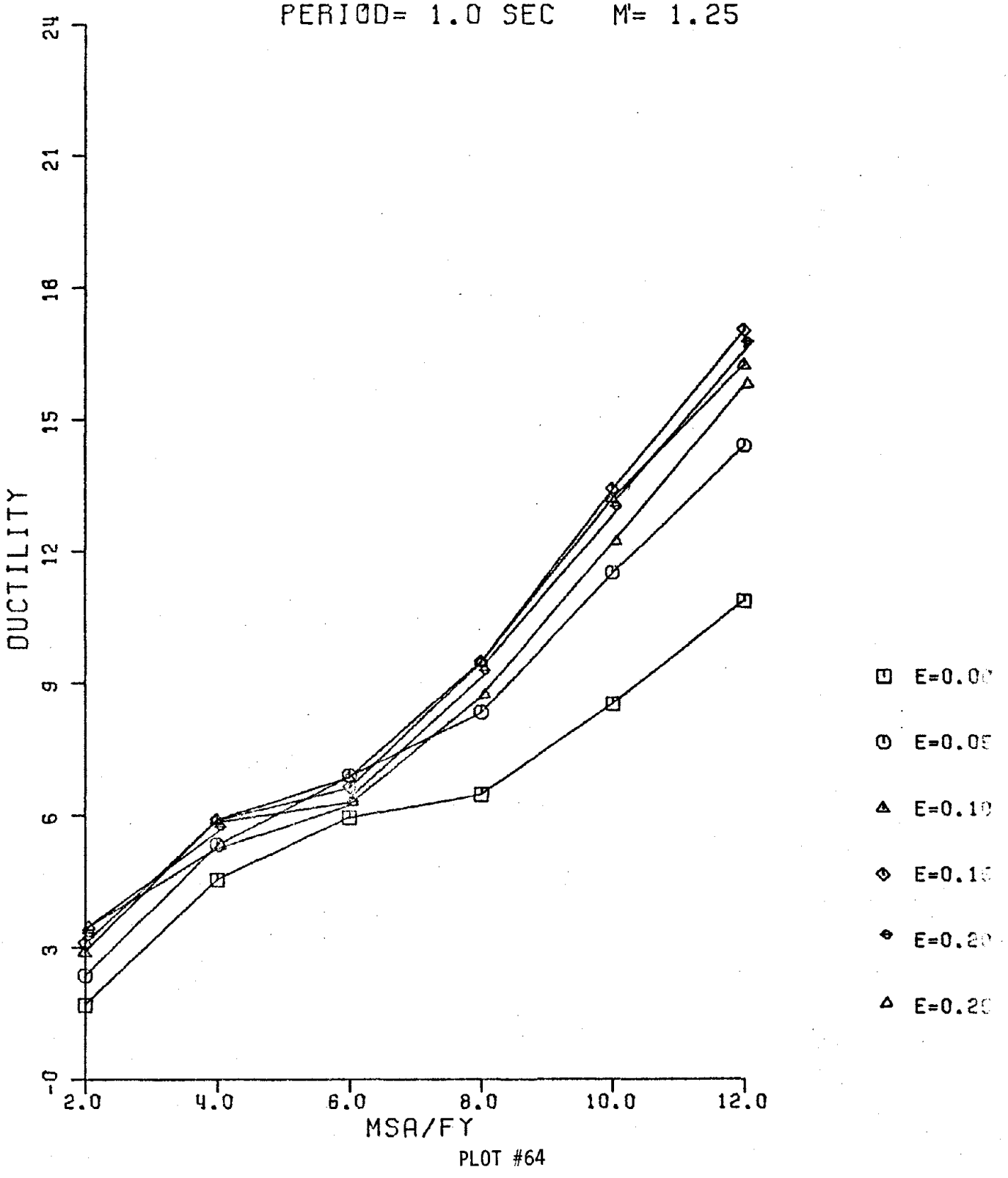

PLOT #64

KERN COUN., TAFT N21E

PERIOD= 1.0 SEC M'= 1.50

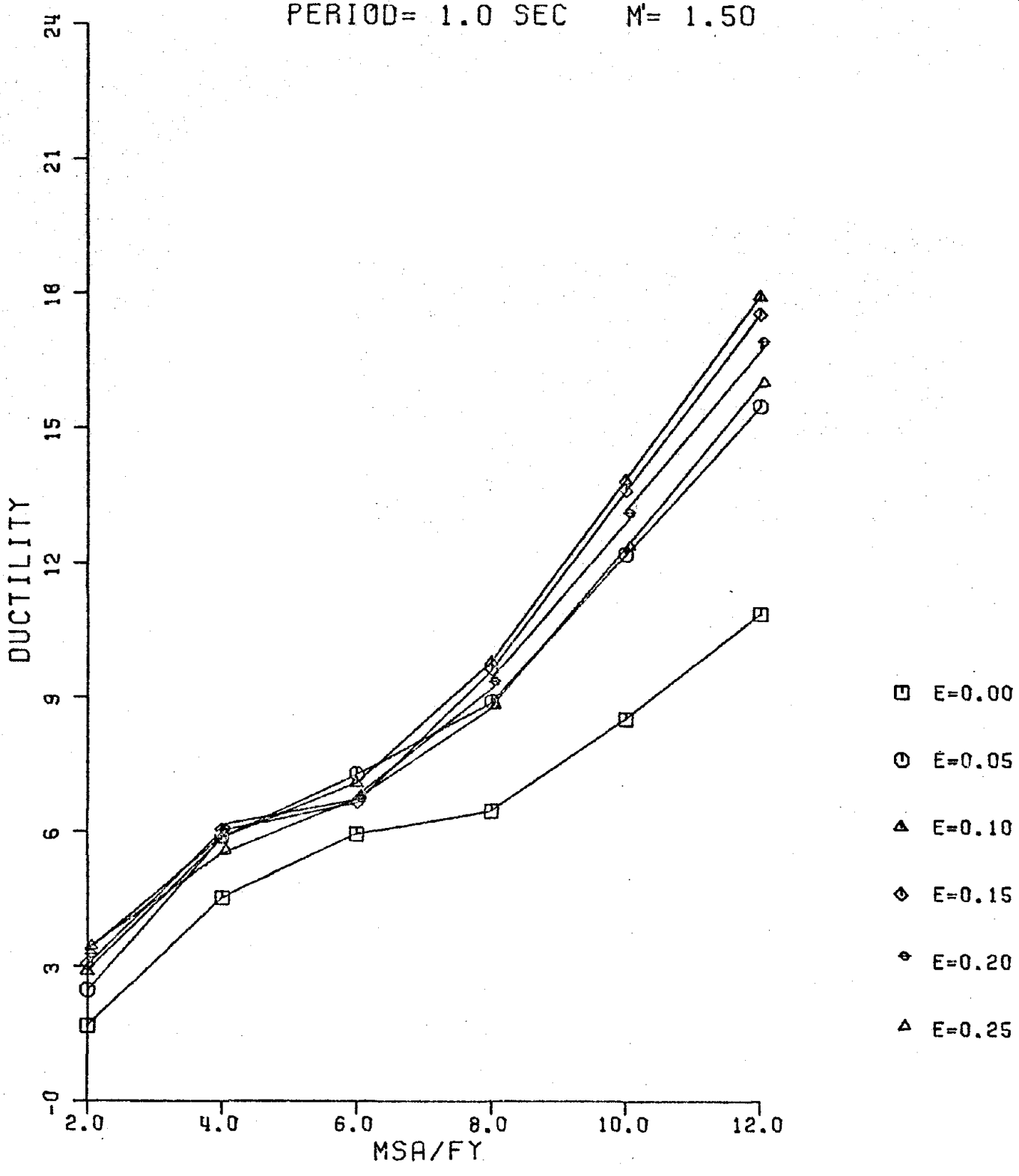

PLOT #65

KERN COUN., TAFT N21E

PERIOD= 1.0 SEC M'= 1.75

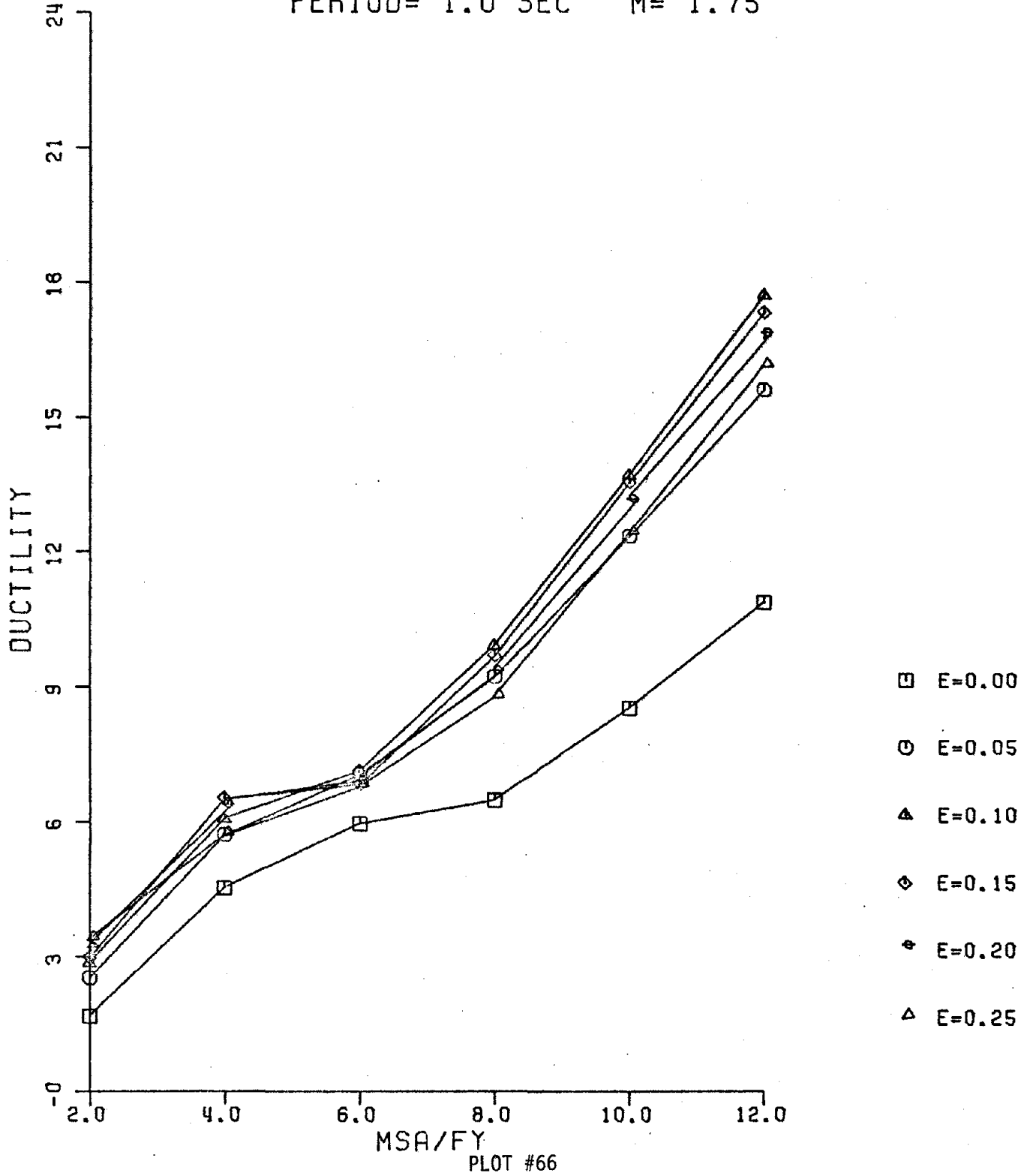

PLOT #66

KERN COUN., TAFT N21E

PERIOD= 1.5 SEC M= 0.50

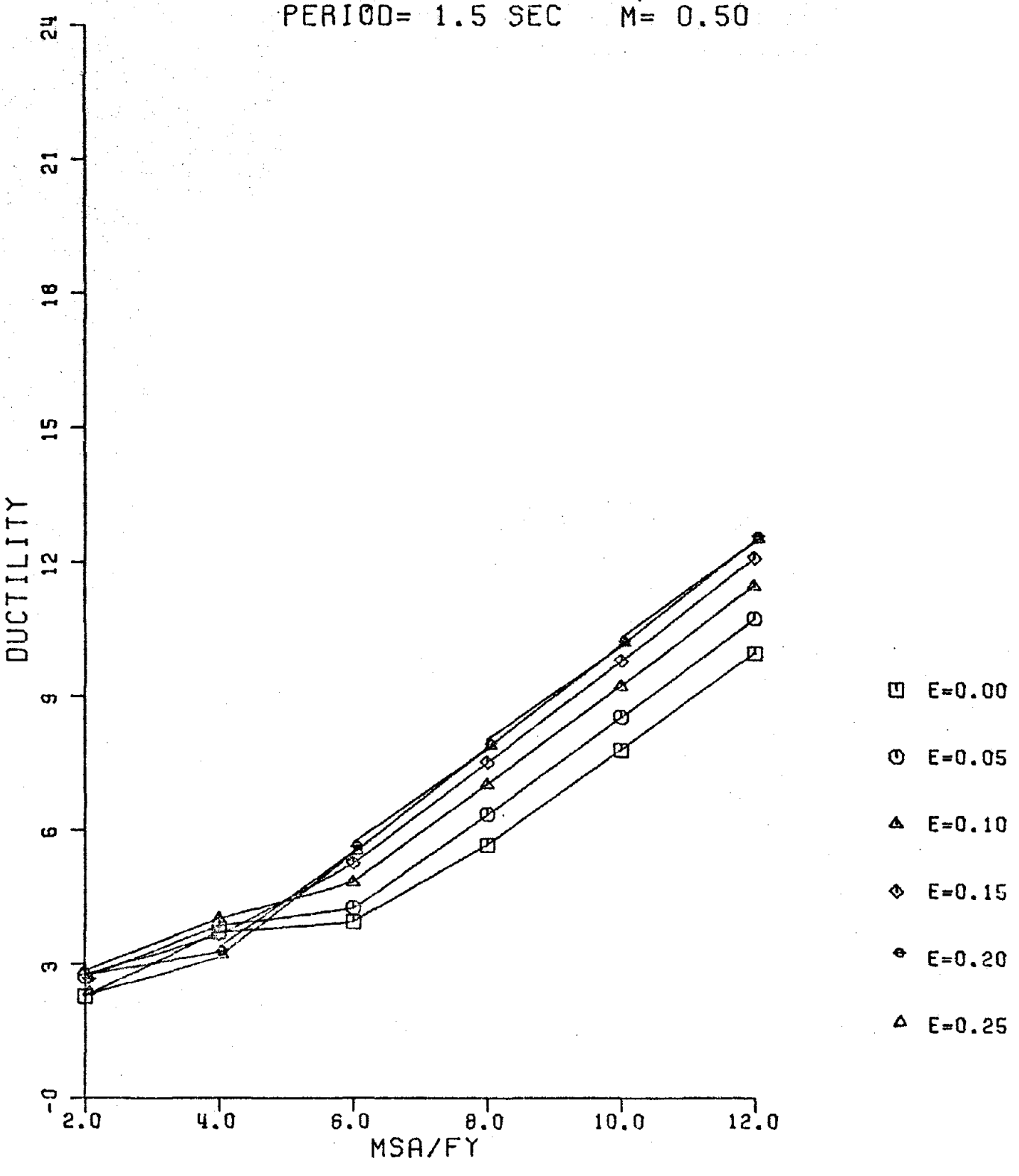

PLOT #67

KERN COUN., TAFT N21E

PERIOD= 1.5 SEC M'= 0.75

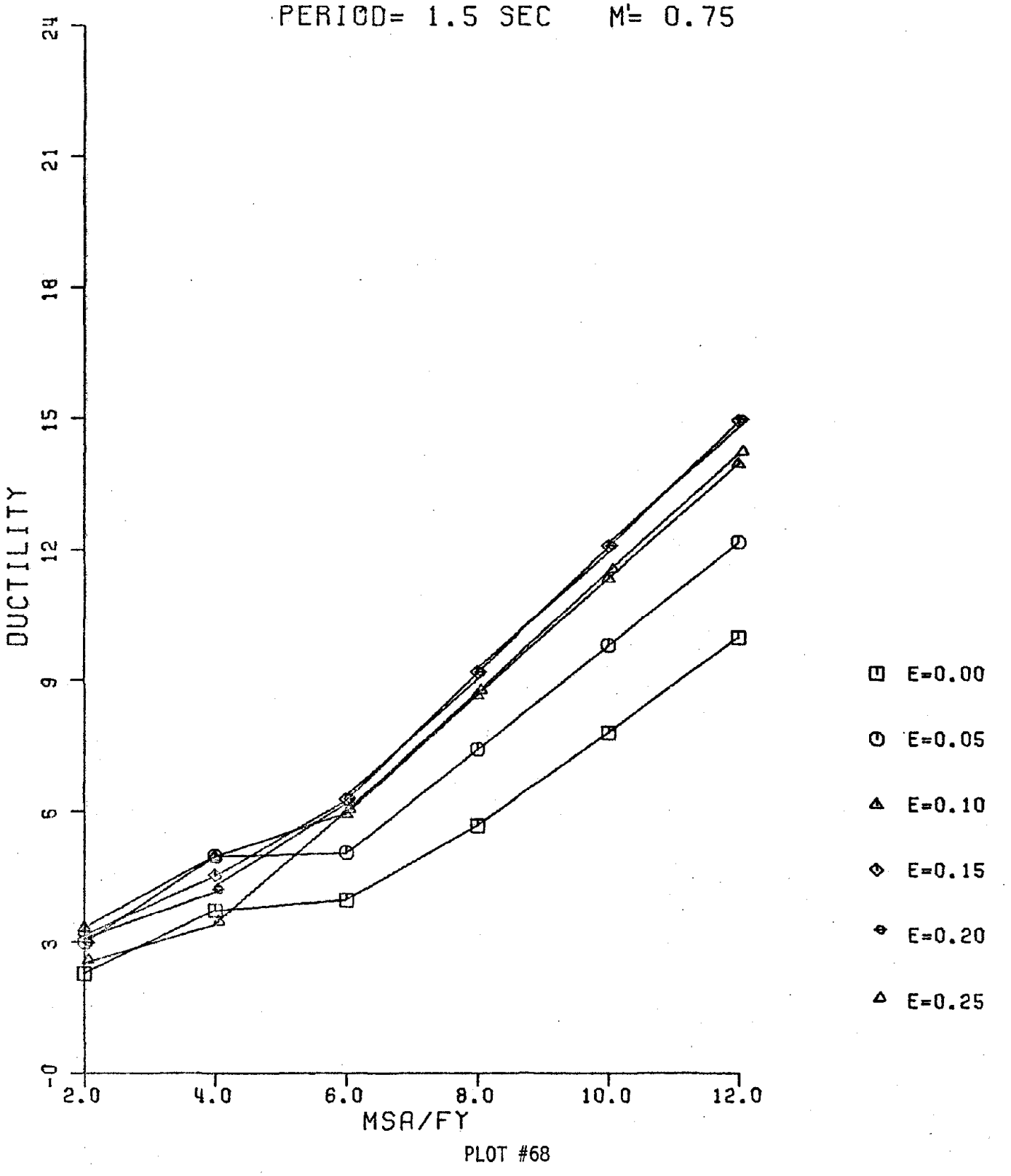

PLOT #68

KERN COUN., TAFT N21E

PERIOD= 1.5 SEC M= 1.00

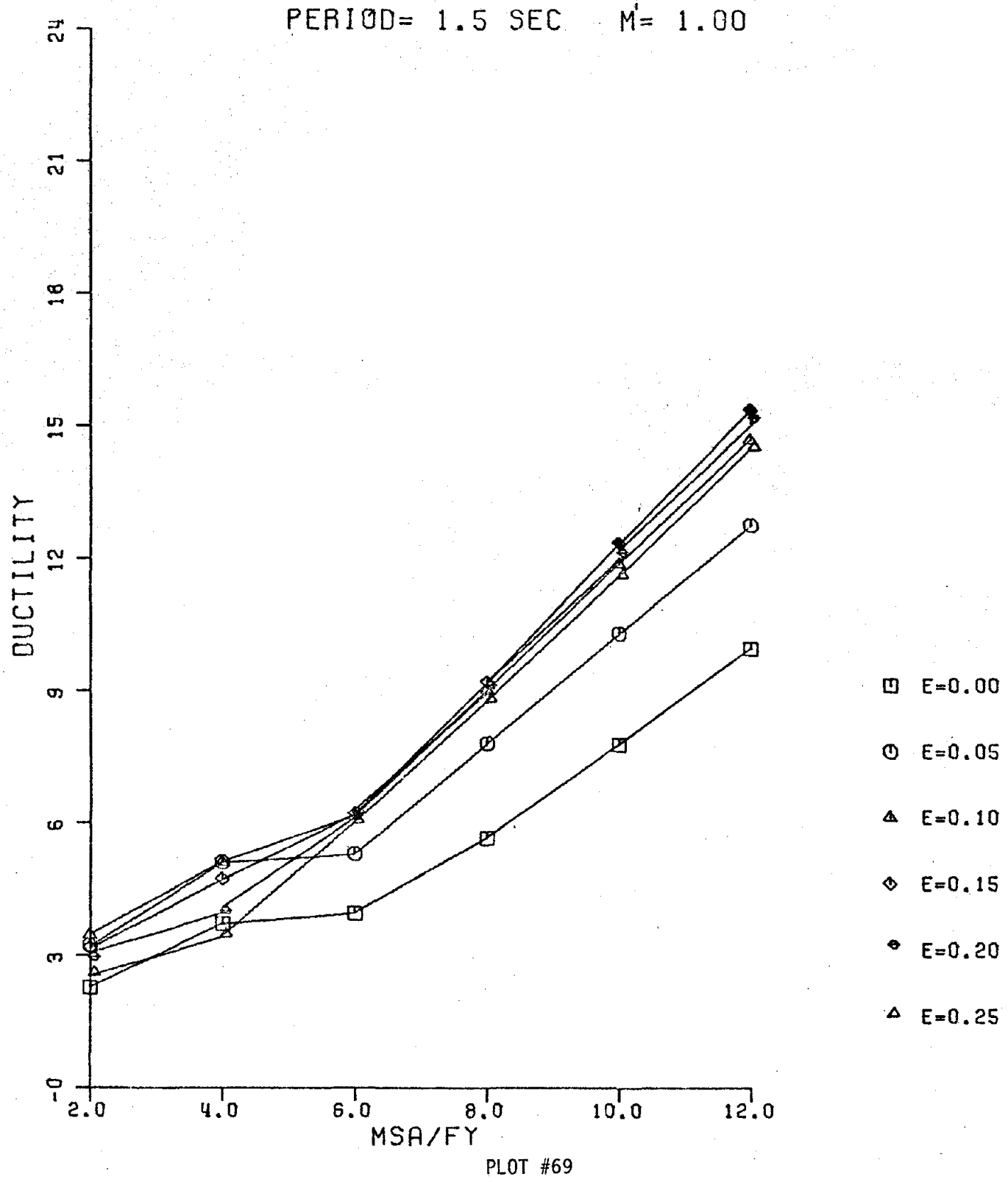

PLOT #69

KERN COUN., TAFT N21E

PERIOD= 1.5 SEC M'= 1.25

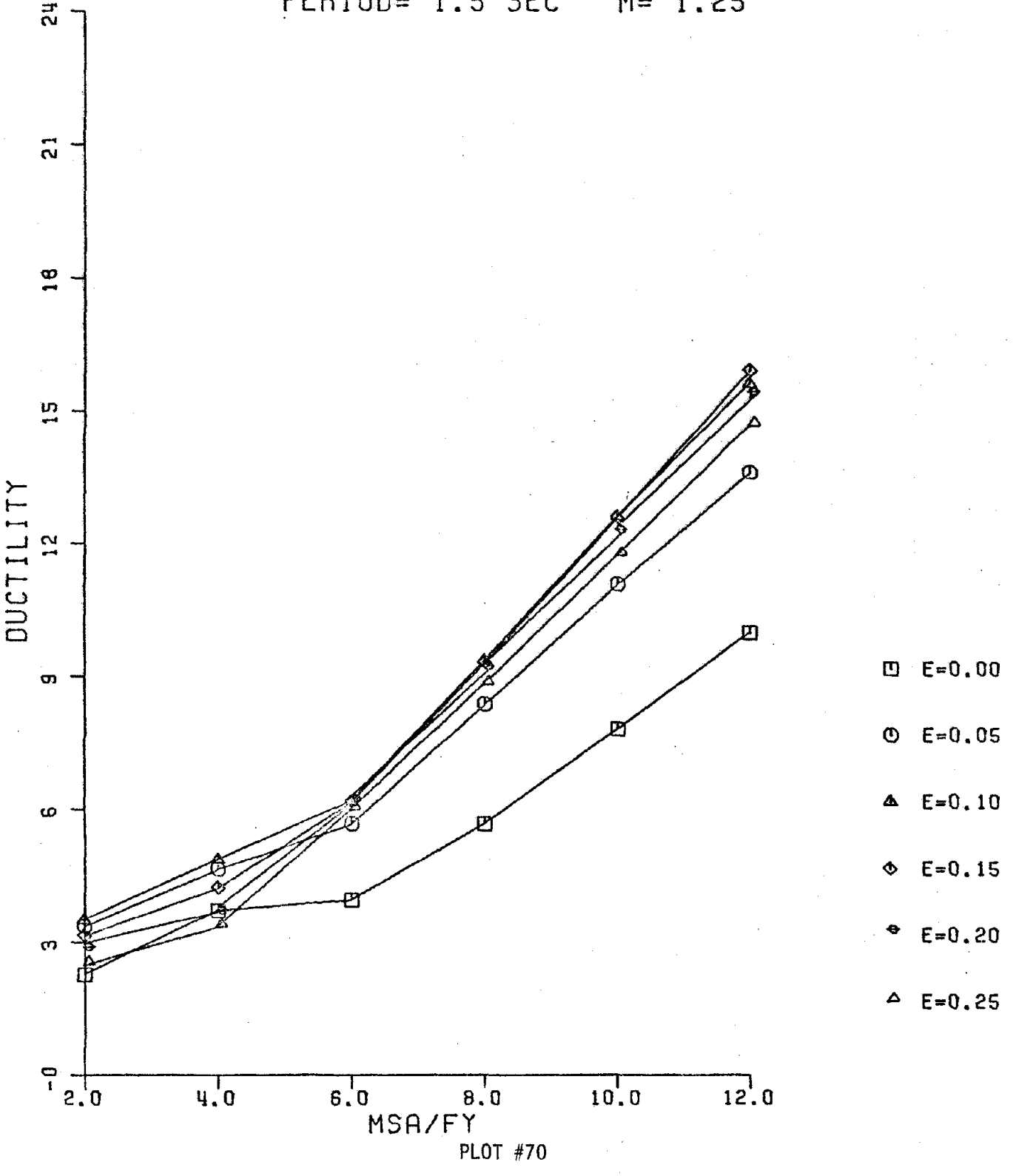

PLOT #70

KERN COUN., TAFT N21E

PERIOD= 1.5 SEC M'= 1.50

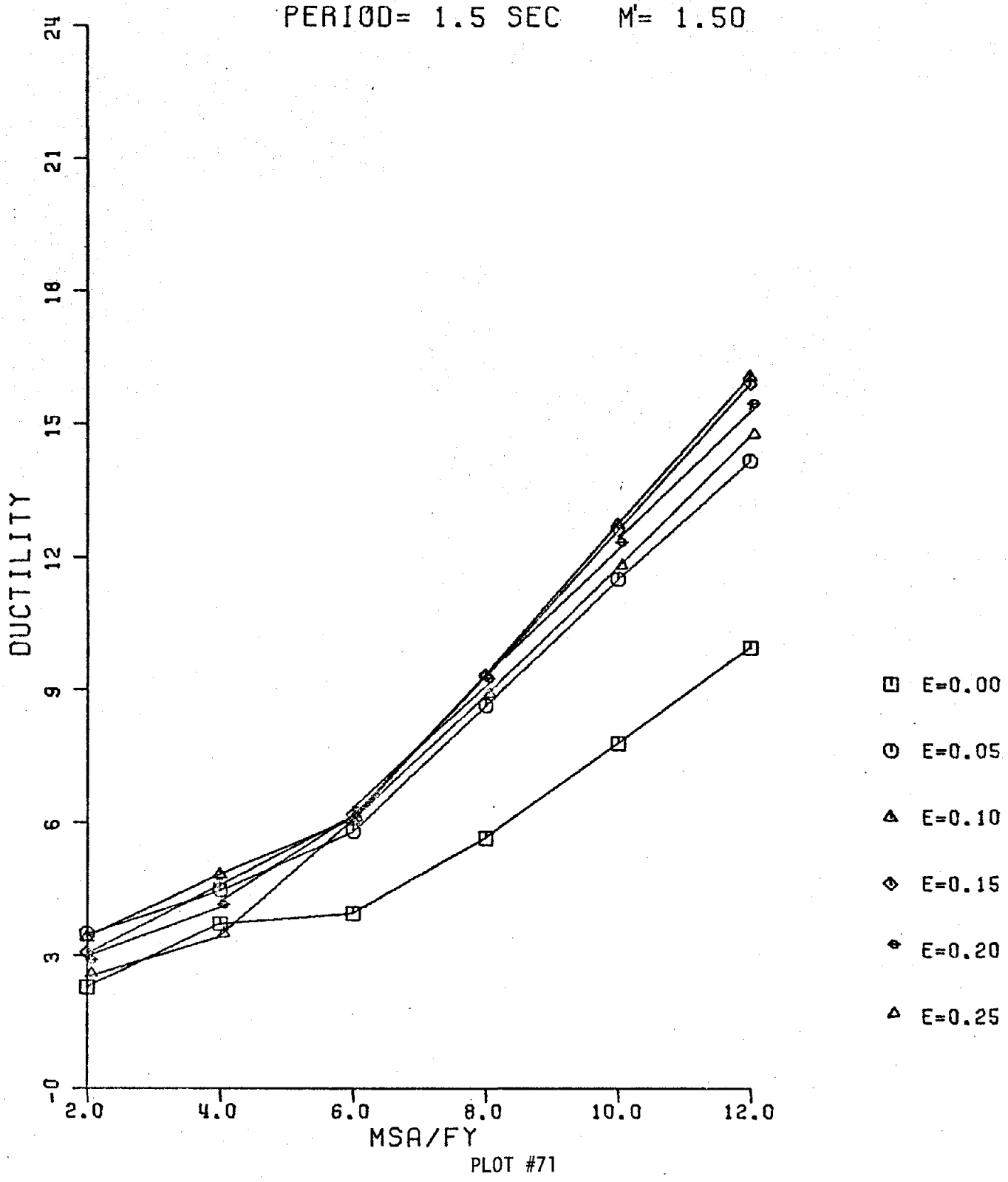

PLOT #71

KERN COUN., TAFT N21E

PERIOD= 1.5 SEC M= 1.75

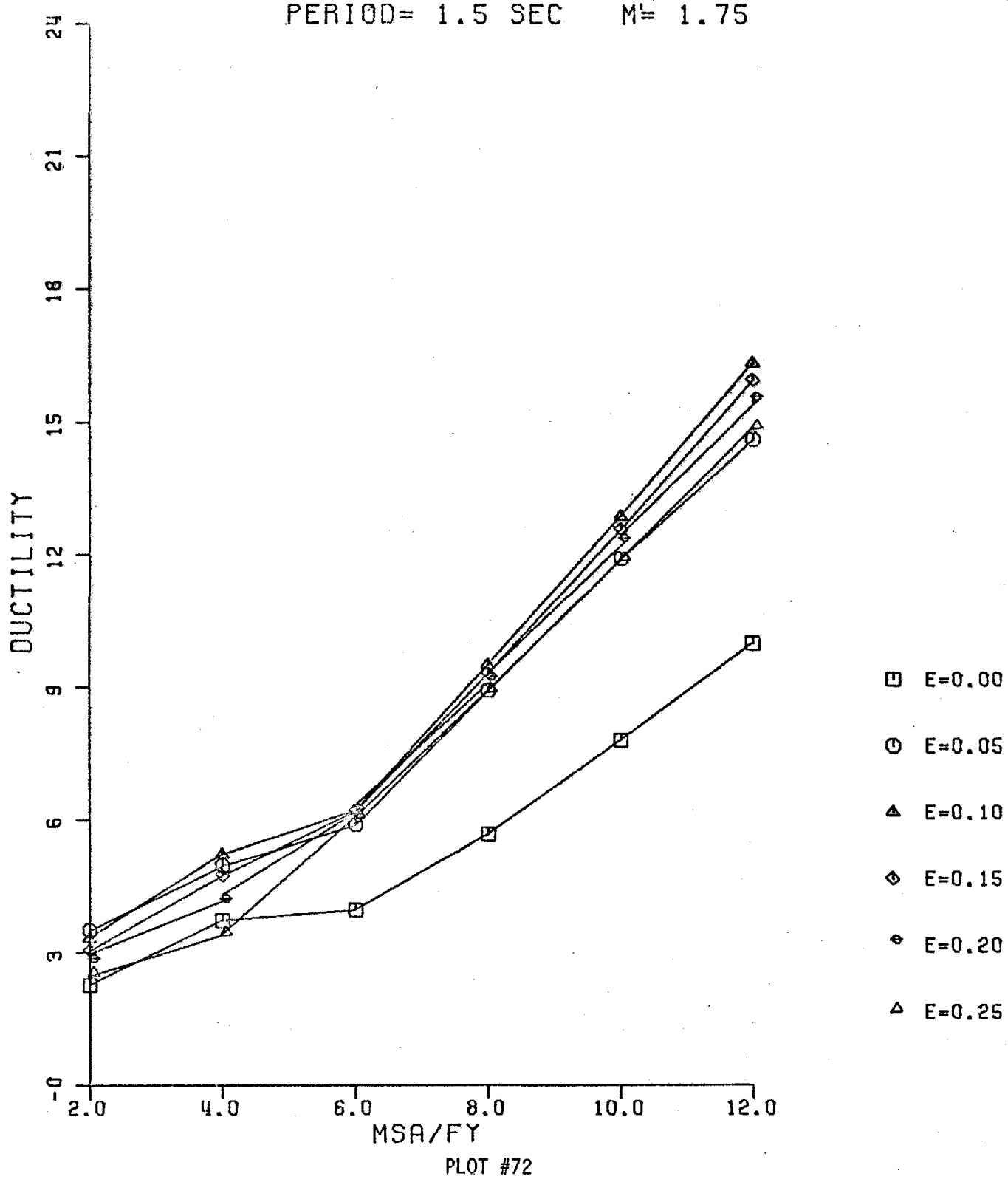

PLOT #72

KERN COUN., TAFT N21E

PERIOD= 2.0 SEC M'= 0.50

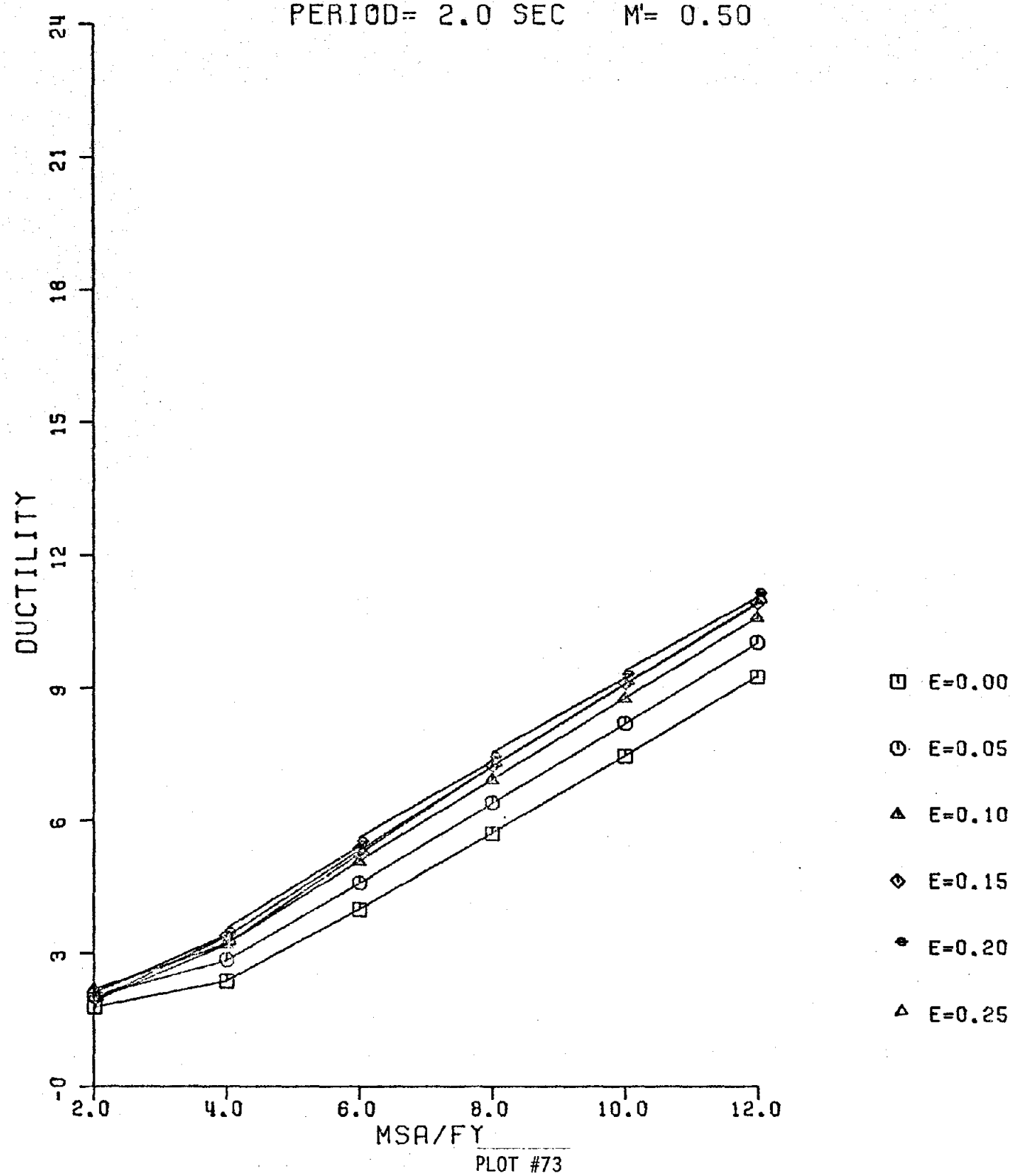

PLOT #73

KERN COUN., TAFT N21E

PERIOD= 2.0 SEC M'= 0.75

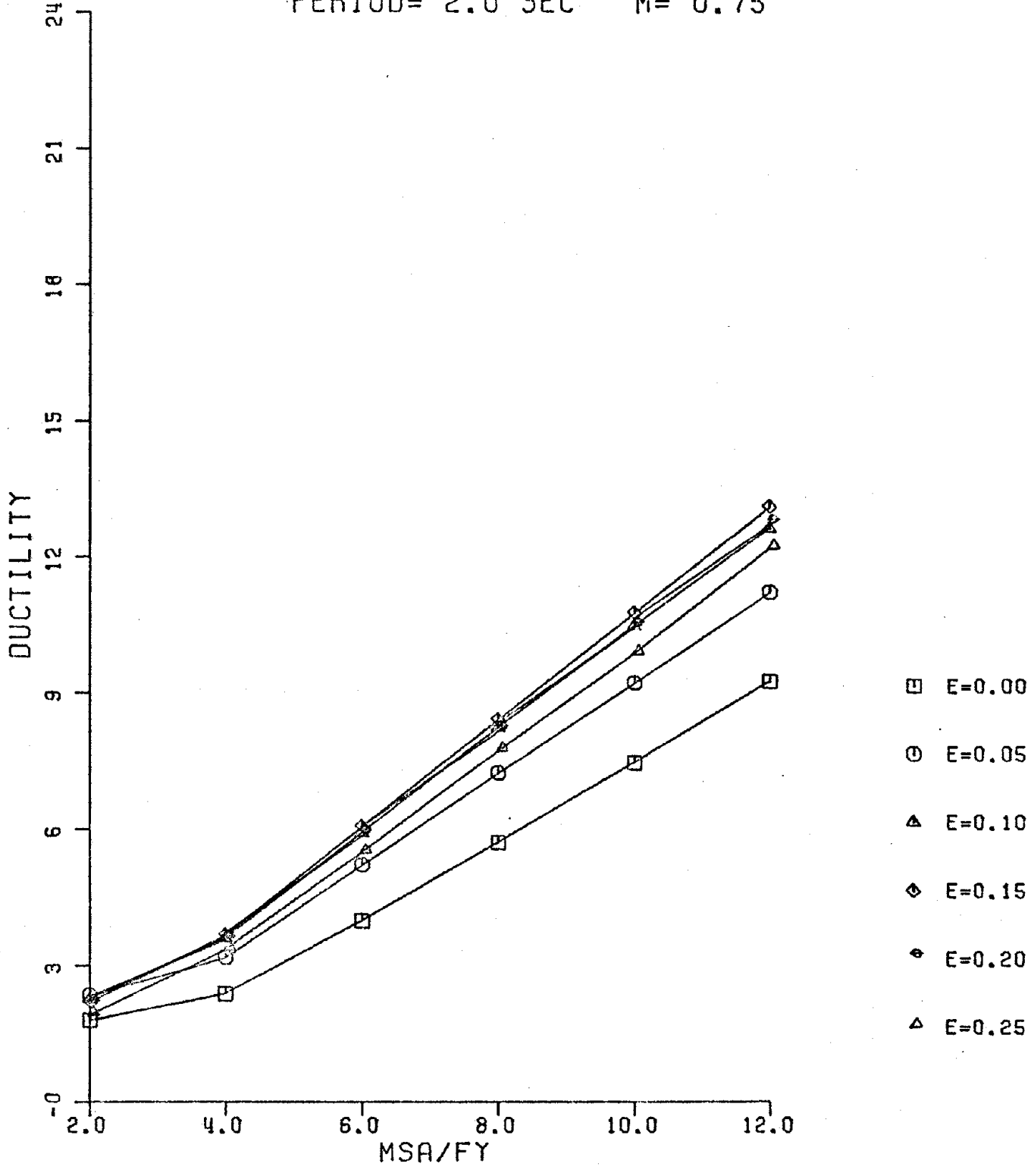

PLOT #74

KERN COUN., TAFT N21E

PERIOD= 2.0 SEC M= 1.00

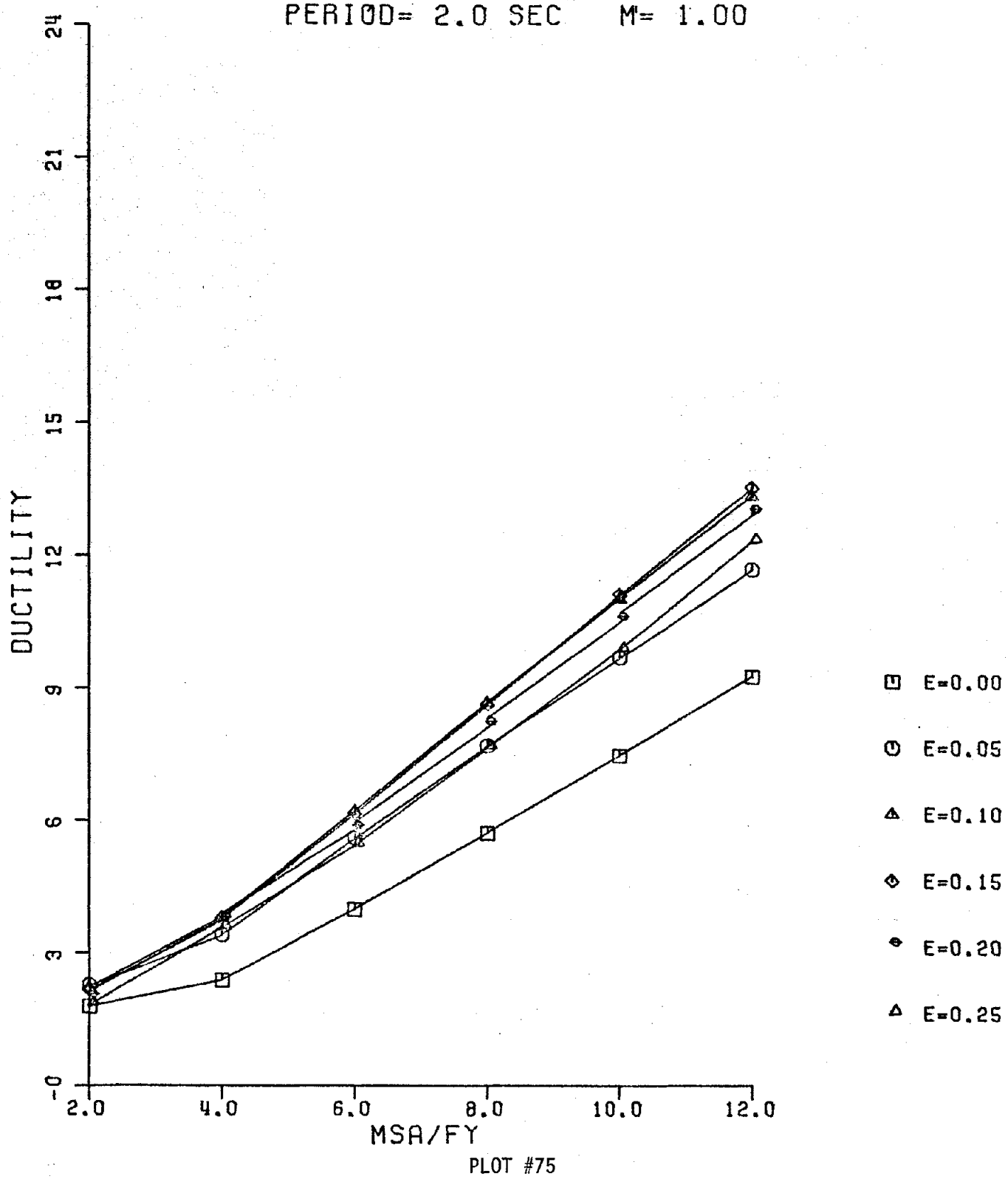

PLOT #75

KERN COUN., TAFT N21E

PERIOD= 2.0 SEC M= 1.25

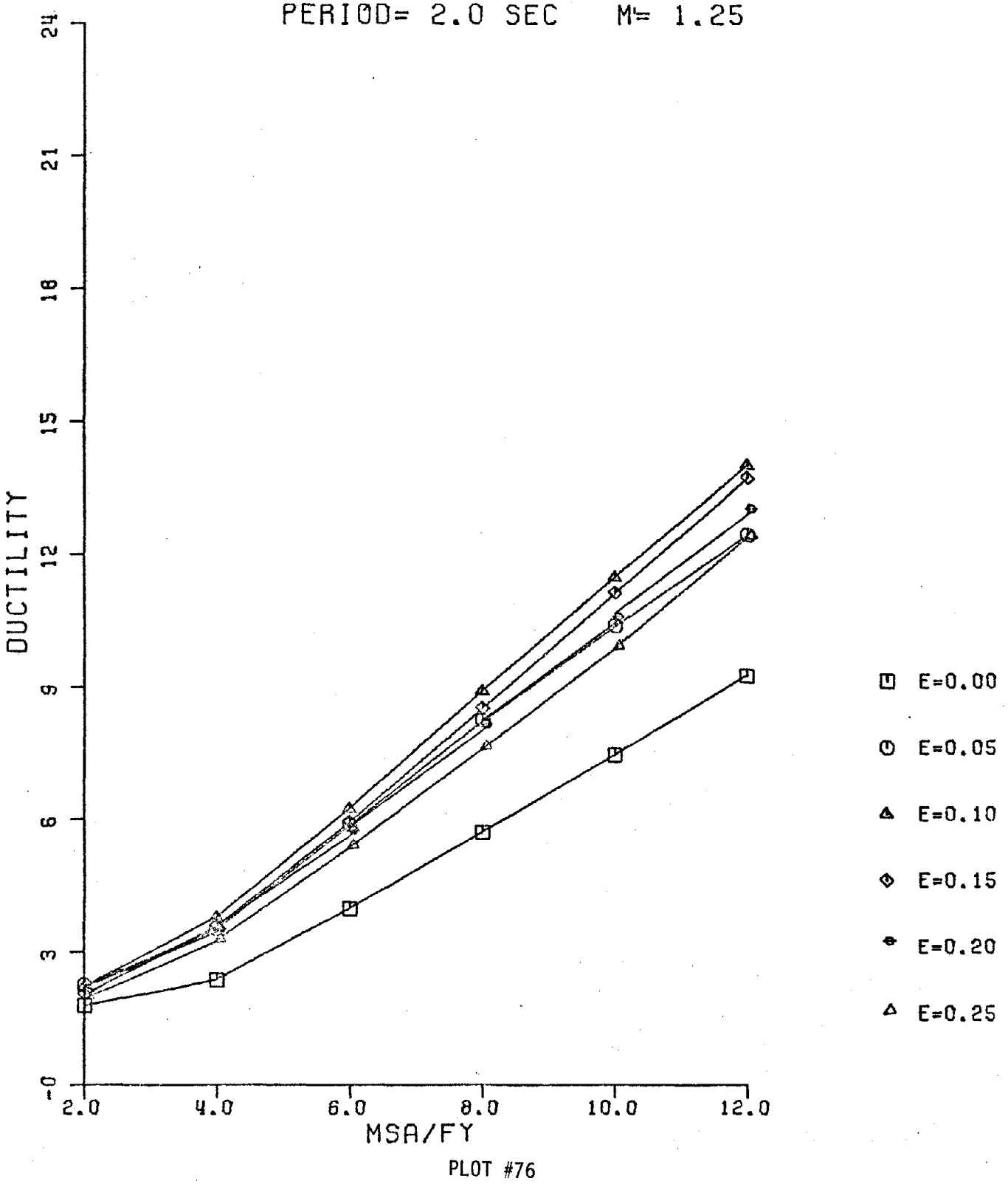

PLOT #76

KERN COUN., TAFT N21E

PERIOD= 2.0 SEC M'= 1.75

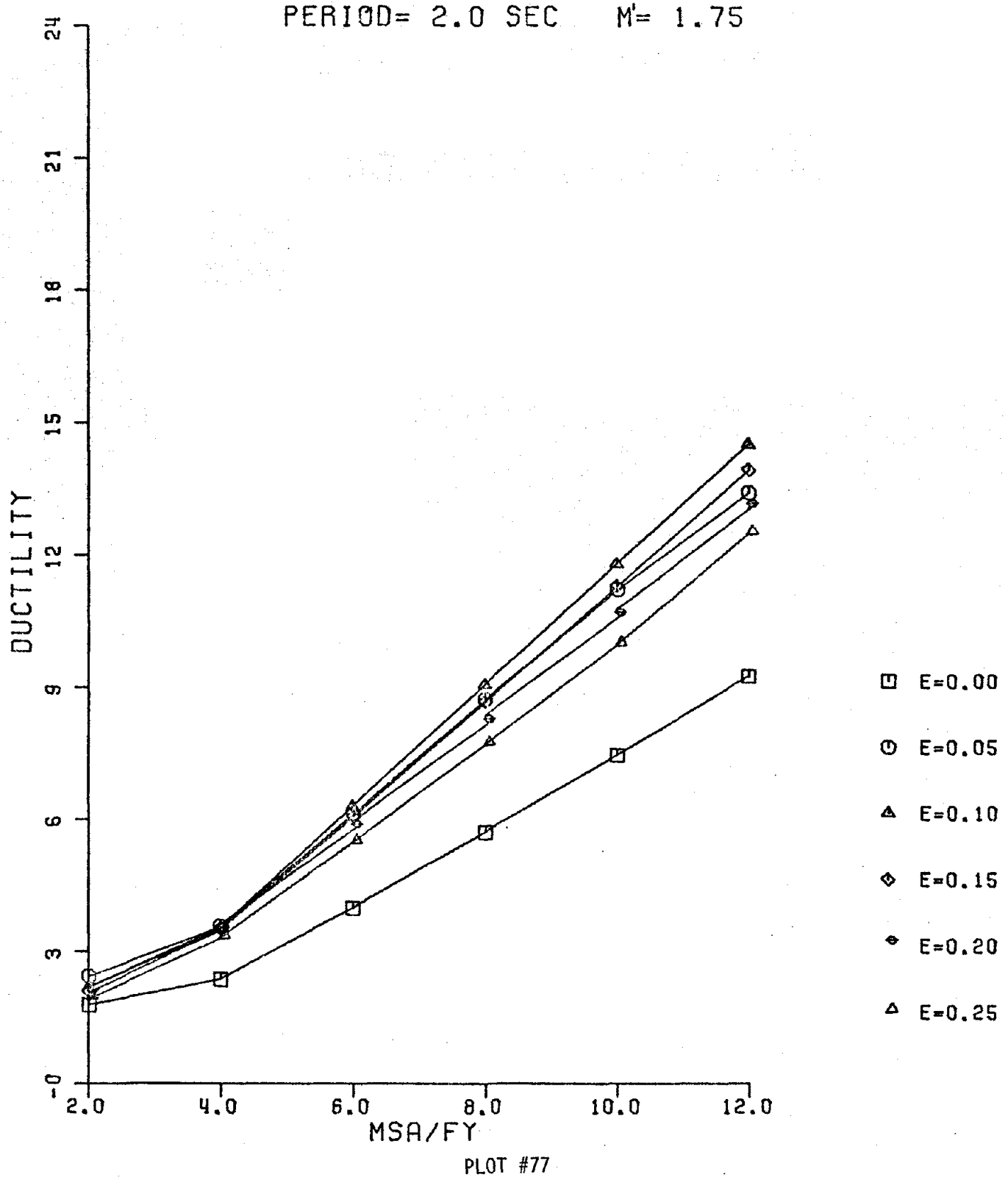

PLOT #77

KERN COUN., TAFT N21E

PERIOD= 2.0 SEC M'= 1.50

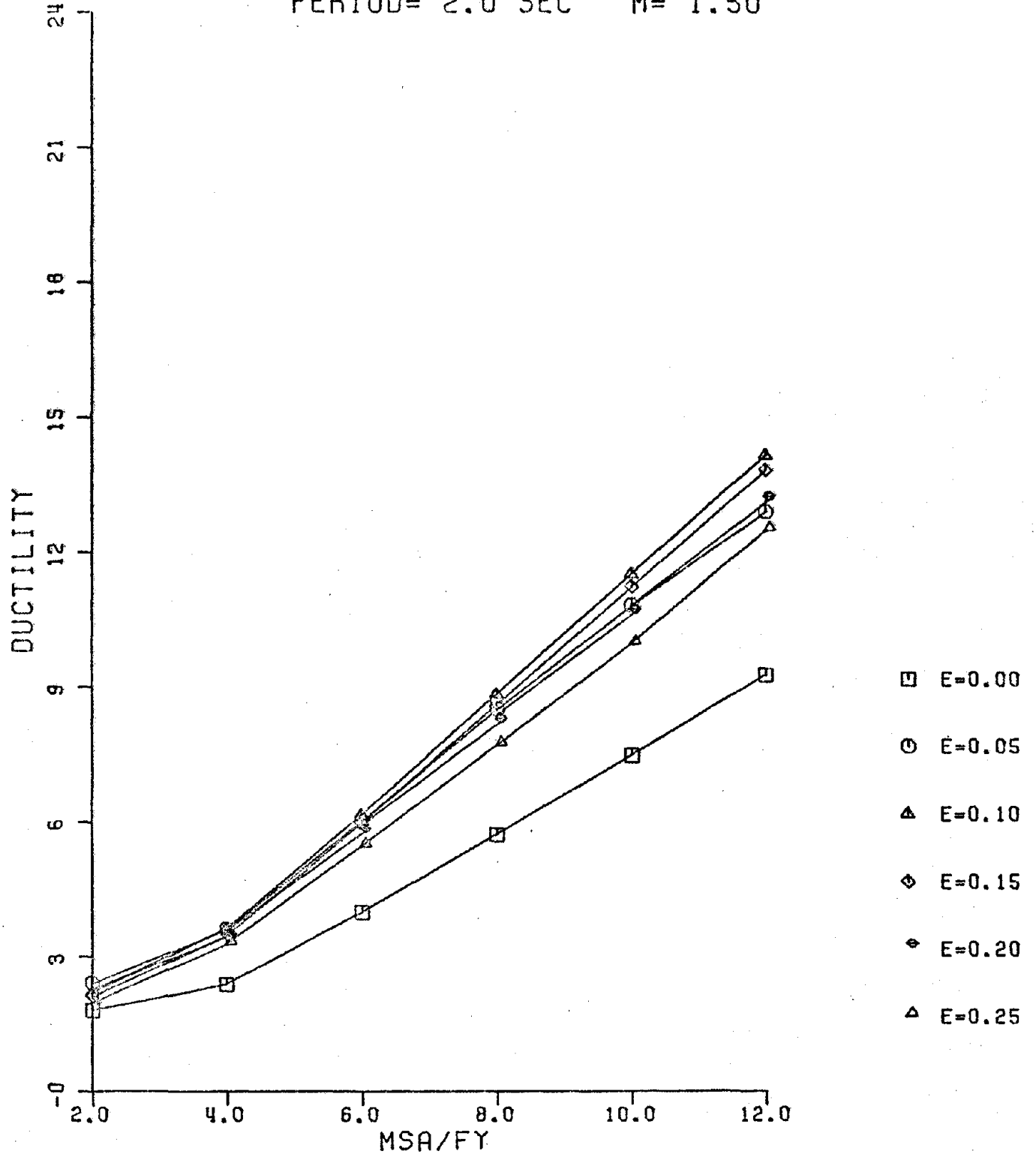

PLOT #78

ARTIFICIAL MOTIONS

PLOTS 79 - 108

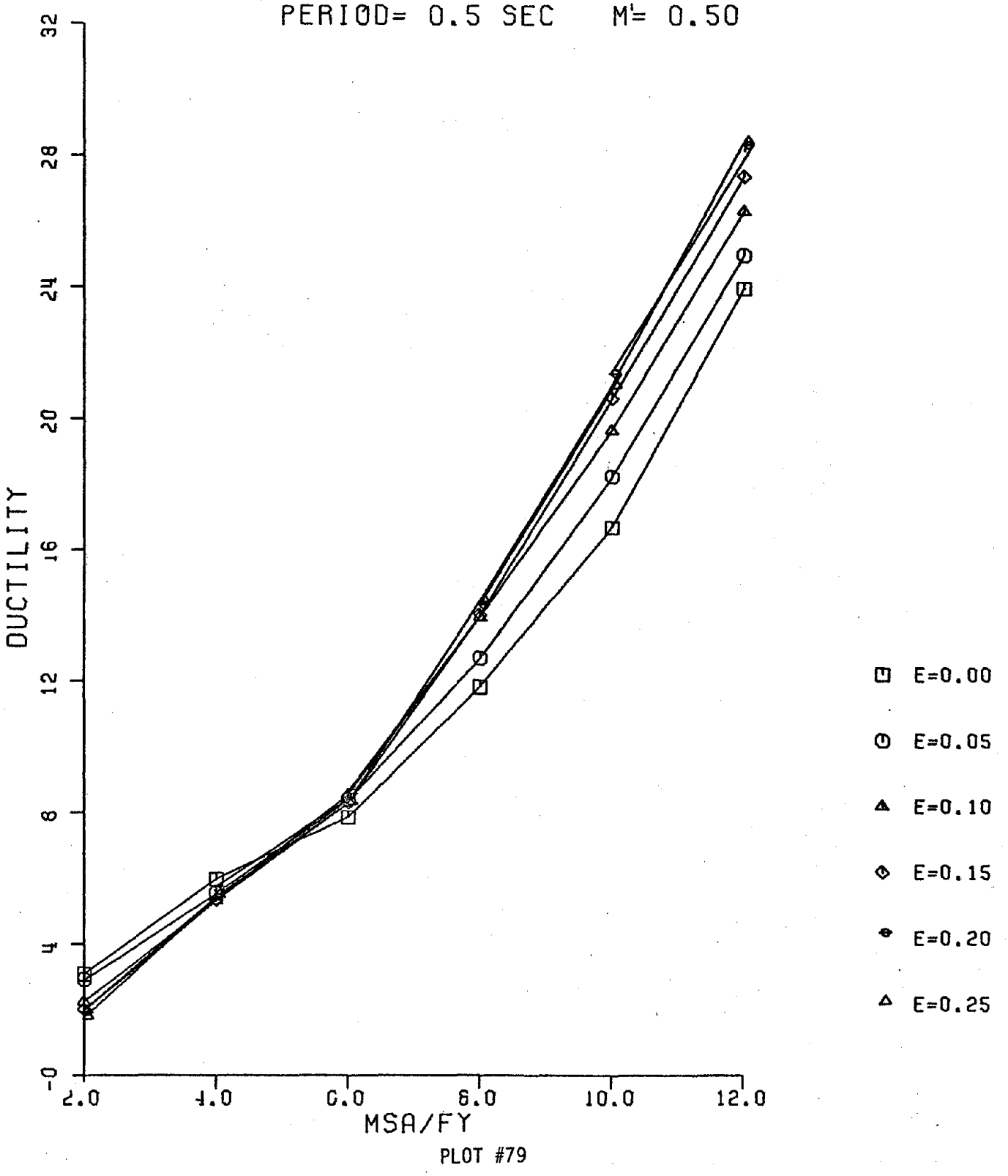
ARTIFICIAL MOTION
PERIOD= 0.5 SEC M= 0.50
DUCTILITY
0
4
8
12
16
20
24
28
32
2.0
4.0
6.0
8.0
10.0
12.0
MSA/FY
E=0.00
E=0.05
E=0.10
E=0.15
E=0.20
E=0.25

PLOT #79

ARTIFICIAL MOTION

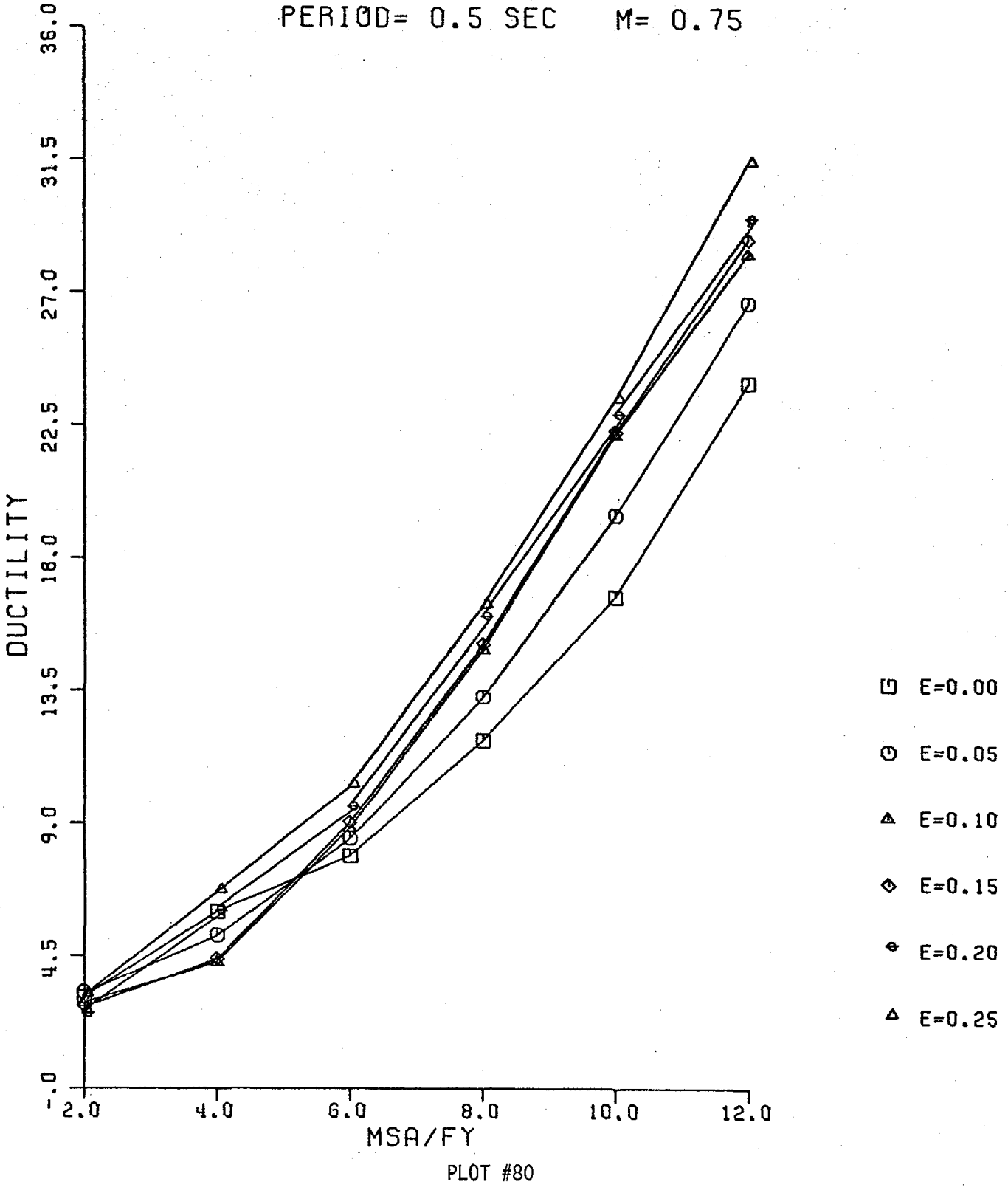

PLOT #80

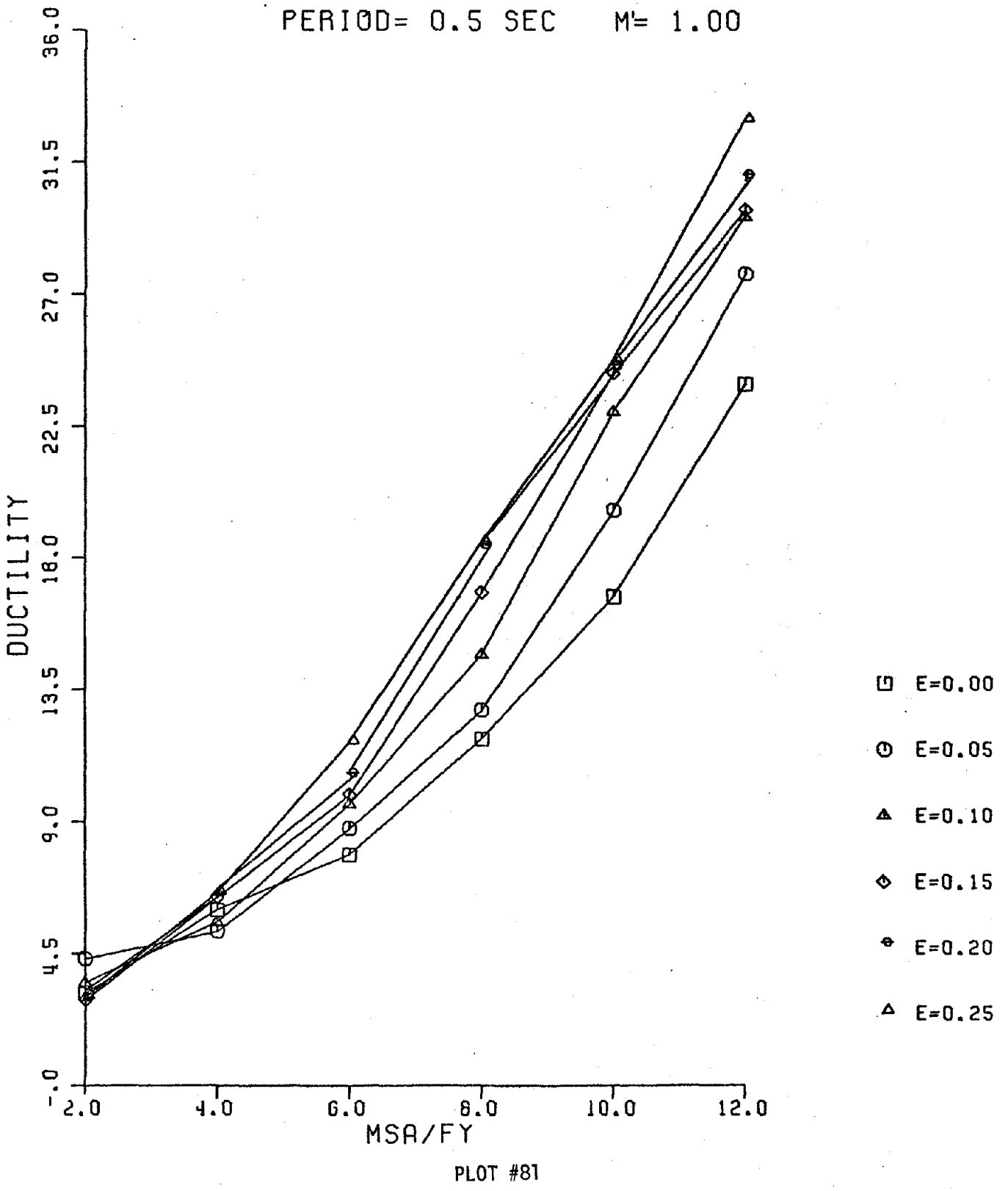
ARTIFICIAL MOTION
PERIOD= 0.5 SEC M= 1.00
DUCTILITY
-.0
4.5
9.0
13.5
18.0
22.5
27.0
31.5
36.0
2.0
4.0
6.0
8.0
10.0
12.0
MSA/FY
E=0.00
E=0.05
E=0.10
E=0.15
E=0.20
E=0.25

PLOT #81

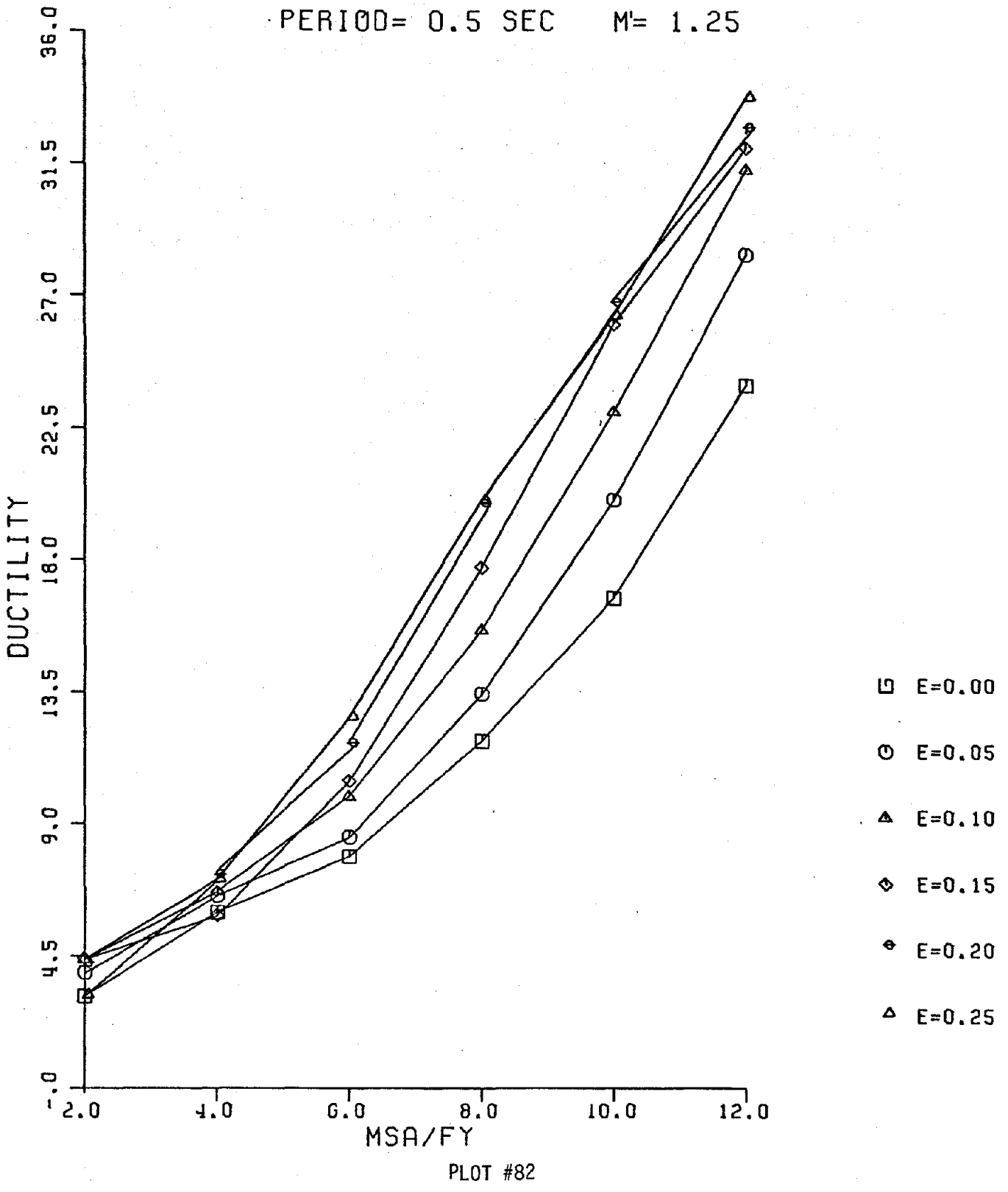
ARTIFICIAL MOTION
PERIOD= 0.5 SEC M'= 1.25
DUCTILITY
36.0
31.5
27.0
22.5
18.0
13.5
9.0
4.5
-.0
2.0
4.0
6.0
8.0
10.0
12.0
MSA/FY
E=0.00
E=0.05
E=0.10
E=0.15
E=0.20
E=0.25

PLOT #82

ARTIFICIAL MOTION

PERIOD= 0.5 SEC M'= 1.50

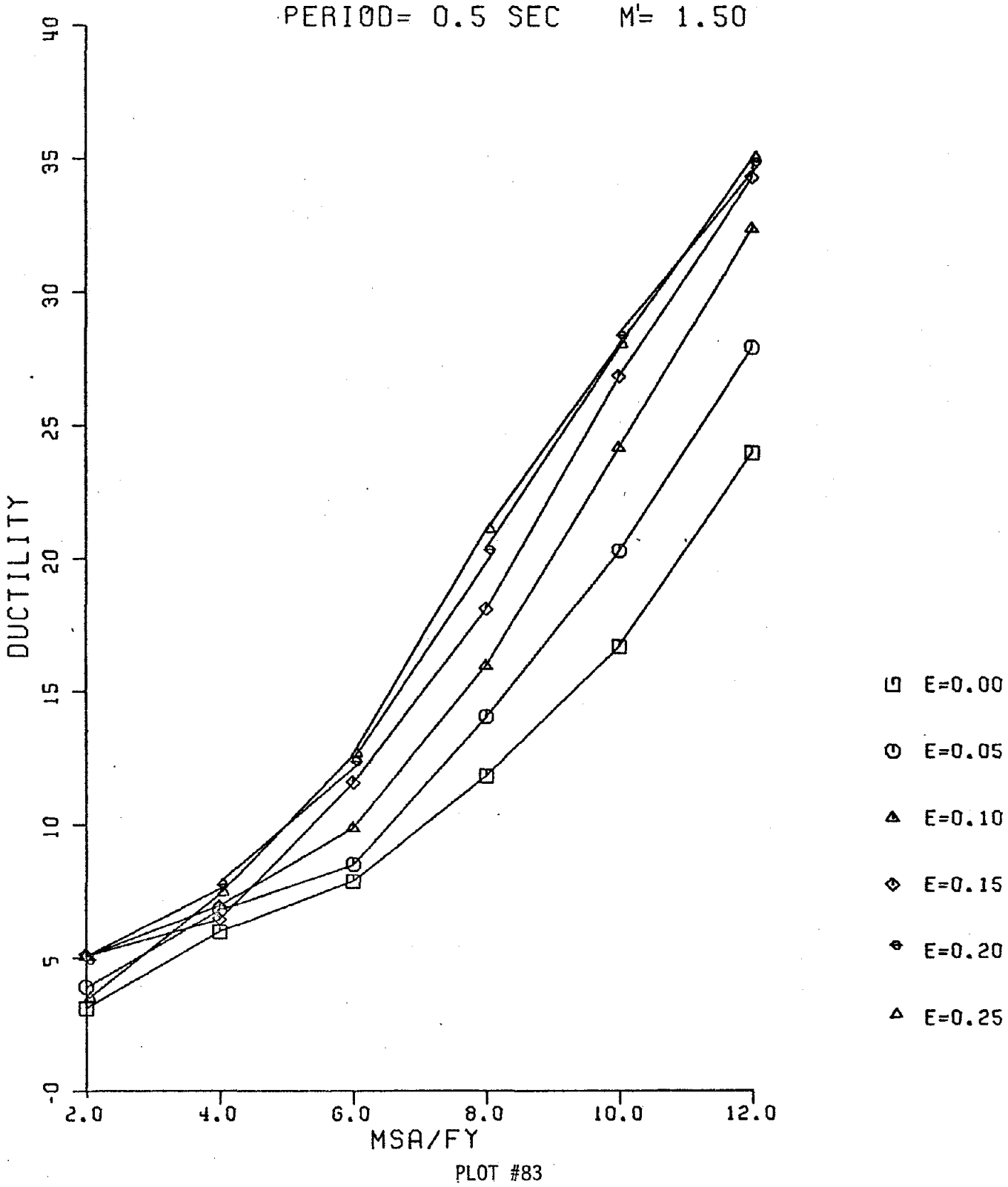

PLOT #83

ARTIFICIAL MOTION

PERIOD= 0.5 SEC M= 1.75

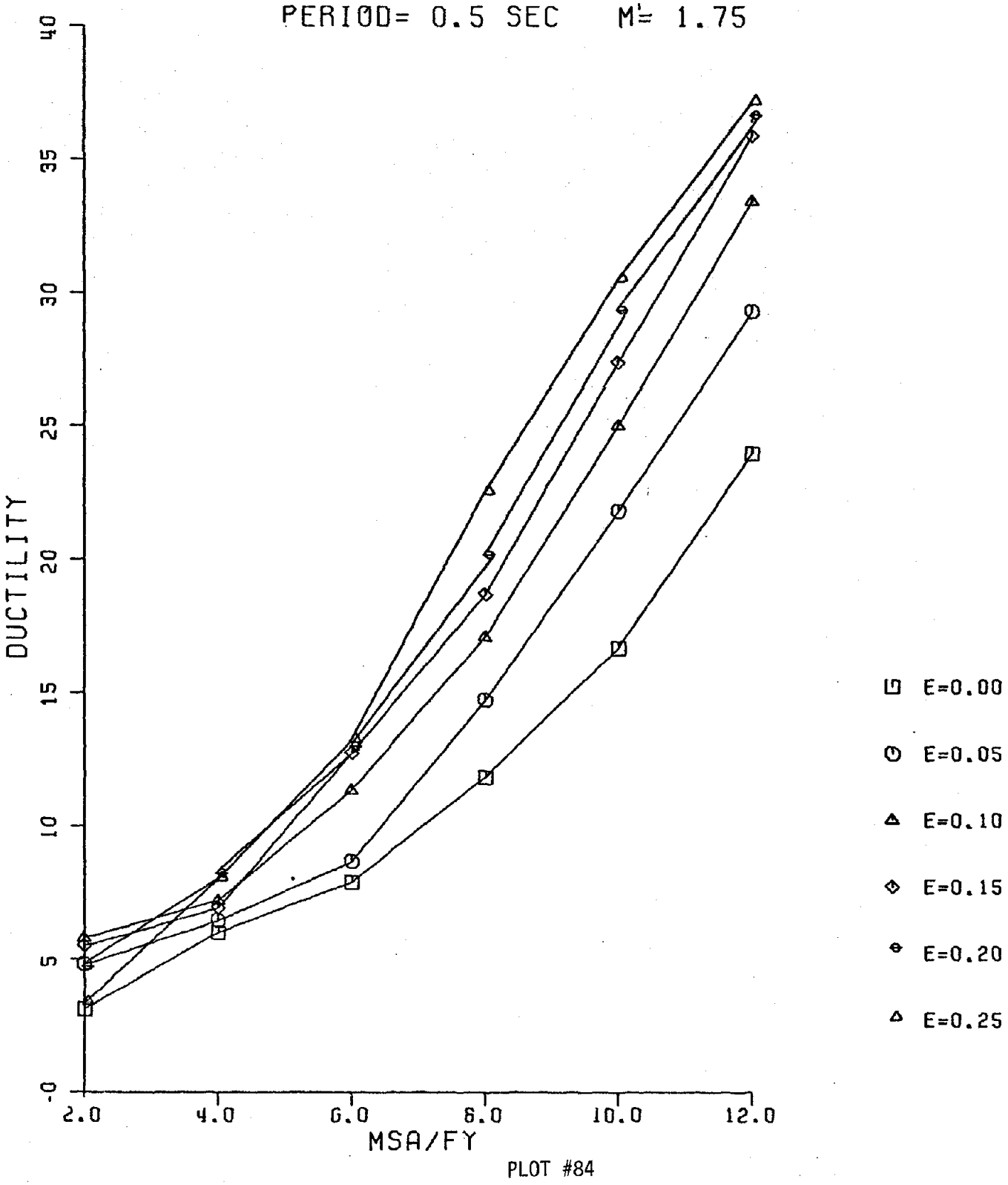

PLOT #84

ARTIFICIAL MOTION

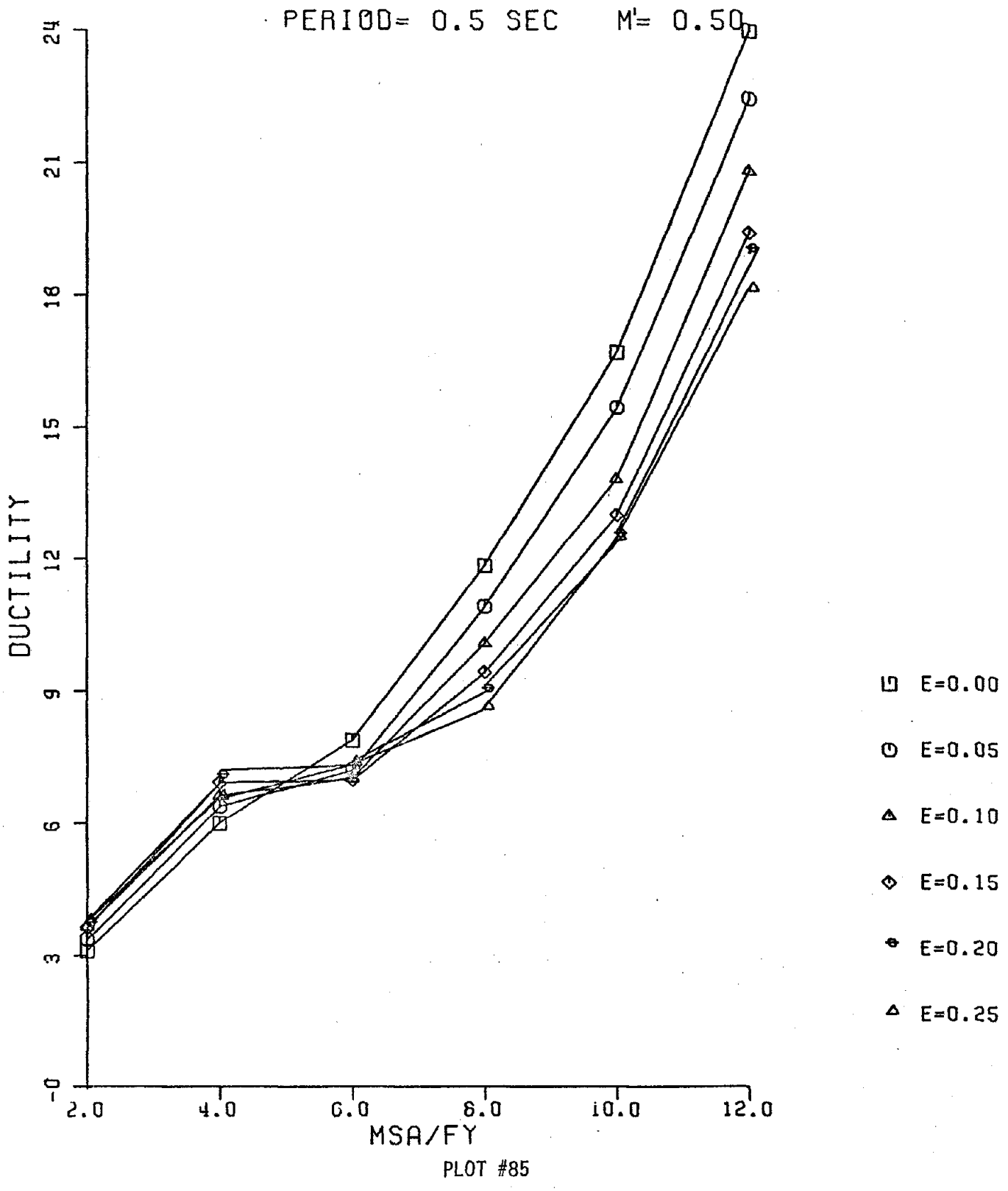

PLOT #85

ARTIFICIAL MOTION

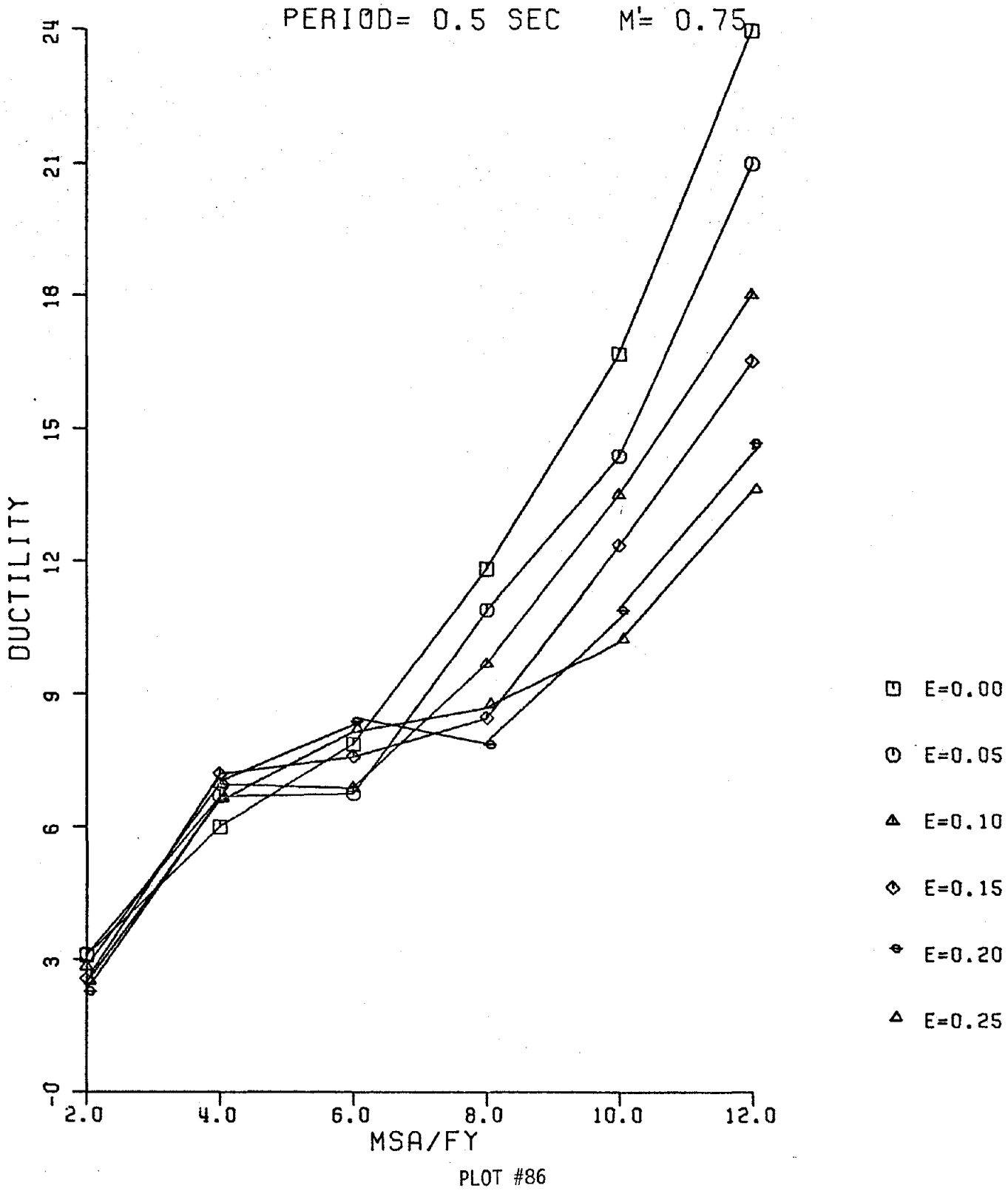

PLOT #86

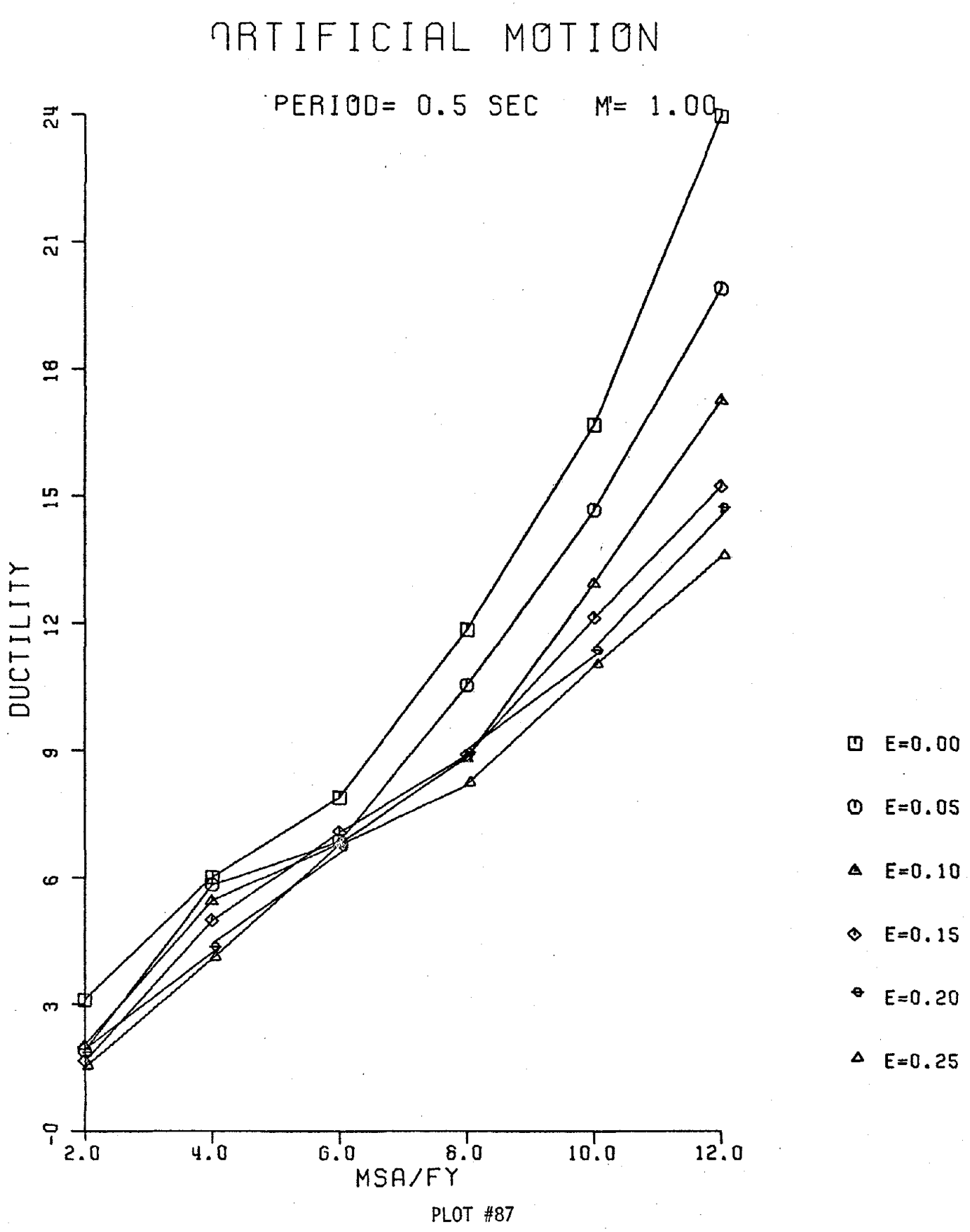
ARTIFICIAL MOTION
PERIOD= 0.5 SEC M'= 1.00
DUCTILITY
MSA/FY
-0
3
6
9
12
15
18
21
24
2.0
4.0
6.0
8.0
10.0
12.0
E=0.00
E=0.05
E=0.10
E=0.15
E=0.20
E=0.25

PLOT #87

ARTIFICIAL MOTION

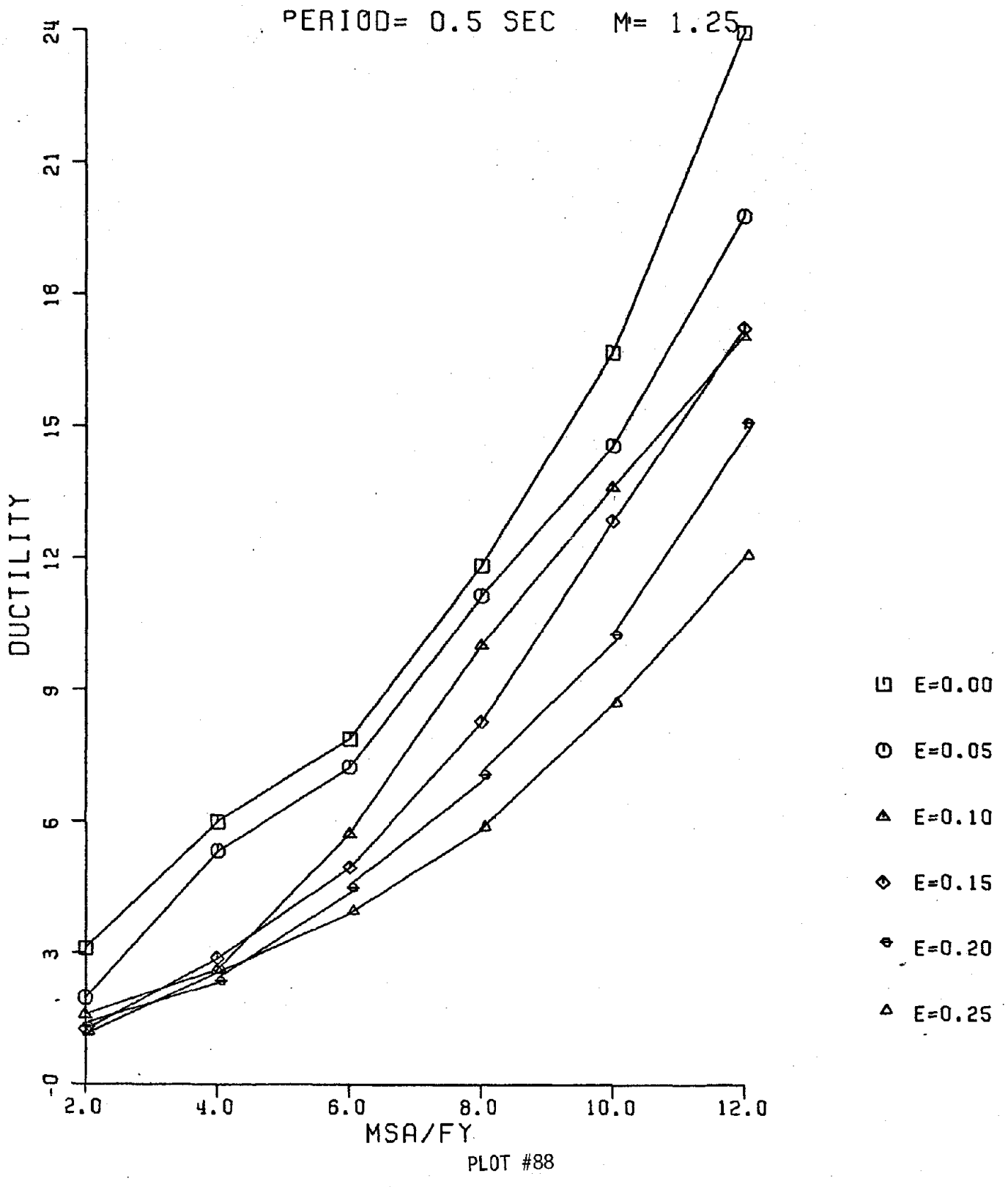

PLOT #88

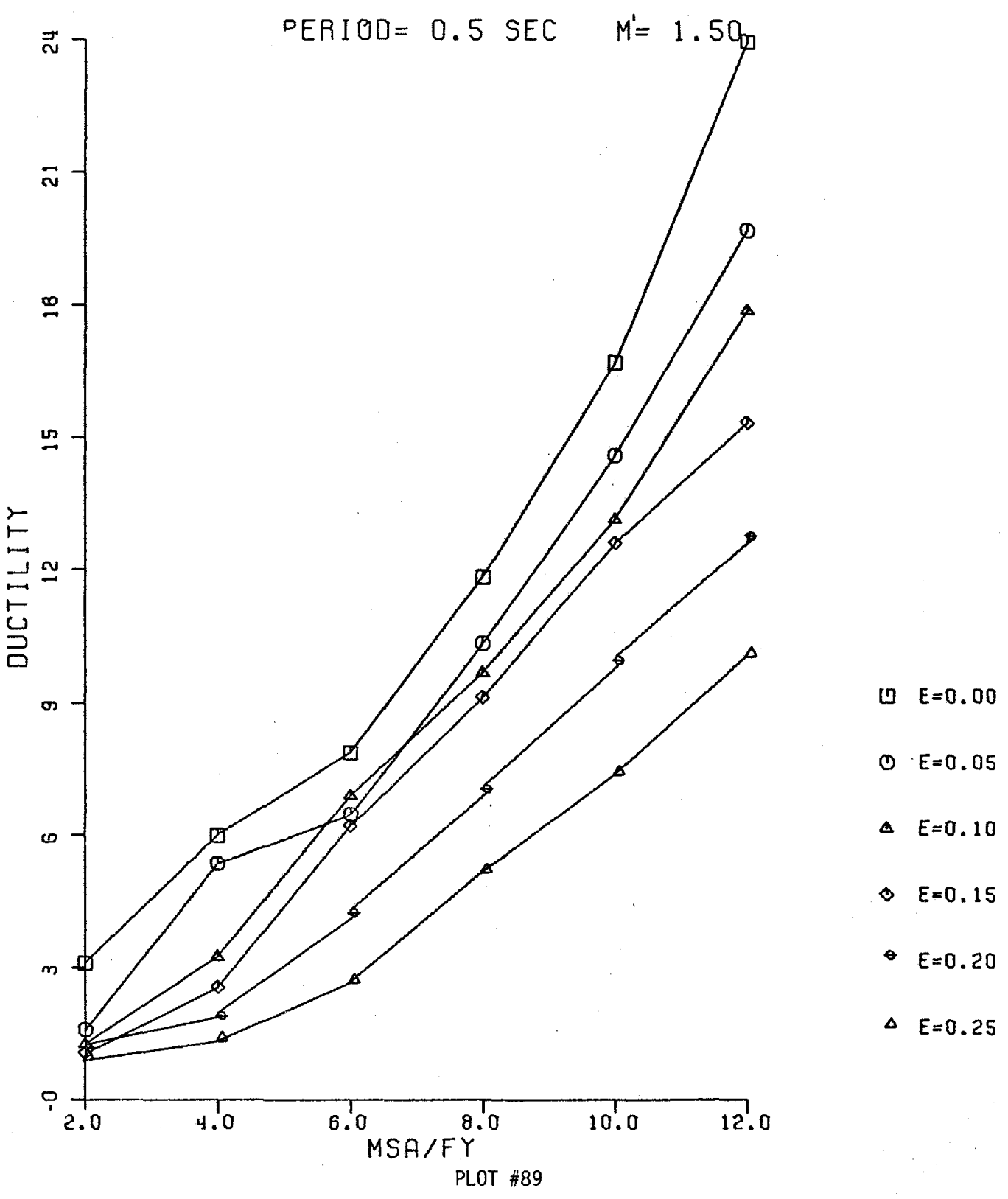
ARTIFICIAL MOTION
PERIOD= 0.5 SEC M'= 1.50
DUCTILITY
-0
3
6
9
12
15
18
21
24
2.0
4.0
6.0
8.0
10.0
12.0
MSA/FY
PLOT #89
E=0.00
E=0.05
E=0.10
E=0.15
E=0.20
E=0.25

ARTIFICIAL MOTION

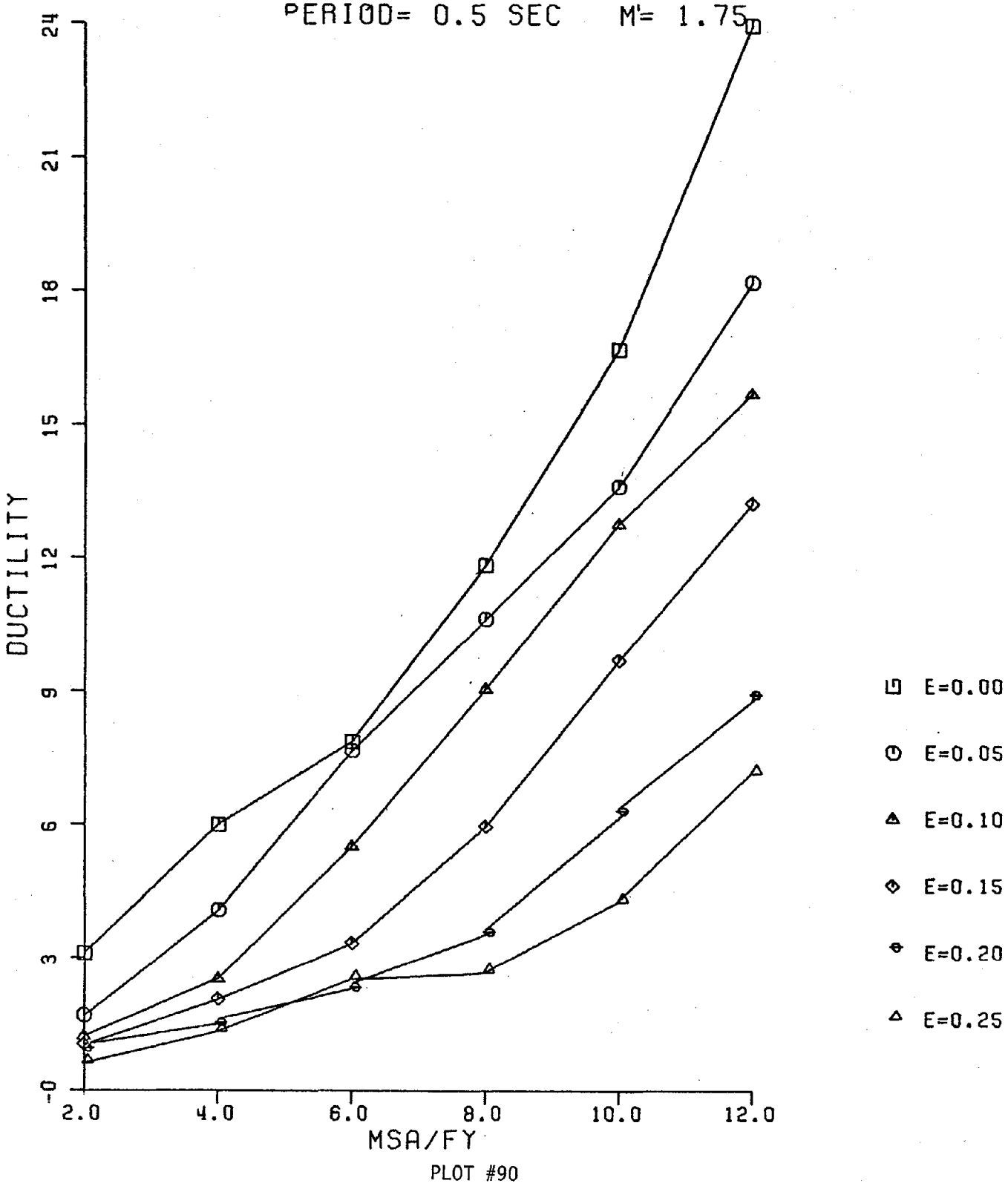

PLOT #90

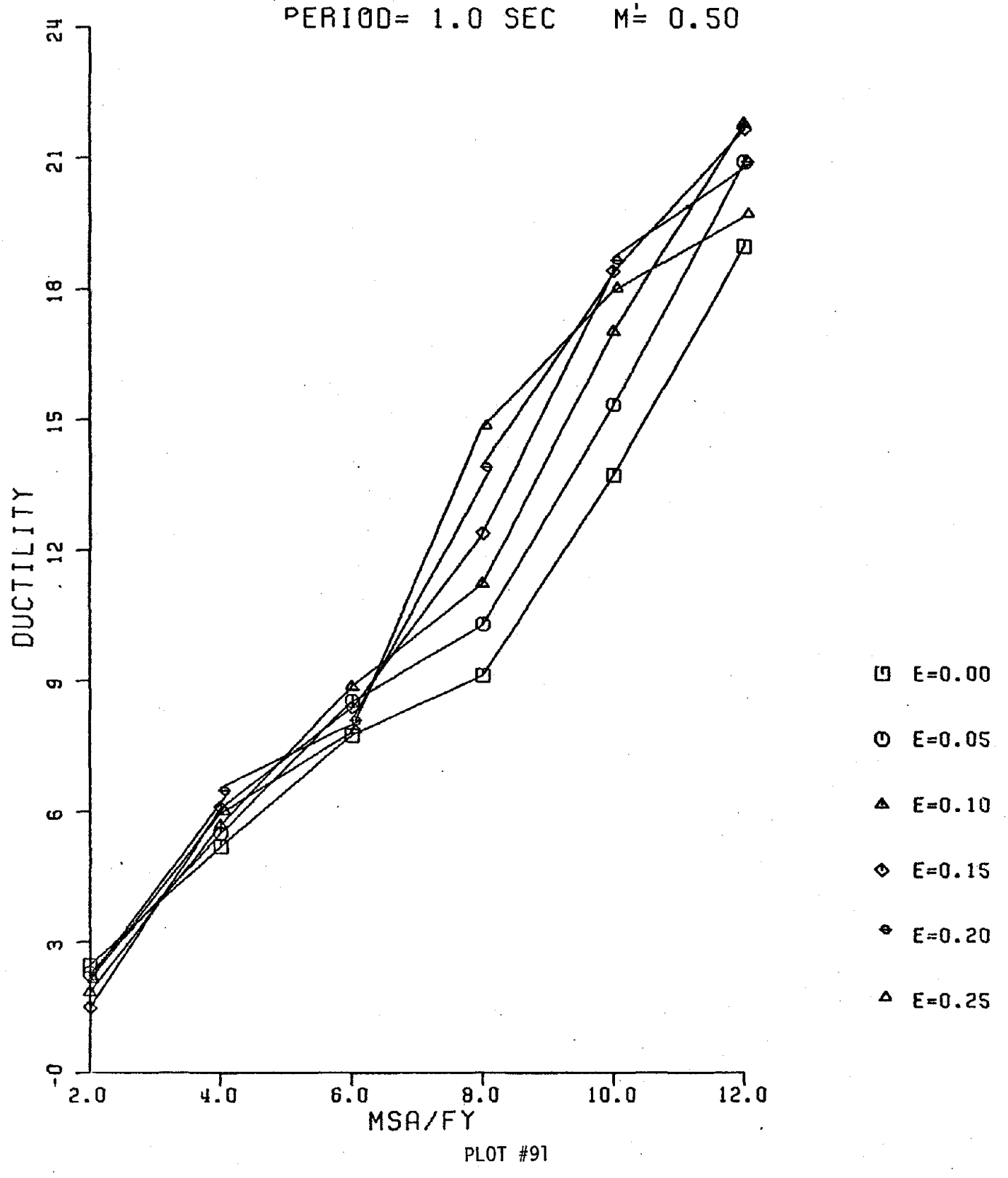
ARTIFICIAL MOTION
PERIOD= 1.0 SEC M= 0.50
DUCTILITY
MSA/FY
-0
3
6
9
12
15
18
21
24
2.0
4.0
6.0
8.0
10.0
12.0
E=0.00
E=0.05
E=0.10
E=0.15
E=0.20
E=0.25
PLOT #91

ARTIFICIAL MOTION

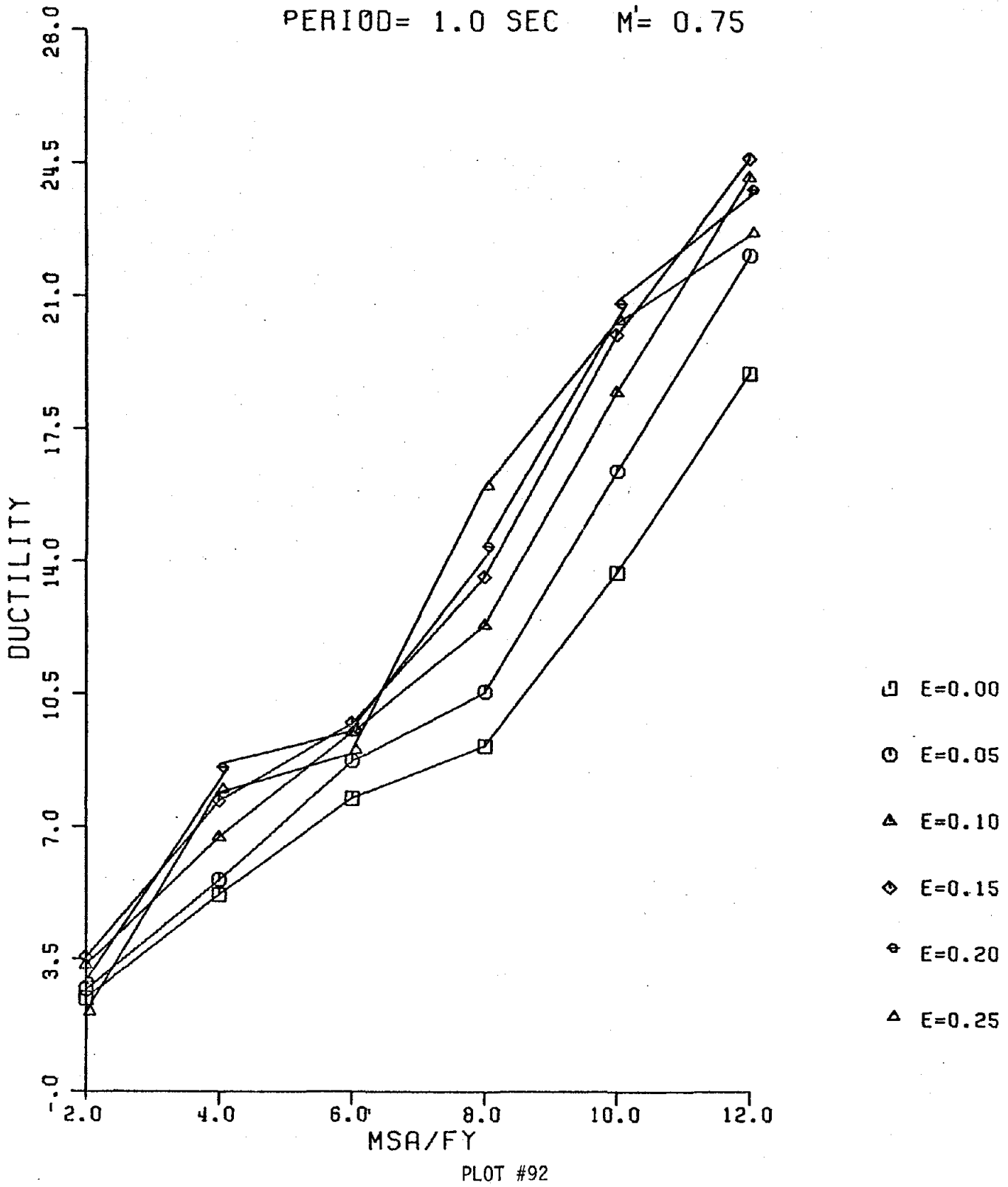

PLOT #92

ARTIFICIAL MOTION

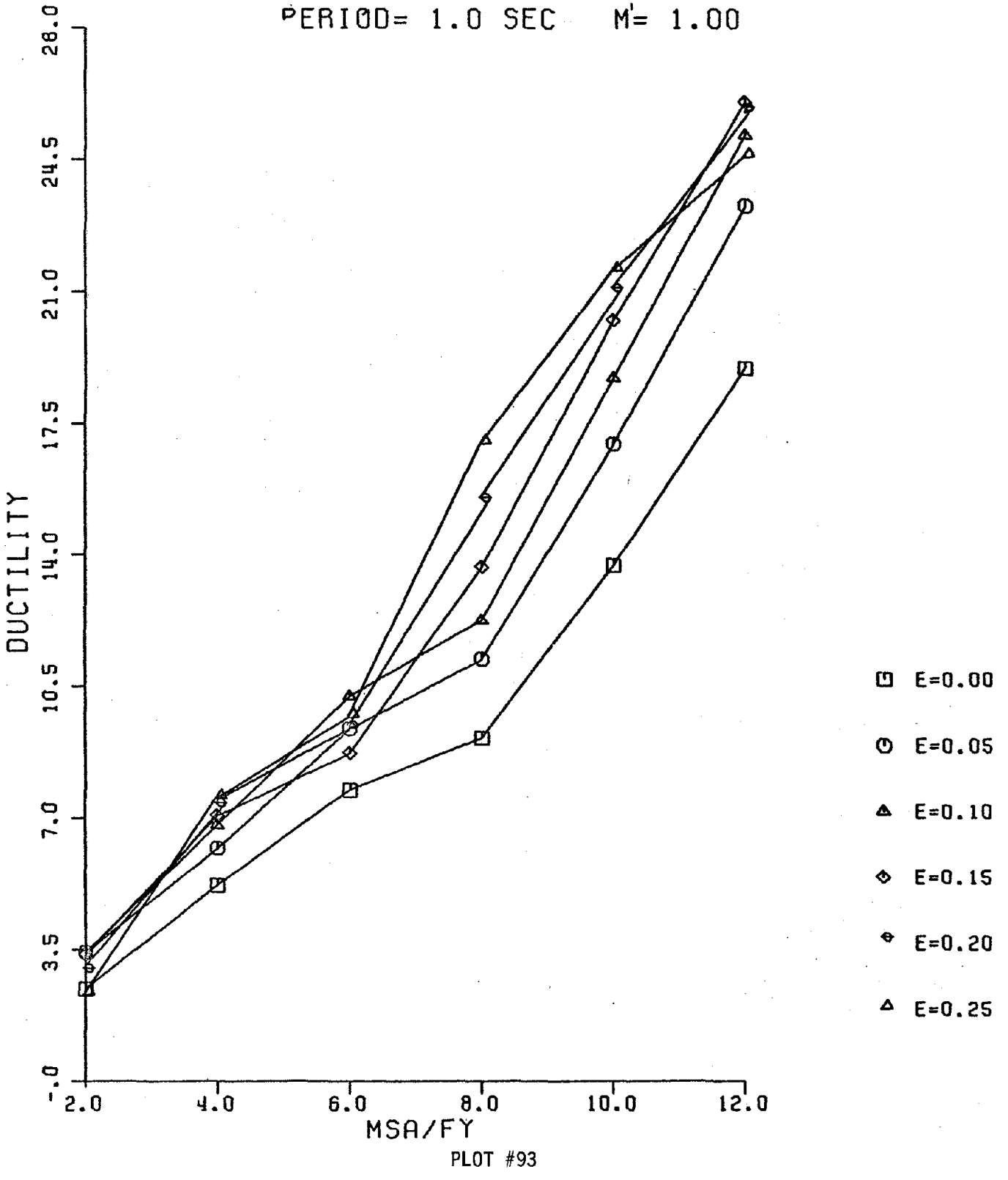

PLOT #93

ARTIFICIAL MOTION

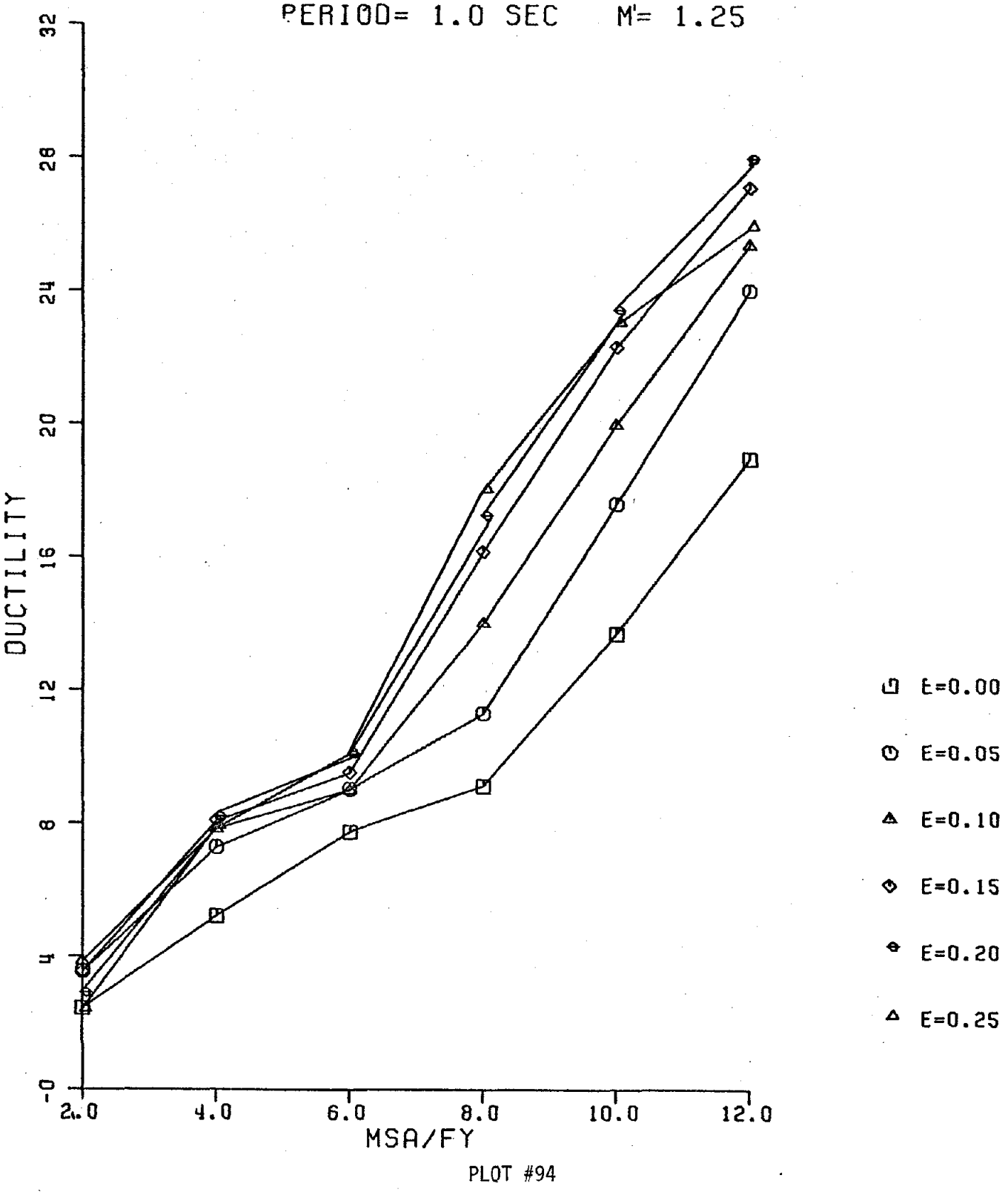

PLOT #94

ARTIFICIAL MOTION

PERIOD= 1.0 SEC M= 1.50

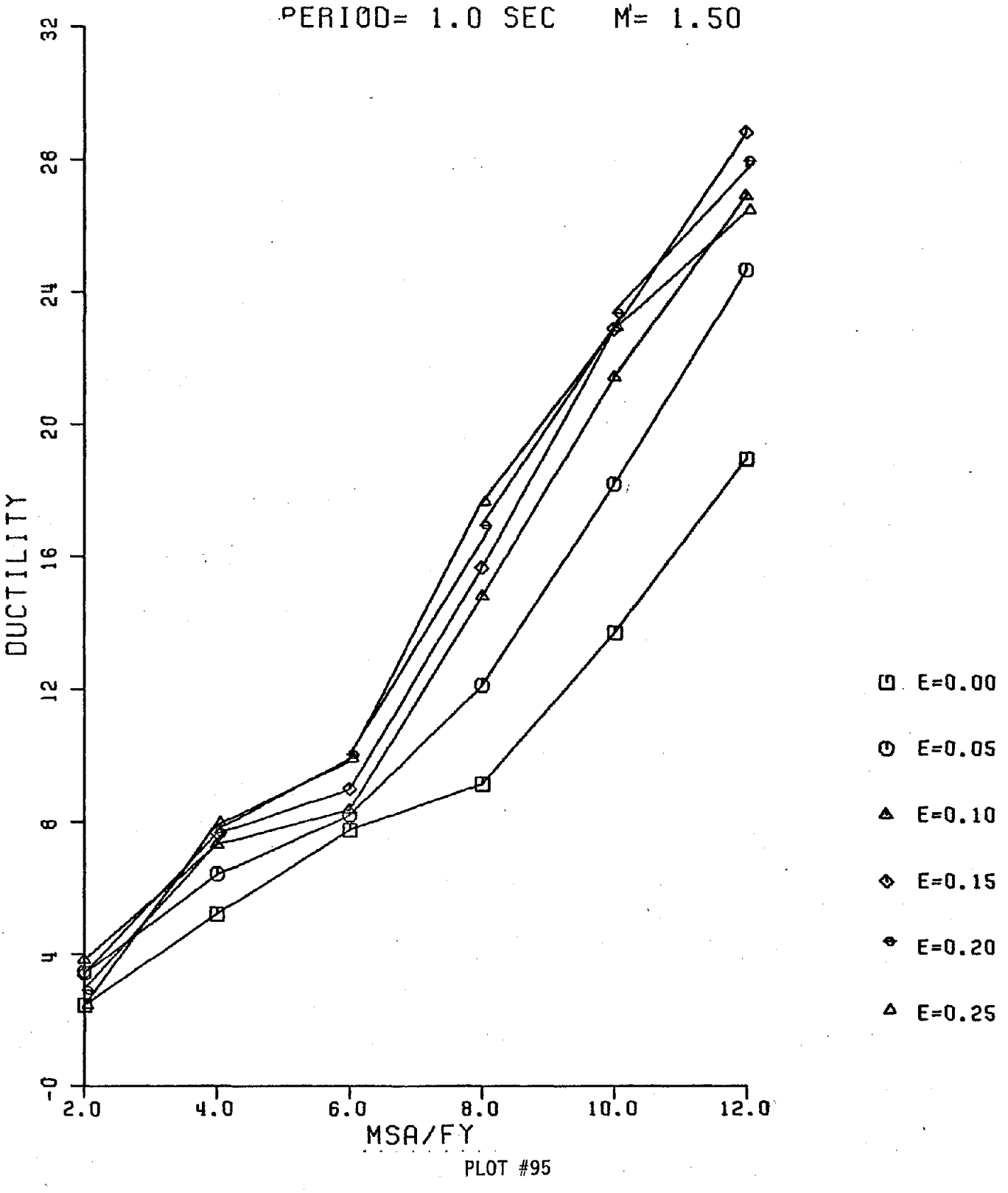

PLOT #95

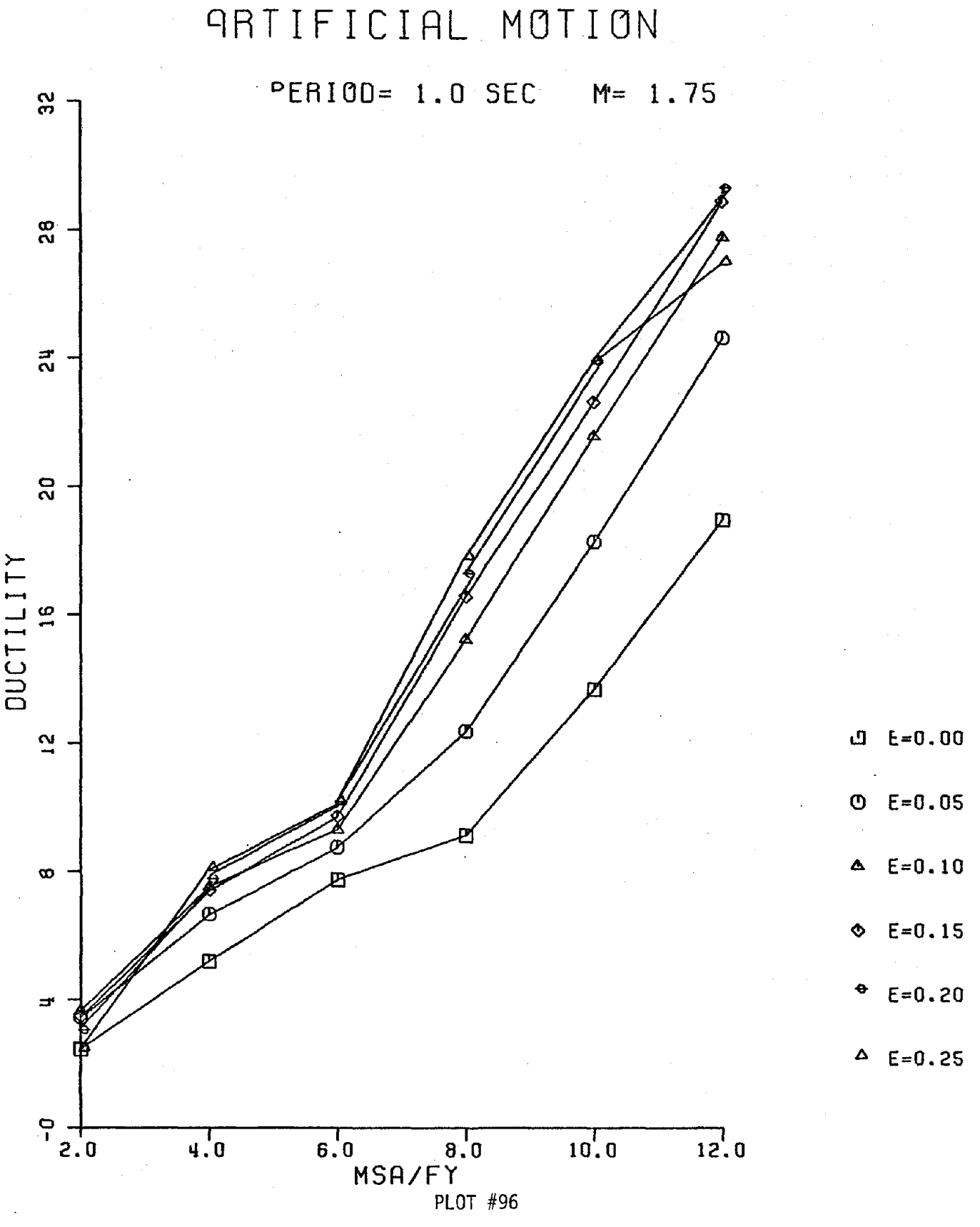
ARTIFICIAL MOTION
PERIOD= 1.0 SEC M= 1.75
DUCTILITY
-0
4
8
12
16
20
24
28
32
2.0
4.0
6.0
8.0
10.0
12.0
MSA/FY
E=0.00
E=0.05
E=0.10
E=0.15
E=0.20
E=0.25

PLOT #96

ARTIFICIAL MOTION

PERIOD= 1.5 SEC M'= 0.50

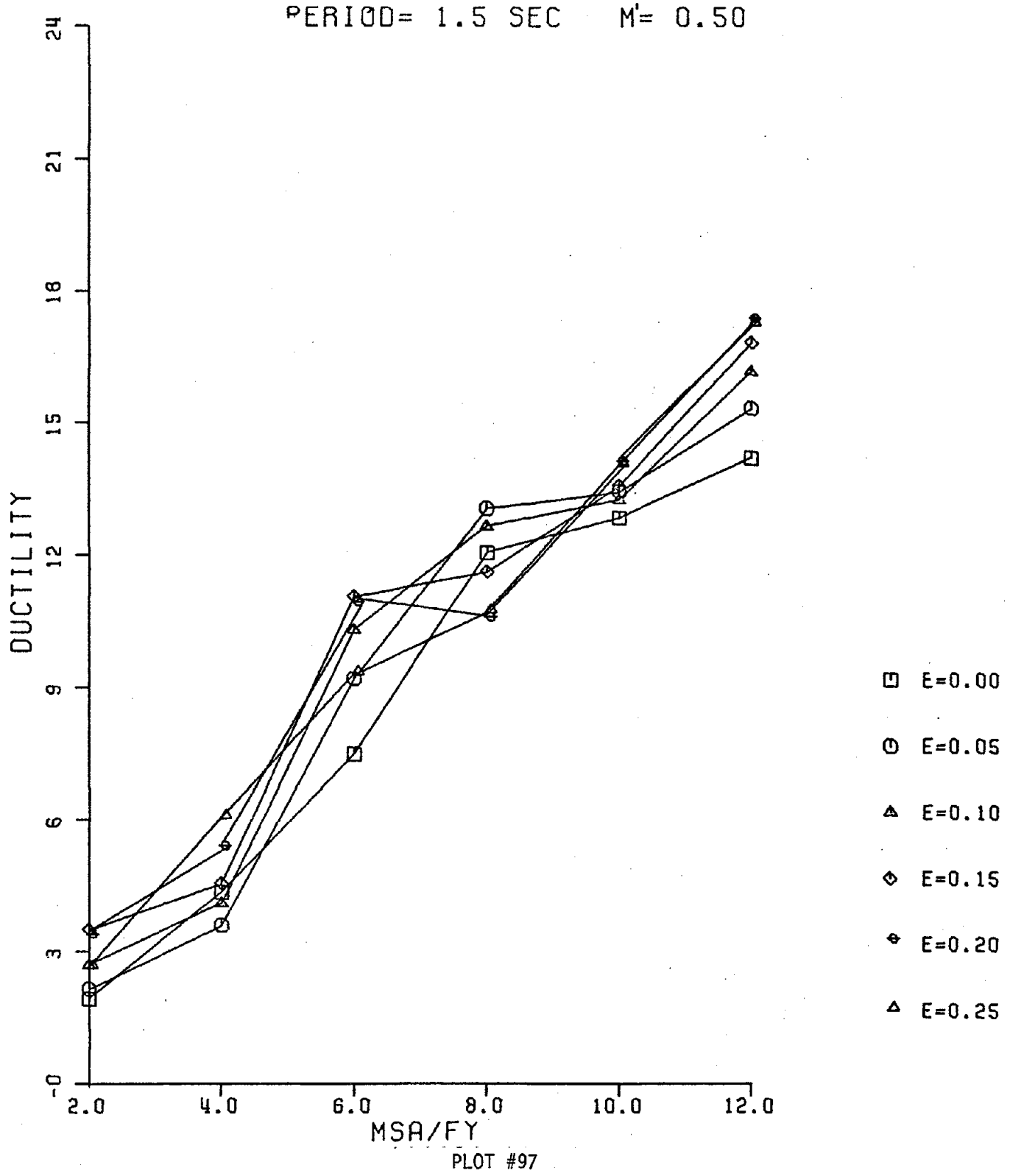

PLOT #97

ARTIFICIAL MOTION

PERIOD= 1.5 SEC M'= 0.75

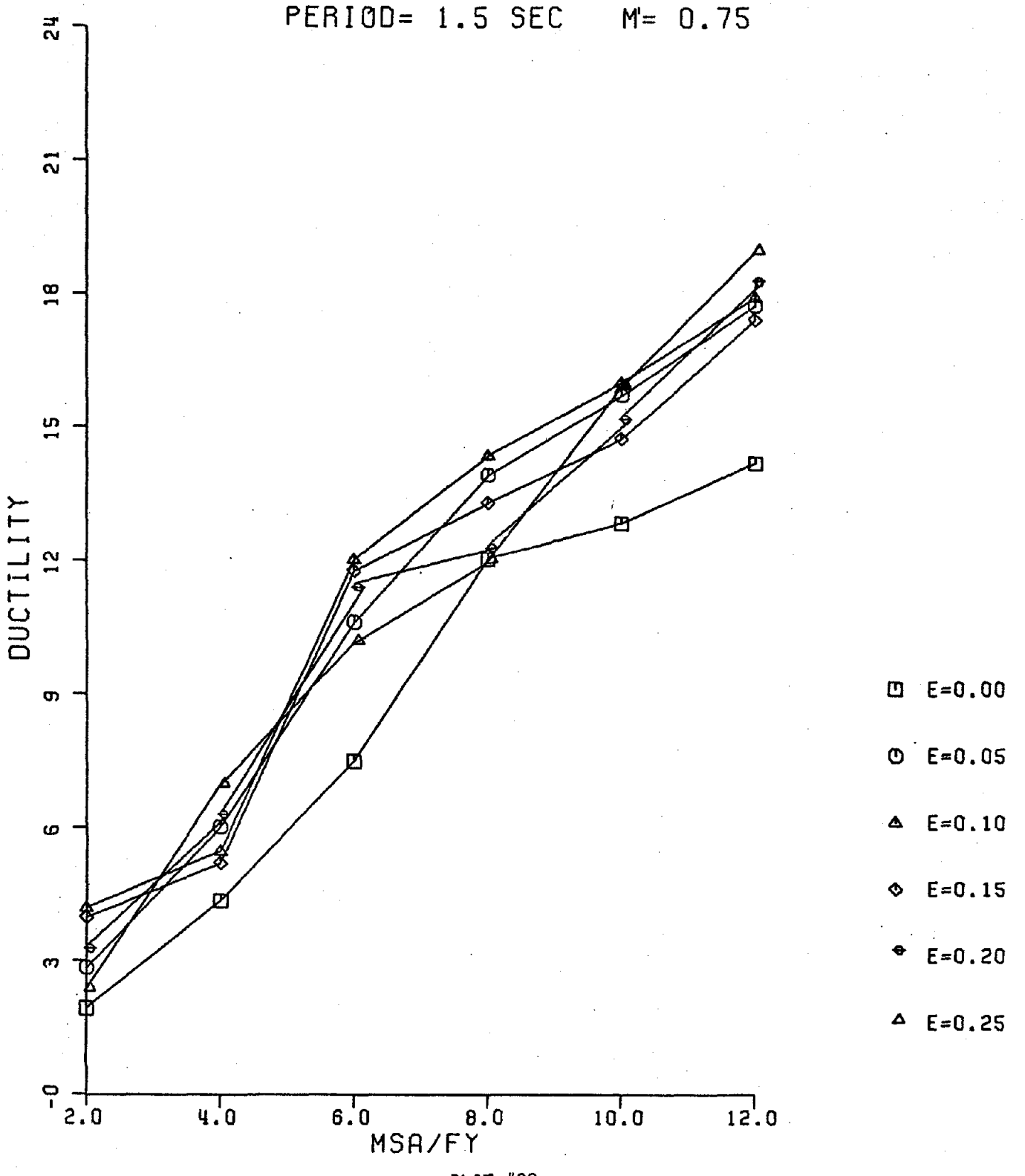

PLOT #98

ARTIFICIAL MOTION

PERIOD= 1.5 SEC M= 1.00

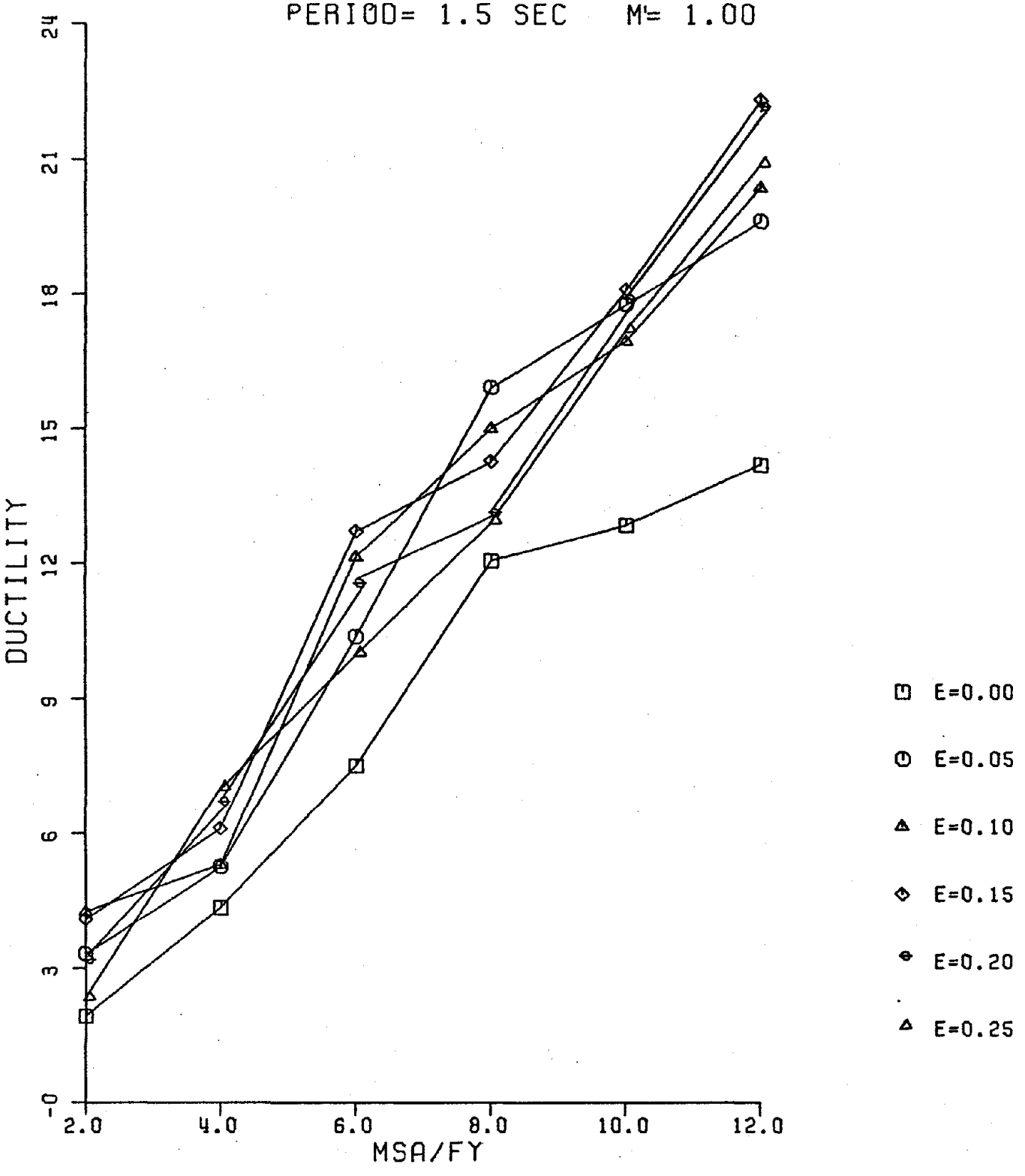

PLOT #99

ARTIFICIAL MOTION

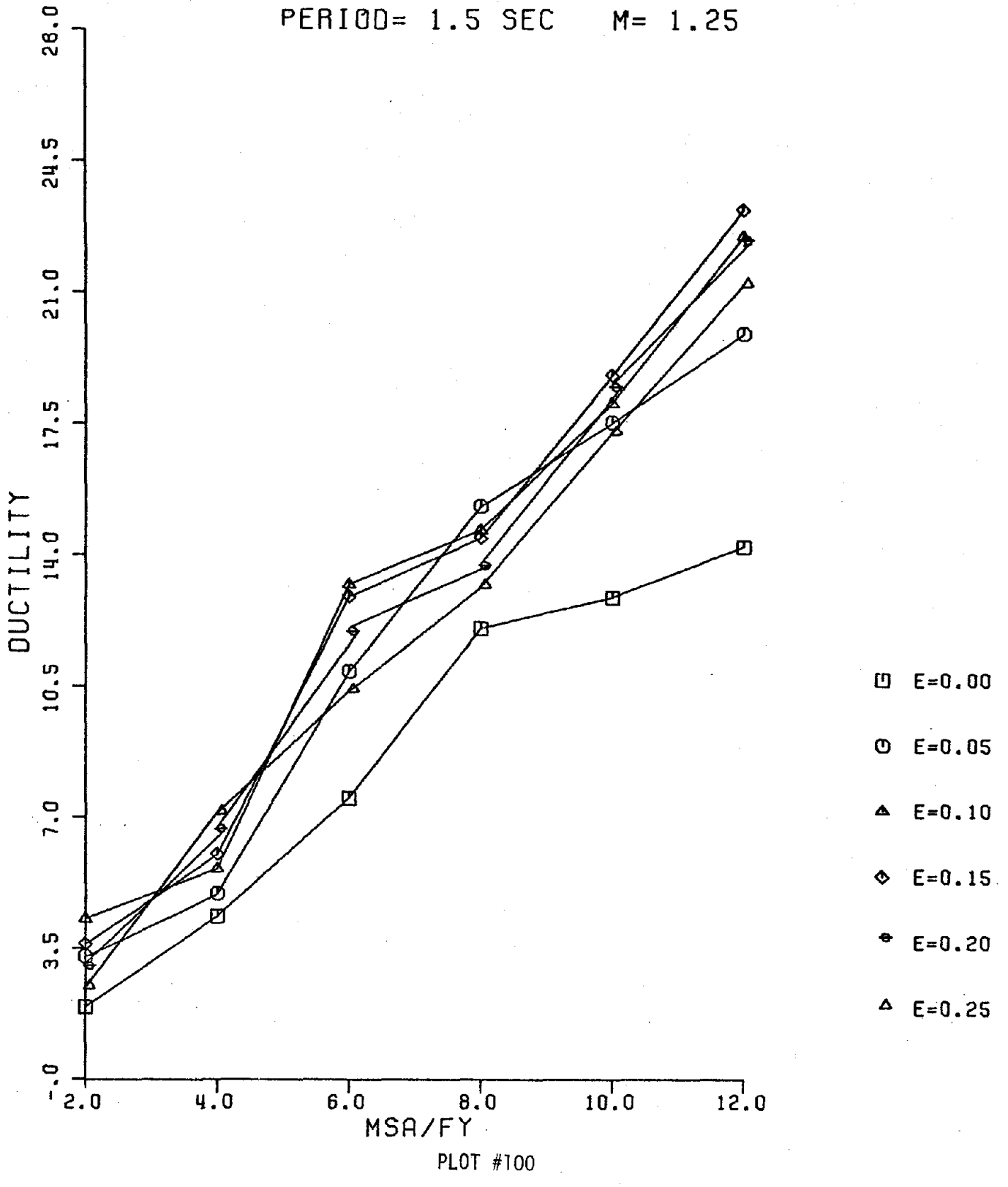

ARTIFICIAL MOTION

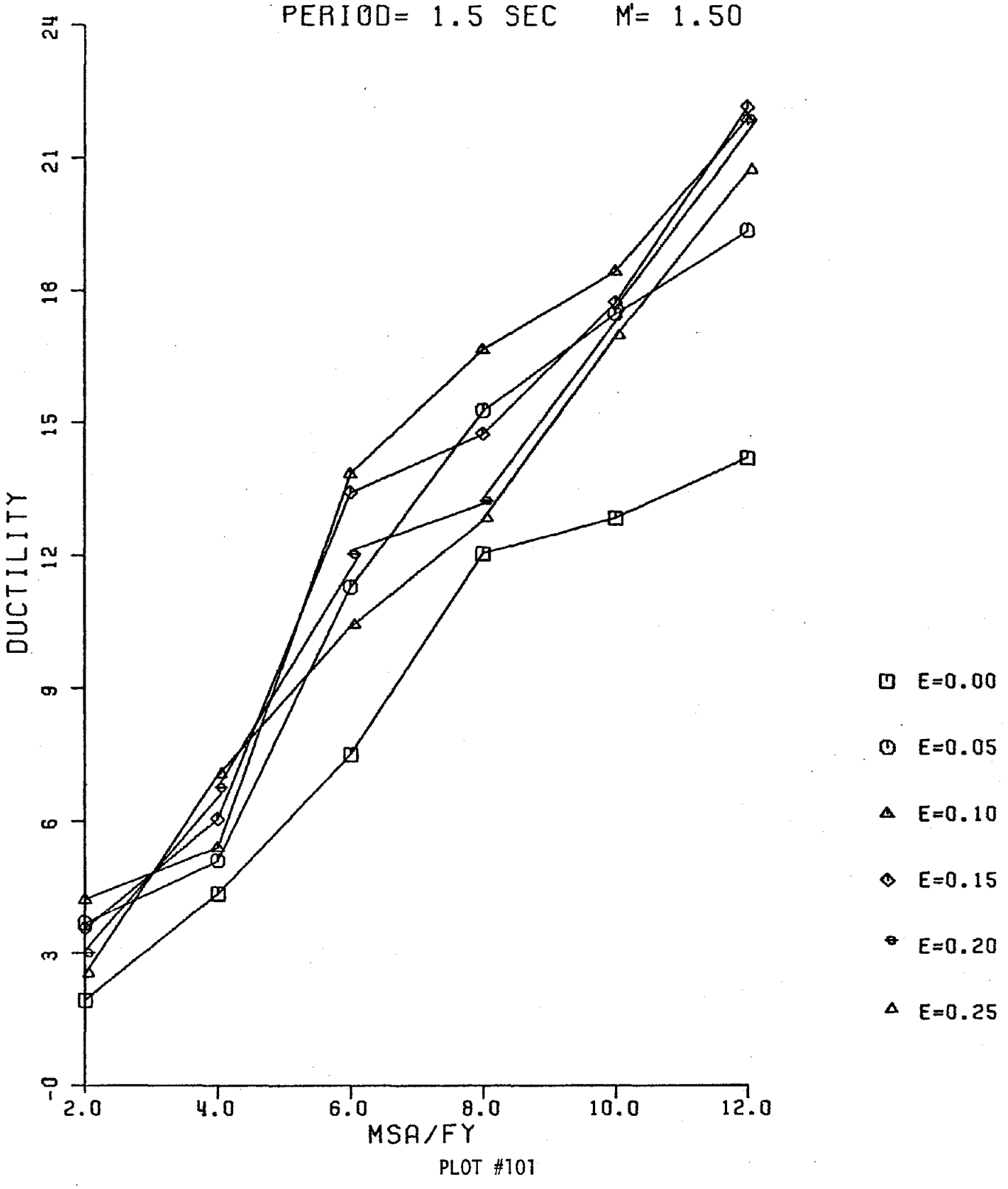

ARTIFICIAL MOTION

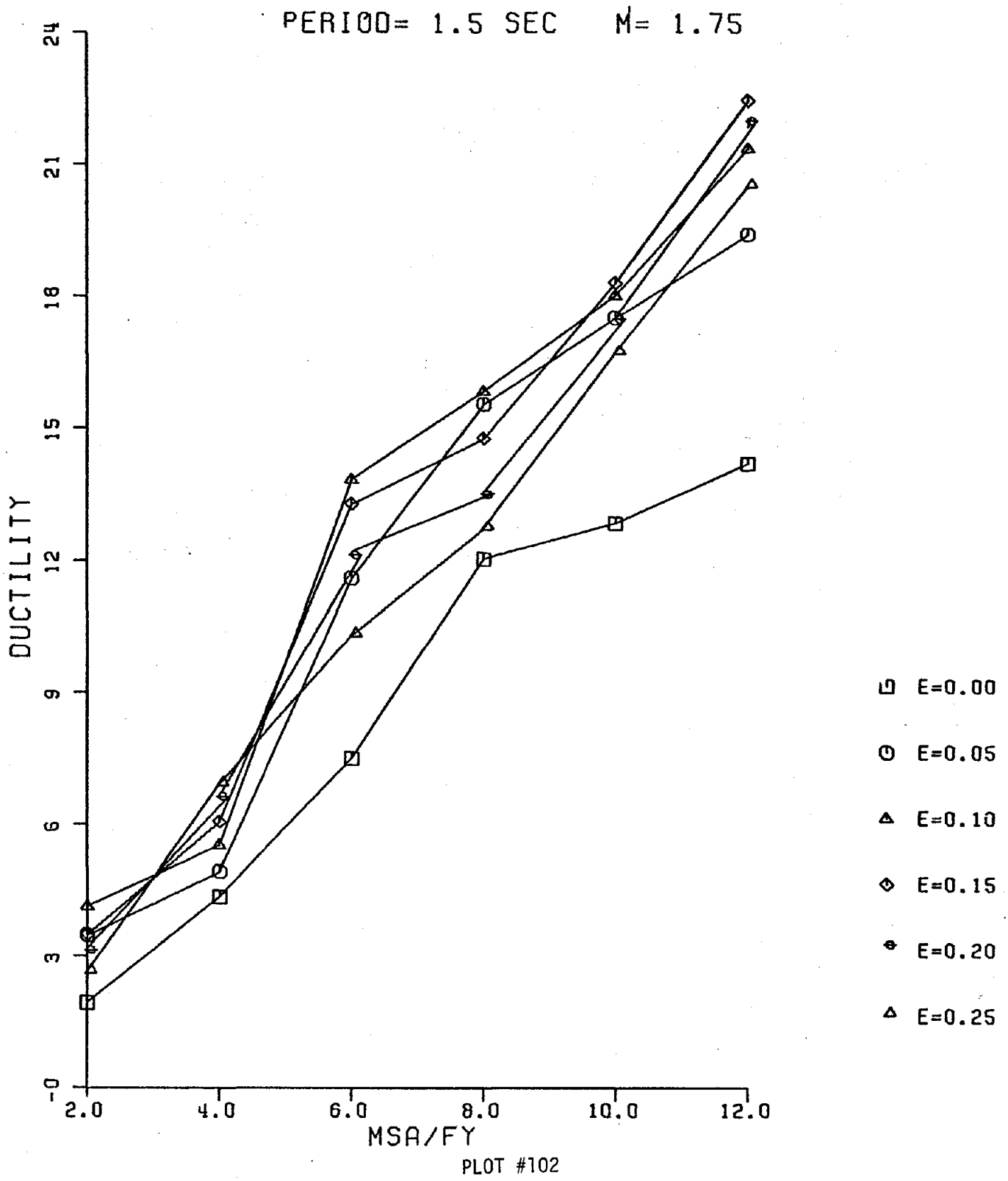

ARTIFICIAL MOTION

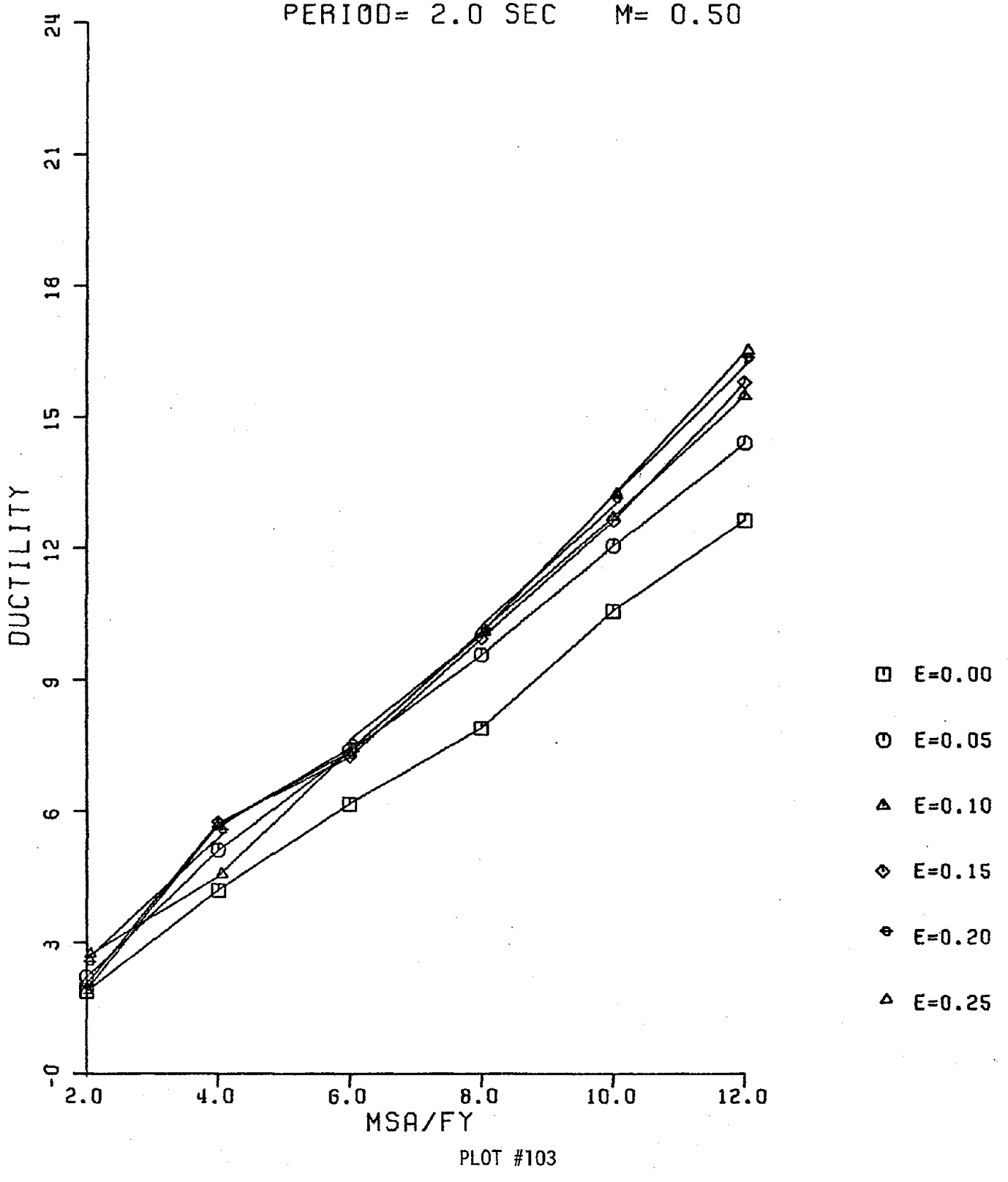

PLOT #103

ARTIFICIAL MOTION

PERIOD= 2.0 SEC M'= 0.75

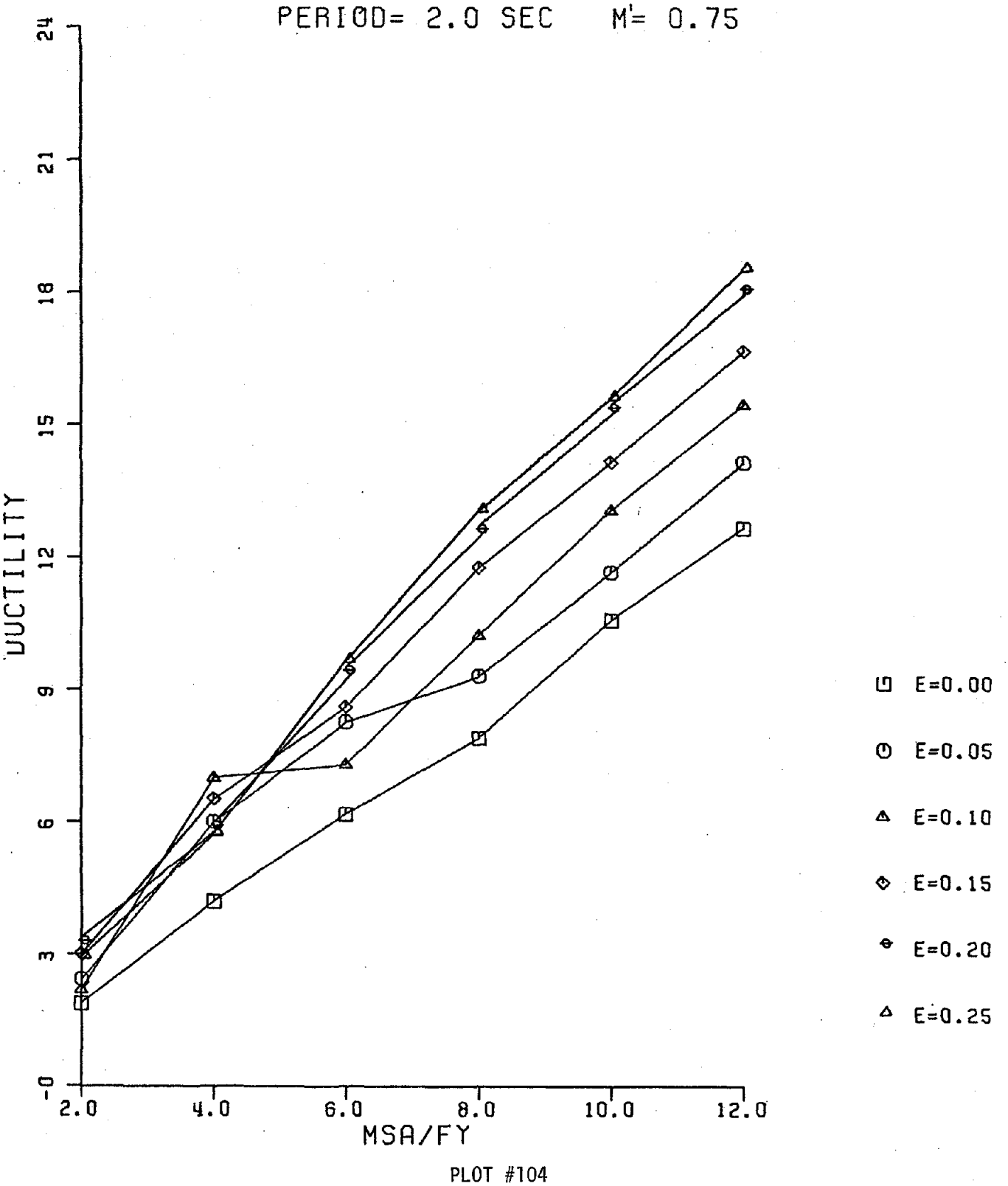

PLOT #104

ARTIFICIAL MOTION

PERIOD= 2.0 SEC M'= 1.00

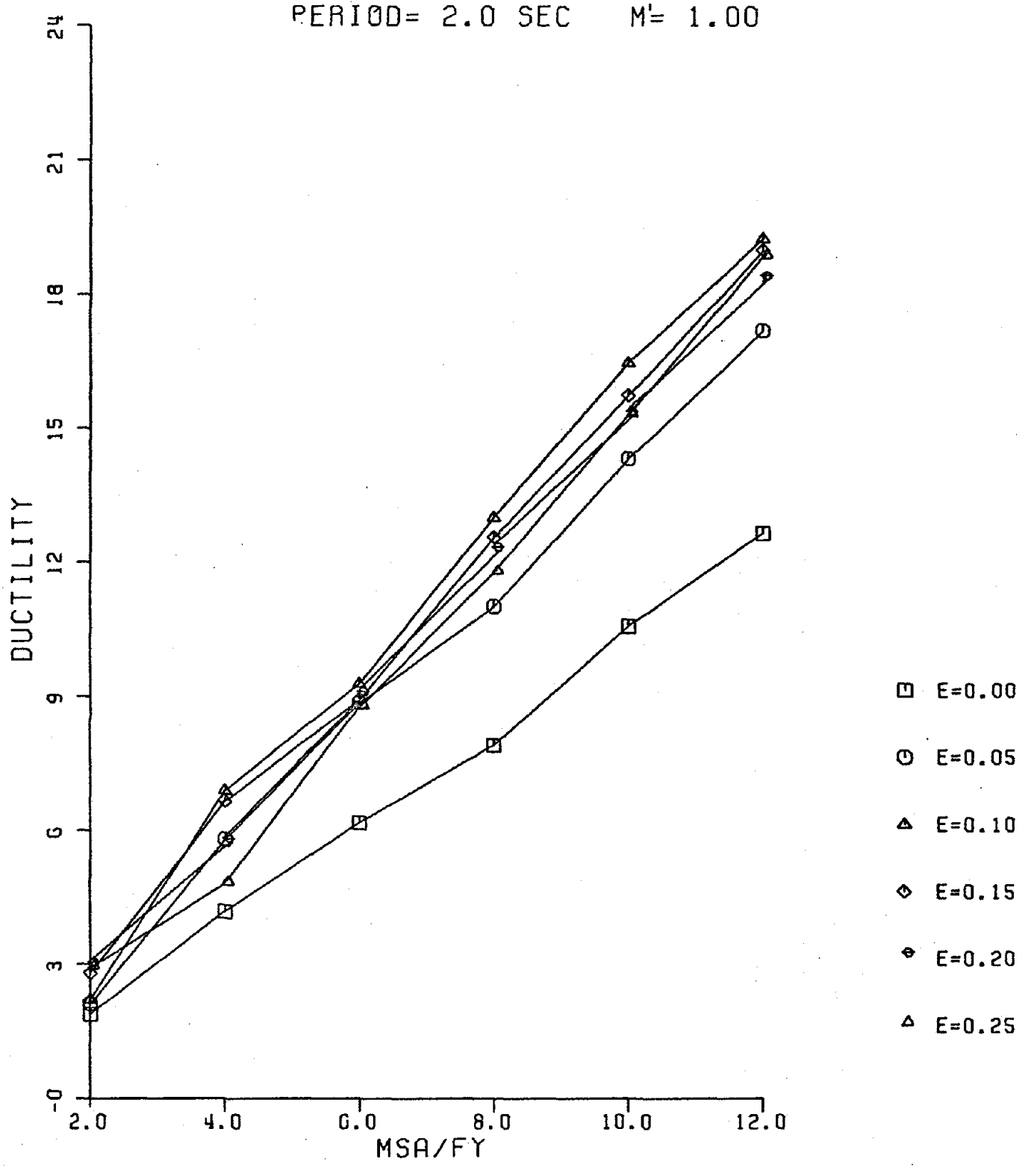

PLOT #105

ARTIFICIAL MOTION

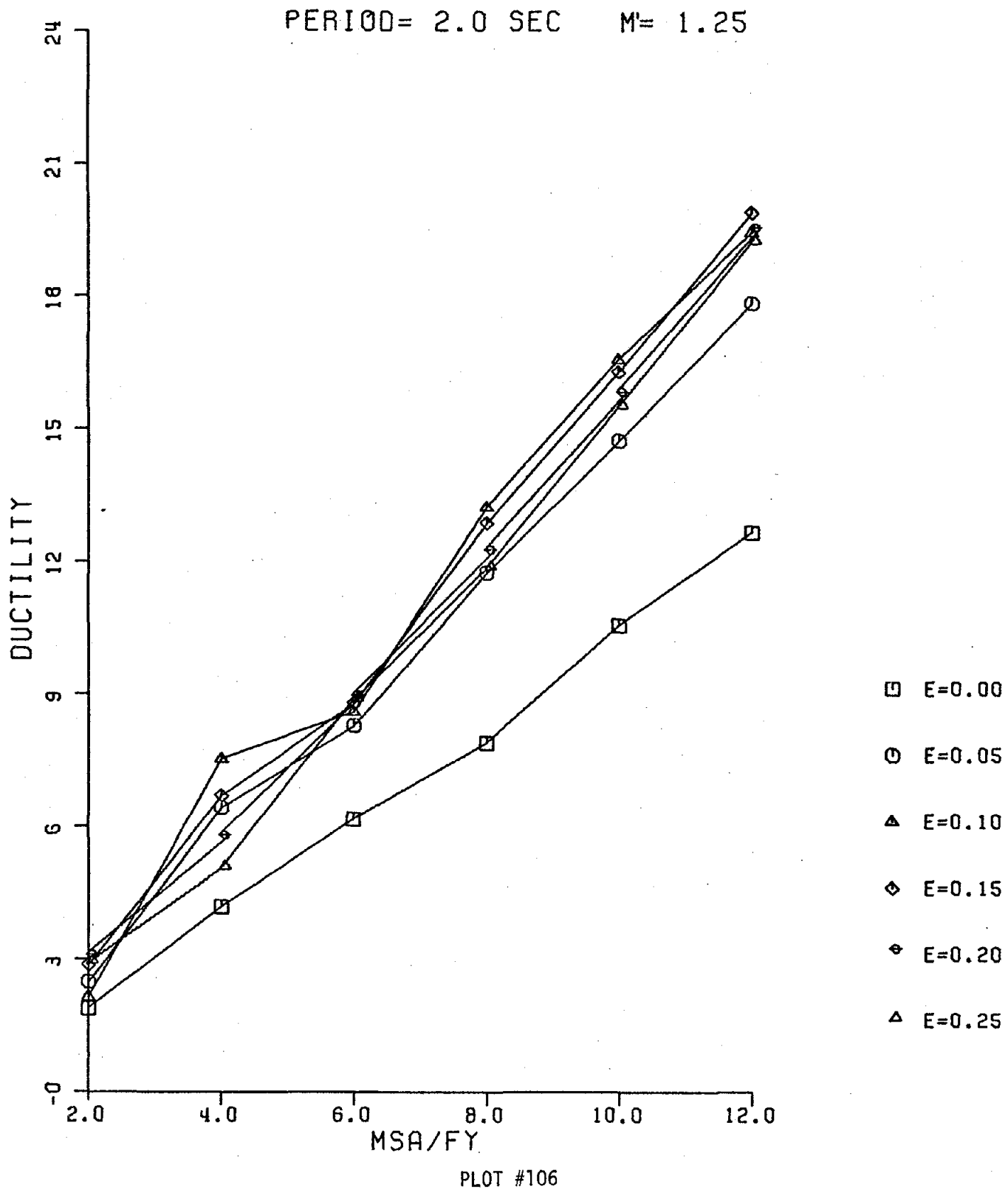

PLOT #106

ARTIFICIAL MOTION

PERIOD= 2.0 SEC M'= 1.50

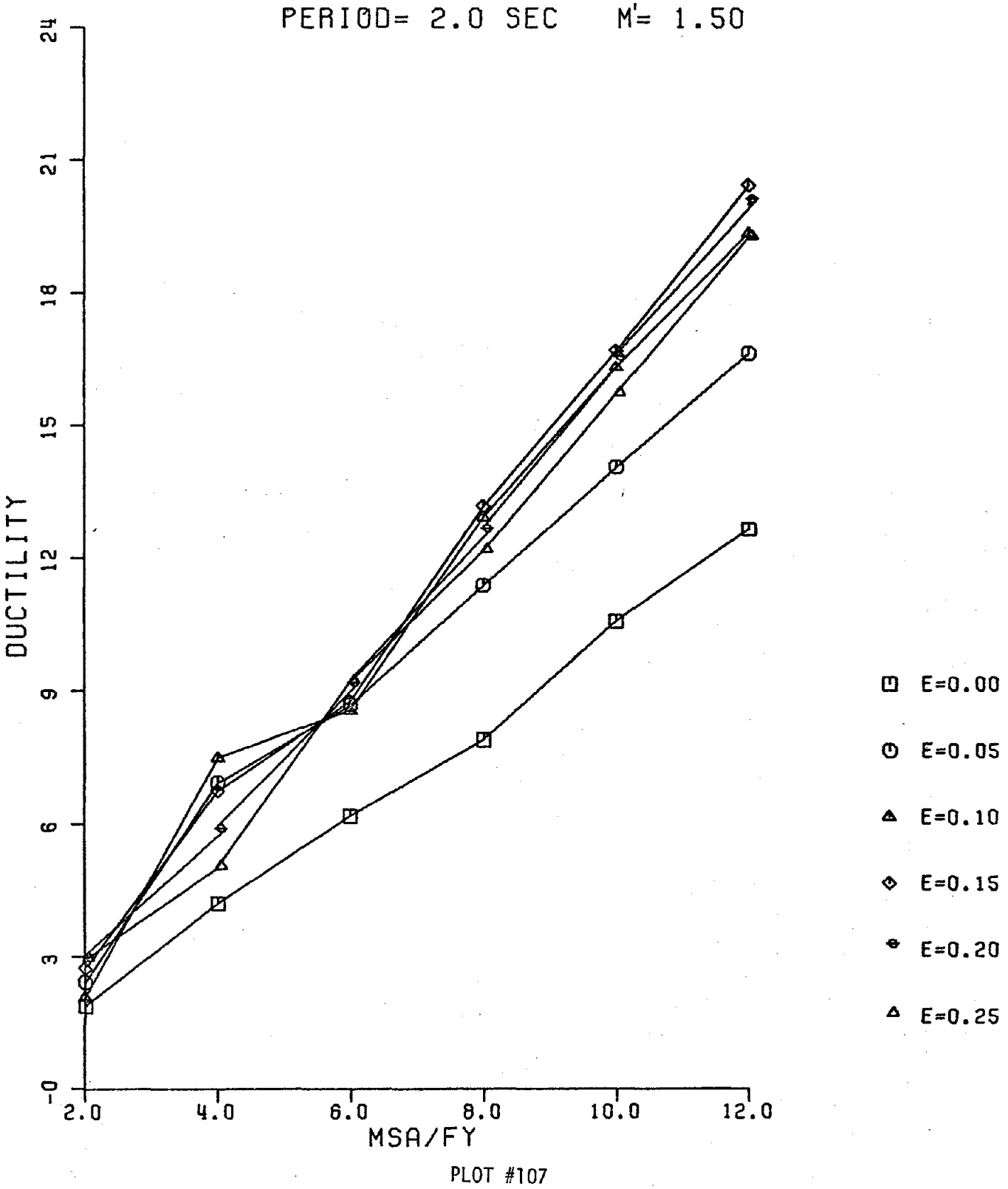

PLOT #107

ARTIFICIAL MOTION

PERIOD= 2.0 SEC M'= 1.75

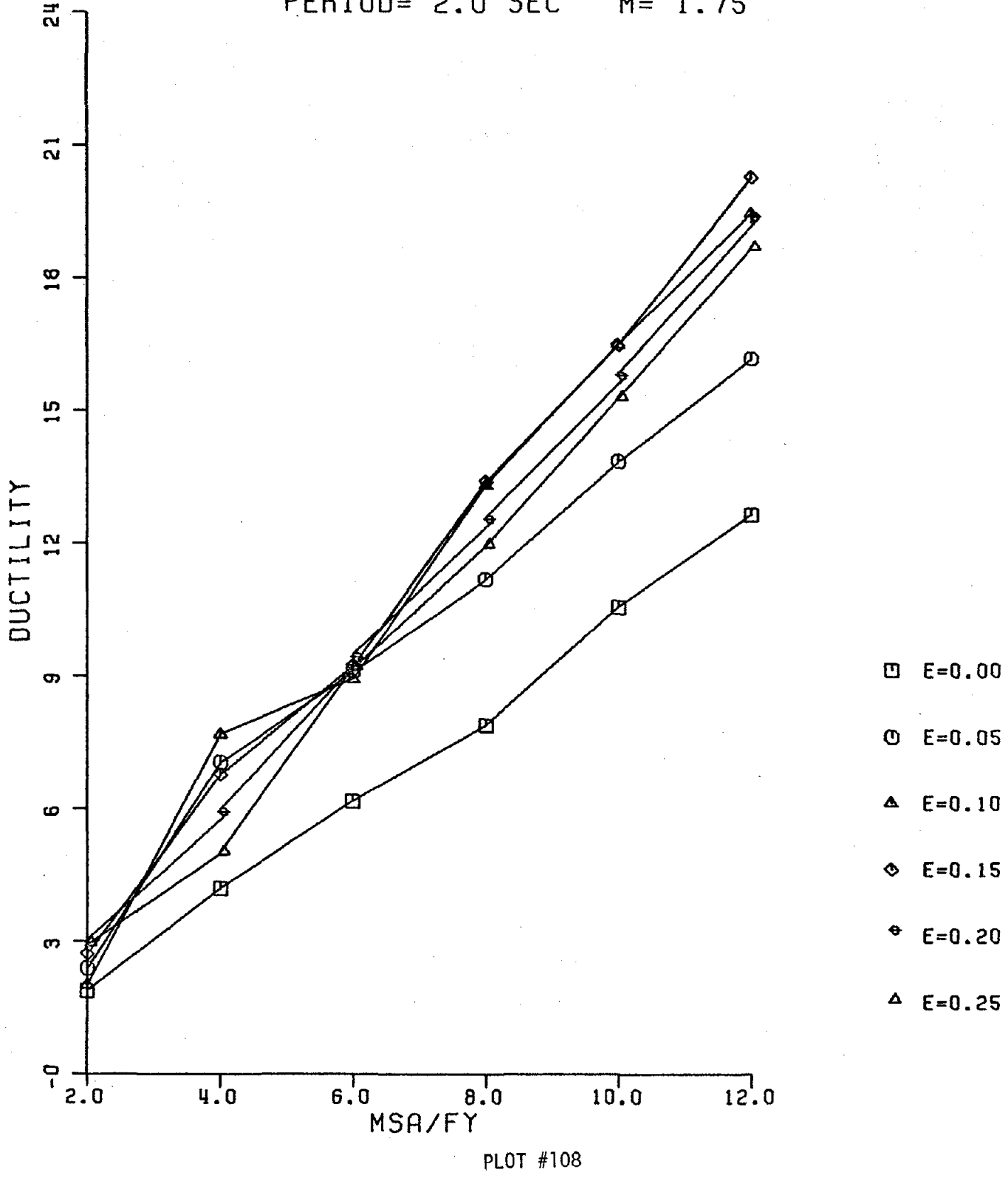

PLOT #108

CHAPTER V - DISCUSSION AND CONCLUSIONS

In plots 1 through 108 peak ductility demands (P.D.D.) are plotted against the parameter α (ratio of mass times spectral acceleration divided by yield strength), for eccentricities ranging from zero (symmetric case) to 0.25. Each plot accounts for a specific value of the parameter L/2r. Every six plots account for one specific translational period (ranging from 0.5 to 2 secs.). Four representative periods of 0.5, 1., 1.5 and 2.0 secs. are used in each earthquake motion, El-Centro, Pacoima Dam, Kern-County Taft, and an artificial motion.

Plot 59 is typical. The value of P.D.D. increases with parameter α in an essentially linear fashion. The line for zero eccentricity (marked with squares) is the bottom line. The first line above is the line corresponding to an 0.05 eccentricity, the next line above that is almost solely the line with 0.1 eccentricity, except at α = 12. An eccentricity of 0.25 yields a lower ductility than the lines with eccentricities of 0.10, 0.15, or 0.20. The line of the zero eccentricity case doesn't depend on L/2r, so it is unchanged for specified translational periods. See, for example, the curves marked with squares from plots 55 to 60.

It should be noted that if the structure behaved elastically, then the lines in the plot should be perfectly straight, due to the fact that in the elastic analysis the response is linear to the magnitude of the input acceleration.

Going through the plots, we observe that the curves for small values of the parameter L/2r lie almost one on the other (see plot 31), but as L/2r increases, they tend to diverge (see plots 32, 33, 34, 35, and 36). The same trend is noticeable also in plots 55 through 60, 61 through 66, etc.

This observation leads us to believe that eccentricity is largely unimportant for small values of L/2r, although it becomes more important for larger values of L/2r. The trend can be shown in an analytical manner.

Expressing formulae (3.2.4) as a function of our parametric study, we obtain

$$u_1 = -\frac{-\frac{r^2}{L^2}\Omega^2 + \frac{K^V}{2M}(\varepsilon + \frac{1}{2})}{\frac{r^2}{L^2}\Omega^4 - \frac{K^V}{2M}\Omega^2(\frac{1}{2} + 2\varepsilon^2 + 2(\frac{r}{L})^2) + \frac{K^{V2}}{4M^2}} \cdot \ddot{U}_g$$

$$u_2 = -\frac{\frac{r^2}{L^2}\Omega^2 + \frac{K^V}{2M}(\varepsilon - \frac{1}{2})}{\frac{r^2}{L^2}\Omega^2 - \frac{K^V}{2M}\Omega^2(\frac{1}{2} + 2\varepsilon^2 + 2(\frac{r}{L})^2) + \frac{K^{V2}}{4M^2}} \cdot \ddot{U}_g$$

or

$$u_1 = -\frac{-\frac{\Omega^2}{4(L/2r)^2} + \frac{2\pi^2}{T^2}(\varepsilon + \frac{1}{2})}{\frac{\Omega^4}{4(L/2r)^2} - \frac{2\pi^2}{T^2}\Omega^2(\frac{1}{2} + 2\varepsilon^2 + \frac{1}{2}\frac{1}{(L/2r)^2}) + \frac{4\pi^4}{T^4}} \cdot \ddot{U}_g$$

$$u_2 = -\frac{+\frac{\Omega^2}{4(L/2r)^2} + \frac{2\pi^2}{T^2}(\varepsilon - \frac{1}{2})}{\frac{\Omega^4}{4(L/2r)^2} - \frac{2\pi^2}{T^2}\Omega^2(\frac{1}{2} + 2\varepsilon^2 + \frac{1}{2}\frac{1}{(L/2r)^2}) + \frac{4\pi^2}{T^4}} \cdot \ddot{U}_g$$

From this we observe that the first term of the numerator in both equations is the dominant one for small values of L/2r. This implies that for small values of L/2r the term $\frac{\Omega^2}{4(L/2r)^2}$ will dominate the term

$\frac{2\pi^2}{T^2}(\varepsilon \pm \frac{1}{2})$ until it becomes important (for small translational periods). Of course, the equations are valid only for the elastic case. Nevertheless, they can always give us useful information for the behavior even in the inelastic case. The basic difference is that transfer functions assume constant stiffness matrix and steady-state response, whereas the earthquake motion is short and strong, so that the structural elements enter the inelastic range. The transfer function relates input amplitudes with output amplitudes at a specific driving frequency, so we can at least obtain some information about the amplification that takes place. However, it should not be overlooked that the P.D.D. don't give any information about the details of the response, cumulative ductilities, etc.

Plots 1-6, 13-84, 91-108 show the peak ductility demand of the frame closest to the center of mass, which as mentioned in Chapter 3 is expected to exhibit the maximum ductility. However, as has been pointed out in the elastic study of Dempsey and Irvine, this was not always the case. In certain instances the situation reverses and the frame farthest from the center of mass can exhibit larger ductilities than the frame closest to the center of mass. The analytical studies performed in Chapter 3 determined the conditions under which such a phenomenon can occur, and it was shown that this should be expected for small values of L/2r, and under a specific Fourier amplitude spectrum of the input motion, which is characterized by accumulation of power at lower frequencies. So if something like this does happen, it would be evident in the plots with the lowest values of L/2r, namely, plots 1, 31, 55, 79.

Plot 1 illustrates clearly the point. In this plot the curve for zero eccentricity lies on the top of all the curves with eccentricity showing

that, as the eccentricity increases, the P.D.D. for the frame closest to the center of mass become smaller and smaller which, in simple words, means that as the center of mass moves towards the one frame, the other frame is excited more strongly. In Plot 31 this phenomenon doesn't appear; however, the curves are bunched close together. In Plot 58 the phenomenon appears again, but Plot 79 does not show the above trend. Instead it exhibits a regular increase of P.D.D. with eccentricity. Artificial motions do not exhibit the above property because the Fourier amplitude spectra are artificially even.

Coming back to Plot 1, we observe a nearly perfect negative correlation with eccentricity. This property is observed in Plot 2. In Plot 3 it is less apparent and, from Plot 4 to Plot 6, the curves have their natural order. In Plots 7 to 12 the P.D.D. of the offset frame are pictured. Indeed, we observe in Plot 7 that the curves for the eccentric cases lie on (and sometimes above) the curve for the symmetric case, showing that the frame offset from the center of mass exhibits larger P.D.D. Slowly this property vanishes, mixing with the other curves in Plot 8 and finally ordering in physical order in Plots 9 through 12. However, as can be seen from these results, half the sum of the P.D.D. of the closest frame plus the P.D.D. of the farthest frame is almost equal to the P.D.D. of the symmetric cases, or

$$\frac{\mu_1 + \mu_2}{2} = \mu_{\text{symm.}} \quad ,$$

a result which has an intuitive appeal.

We also observe that the P.D.D. is very much dependent on the earthquake motion and, more specifically, on the value of the spectral acceleration associated with a specific translational natural frequency. However,

during the motion the translational period increases, and this tends to mask cause and effect. In addition to this, the P.D.D. depend very much on the shape of the input motion, and this could not be quantified in the present parametric study.

The conclusions to be drawn from this study appear to be as follows.

In almost all cases there appears to be a broadly linear trend between peak ductility demands and the parameter $\alpha(= MS_a/F_y)$. For the period range considered here, which was chosen to reflect a wide range of typical multistory structures, this trend is well known, at least for symmetric structures.

There is considerable scatter in results for large values of the ratio of frame spacing to the radius of gyration of the floor diaphragm. In analogous multistory structures this scatter would perhaps be associated with buildings with a peripheral frame.

By and large, peak ductility demands are more severe for frames closest to the center of mass than for frames further away. However, this is not always the case when the ratio of frame spacing to radius of gyration of the diaphragm is small, as might arise with buildings arranged around a central core. This behavior has been predicted in other elastic studies (2) and was found to be present in the present elastic response studies. It would appear that a simple frequency domain analysis, such as that presented here, suffices to explain this phenomenon. Even though this changeover occurs, the results nevertheless support a conclusion with some intuitive appeal—namely, that the mean ductility demand when eccentricity is present is little different from the ductility demand of the symmetric structure.

However, the most interesting conclusion that may be drawn from the present work is that there does not appear to be a strong correlation between peak ductility and eccentricity, Provided that the eccentricity ratio is limited to about 0.25, which more than covers most cases of practical interest, the differences in ductility demand between eccentric and symmetric buildings remain small, at least for small to moderate values of α ($=MS_a/F_y$). In this range the ratio of frame spacing to radius of gyration of the floor diaphragm does not significantly affect the results either.

Because this conclusion is seen to be of interest to those charged with the responsibility of drafting codes of practice for seismic loading, and because such activity in relation to torsional effects in buildings is widespread at present, it was decided to do a regression analysis of the data generated for the ductility demand of the most heavily loaded frame. The range of values of α was restricted to an upper limit of six, since ductility demands much greater than 10, say, are difficult to generate in normal structure elements. For all such data points 50% were found to lie below

$$\mu_{50} \simeq -0.2 + 1.2\,\alpha$$

while 90% of the data lay below $\qquad \varepsilon \leq 0.25,\ \alpha \leq 6$

$$\mu_{90} \simeq 2.1 + 1.2\,\alpha.$$

In the case of the data for zero eccentricity

$$\mu_{50} \simeq 0.1 + 0.9\,\alpha$$

$$\varepsilon \leq 0.25,\ \alpha \leq 6$$

and $\qquad \mu_{90} \simeq 1.7 + 0.9\,\alpha.$

On comparing respective pairs of lines one sees that the ductility demand in eccentric buildings is rarely more than about 30% higher than in symmetric structures experiencing realistic ductility demands.

We may close by reiterating that our simple model derives its eccentricity from variations in the location of the center of mass of the diaphragm and not, as is more common, by variations in stiffness of the frames. Strictly speaking, therefore, our results apply to that case and to no other. Nevertheless, our feeling is that the conclusions may be applied more generally, even though we have not proved it. The extent to which the conclusions drawn may be applied to multistory structures is obviously a matter for individual judgement. It is, however, rather unlikely that sufficiently comprehensive parameter studies can be done to resolve that question and, as in the past, reliance will have to be placed on the extrapolation of results from simplified building models.

As they stand at present, torsional provisions in some loading codes, which provide a dynamic increment to the existing eccentricity, in addition to an inclusion for accidental eccentricity, may be somewhat conservative (5, 6). It seems that, if in the equivalent static approach the seismic forces are required to act through the respective centers of mass and if some allowance is made for accidental eccentricity, a reasonable provision will have been made for the seismic elastic and inelastic effects of torsion in most buildings. It is interesting to note that the recent provisions of ATC are in accordance with this view.

References

1. Hoerner, J. B., "Modal Coupling and Earthquake Response of Tall Buildings," PhD Thesis, Report No. EERL 71-07, California Institute of Technology, Pasadena, California, 1971.

2. Dempsey, K.M., Irvine, H. M., "Envelopes of Maximum Seismic Response for a Partially Symmetric Single-storey Building Model," Earthquake Engineering and Structural Dynamics, Vol. 7, pp.161-180, 1979.

3. Anagnostopoulos, S.A., "Nonlinear Dynamic Response and Ductility Requirements of Buildings Subjected to Earthquakes," M.I.T. Department of Civil Engineering, Research Report R72-54, Sept.1972.

4. Anagnostopoulos, S.A., "A Computer System for Approximate Analysis of Multistory Buildings under Earthquake Loads," M.I.T. Department of Civil Engineering Research Report R70-7, January 1970.

5. Rutenberg, A., "A Consideration of the Torsional Response of Building Frames," Bulletin of the New Zealand National Society for Earthquake Engineering, Vol. 12, No. 1, March 1979.

6. Elms, D.G., "Seismic Torsional Effects on Buildings," Bulletin No. 2, N.S.E.E., Vol. 9, No.1, 1976, pp. 79-83.

7. Frank, R.A., Anagnostopoulos, S.A., Biggs, J. M., and Vanmarcke, E.H., "Variability of Inelastic Structural Response Due to Real and Artificial Ground Motions," M.I.T. Department of Civil Engineering Research Report R76-6, January 1976.

8. Kan, C.L., and Chopra, A.K., "Elastic Earthquake Analysis of a Class of Torsionally Coupled Buildings," ASCE Journal of the Structural Division, ST4, April 1977, pp. 821-838.

9. Vanmarcke, E., "Earthquake Ground Motion Input for Seismic Analysis and Design," Techn. Report, Waterways Experiment Station, 1979.

10. Gasparini, D.A., and Vanmarcke, E.H., "Simulated Earthquake Motion Compatible with Prescribed Response Spectra," Evaluation of Seismic Safety of Buildings Report No. 2, M.I.T. Department of Civil Engineering Research Report No. R76-4, Order No.527, January 1976.

APPENDIX I

EQUATIONS OF COUPLED MOTION WITH RESPECT TO THE CENTER OF MASS AND CENTER OF STIFFNESS

1. Equations of coupled motion with respect to the center of mass.

In Figure A.1.1 our model is sketched in the undeformed and deformed configuration.

The motion of the center of mass and center of stiffness are portrayed in Figure A.1.2. If V is the displacement of the center of mass, then $V - \varepsilon\theta$ is the displacement of the center of stiffness, where ε is the distance between center of mass and center of stiffness and θ is the angle of the deformed to the undeformed configuration.

Apply force F and Moment T at the center of mass and sketch spring resistances and inertia of the center of mass in Figure A.1.2. Then take the two equations of equilibrium equating the sum of forces equal to F and the sum of moments equal to T:

$$M\ddot{V} + K^V(V - \varepsilon\theta) = F$$

$$J_o\ddot{\theta} + K^\theta\theta - K^V(V - \varepsilon\theta)\varepsilon = T$$

or

$$\begin{vmatrix} M & 0 \\ 0 & J_o \end{vmatrix} \begin{vmatrix} \ddot{V} \\ \ddot{\theta} \end{vmatrix} + \begin{vmatrix} K^V & -K^V\varepsilon \\ -K^V\varepsilon & K^\theta + K^V\varepsilon^2 \end{vmatrix} \begin{vmatrix} V \\ \theta \end{vmatrix} = \begin{vmatrix} F \\ T \end{vmatrix}$$

In our case

$$\begin{vmatrix} F \\ T \end{vmatrix} = - \begin{vmatrix} M\ddot{u}_g \\ 0 \end{vmatrix}$$

Hence

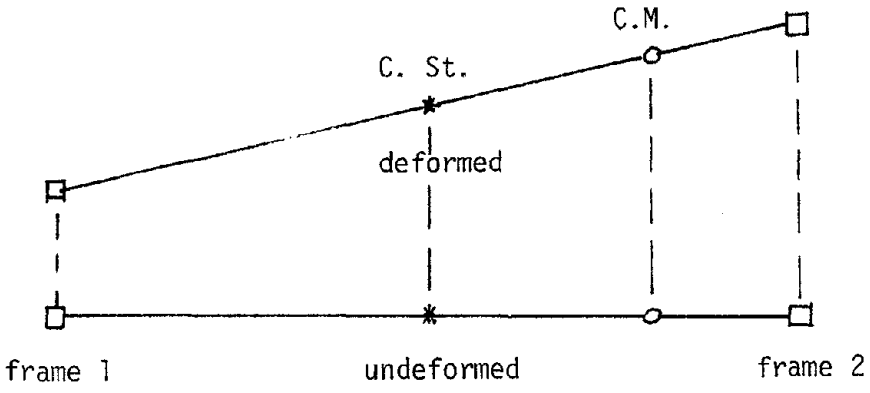

Figure A.1.1 - Model in Undeformed and Deformed Configuration

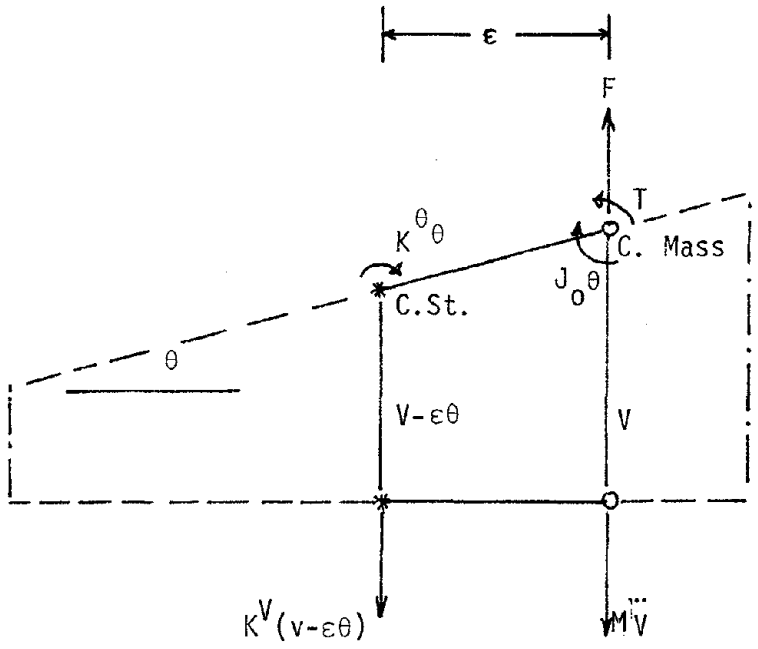

Figure A.1.2 - Forces and Resistances on Center of Mass and Centers of Stiffness

$$\begin{bmatrix} M & 0 \\ 0 & J_o \end{bmatrix} \begin{vmatrix} \ddot{V} \\ \ddot{\theta} \end{vmatrix} + \begin{bmatrix} K^V & -K^V\varepsilon \\ -K^V\varepsilon & K^\theta + K^V\varepsilon^2 \end{bmatrix} \cdot \begin{vmatrix} V \\ \theta \end{vmatrix} = - \begin{vmatrix} M\ddot{u}_g \\ 0 \end{vmatrix} \qquad \text{(A.1.3)}$$

Since the eccentricity, ε, and angle, θ, are algebraic quantities according to the sign convention, we obtain the corresponding equation.

2. Equations of motion with respect to the center of stiffness.

Now we apply the force F and moment T at the center of stiffness. The displacement of the center of stiffness is designated as V and hence the displacement of the center of mass is $V + \varepsilon\theta$. We sketch on Figuure A.1.3 the spring and inertia resistances and equate forces with F and moments with T.

$$M(\ddot{V} + \ddot{\theta}\varepsilon) + K^V V = F$$
$$J_o\ddot{\theta} + K^\theta\theta + M(\ddot{V} + \ddot{\theta}\varepsilon)\varepsilon = T$$

or

$$\begin{vmatrix} M & M\varepsilon \\ M\varepsilon & J_o + M\varepsilon^2 \end{vmatrix} \begin{vmatrix} \ddot{V} \\ \ddot{\theta} \end{vmatrix} + \begin{vmatrix} K^V & 0 \\ 0 & K^\theta \end{vmatrix} \begin{vmatrix} V \\ \theta \end{vmatrix} = + \begin{vmatrix} F \\ T \end{vmatrix}$$

if

$$\begin{vmatrix} F \\ T \end{vmatrix} = \begin{vmatrix} -M\ddot{u}_g \\ 0 \end{vmatrix}$$

Then

$$\begin{vmatrix} M & M\varepsilon \\ M\varepsilon & J_o + M\varepsilon^2 \end{vmatrix} \begin{vmatrix} \ddot{V} \\ \ddot{\theta} \end{vmatrix} + \begin{vmatrix} K^V & 0 \\ 0 & K^\theta \end{vmatrix} \begin{vmatrix} V \\ \theta \end{vmatrix} = - \begin{vmatrix} M\ddot{u}_g \\ 0 \end{vmatrix}$$

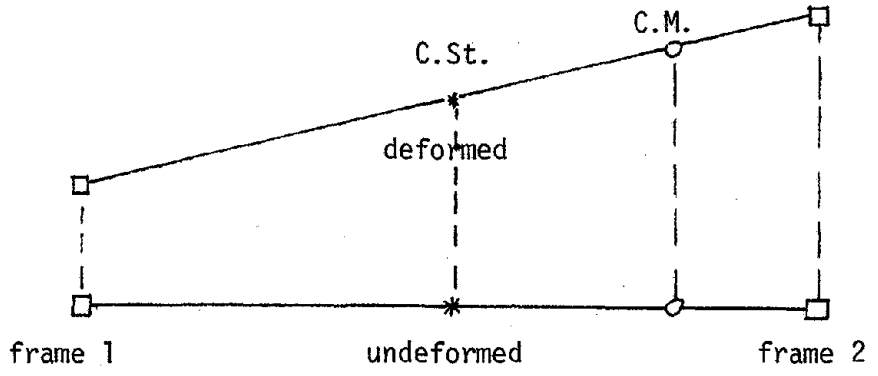

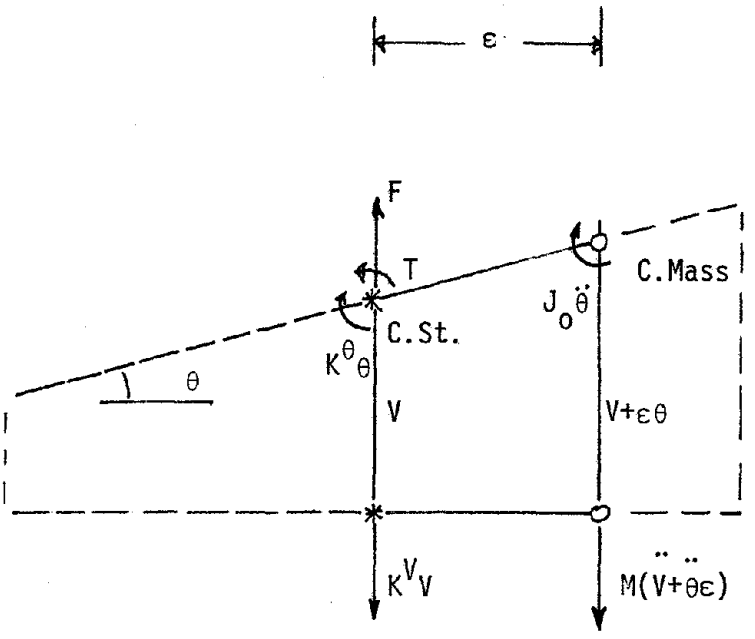

Figure A.1.3 - Model in Undeformed and Deformed Configuration. Forces and Resistances on Center of Mass and Center of Stiffness.

APPENDIX II - SUBROUTINE BILIN

In subroutine BILIN the force vector at n is calculated from a given force vector at n-1, and from given displacements both at n and n-1. The listing of subroutine BILIN is on Figure A.2.1.

The symbols used in the subroutine are:

FY = yield force

RK1 = primary stiffness

RK2 = secondary stiffness

FO = force at n-1

YO = displacement at n-1

FN = force at n (to be calculated)

YN = displacement at n

IFLAG = a flag used to calculate the INDEX

INDEX = an index of whether we ascend, descend, or are on the second branch.

Looking at Figure A.2.2, let BC be equal to a known value X. Also let the angle between OC and OA, OB and OA be β and α respectively.

Then $OA = (AB + X) \cot \beta$

but $AB = OA \tan \alpha$

Hence $OA = (OA \tan \alpha + X) \cot \beta$

or $$OA = \frac{X}{\tan \beta - \tan \alpha}$$

But in our case $\tan \beta$ equals RK1 and $\tan \alpha$, RK2. So

$$OA = \frac{X}{RK1 - RK2} \qquad (A.2.1)$$

```
      SUBROUTINE BILIN(FY,RK1,RK2,FO,YO,FN,YN,JFLAG,JNDEX)
      INTEGER*2 JFLAG,JNDEX,MCYCL
C---JNDEX=1  WE ASCEND  JNDEX=2  WE DESCEND,JNDEX=3  WE ARE ON THE SECOND SLOPE
      GO TO (10,20,30),JNDEX
   10 TEMP=(RK1*YO-FO)/(RK1-RK2)
      FN=FO+(YN-YO)*RK1
      FMAX=FY+RK2*TEMP
C---
      IF(FN-FMAX) 40,50,50
   40 JNDEX=1+JFLAG
      GO TO 100
   50 YMAX=FY/RK1+TEMP
      FN=FMAX+(YN-YMAX)*RK2
      JNDEX=3-JFLAG
      GO TO 100
   20 TEMP=(RK1*YO-FO)/(RK1-RK2)
      FN=FO+(YN-YO)*RK1
      FMAX=-FY+RK2*TEMP
      IF(FN-FMAX)60,60,70
   70 JNDEX=2-JFLAG
      GO TO 100
   60 YMAX=-FY/RK1+TEMP
      FN+FMAX+(YN-YMAX)*RK2
      JNDEX=3-2*JFLAG
      GO TO 100
   30 FN=FO+(YN-YO)*RK2
      IF(FN)80,80,90
   80 JNDEX=3-2*JFLAG
      GO TO 100
   90 JNDEX=3-JFLAG
  100 RETURN
      END
```

Figure A.2.1 - Subroutine BILIN

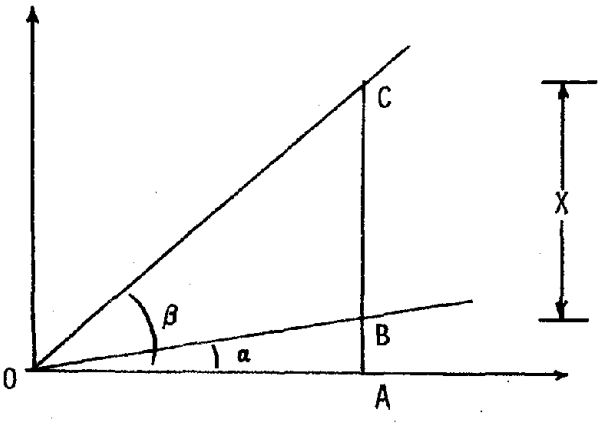

Figure A.2.2 - Calculation of X

Let us analyze the ascending case. (The descent is exactly analogous). In the ascent three cases are possible:

(1) FO is in the elastic range and FN cannot attain the value of FY. In this case FN will be located on the primary slope between FO and FY (Figure A.2.3a).

(2) FO is in the elastic range and FN exceeds the value of FY. In this case FN will be located on the secondary slope, and will be on the right of FY (Figure A.2.3b).

(3) FO is in the inelastic range (on the secondary slope) and is of course larger than FY. FN will be also on the secondary slope to the right of FO (Figure A.2.3c).

In the first case the new force will be:

$$PN = FO + (YN - YO) \cdot RK1$$

In the second case the new force will be

$$FN - FMAX + (YN - YMAX) \cdot RK2$$

where FMAX and YMAX are the yield force and displacement in the new position where the origin is shifted due to permanent displacements.

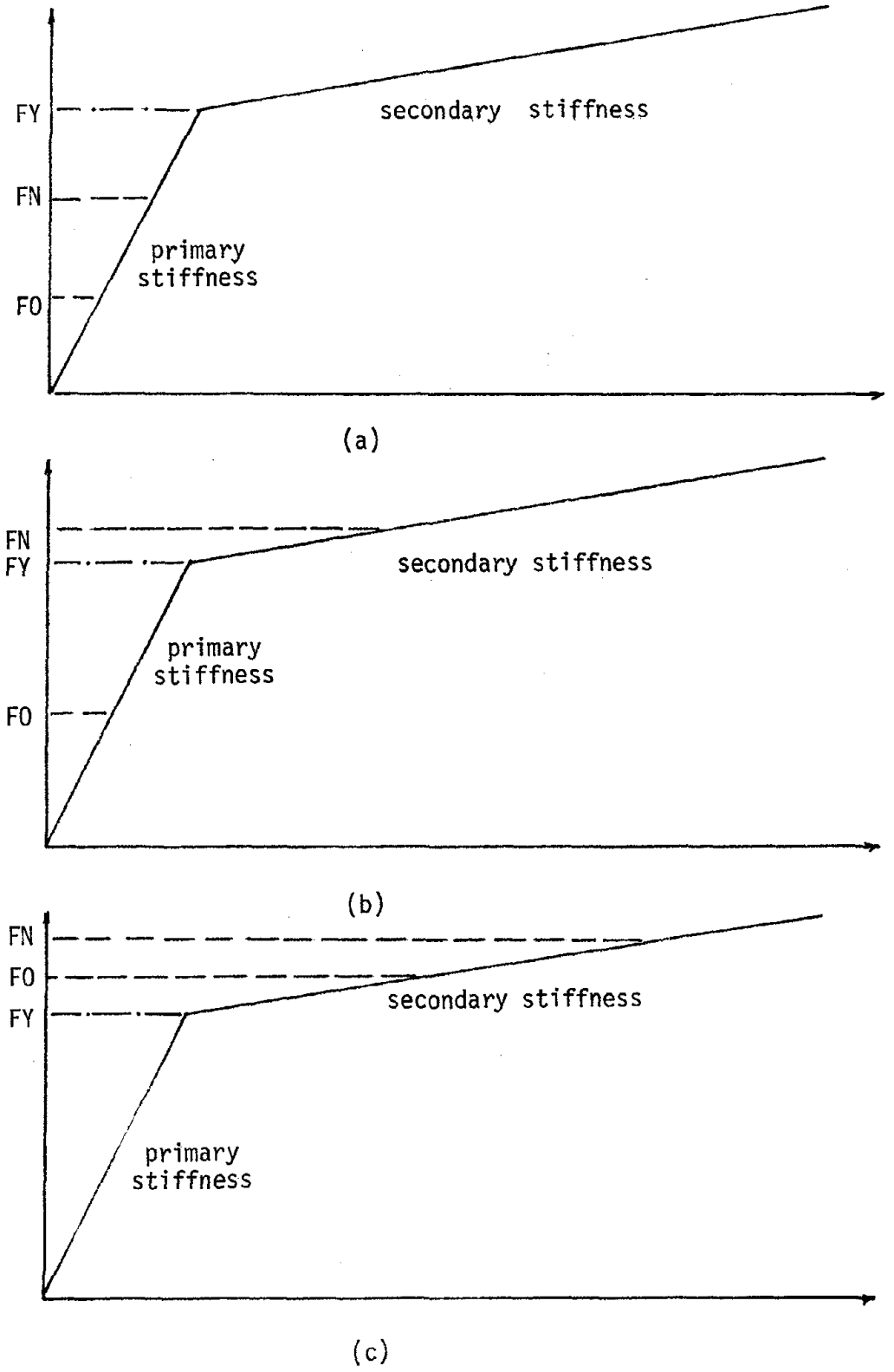

Figure A.2.3 - Position of the New Force Vector on the Bilinear Model

In order to illustrate the above, the ordinate of point A is the yield force FY. Now imagine that the motion starts from rest (point 0). For a displacement u_1 we come on point C on the curve. Then if the new displacement is u_2 we descend to E. Now ascending, the yield point is at B. The force at this point is designated FMAX and the displacement YMAX.

This is implemented in the program in the following way. First a value TEMP is calculated:

$$TEMP = (RK1 \cdot Y0 - F0)/(RK1 - RK2)$$

Comparing with equation (A.2.1, we realize that TEMP is the horizontal distance between B and Y in Figure A.2.4. Then

$$FMAX = FY + TEMP \cdot RK2$$

which is the ordinate of point B. The coordinates of point B are very important, because they define the yielding point. Having obtained the FMAX:

$$YMAX = \frac{FY}{RK1} + TEMP \quad ,$$

and

$$FN = FMAX + (YN - YMAX) \cdot RK2 \quad .$$

In the third case we move entirely on the second slope. So:

$$FN = F0 + (YN - Y0) \cdot RK2 \quad .$$

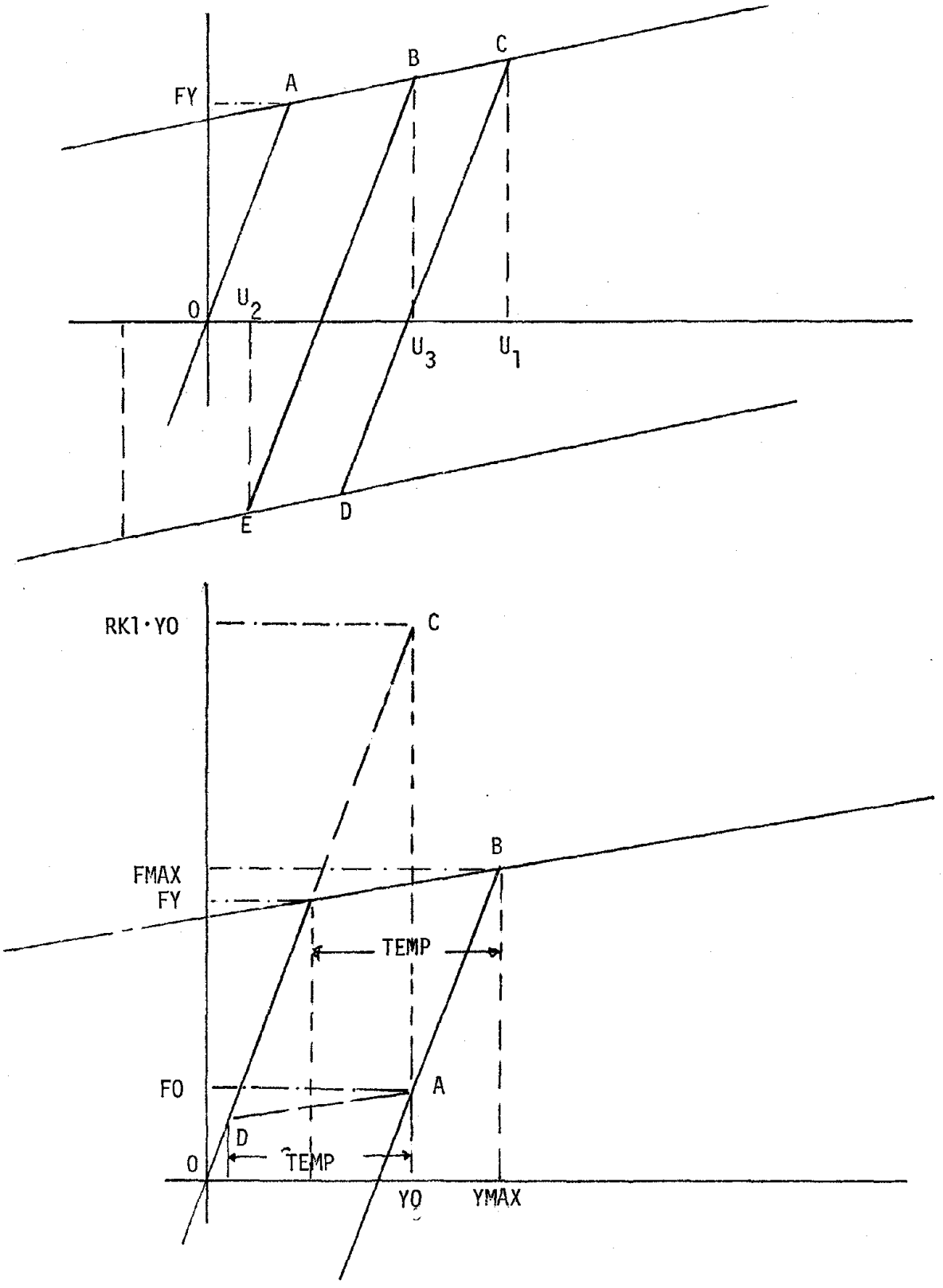

Figure A.2.4 - The Bilinear Model